



HAL
open science

Toward green processes organic synthesis by catalysis with metal-doped solids

Sophie Borghèse

► **To cite this version:**

Sophie Borghèse. Toward green processes organic synthesis by catalysis with metal-doped solids. Other. Université de Strasbourg, 2013. English. NNT : 2013STRAF008 . tel-01017796

HAL Id: tel-01017796

<https://theses.hal.science/tel-01017796>

Submitted on 3 Jul 2014

HAL is a multi-disciplinary open access archive for the deposit and dissemination of scientific research documents, whether they are published or not. The documents may come from teaching and research institutions in France or abroad, or from public or private research centers.

L'archive ouverte pluridisciplinaire **HAL**, est destinée au dépôt et à la diffusion de documents scientifiques de niveau recherche, publiés ou non, émanant des établissements d'enseignement et de recherche français ou étrangers, des laboratoires publics ou privés.

ÉCOLE DOCTORALE DES SCIENCES CHIMIQUES

Institut de Chimie, UMR 7177

THÈSE

présentée par

Sophie BORGHÈSE

soutenue le : 15 février 2013

pour obtenir le grade de

Docteur de l'université de Strasbourg

Discipline/ Spécialité : Chimie Organique

Toward Green Processes
Organic Synthesis by Catalysis with
Metal-Doped Solids

THÈSE dirigée par :

M. PALE Patrick

Professeur, Université de Strasbourg

RAPPORTEURS :

Mme MASSIANI Pascale

M. PRAKASH Surya G. K.

Directeur de Recherches, Université Pierre et Marie CURIE
Professeur, Loker Hydrocarbon Research Institute

MEMBRES DU JURY :

M. BAATI Rachid

M. EVANO Gwilherm

Directeur de Recherches, Université de Strasbourg
Professeur, Université Libre de Bruxelles

Acknowledgements

Je tiens tout d'abord à remercier les membres du jury d'avoir accepté de juger ce travail : Mme Pascale Massiani, Mr Surya Prakash, Mr Rachid Baati et Mr Gwilherm Evano.

J'adresse mes plus chaleureux remerciements aux deux professeurs qui m'ont choisi pour réaliser cette thèse et qui m'ont accueilli dans leur laboratoire : Patrick Pale et Jean Sommer. Je ressors réellement enrichie d'avoir étudié pendant ces trois années des domaines très divers, choisis ou non, autour de quatre projets différents.

Je tiens bien sûr à remercier les encadrants du laboratoire avec qui j'ai – pour la plupart - collaboré sur ces différents sujets et qui m'ont aidé à progresser, humainement et/ou scientifiquement. Je pense au Dr Valérie Bénéteau : merci pour ta présence et ta gentillesse, qui ont été un soutien important tout au long de cette thèse. Merci au Dr Benoît Louis, pour ses enseignements sur la vie et les relations humaines. Merci au *Professeur* Jean-Marc Weibel (encore désolée!) pour les moments de rigolade – même si j'ai souvent eu du mal à comprendre ton langage ! Enfin, mention spéciale à Mr Aurélien Blanc, avec qui j'ai partagé pendant ces trois années bien plus que de la chimie. La liste est longue et s'étend des identifications de produits par RMN à la customisation de blouse. Ce qui est sûr, c'est que ton caractère bien trempé m'a parfois mis en boule, mais j'ai vraiment apprécié ton honnêteté permanente, une qualité bien rare de nos jours. Merci pour tout ce que tu as fait pour moi professionnellement : mes deux seules publiés à ce jour en sont le premier témoignage, et pour l'amitié qu'on a créée autour.

Merci à tous les collègues thésards, postdocs et stagiaires, pour l'ambiance agréable et chaleureuse à laquelle ils ont contribué au labo, et pour les nombreux pots et soirées mémorables qu'on a partagés ensemble : Auré A., Simon, Andrea, Thomas, Guillaume, Béa, Florian, Nico C., Paco, Nico K., Damien, Marilyne, Claire, Julie, Anne-Sophie, Rofia, Ani. Non Matthieu je ne t'ai pas oublié, tu fais définitivement parti de ce labo je pense ! Merci à toi pour les bons moments qu'on a passés cette dernière année. Une pensée particulière à ma petite Marie, dont la présence féminine dans le bureau a été d'un grand secours ! Nos discussions 'potins' vont me manquer, c'est sûr ! Merci d'avoir été là pour moi quand j'étais dans la m****, mais aussi pour ta bonne humeur et ton entrain à faire la fête.

Au cours de ces trois ans, j'ai eu la nécessité et la chance de partir quatre fois à Los Angeles, et de prendre l'avion pour la première fois de ma vie, pendant 12h. Merci à Jean qui est à l'origine de tout cela. Merci au Loker Institute et au Pr Prakash pour le soutien financier qui m'a été accordé. J'en profite pour remercier également les personnes qui m'ont accueilli là-

bas, notamment Alain Goeppert, qui m'a fait découvrir la ville autrement qu'en bus, Robert Aniszfeld, qui s'est toujours montré disponible et efficace, et mes collègues et amis : Miklos, Nan, Clement et Somesh : merci pour ton amitié et pour le road trip à Santa Barbara, inoubliable !

Mes remerciements vont également à ma famille, plus précisément ma maman, mon papa, ma sœur et Philippe. Malgré la distance qui nous sépare depuis maintenant 6 ans, j'ai toujours pu compter sur vous, dans les bons et les moins bons moments. Vos encouragements et votre soutien ont été un bien précieux. Je suis vraiment heureuse d'avoir pu en retour vivre avec vous cette journée de soutenance, un moment de grande joie et de satisfaction, réussi à tous les niveaux.

Merci à ma constante, l'une de mes premières rencontres à Strasbourg, avec qui j'ai parcouru à pied un nombre incalculable de fois les ruelles de la Krutenau. Merci pour tous les moments inoubliables vécus depuis ce fameux soir à Amitel. Comme dans notre série préférée, j'espère bien qu'on saura toujours se retrouver et apprécier ces discussions qui nous sont chères, à n'importe quelle époque et dans n'importe quel lieu.

Merci à tous les membres du groupe, avec qui j'ai vécu les meilleurs moments de ma vie étudiante pendant ces 6 années à Strasbourg, et qui comptent beaucoup pour moi. On a tellement évolué depuis la première soirée (crêpes !), tout en restant les mêmes, au fond : Juju, toujours insortable, et partant pour les idées les plus barges, Adrien, métrosexuel sosie de Beigbeider, toujours branché, et Le Big, le blond fidèle à lui-même, tellement attachant. Une pensée pour ceux qui sont loin maintenant, et pour ceux qui sont arrivés en cours de route : Carine, Benoît-Jérémy, Nadège, Geoffrey, Yohan, Salomé, Laurence. Les amis, n'oubliez pas que malgré mes défauts, les années et les sorties, je suis restée VOMIT FREE (très important).

Merci à ma BF que j'ai enrôlé dans ce groupe, et avec qui j'ai traversé avec plaisir des années et moments intenses à l'ECPM. Tu restes ma **BFE**, même de l'autre côté de l'Atlantique !

Spéciale dédicace à Mr Bingo, un mec super qui tire aussi bien à la carabine qu'il joue au bad ou fait la galipette, avec qui on rit, mais on rit !! Et surtout qui est devenu un *VRAI* ami.

Merci à la team mayennaise, une vraie bande de cassos, connue depuis peu mais avec qui on se tape des barres de rire à chaque fois, et que j'adore : Léo, Julie, Arnaud, Jocelyn, Vince, Thomas, Caro, Francis, et Estefania.

Enfin, un immense merci à celui qui me les a fait connaître, et qui reste le meilleur à mes yeux. Ta patience, ton soutien constant et tes conseils ont été des facteurs directs de ma réussite. Maintenant, c'est fait et j'ai hâte qu'on écrive la suite de nos aventures.

Abbreviations and formulas

Å	Ångström
aq	aqueous
Ac	acetyl
BEA	Beta
BINAP	2,2'-bis(diphenylphosphino)-1,1'-binaphthyl
Boc	<i>tert</i> -butyloxycarbonyl
<i>i</i> -Bu	<i>iso</i> -butyl
<i>t</i> -Bu	<i>tert</i> -butyl
<i>n</i> -BuLi	<i>n</i> -butyllithium
cat.	catalytic amount
CDCl ₃	deuterated chloroform
<i>m</i> -CPBA	meta-chloroperbenzoic acid
DCM	dichloromethane
DVB	divinylbenzene
<i>E</i>	<i>entgegen</i>
EDX	Energy-dispersive X-ray
ee	enantiomeric excess
equiv.	equivalent
Et	ethyl
Et ₂ O	Diethyl ether
EtOAc	Ethyl acetate
EtOH	ethanol
ESI	electrospray ionisation
eV	electronvolt
EWG	Electron Withdrawing Group
FAU	Faujasite
FT-IR	Fourier-Transformed InfraRed
g	gram
GC	Gas Chromatography
h	hour
HMPA	Hexamethylphosphoramide

HOMO	Highest Occupied Molecular Orbital
HPA	HeteroPoly Acid
HRMS	High Resolution Mass Spectroscopy
Hz	Herz
<i>J</i>	coupling constant
LUMO	Lowest Unoccupied Molecular Orbital
MAS	Magic Angle Spinning
Me	methyl
MeCN	acetonitrile
MeOH	methanol
MFI	Mordenite Framework Inverted
mg	milligram
min	minute
mL	milliliter
mmol	millimole
mol	mole
MOR	Mordenite
MS 4 Å	molecular sieves 4 Å
NMR	Nuclear Magnetic Resonance
Ph	phenyl
PhMe	toluene
PPh ₃	triphenylphosphine
POM	PolyOxoMetalate
ppm	parts per million
<i>R_f</i>	retardation factor
r.t.	room temperature
SEM	Scanning Electron Microscopy
TBAF	<i>tert</i> -butyl ammonium fluoride
TBS	<i>tert</i> -butyldimethylsilyl
TBDPS	<i>tert</i> -butyldiphenylsilyl
TEA	triethylamine
THF	TetraHydroFuran
TLC	Thin Layer Chromatography
USY	Ultra Stable Y

XRD	X-Ray Diffraction
ZSM-5	Zeolite Socony Mobil-5
wt%	weight %
Z	<i>zusammen</i>

Table of contents

General Introduction.....	3
Chapter 1 : From the use of transition metals in organic synthesis to the development of new heterogeneous catalysts for green chemistry	3
1. Environmental considerations with respect to modern chemical industry.....	5
1.1. The Green Chemistry concept.....	5
1.2. Important green metrics for assessing environmental impact.....	6
2. Importance of transition metals in organic synthesis	8
2.1. Particular properties of coinage metals	9
2.2. Utility of recycling transition metal catalysts	20
3. Heterogeneous catalysts for greener organic transformations	22
3.1. Heterogeneization of homogeneous catalysts: the different solid supports	22
3.2. Zeolites	24
3.3. Polyoxometalates	44
4. Objectives of the thesis	54
4.1. Development of heterogeneous procedures catalyzed by metal-doped solids ...	54
4.2. Comprehension of the mechanisms of hydrocarbon conversion	55
Chapter 2 : Activation of small alkanes on solid acids : study of the hydride transfer reaction by isotopic exchange between ^2H - and ^{13}C - labeled isobutanes.....	57
1. Mechanisms of hydrocarbon conversion on solid acids : an overview.....	59
1.1. Hydrocarbon cracking: an illustration of the early issues concerning the first step of alkane conversion.....	59
1.2. The emergence of H/D exchange studies	64
2. Focus on an important step of alkane conversion: the hydride transfer reaction.....	71
2.1. Preparation of ^{13}C and ^2H labeled isobutanes	73
2.2. The hydride transfer study: experimental results	76
2.3. The hydride transfer study: interpretation of the results	79
Chapter 3 : Silver(I)-heteropolyacids as “green” catalysts for the synthesis of furans from alkyloxiranes	89
1. Furans: utility and accessibility.....	91
2. Precedents for the rearrangement of allenes and alkyne derivatives to furans by silver(I) catalysis	93

3. Silver(I)-heteropolyacids as bifunctional heterogeneous catalysts for the rearrangement of alkynyloxiranes into furans.....	98
3.1. Preparation of the bifunctional Ag-H-POMs	99
3.2. Characterization of the Ag-H-POMs catalysts.....	100
3.3. Screening of reaction conditions using Ag-H-POMs catalysts.....	104
3.4. Scope of the Ag-H-POMs catalyzed rearrangement of alkynyloxiranes	106
3.5. Recycling of the catalyst	109
Chapter 4 : Synthesis of ketals and spiroketals by Ag-zeolite catalyzed dihydroalkoxylation of alkyne diols.....	113
1. The spiroketal moiety: importance and accessibility	115
1.1. Traditional approaches toward spiroketal moieties	116
1.2. Recent strategies based on C=C bond creation	119
1.3. The dihydroalkoxylation of alkyne diols	120
1.4. The silver(I)-catalyzed cycloisomerization of alkynols and alkyne diols.....	124
2. Ag ^I -zeolite catalyzed cycloisomerization of alkynols and alkyne diols	127
2.1. Preparation of silver-doped zeolites	127
2.2. Characterization of the materials.....	128
2.3. Influence of the zeolite topology on the hydroalkoxylation of alkynols.....	132
2.4. Screening of reaction conditions for the cyclization of alkynols	134
2.5. Screening of reaction conditions for the dihydroalkoxylation of alkyne diols ...	136
2.6. Scope of the Ag-USY catalyzed cyclization of alkynols and alkyne diols.....	139
2.7. Discussion concerning the reaction mechanism.....	143
2.8. Recyclability of Ag-USY	147
3. Conclusion.....	148
Chapter 5 : Toward the total synthesis of acortatarin A, using a Ag ^I -catalyzed spiroketalization strategy.....	151
1. Acortatarin A: a natural product of biological interest.....	153
2. Previous total syntheses of acortatarin A	155
3. Our approach toward acortatarin A	158
4. Toward a copper-zeolite catalyzed amidative cross-coupling	162
4.1. Ynamines: a versatile functional group.....	162
4.2. Emergence of ynamides	164
4.3. Toward a Cu-zeolite catalyzed amidative cross-coupling.....	172
5. Ag-USY catalyzed spiroketalization of ynamide diols	178

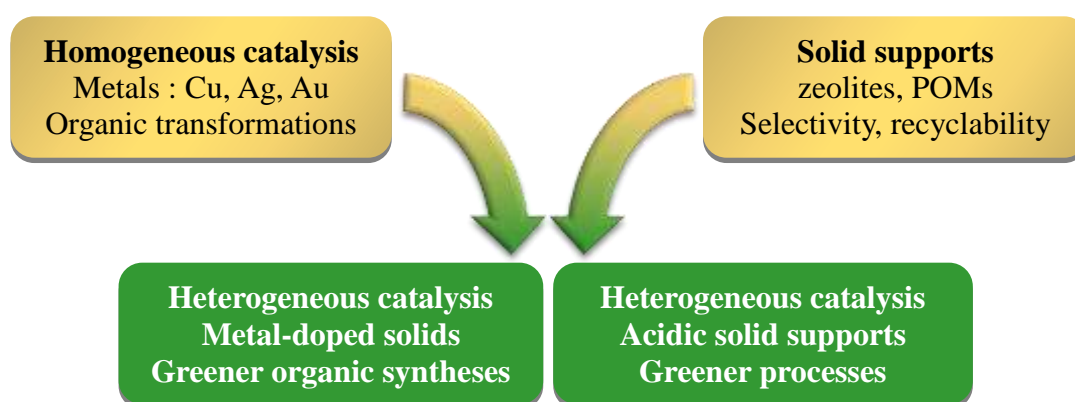
5.1. Spiroketalization of aliphatic ynamide diols	178
5.2. Toward the tricyclic core of acortatarin A	184
6. Synthesis of the sugar moiety of acortatarin A	188
7. Perspectives concerning the total synthesis of acortatarin A	196
Conclusion	201
Experimental Data	207
1. Activation of small alkanes on solid acids	209
1.1. General information	209
1.2. Synthesis of ² H and ¹³ C labeled isobutanes	209
1.3. <i>In situ</i> MAS NMR experiments	210
2. Ag-H-POMs catalyzed rearrangement of alkynyloxiranes to furans	212
2.1. General Information	212
2.2. Preparation of silver-containing POMs	212
2.3. Characterization of the products	213
3. Synthesis of ketals and spiroketals under Ag-zeolite catalysis	219
3.1. General information	219
3.2. Ag-zeolites preparation	220
3.3. Characterization of the products	220
4. Toward the total synthesis of Acortatarin A	229
4.1. General Information	229
4.2. Cu-USY preparation	229
4.3. Characterization of the products	230
Résumé	248
Abstract	248

General Introduction

With the development of the modern chemical industry, environmental concerns related to the disposal of waste and the reduction of the worldwide resources have gained increasing importance. To tackle these issues, the introduction of the Green Chemistry¹ concept has provided theoretical guidelines to the chemical community and enabled to highlight the novel priorities that have to be considered. Among them, the use of catalytic reagents instead of stoichiometric quantities is getting increasingly important with the rarefaction of the resources, including transition metals.

In parallel, homogeneous catalysis with transition metals has become a strategic tool in organic synthesis over the last decades, enabling the construction of complex molecules from simple starting materials, sometimes in short reaction sequences.²

The shift from homogeneous to heterogeneous procedures *via* the use of solid supported transition metals is an efficient way to take benefit from these methodologies while reducing their environmental and economic impact at the same time. By combining the ability of transition metals to promote organic transformations, with the properties of solid supports such as zeolites or polyoxometalates, we aimed to design green heterogeneous pathways to attractive building blocks of organic synthesis (Scheme 1).



Scheme 1. Objectives of the Ph.D. thesis

This objective is at the heart of the present Ph.D. thesis, which lies at the interface between organic synthesis, heterogeneous catalysis, and materials science.

¹ Anastas, P. T.; Warner, J. C. *Green Chemistry, Theory and Practice*; Oxford University Press: Oxford, **1998**.

² (a) Beller, M. ; Bolm, C. *Transition Metals for Organic Synthesis, 2nd Ed.*; Wiley-VCH, **2004**. (b) Hegedus, L. S. *Transition Metals in the Synthesis of Complex Organic Molecules, 2nd Ed.*; University Science Books, Sausalito, **1999**.

Introduction

After a brief introduction on the challenges set up by Green Chemistry, the first section of chapter 1 will highlight the properties and importance of coinage metals, *i.e.* copper, silver and gold, as catalysts in organic synthesis. In a second place, we will present the different types of solid supports available to host transition metals, with an emphasis on zeolites and polyoxometalates, which were studied more in depth during the Ph.D. thesis. The second chapter will concern another field of application of heterogeneous catalysts, *i.e.* hydrocarbon conversion in petrochemical processes. We will focus on the hydride transfer reaction and try to understand the mechanisms taking place between acidic zeolites and hydrocarbons. In the third chapter, we will detail the use of silver-doped polyoxometalates as bifunctional heterogeneous catalysts for the rearrangement of alkynyloxiranes into furans. The fourth chapter is dedicated to the synthesis of ketals and spiroketals by hydroalkoxylation of alkynediols, using silver-doped zeolites as recyclable catalysts. After the optimization of the methodology, we will try to demonstrate in a last chapter how such environmental friendly procedures can take part in the total synthesis of a natural molecule of biological interest, and constitute useful methods to reach complex targets in a green fashion.

Chapter 1 :

From the use of transition metals in organic synthesis to the development of new heterogeneous catalysts for green chemistry

1. *Environmental considerations with respect to modern chemical industry*

1.1. The Green Chemistry concept

The “environmental movement” emerged 50 years ago and is known to be related to the publication of Rachel Carson’s book ‘Silent Spring’ in 1962,³ which denounced the hazards of environmental pollution - notably pesticides - for flora and fauna, but also human beings. Although not a scientific book, it clearly helped to make public aware of the importance of environmental issues. Subsequently, the “environmental movement” slowly extended through the creation of institutions like the Environmental Protection Agency (EPA) and the development of environmental policies shifted toward the prevention of waste, rather than the “end-of-pipe control”.

In the mid 1990’s, Paul Anastas of the EPA and John Warner introduced the concept of green chemistry.¹ To tackle the environmental issues, but also the economic and social dimensions that the modern chemical industry presupposed, they formulated 12 principles indicating how practically the production of chemicals must be carried out to be sustainable:⁴

1. Waste prevention instead of remediation
2. Atom economy or efficiency
3. Use of less hazardous and toxic chemicals
4. Safer products by design
5. Innocuous solvents and auxiliaries
6. Energy efficiency by design
7. Preferred use of renewable raw materials
8. Shorter syntheses (avoid derivatization)
9. Catalytic rather than stoichiometric reagents
10. Design products to undergo degradation in the environment
11. Analytical methodologies for pollution prevention
12. Inherently safer processes

³ Carson, R. *Silent Spring, 40th anniversary edition*; Houghton Mifflin, Boston, **1962**.

⁴ Green Chemistry (URL: <http://www.organic-chemistry.org/topics/green-chemistry.shtm>)

The 9th principle underlines the fact that catalytic reagents instead of stoichiometric ones can prevent the formation of wastes. If most catalysts and solvents can be recycled, the process is even more sustainable.

1.2. Important green metrics for assessing environmental impact

In the early 1980's, the big chemical companies started to realize that the disposal of waste had an economic impact as important as the profit generated by the production of their chemicals. Consequently, people began looking for ways to assess and measure the impact of chemical processes on the environment. In this context, Sheldon introduced the E(nvironmental) factor,⁵ defined as the ratio of waste to the desired product (kg/kg). Thus, the ideal E factor is 0. It can be easily calculated as the amount of raw materials in, minus the amount of desired product, divided by the amount of product out. Water itself is excluded from the calculation, but any chemical diluted in the aqueous stream must be considered. At first sight, the E factor gives interesting information concerning different industry segments (Table 1).⁵

Table 1. E factor in the chemical industry

Industry segment	Product tonnage	E factor (kg waste/kg product)
Oil refining	10 ⁶ -10 ⁸	< 0.1
Bulk chemicals	10 ⁴ -10 ⁶	<1-5
Fine chemicals	10 ² -10 ⁴	5-50
Pharmaceuticals	10-10 ³	25-100

The E factor of oil refining is close to 0, due to a large utilization of heterogeneous catalysts – especially zeolites - which have replaced toxic and hazardous acids in various refining processes. On the contrary, and despite a lower product tonnage, pharmaceutical industries exhibit a high E factor, in agreement with the fact that usual organic transformations often employ stoichiometric reagents rather than catalysts. It is noteworthy to mention that all these considerations have to be balanced by the toxicity of waste. For this purpose, Sheldon invented the unfriendliness quotient Q, which should be close to one for ‘inoffensive’ waste -

⁵ (a) Sheldon R. A. *Chem. Ind.* **1992**, 903–906. (b) Sheldon, R. A. *Green Chem.* **2007**, 9, 1273–1283.

NaCl for instance - and very high for heavy metal salts like chromium. Hence, by multiplying the E factor by Q, we should get closer to the real impact of a process.

During the same period, Trost popularized the concept of atom efficiency or atom economy, which can be sum up as how much of the reactants end up in the product (Equation 1).⁶

$$\% \text{ Atom efficiency} = \frac{\text{MW}_{(\text{desired product})}}{\text{MW}_{(\text{all substances formed})}} \times 100$$

Equation 1. Definition of the atom efficiency

Contrary to the E factor, the atom efficiency is a theoretical number which assumes a quantitative yield and does not consider the chemicals besides the stoichiometric equation. A theoretical E factor can be deduced from the atom efficiency (Equation 2).

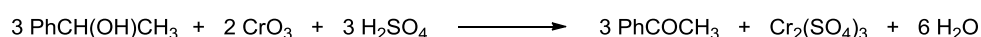
$$E_{\text{theo}} = \frac{100 - \text{atom efficiency}}{\text{atom efficiency}}$$

Equation 2. Definition of the theoretical E factor

The real E factor is usually much higher since it takes into account actual yields and chemicals involved.

As an example, atom efficiency and theoretical E factor have been assessed for the stoichiometric *versus* catalytic oxidation of 1-phenylethanol in acetophenone (Scheme 2).^{5b}

Stoichiometric:

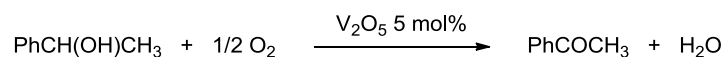


$$\% \text{ Atom efficiency} = \frac{3 \times 120}{3 \times 120 + 392 + 6 \times 18} = 42 \%$$

$$E_{\text{theo}} = 1,5$$

$$Q = 100 - 1000 \text{ (chromium salts)}$$

Catalytic:



$$\% \text{ Atom efficiency} = \frac{120}{120 + 18} = 87 \%$$

$$E_{\text{theo}} = 0,1 \text{ (0)}$$

$$Q = 1$$

Scheme 2. Stoichiometric *versus* catalytic oxidation of 1-phenylethanol in acetophenone

The Jones oxidation employing chromium trioxide, sulfuric acid, and generating toxic chromium salts and water has a poor atom efficiency of 42%, while the oxidation by simple

⁶ Trost, B. M. *Science* **1991**, 254, 1471–1477.

oxygen and using a vanadium catalyst⁷ generates only water and has an atom efficiency of 87%.

In his publication,⁶ Trost upholds that “*The ability of transition metal complexes to activate organic molecules makes them attractive prospects for developing catalytic processes with high atom economy.*”

2. *Importance of transition metals in organic synthesis*

In the field of organic synthesis, transition metal catalyzed reactions represent very attractive methodologies, due to their ability to build up complex molecules from simple starting materials under mild conditions.²

Indeed, it is very rare today to find a total synthesis that does not involve at least one transition-metal mediated step. In this context, palladium has gained widespread use and is nowadays the most popular transition metal catalyst.⁸

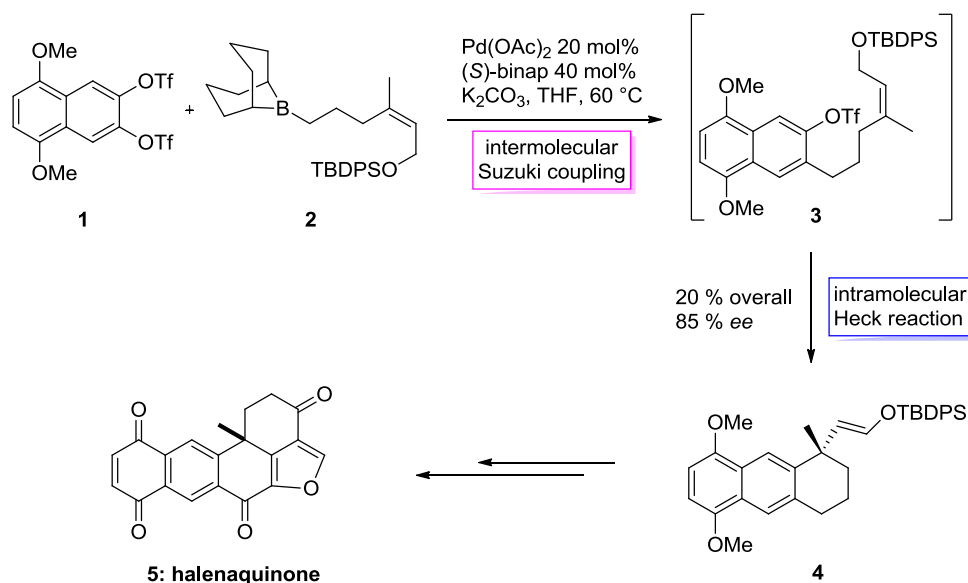
Its ability to undergo oxidative additions has enabled the emergence of powerful synthetic methodologies for the synthesis of C-C and C-Heteroatom bonds between or within functionalized substrates, namely the well-known Heck, Stille, Suzuki, Sonogashira, Tsuji–Trost, Negishi and Buchwald-Hartwig reactions.⁹ Developed during the last quarter of the 20th century, these transformations provided new synthetic tools for the total synthesis of complex molecules (Scheme 3).¹⁰

⁷ Velusamy, S.; Punniyamurthy, T. *Org. Lett.* **2004**, *6*, 217–219.

⁸ Tsuji, J. In *Palladium Reagents and Catalysts: New Perspectives for the 21st Century*; John Wiley & Sons, Ltd., Chichester, **2004**.

⁹ (a) De Meijere, A.; Diederich, F. *Metal-Catalyzed Cross-Coupling Reactions*, 2nd ed., Wiley-VCH, Weinheim, **2004**. (b) Negishi, E. *Handbook of Organopalladium Chemistry for Organic Synthesis*, Wiley Interscience, New York, **2002**; (c) Miyaura, N. *Cross-Coupling Reactions: A Practical Guide*, Springer, Berlin, **2002**.

¹⁰ Nicolaou, K. C.; Bulger, P. G.; Sarlah, D. *Angew. Chem. Int. Ed.* **2005**, *44*, 4442–4489.



Scheme 3. Palladium catalyzed reactions for the synthesis of halenaquinone

The group of Shibasaki developed elegant syntheses of halenaquinone and its derivatives based on palladium catalyzed transformations.¹¹ They successfully obtained the tricyclic system 4 *via* an intermolecular Suzuki–Miyaura coupling/intramolecular asymmetric Heck cyclization cascade sequence. Despite a low yield due to the formation of side products (reduction of bistriflate 1 and double Suzuki coupling product), the palladium catalyzed cascade enabled the one pot creation of 2 new C–C bonds, a new ring and a quaternary center enantioselectively.

2.1. Particular properties of coinage metals

Due to its efficiency in various coupling reactions, palladium actually took over copper catalysts, known for a century for promoting C–C and C–O bonds formation. Lying just between transition metals and main group elements, copper belongs to the so-called coinage metals triad: Cu, Ag and Au or group 11 elements. With a s^1d^{10} electronic configuration (Figure 1), coinage metals are very prone to lose one electron for giving the corresponding Lewis acidic metal cations (Cu^+ , Ag^+ , Au^+).

¹¹ (a) Kojima, A.; Takemoto, T.; Sodeoka, M.; Shibasaki, M. *J. Org. Chem.* **1996**, *61*, 4876–4877. (b) Kojima, A.; Takemoto, T.; Sodeoka, M.; Shibasaki, M. *Synthesis* **1998**, 581–589.

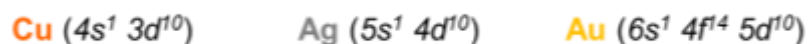


Figure 1. Electronic configuration of Cu, Ag and Au

However, it is noteworthy to mention that the three metals exhibit considerable differences regarding their oxidation state in aqueous solution.¹² Copper(I) and (II), silver(I) and gold(I) and (III) are the most common oxidation states, whereas copper(III), silver(III) and gold(II) occur very rarely.¹³ Among the various factors responsible for the stability of one particular oxidation state, atomic properties and especially relativistic effects have a great importance. Relativistic effects typically occur for heavy elements, when the velocity of electrons is considered to become significant with respect to the speed of light.¹⁴ This can be expressed mathematically by the Lorentz equation (Equation 3), where m is the corrected mass, m_0 is the non-relativistic mass, v is the electron velocity and c the speed of light.

$$m = m_0 / (1 - (v / c)^2)^{1/2}$$

$$m \longrightarrow \infty$$

$$v \longrightarrow c$$

Equation 3. Definition of the Lorentz equation

Since the Bohr radius is inversely proportional to the mass of the electron, the increase in mass results in a decrease in radius. Electrons of s and p orbitals are stabilized and contracted closer to the nucleus, but this provokes an opposite effect: the destabilization and expansion of d and f orbitals, due to a stronger shielding of the nuclear attraction. The orbital frontier energies of coinage metals are shown in Figure 2.^{14c}

¹² Walker, N. R.; Wright, R. R.; Barran, P. E.; Murrell, J. N.; Stace, A. J. *J. Am. Chem. Soc.* **2001**, *123*, 4223–4227.

¹³ (a) Levason, W.; Spicer, M. D. *Coord. Chem. Rev.* **1987**, *76*, 45–120. (b) Po, H. N. *Coord. Chem. Rev.* **1976**, *20*, 171–195.

¹⁴ (a) Gorin, D. J.; Toste, F. D. *Nature* **2007**, *446*, 395–403. (b) Pyykkö, P. *Angew. Chem. Int. Ed.* **2004**, *43*, 4412–4456. (c) Vallet, V. *Actualité Chimique* **2003**, *260*, 3–11. (d) Pyykko, P. *Chem. Rev.* **1988**, *88*, 563–594. (e) Desclaux, J. P.; Pyykkö, P. *Chem. Phys. Letters* **1976**, *39*, 300–303.

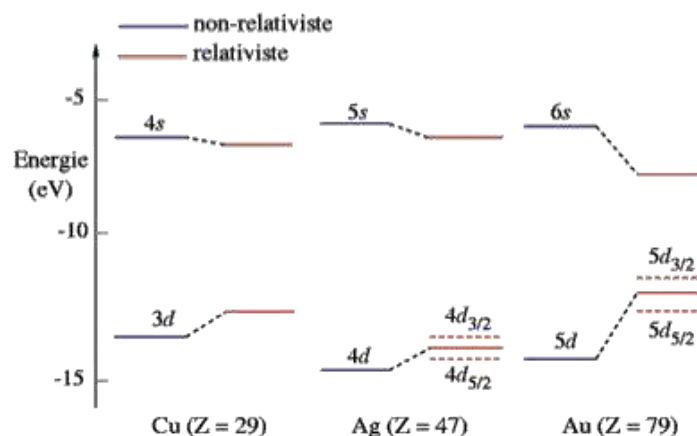


Figure 2. Orbital frontier energies of Cu, Ag and Au

Relativistic effects increase down the group and become particularly significant for gold. As a consequence, its first ionization is high compared to copper and silver (Table 2).^{13a,15} The second ionization energy is higher when going from copper to silver, due to the increase in nuclear charge. On the contrary, it decreases from silver to gold, because of the destabilization of the $5d$ orbital electrons. This indirect relativistic effect is so influential for gold that its third ionization energy is still much lower compared to copper and silver, which accounts for the preferred Au^{III} oxidation state.

Table 2. Ionization energies of Cu, Ag and Au

	Ionization energies [eV]		
	1st	2nd	3rd
Cu	7,721	20,29	36,74
Ag	7,576	21,48	34,82
Au	9,214	20,52	30,00

Contraction and stabilization of the lowest unoccupied molecular orbital (LUMO) of coinage metal cations make them very strong Lewis acids, able to coordinate easily electron donating ligands, either in a σ or a π -fashion. This Lewis acidity is especially marked for gold salts, and reinforced by their high electron affinity (2.4) compared to silver and copper (≈ 1.9). Yamamoto and co-workers calculated the heat of formation of various Lewis acid complexes

¹⁵ Wiberg, N.; Holleman, A. F.; Wiberg, E. *Inorganic Chemistry, 1st English Ed.*, San Diego: Academic Press; Berlin; New York: De Gruyter, **2001**.

with representative unsaturated compounds (aldehydes, imines, alkynes, alkenes) and reached interesting trends (Table 3).¹⁶ Copper chlorides bind preferentially to heteroatoms, just like classical Lewis acids. On the other hand, silver and gold chlorides have a higher tendency to make π -coordination to carbon-carbon multiple bonds. One can also deduce from these data that the lower oxidation state of the metal (Cu^{I} versus Cu^{II} , Au^{I} versus Au^{III}) seems to strengthen the coordination to C-C multiple bonds.

Table 3. Computed heats of formation of various Lewis acid complexes with representative unsaturated compounds (kcal.mol^{-1}).

$$\text{R}-\text{C}\equiv\text{C}-\text{X} \xrightarrow{\text{MetCl}_n} \text{R}-\text{C}\equiv\text{C}-\text{X} \cdots \text{MetCl}_n \quad \text{or} \quad \text{R}-\text{C}\equiv\text{C}-\text{X} \cdots \text{MetCl}_n$$

	LA	BCl₃	CuCl	CuCl₂	AgCl	AuCl	AuCl₃
π -donors	Ph— \equiv	0,9	33,1	14,3	22,6	34,7	32,5
	Ph— $=$	0,4	33,6	18,1	24,4	37,5	36,8
σ -donors	Ph— $=\text{O}$	18,9	37,4	25,4	26,4	33,1	35,9
		$\sigma \gg \pi$	$\sigma > \pi$	$\sigma \approx \pi$	$\pi \geq \sigma$		

To sum up, coinage metals exhibit both alkyno(alkeno)philicity and oxo(aza)philicity, more or less pronounced depending on the metal. Due to their just mentioned versatile properties, they have found wide applications as homogeneous catalysts in a range of organic transformations.¹⁷

2.1.1. Rise, fall and revival of copper catalysis in organic synthesis

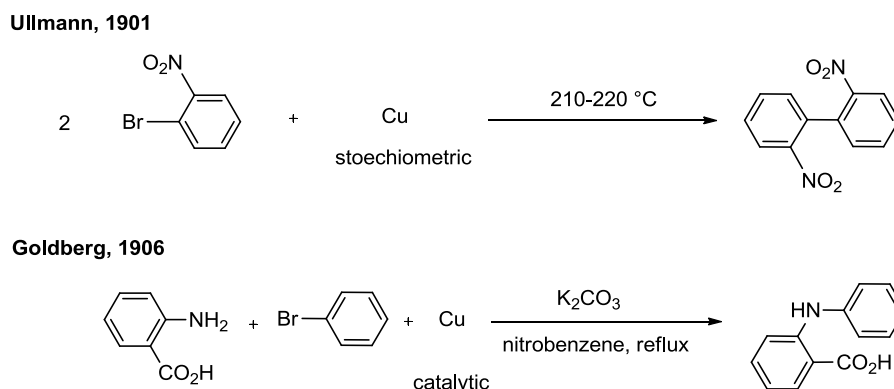
Contrary to the rather recent expansion of palladium (1970's) and gold (21th century) catalyzed chemistry, copper salts have been utilized for a very long time in organic synthesis. Their first remarkable application – in the first examples of cross-coupling reactions! - was certainly reported by Ullman¹⁸ and Goldberg¹⁹ at the turn of the 20th century (Scheme 4),

¹⁶ Yamamoto, Y. *J. Org. Chem.* **2007**, 72, 7817–7831.

¹⁷ For a recent review on the applications of coinage metals, see the special issue “Coinage Metals in Organic Synthesis” *Chem. Rev.* **2008**, 108, 8, 2793–3442.

¹⁸ Ullmann, F.; Bielecki, J. *Ber. Dtsch. Chem. Ges.* **1901**, 34, 2174–2185.

long before the name of palladium becomes inseparable from the term “cross-coupling”. The discovery of these reactions allowed the development of versatile methods for the synthesis of biaryls linkages and the building of C-N, C-O, C-S and some other bonds.²⁰



Scheme 4. The Ullmann and Goldberg reactions

Started in the early 1950's with the work of Gilman,²¹ organocopper chemistry constituted a practical tool for the alkylation of carbon electrophiles. The reactivity of organocuprates R_2CuLi , named Gilman's reagents in reference to his pioneering work, was subsequently investigated by House²² in the well-known 1,4-addition to α,β -unsaturated carbonyl compounds. Corey also demonstrated their efficiency in total synthesis for the stereoselective formation of trisubstituted alkenes.²³ Until the apparition of palladium catalyzed cross-couplings, conjugate additions and substitutions promoted by organocopper reagents provided methods of choice for the selective formation of C-C bonds,²⁴ especially in the total synthesis of complex molecules.²⁵

¹⁹ Goldberg, I. *Ber. Dtsch. Chem. Ges.* **1906**, *39*, 1691–1692.

²⁰ (a) Ley, S. V.; Thomas, A. W. *Angew. Chem. Int. Ed.* **2003**, *42*, 5400–5449. (b) Hassan, J.; Sévignon, M.; Gozzi, C.; Schulz, E.; Lemaire, M. *Chem. Rev.* **2002**, *102*, 1359–1470.

²¹ Gilman, H.; Jones, R. G.; Woods, L. A. *J. Org. Chem.* **1952**, *17*, 1630–1634.

²² House, H. O.; Respass, W. L.; Whitesides, G. M. *J. Org. Chem.* **1966**, *31*, 3128–3141.

²³ Corey, E. J.; Katzenellenbogen, J. A.; Gilman, N. W.; Roman, S. A.; Erickson, B. W. *J. Am. Chem. Soc.* **1968**, *90*, 5618–5620.

²⁴ (a) Alexakis, A.; Bäckvall, J. E.; Krause, N.; Pàmies, O.; Diéguez, M. *Chem. Rev.* **2008**, *108*, 2796–2823. (b) Breit, B.; Schmidt, Y. *Chem. Rev.* **2008**, *108*, 2928–2951. (c) Harutyunyan, S. R.; den Hartog, T.; Geurts, K.; Minnaard, A. J.; Feringa, B. L. *Chem. Rev.* **2008**, *108*, 2824–2852.

²⁵ Krause, N.; Gerold, A. *Angew. Chem. Int. Ed.* **1997**, *36*, 186–204.

Left aside and neglected during the explosion of palladium catalysis, it seems that copper catalysts currently experience kind of a revival. High cost as well as certain limitations of palladium(II) complexes (propension to decompose by β -hydride elimination for instance) encouraged synthetic chemists to explore over again the potential of copper in coupling reactions. Unlike palladium, copper is an inexpensive, earth-abundant metal with good flexibility in oxidation state, from 0 to +3. Palladium is more 'restricted' to its two most stable oxidation states, 0 and +2. However, the advantage of palladium chemistry lies in a good understanding of reaction mechanisms, as well as complete characterization of reaction intermediates.²⁶ Unfortunately up to now, mechanisms of copper catalyzed cross-couplings have remained controversial,²⁷ due in part to the lack of characterization of reaction intermediates, notably organo-Cu^{III} species. This problem recently turned into a challenge for the synthetic community, with tremendous efforts devoted to the preparation and applications of high-valent organocopper (and palladium) complexes.²⁸

In a more classical approach, recent years have seen the revival of copper catalyzed coupling reactions.²⁹ Since the pioneering work of Ullmann and Goldberg, considerable improvements have been made for providing mild and high yield procedures. These new methods are based on efficient catalytic systems combining copper salts and appropriate ligands, and tolerate a wide range of functional groups. Among them, the copper catalyzed cross-coupling of amides and alkynyl bromides provides a very convenient access to ynamides, a modern and attractive functional group gaining increasing interest.³⁰ For all these reasons, it is likely that copper catalyzed reactions will be particularly useful in the future and will take growing part in the total synthesis of complex molecules.

²⁶ Hartwig, J. F. *Inorg. Chem.* **2007**, *46*, 1936–1947.

²⁷ Sperotto, E.; van Klink, G. P. M.; van Koten, G.; de Vries, J. G. *Dalton Trans.* **2010**, *39*, 10338–10351.

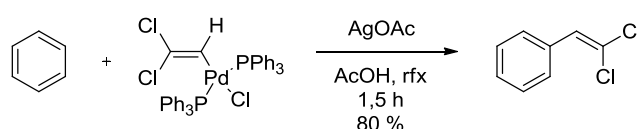
²⁸ Hickman, A. J.; Sanford, M. S. *Nature* **2012**, *484*, 177–185.

²⁹ (a) Kunz, K.; Scholz, U.; Ganzer, D. *Synlett* **2003**, *2003*, 2428–2439. (b) Beletskaya, I. P.; Cheprakov, A. V. *Coord. Chem. Rev.* **2004**, *248*, 2337–2364. (c) Evano, G.; Blanchard, N.; Toumi, M. *Chem. Rev.* **2008**, *108*, 3054–3131. (d) Liu, Y.; Wan, J.-P. *Chem. Asian J.* **2012**, *7*, 1488–1501.

³⁰ (a) Evano, G.; Coste, A.; Jouvin, K. *Angew. Chem. Int. Ed.* **2010**, *49*, 2840–2859. (b) De Korver, K. A.; Li, H.; Lohse, A. G.; Hayashi, R.; Lu, Z.; Zhang, Y.; Hsung, R. P. *Chem. Rev.* **2010**, *110*, 5064–5106.

2.1.2. Homogeneous catalysis by silver salts in organic synthesis

Similarly to its neighbor copper, silver has a long history in organic chemistry, but for a long time silver salts were mainly used stoichiometrically as halogen scavengers. This halogenophilicity served as a driving force in various transformations, notably nucleophilic substitutions,³¹ eliminations,³² and organometallics mediated reactions. As an example, the vinylation of benzene³³ (Scheme 5) has been successfully carried out in the presence of silver acetate, which abstracted chloride from the vinylpalladium(II) complex, enabling the coordination of benzene. The product was finally obtained after reductive elimination.



Scheme 5. Vinylation of benzene in the presence of silver acetate

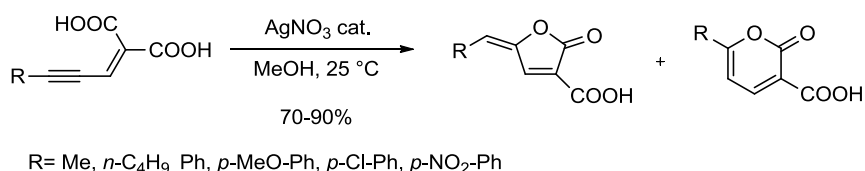
Inter and intramolecular nucleophilic additions to unsaturated molecules have been known for the end of the 19th century, however π -Lewis acidic silver salts were found interesting for this class of reactions only since the 1960's. Heterocyclizations starting from alkynes and allenes are particularly useful in organic synthesis, since the products obtained still contain a double bond, able to react further to give more complex molecules. Concerning the latter area, the preparation of 5-membered lactones has attracted more particularly the attention of organic chemists, due to the large number of biologically active compounds containing this motif. To achieve this goal, they tried to design strategies based on the cyclization of alkynoic acids. The first example probably dates from 1958, when Castañer and Pascual reported that γ -benzylidene- α -carboxybutenolide could be obtained from the internal cyclization of phenylpropargylidene malonic acid, either by thermal isomerization, or in the presence of catalytic silver nitrate at room temperature (Scheme 6).³⁴

³¹ (a) Honda, T.; Ushiwata, M.; Mizutani, H. *Tet. Lett.* **2006**, *47*, 6251–6254. (b) Schultheiss-Reimann, P.; Kunz, H. *Angew. Chem. Int. Ed.* **1983**, *22*, 62–63.

³² Jüres, S.; Werschkun, B.; Thiem, J. *Eur. J. Org. Chem.* **2006**, *2006*, 4451–4462.

³³ Moritani, I.; Fujiwara, Y.; Danno, S. *J. Organomet. Chem.* **1971**, *27*, 279–282.

³⁴ Castañer, J.; Pascual, J. *J. Chem. Soc.* **1958**, 3962–3964.



Scheme 6. Internal cyclization of alkynoic acids catalyzed by silver nitrate

It was shown that aromatic substituted alkynes gave only butenolides, whereas alkyl substituted alkynes afforded mixtures of butenolides and α -pyrones in various ratios.³⁵

Surprisingly, other types of heterocyclizations catalyzed by silver salts were not studied before the end of the 1970's. Goré³⁶ and Balme³⁷ started this work again with the cyclization of γ -allenic alcohols. Following these results, many other heterocyclizations based on the addition of O and N nucleophiles to C-C multiple bonds activated by silver(I) (especially alkynes, but also allenes and alkenes) were reported.³⁸ Depending on the reaction conditions (silver counterion, solvent, nature of the substrate), *endo* or *exo* cyclization products could be isolated (Scheme 7).³⁹

Besides heterocyclizations, the activation of a triple bond by silver(I) can also lead to another type of reactivity. Indeed, upon coordination to a terminal or silylated alkyne, the latter can evolve toward the corresponding silver acetylide.⁴⁰ Alkynyl silvers are mild nucleophiles with low basicity, able to trap any electrophilic species present in the reaction mixture. Silver acetylides can also be transmetalated and thus perform cross-coupling reactions (Scheme 7).^{38b,40-41}

³⁵ Belil, C.; Pascual, J.; Serratosa, F. *Tetrahedron* **1964**, *20*, 2701–2708.

³⁶ Audin, P.; Doutheau, A.; Ruest, L.; Gore', J. *Bull. Soc. Chim. Fr. II* **1981**, 313–318.

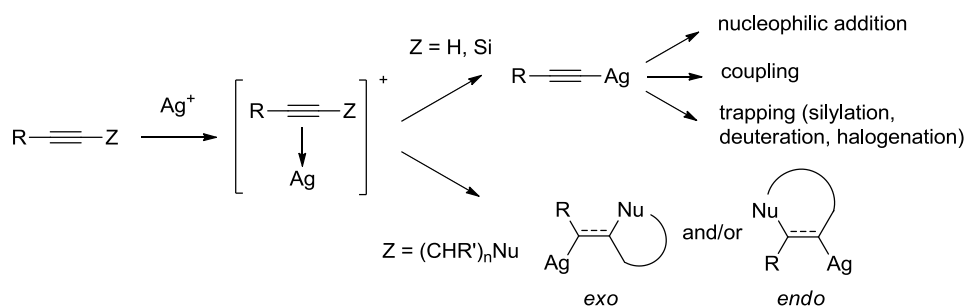
³⁷ Balme, G. Ph.D. Thesis, University Claude Bernard, Lyon, **1979**.

³⁸ (a) Álvarez-Corral, M.; Muñoz-Dorado, M.; Rodríguez-García, I. *Chem. Rev.* **2008**, *108*, 3174–3198. (b) Weibel, J.-M.; Blanc, A.; Pale, P. *Chem. Rev.* **2008**, *108*, 3149–3173.

³⁹ Anastasia, L.; Xu, C.; Negishi, E.-i. *Tetrahedron. Lett.* **2002**, *43*, 5673–5676.

⁴⁰ Halbes-Letinois, U.; Weibel, J.-M.; Pale, P. *Chem. Soc. Rev.* **2007**, *36*, 759–769.

⁴¹ Yamamoto, Y. *Chem. Rev.* **2008**, *108*, 3199–3222.



Scheme 7. Reactivity of alkyne derivatives in the presence of silver(I) salts

The σ -Lewis acid character of silver salts has already been exploited in various asymmetric reactions.⁴² One of the most popular example is probably the enantioselective allylation of aldehydes with allylic stannanes, promoted by the Yamamoto-Yanagisawa catalytic system (BINAP + silver(I)).⁴³ This area is growing, due to the efficiency of silver catalysts, which provide fast and high yielding reactions in mild conditions.

Silver salts are also known to be used as cocatalysts with other transition metals, namely Au,⁴⁴ Cu,⁴⁵ Pd,⁴⁶ and others. In most cases, the halogenophilicity of silver is exploited to generate a more active cationic species. The addition of silver cocatalyst proves often critical toward the efficiency of the reaction. This ‘silver effect’ has been recently highlighted in gold(I) catalysis by Wang and co-workers, in an elegant study.⁴⁷ They investigated 14 reactions catalyzed by gold and distinguished 3 cases: type I or catalysis by gold(I) only, type II or catalysis by Au/Ag mixtures only, and type III or silver assisted catalysis, in which different reactivities are obtained with and without Ag. The synthesis of cyclopentadienyl acetates *via* tandem Au^I-catalyzed 3,3- rearrangement/Nazarov reaction of propargylic esters (in anhydrous conditions) seems to be a case of truly Au/Ag bimetallic catalysis, since only traces of product are obtained with either Au^I or Ag^I catalyst alone (Scheme 8).

⁴² Naodovic, M.; Yamamoto, H. *Chem. Rev.* **2008**, *108*, 3132-3148.

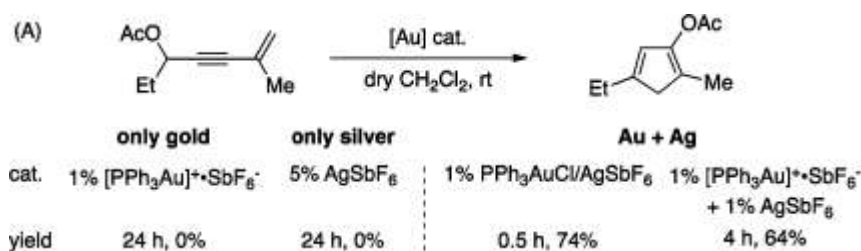
⁴³ Yanagisawa, A.; Nakashima, H.; Ishiba, A.; Yamamoto, H. *J. Am. Chem. Soc.* **1996**, *118*, 4723-4724.

⁴⁴ Han, X.; Widenhoefer, R. A. *Angew. Chem. Int. Ed.* **2006**, *45*, 1747-1749.

⁴⁵ Mancheño, O. G.; Arrayás, R. G.; Carretero, J. C. *J. Am. Chem. Soc.* **2003**, *126*, 456-457.

⁴⁶ Trost, B. M.; Godleski, S. A.; Genet, J. P. *J. Am. Chem. Soc.* **1978**, *100*, 3930-3931.

⁴⁷ Wang, D.; Cai, R.; Sharma, S.; Jirak, J.; Thummanapelli, S. K.; Akhmedov, N. G.; Zhang, H.; Liu, X.; Petersen, J. L.; Shi, X. *J. Am. Chem. Soc.* **2012**, *134*, 9012-9019.



Scheme 8. Tandem Au^I-catalyzed 3,3- rearrangement/Nazarov reaction of propargylic esters

Although neglected for a long time by organic chemists, silver catalysts are currently gaining increasing interest due to their amazing properties of halogenophilicity, as well as σ and π -Lewis acidity.⁴⁸ In the near future, the development of silver chemistry will certainly keep growing, along with the recent explosion of gold chemistry.

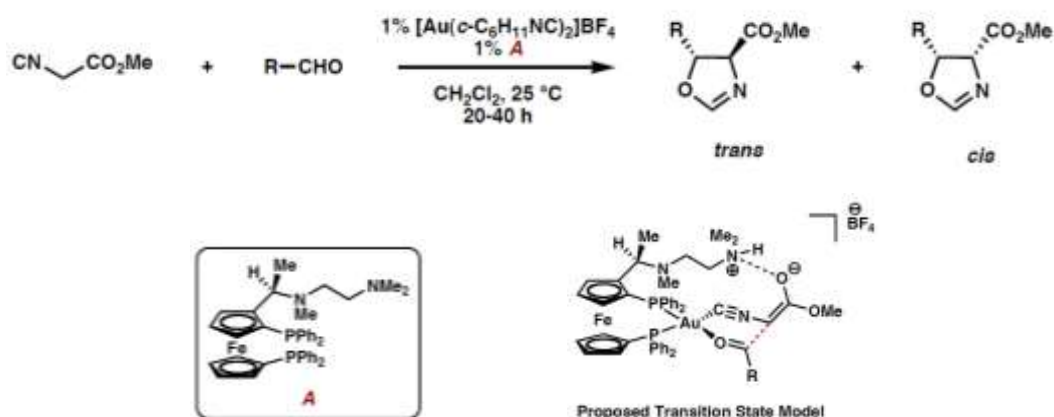
2.1.3. About the recent development of gold chemistry

Surprisingly, gold salts were for a long time regarded as “catalytically dead”, but this is rapidly changing,⁴⁹ thanks to a few key reactions reported at the end of the 20th century, which initiated extensive research in this area. An important breakthrough was made by Ito and Hayashi in 1986, who reported an asymmetric aldol reaction catalyzed by a chiral ferrocenylphosphine-gold(I) complex (Scheme 9).⁵⁰

⁴⁸ Harmata, M. *Silver in Organic Chemistry*; John Wiley & Sons, Inc., **2010**.

⁴⁹ For recent reviews on homogeneous gold catalysis, see the special issue “Coinage Metals in Organic Synthesis” *Chem. Rev.* **2008**, 108, 8, 2793–3442, and also: (a) Hashmi, A. S. K.; Rudolph, M. *Chem. Soc. Rev.* **2008**, 37, 1766–1775. (b) Marion, N.; Nolan, S. P. *Chem. Soc. Rev.* **2008**, 37, 1776–1782. (c) Shapiro, N. D.; Toste, F. D. *Synlett* **2010**, 2010, 675–691. (d) Wang, S.; Zhang, G.; Zhang, L. *Synlett* **2010**, 2010, 692–706.

⁵⁰ Ito, Y.; Sawamura, M.; Hayashi, T. *J. Am. Chem. Soc.* **1986**, 108, 6405–6406.



Scheme 9. Gold(I) catalyzed asymmetric aldol reaction reported by Ito and Hayashi

The reaction between isocyanoacetates and aldehydes afforded 5-alkyl-2-oxazoline-4-carboxylates almost quantitatively with high enantio (> 90% *ee*) and *trans* selectivity (> 97%). The terminal dialkylamino group on ligand A proved essential to reach high stereoselectivity. It must be noticed that silver and copper catalysts were also far less selective than gold(I).

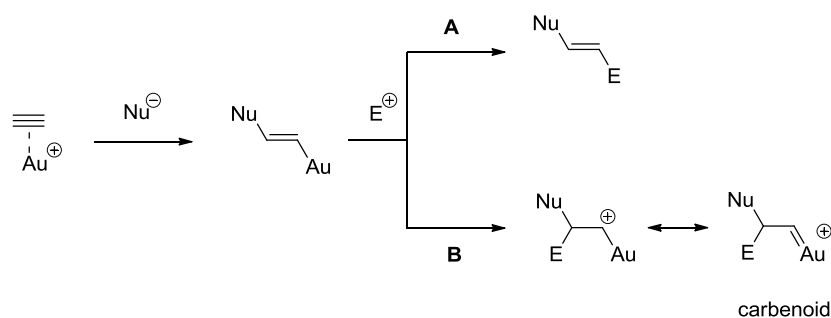
The reactivity of gold can be rationalized by theoretical study of its electronic structure and properties.^{14a} Important contraction of the *s* orbital (*vide infra*) leads to very strong interaction of gold(I) with electron-donating ligands. Computational calculations revealed that the $6s$ occupancy of Au-PPh_3^+ was 0,438 electron *versus* 0,156 electron for Ag-PPh_3^+ ,⁵¹ suggesting a strongly covalent Au-phosphine bond. Since Au^{I} is a large cation sharing its positive charge with the phosphine ligand, Au-PPh_3^+ is considered as a soft electrophile interacting preferentially with soft electrophiles, such as π -systems. The work of Teles *et al.*⁵² on the addition of alcohols to alkynes catalyzed by highly efficient phosphine-gold(I) complexes is an elegant illustration of this reactivity, and probably initiated the research on the addition of other hetero⁵³ as well as carbon⁵⁴ nucleophiles to alkynes (Scheme 10 path A).

⁵¹ Schwerdtfeger, P.; Hermann, H. L.; Schmidbaur, H. *Inorg. Chem.* **2003**, *42*, 1334–1342.

⁵² Teles, J. H.; Brode, S.; Chabanas, M. *Angew. Chem. Int. Ed.* **1998**, *37*, 1415–1418.

⁵³ (a) Mizushima, E.; Hayashi, T.; Tanaka, M. *Org. Lett.* **2003**, *5*, 3349–3352. (b) Akana, J. A.; Bhattacharyya, K. X.; Müller, P.; Sadighi, J. P. *J. Am. Chem. Soc.* **2007**, *129*, 7736–7737.

⁵⁴ (a) Hashmi, A. S. K.; Schwarz, L.; Choi, J.-H.; Frost, T. M. *Angew. Chem. Int. Ed.* **2000**, *39*, 2285–2288. (b) Hashmi, A. S. K.; Frost, T. M.; Bats, J. W. *J. Am. Chem. Soc.* **2000**, *122*, 11553–11554. (c) Corkey, B. K.; Toste, F. D. *J. Am. Chem. Soc.* **2005**, *127*, 17168–17169. (d) Markham, J. P.; Staben, S. T.; Toste, F. D. *J. Am. Chem. Soc.* **2005**, *127*, 9708–9709.



Scheme 10. Addition of nucleophiles to alkynes in the presence of gold salts

In addition to their Lewis acid character, it has been demonstrated that gold salts possess strong backbonding ability, especially toward vacant p orbitals.⁵⁵ The latter seem low enough in energy to correctly overlap with full $5d$ orbitals of gold(I). On the contrary, in Au-alkyne⁵⁶ and Au-carbonyl complexes,⁵⁷ the coordination is mostly σ -type and weak or almost no backbonding occurs. The cycloisomerization of enynes is the first example in which the carbenoid character of gold complexes has been widely debated.⁵⁸ This reaction proceeds through carbocationic intermediates, and gold carbenoid species have been proposed to stabilize the positive charge by delocalization (Scheme 10 path B). However, the preference for one or the other intermediate has not been unambiguously demonstrated so far. Isolation of gold complexes with carbenoid character is one of the challenges of tomorrow, along with the determination of the exact nature of the active catalyst, and a better understanding of reaction mechanisms.

2.2. Utility of recycling transition metal catalysts

While the utility and interest in coinage metals is currently growing in synthetic organic chemistry, the price of these “noble metals” increases simultaneously. In almost ten years, the price of copper, silver and gold has been multiplied by 6, approximately (Figure 3).⁵⁹

⁵⁵ (a) Barysz, M.; Pyykkö, P. *Chem. Phys. Lett.* **1998**, 285, 398–403. (b) Irikura, K. K.; Goddard, W. A. *J. Am. Chem. Soc.* **1994**, 116, 8733–8740.

⁵⁶ Nechaev, M. S.; Rayón, V. M.; Frenking, G. *J. Phys. Chem. A* **2004**, 108, 3134–3142.

⁵⁷ Xu, Q.; Imamura, Y.; Fujiwara, M.; Souma, Y. *J. Org. Chem.* **1997**, 62, 1594–1598.

⁵⁸ (a) Luzung, M. R.; Markham, J. P.; Toste, F. D. *J. Am. Chem. Soc.* **2004**, 126, 10858–10859. (b) Mamane, V.; Gress, T.; Krause, H.; Fürstner, A. *J. Am. Chem. Soc.* **2004**, 126, 8654–8655. (c) Nieto-Oberhuber, C.; Muñoz, M. P.; Buñuel, E.; Nevado, C.; Cárdenas, D. J.; Echavarren, A. M. *Angew. Chem. Int. Ed.* **2004**, 43, 2402–2406.

⁵⁹ <http://www.infomine.com/>

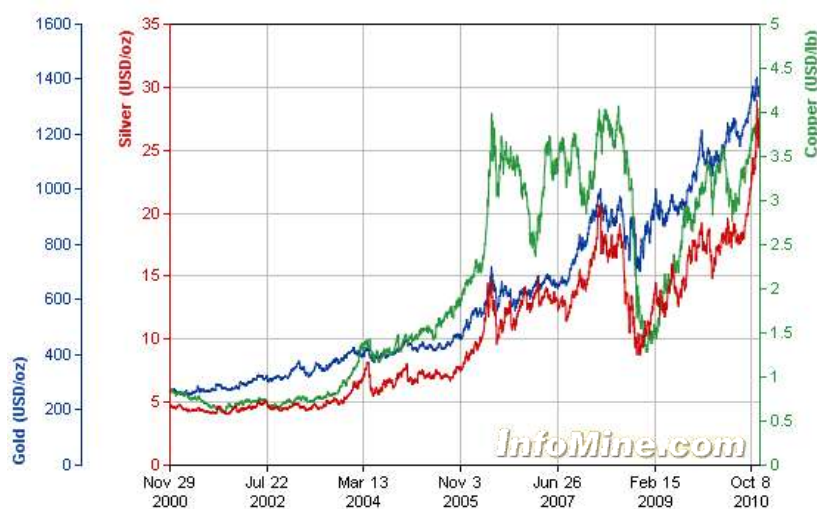


Figure 3. The price of copper, silver and gold over ten years, from December 2000 to December 2010.

This increase in price is directly linked with the diminution of the worldwide reserves (Table 4).⁶⁰ Based on the estimated worldwide annual production in 2011, we should come close to the end of resources starting from 2030.

Table 4. World mine reserves and production for copper, silver and gold in 2011 (assessments).

	Reserves [Mt]	Production [Mt]	Approximate end of resource (year)
Cu	690000	16100	2054
Ag	530000	23800	2033
Au	51000	2700	2030

Consequently, the mine industry has begun recycling the “old scrap” derived from the consumption of these noble metals. In 2011, the recycling of copper accounted for 7% of its global consumption. However, great efforts remain to accomplish in this area. Concerning the chemical industry and the utilization of noble metals in catalysis, an efficient way to avoid waste is to shift from homogeneous to heterogeneous processes. Hence, the design of green

⁶⁰ <http://minerals.usgs.gov/>

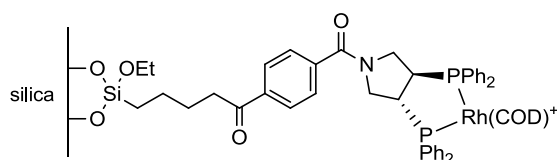
reactions catalyzed by transition metals supported on retrievable solids constitutes one of the most important challenges of modern synthetic chemistry.

3. *Heterogeneous catalysts for greener organic transformations*

3.1. Heterogeneization of homogeneous catalysts: the different solid supports

In addition to environmental concerns, heterogeneization of homogeneous catalysts has become necessary to overcome the limitations they induced, namely corrosiveness and difficulty of separation from fluid-phase products. Moreover, asymmetric reactions often rely on very complex and expensive chiral ligands, which account for an extra economic impact. To tackle these issues, several strategies have been and are still employed to fix the metal or metal complex of interest on a retrievable solid support.

In a first approach, the metal is anchored to the support *via* a bifunctional ligand.⁶¹ The most common support is silica, due to its chemical inertness, low surface acidity, high specific surface area and good thermal stability. For example, phosphine-Rh^I complexes have been anchored *via* OH or NH functional groups on silica, providing a grafted catalyst able to efficiently catalyze enantioselective hydrogenation reactions (Scheme 11).⁶²



Scheme 11. Example of phosphine-Rh^I complex anchored to silica


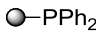
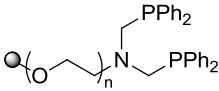
Despite satisfying catalytic activity, solids prepared by this method are not considered viable industrially, due to significant metal leaching, as well as possible dimers formation at high metal loading.

⁶¹ Choplin, A.; Quignard, F. *Coord. Chem. Rev.* **1998**, 178–180, Part 2, 1679–1702.

⁶² (a) Nagel, U.; Kinzel, E. *J. Chem. Soc., Chem. Commun.* **1986**, 1098–1099. (b) Pugin, B.; Müller, M. *Stud. Surf. Sci. Catal.*, **1993**, 78, 107–114.

A second strategy consists in grafting the metal to a polymer support, usually polystyrene derivatives.⁶³ This class of solids has been widely used for the production of compounds library,⁶⁴ and various metals and reactions were tested (Table 5).

Table 5. Some applications of polymer-supported phosphine ligands and their metal complexes.

Polymer	Supported phosphine	Metal	Preparation	Catalytic application
Polystyrene		Pd	Ligand exchange with PdCl ₂ (PPh ₃) ₂	Heck arylation ⁶⁵
Polystyrene +DVB		Li and Cu	Ligand association with LiCuR ₂	Reactions with unsaturated carbonyls ⁶⁶
Polystyrene/poly(ethylene glycol)		Ru	Ligand exchange from Ru ₆ C(CO) ₁₇	Hydrogenation of olefins ⁶⁷

Copper, palladium, ruthenium and other metallic complexes have been grafted in this way on polystyrene supports, through anchoring of the appropriate ligand. Unfortunately, the catalytic efficiency is often lower than the corresponding homogeneous catalysts, especially in asymmetric synthesis. Metal leaching and side reactions with the polymer itself are major drawbacks. Polymeric supports are not stable under strongly acidic or basic conditions, and the structure is sensitive to osmotic shock. Degradation can thus occur when the support is washed before recycling. In addition, polymer supports are still expensive to purchase and prepare, which makes cost-effective routes highly desirable.⁶⁸

The third possibility is the trapping of the metal in the void of the solid support, for instance the micropores of a zeolite, or the interlayer spaces of a clay.

The introduction of the metal or complex is usually performed by classical cationic exchange. Metal leaching can also occur in some cases, but high catalytic activity and selectivity are usually observed, due to strong interactions between the substrate and the active site,

⁶³ For a recent review, see the special issue “Recoverable Catalysts and Reagents”, *Chem. Rev.* **2002**, 102, 10.

⁶⁴ Kobayashi, S. *Chem. Soc. Rev.* **1999**, 28, 1–15.

⁶⁵ Andersson, C. M.; Karabelas, K.; Hallberg, A.; Andersson, C. *J. Org. Chem.* **1985**, 50, 3891–3895.

⁶⁶ Muralidharan, S.; Freiser, H. *Inorg. Chem.* **1988**, 27, 3251–3253.

⁶⁷ Judkins, C. M. G.; Knights, K. A.; Johnson, B. F. G.; Miguel, Y. R. d.; Raja, R.; Thomas, J. M. *Chem. Commun.* **2001**, 2624–2625.

⁶⁸ Carre, E. L.; Lewis, N.; Ribas, C.; Wells, A. *Org. Process Res. Dev.* **2000**, 4, 606–610.

especially in zeolites. Due to their three dimensional network and hence high surface area, zeolites are by far the most widespread heterogeneous catalysts in the chemical industry, especially in refining processes. This large application is due to their inherent nature and properties which make it very versatile solids, stable and easy to handle and recycle.

Finally, polyoxometalates (POMs) are the last family of solid supports which can host metallic species or metal complexes.

Depending on the solvent and on the nature of the POM, the latter can act as homogeneous or heterogeneous catalyst. The metal of interest can either be introduced as counterion, grafted through the insertion of an organic ligand, or be directly present in the primary structure. Thanks to the multiple possibilities of structures and chemical compositions offered by these solids, POMs have gained prominent interest as recyclable supports for applications in heterogeneous catalysis.

3.2. Zeolites

3.2.1. *Historic evolution and topologies*

Zeolites are microporous crystalline solids with a three-dimensional network that consists of aluminosilicates, tetrahedrally coordinated with each other through shared oxygen atoms. In such structures, Al-O-Al linkages are not favored due to electrostatic repulsions between the negative charges of each aluminate motif (Lowenstein's rule). These natural minerals, mined in many parts of the world, were initially formed by the deposition of volcanic ash in ancient alkaline lakes.

In 1756, the Swedish mineralogist Axel Frederick Cronstedt discovered that stilbite, one of this natural mineral, lost water when heated. He named these materials zeolites from the Greek *zeolithos* (*zeo*: to boil and *lithos*: stone) meaning literally 'boiling stone'.⁶⁹ One century later in 1862, Sainte-Claire Deville reported the first hydrothermal synthesis of a zeolite, levynite.⁷⁰ The concepts of porous structure and molecular sieving were proposed subsequently, based on the experimental observation that several gaseous and liquid

⁶⁹ Cronstedt, A. F. *Akad. Handl. Stockholm* **1756**, *18*, 120–130.

⁷⁰ Sainte-Claire Deville, H. C. R. *Acad. Sci.* **1862**, *54*, 324–327.

molecules were selectively adsorbed by zeolite minerals.⁷¹ At that time, zeolite syntheses suffered from the lack of experimental reproducibility and characterization methods.

These limitations ended with the work of Richard Barrer, who achieved in 1948 the definitive synthesis of a mordenite analog,⁷² and the preparation of a novel non-natural zeolite.⁷³ Up to now, 191 framework types have been identified, approved and listed in the Atlas of Zeolite Structure Types published by the International Zeolite Association Structure Commission (IZA-SC).⁷⁴ This commission assigns a three letters code characteristic of a framework topology and usually derived from the name of the zeolite or type material, e. g. LTA for Linde zeolites type A (Figure 4),⁷⁵ FAU for the faujasite topology, e.g. zeolites X and Y, MOR for the mordenite topology, MFI for the ZSM-5 and silicate topologies.

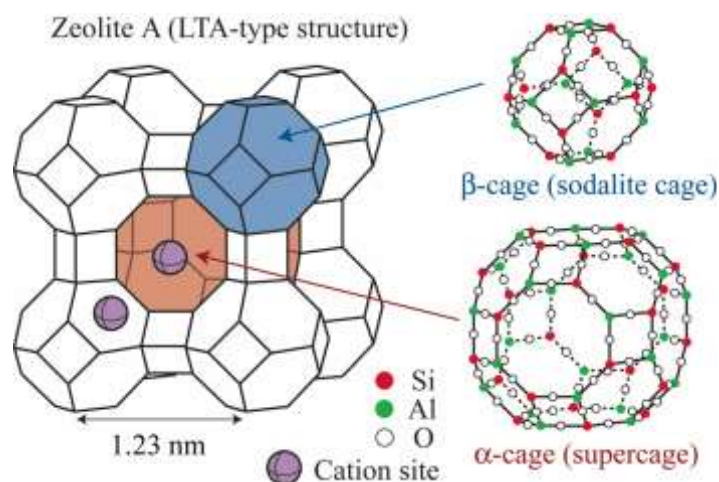


Figure 4. Framework structure of zeolite A (Linde Type A, LTA). Si and Al alternate at the tetrahedral intersections, except that Si substitutes at about 4% of the Al positions.

The three-dimensional network of zeolites gives them a unique and uniform microporous structure (microporosity starts below 20 Å) made of cavities, cages or channels. Pores contain mono or divalent cations – usually alkali or alkaline earth ions like Na^+ , K^+ , Ca^{2+} , Sr^{2+} , Ba^{2+} -

⁷¹ (a) Friedel, G. *Bull. Soc. Fr. Mineral. Cristallogr.* **1896**, 19, 363–390. (b) Friedel, G. *C. R. Acad. Sci.* **1896**, 122, 948–951. (c) Grandjean, F. *C. R. Acad. Sci.*, **1910**, 149, 866–868. (d) Weigel, O.; Steinhoff, E. *Z. Kristallogr.* **1925**, 61, 125–154.

⁷² Barrer, R. M. *J. Chem. Soc.* **1948**, 2158–2163.

⁷³ Barrer, R. M. *J. Chem. Soc.* **1948**, 127–132.

⁷⁴ (a) Baerlocher, C.; Meier, W. H.; Olson, D. H. *Atlas of zeolite framework types*; 6th Edition, Elsevier. **2007**. (b) <http://www.iza-structure.org/databases/>.

⁷⁵ Duan, T.; Nakano, T.; Nozue, Y. *e-J. Surf. Sci. Nanotech.* **2007**, 5, 6–11.

or protons which counterbalance the negative charge of the aluminosilicate framework. Cavities also host water which can freely move in and out, without altering the structure. The pore and cavity dimensions of the most common zeolites are given in Table 6.⁷⁶ These values give an approximate idea of the size of molecules that can fit in the pores of each zeolite. However, one must also consider the flexibility of the cavities due to Si-O-Si bending, and to the type of cations contained in the lattice. Both parameters have an influence on the pores and its dimensions. Consequently, molecules which seem too large at first sight may enter the cavities, especially at high temperatures. In this context, the ‘effective’ pore size has been defined as 110 % of the zeolite dimensions, and should better correspond to the real space offered by zeolite cavities.⁷⁷

Table 6. Important characteristics of the most common zeolites.

Zeolite (IZA)	Pore type	Dimensions (Å)	Si/Al	Molecules adsorbed
A (LTA)	cages	4,1 (pore) 11,4 (cavity)	1	water, methanol
X/Y (Faujasite, FAU)	cages	7,4 (pore) 11,8 (cavity)	5	naphthalene various steroids
ZSM-5 (MFI)	channels	5,3 x 5,6 5,1 x 5,5	30-300	cyclohexane biphenyl
Mordenite (MOR)	channels	6,5 x 7	15-200	neopentane
Beta (BEA)	channels	2,6 x 5,7 7,6 x 6,4 5,5 x 5,5	25	<i>cis</i> -4- <i>tert</i> -butyl cyclohexanol

Due to their unique and regular structure, zeolites have attracted the attention of industrial chemists who sought to commercialize them. In 1957, the discovery of large deposits of natural zeolites in the western United States and other countries marked the beginning of commercial zeolites sold as molecular sieves.

Subsequently between 1950 and 1970 were synthesized the most widespread and industrially important zeolites.

The Union Carbide company initiated the research on synthetic zeolites for applications in purification, separation and catalysis. Advances made in this field can be classified in three categories:

⁷⁶ Sen, S. E.; Smith, S. M.; Sullivan, K. A. *Tetrahedron* **1999**, 55, 12657–12698.

⁷⁷ Payra, P.; Dutta, P. K. In *Handbook of Zeolite Science and Technology*; Taylor & Francis, **2003**.

- **Low silica or aluminum rich zeolites A and X (Si/Al \approx 1).**

Prepared for the first time at the Union Carbide laboratories by Milton and co-workers, zeolites A⁷⁸ (Figure 4) and X⁷⁹ possess a Si/Al ratio close to 1, representing the highest possible aluminum content in a tetrahedral aluminosilicate framework. Consequently they exhibit the highest cations contents and exchange capacities. They are particularly selective for polar solvents and polarizable molecules, leading to various applications in drying, gas or liquid separations and purifications.

Well aware of the possibility for small molecules to enter the zeolite pores, Milton and co-workers tried to introduce noble metals and acid sites *via* ion exchange, in order to create hydrocarbon catalysts. Acid sites were efficiently introduced via NH₄⁺ cation exchange, however the Al-rich zeolites A and X lost crystallinity upon thermal activation.

Faced with these observations, Rabo *et al.* realized that the high aluminum content could create undesirable cation-cation repulsions and thus should be responsible for the instability of the framework.

In addition, Ca-exchange experiments showed that above 40% exchange, bivalent cations were forced to occupy coordinatively deficient surface positions, creating acid sites.⁸⁰ By comparison with amorphous solids, it was also proved that the strong acidity of zeolites was related to their crystallinity.

With the need of more stable materials, resistant to high temperatures and in acidic conditions, Rabo *et al.* prepared zeolites with higher Si/Al ratios.

- **'Intermediate silica' zeolites Y, L, mordenite, natural zeolites (Si/Al \approx 1.5 – 5).**

In 1954, Breck prepared the first Y zeolite⁸¹, with the same framework topology as zeolite X but a Si/Al ratio between 1.5 and 3. First left aside due to its lower adsorbent capacity compared to zeolite X, this novel zeolite soon became the center of interest. Unlike zeolite X, the first acidic Y zeolite prepared by NH₄ exchange and thermal removal of NH₃ conserved its full crystallinity, according to XRD. Moreover, it exhibited acidic properties directly proportional to the NH₄ exchange rate, in contrast with the precedents results obtained with

⁷⁸ (a) Breck, D. W.; Eversole, W. G.; Milton, R. M.; Reed, T. B.; Thomas, T. L. *J. Am. Chem. Soc.* **1956**, *78*, 5972–5977. (b) Milton, R. M. U.S. Patent 2,882,243, **1959**.

⁷⁹ (a) Milton, R. M. U.S. Patent 2,882,244, **1959**. (b) Broussard, L.; Shoemaker, D. P. *J. Am. Chem. Soc.* **1960**, *82*, 1041–1051.

⁸⁰ Rabo, J. A.; Schoonover, M. W. *Appl. Catal. A Gen.* **2001**, *222*, 261–275.

⁸¹ (a) Breck, D. W. U.S. Patent 3, 130,007, **1964**. (b) Breck, D. W. *J. Chem. Ed.* **1964**, *41*, 678–689.

the aluminum rich zeolites. Consequently, Y zeolites were introduced since 1959 as acidic heterogeneous catalysts in various important transformations and especially in petrochemistry for hydrocarbon conversion. Compared to the silica-alumina gel employed at that time, Y zeolites allowed the cracking of hydrocarbons to proceed at much lower temperature, with higher reaction rate and selectivity.

- 'High silica' zeolites beta, ZSM-5 (Si/Al \geq 10).

Between 1960 and 1970, the search for molecular sieves with higher silicon content continued at the Mobil Research & Development Laboratories. Beta⁸² and ZSM-5⁸³ are the most known example. In contrast to zeolites of lower silicon content, their surface is rather hydrophobic and organophilic. Despite low aluminum contents, this type of zeolite is acidic enough to catalyze hydrocarbon conversion.

In the late 1970's, zeolite-like materials – called zeotypes - began to emerge with the discovery of a wide range of AlPO structures,⁸⁴ alternating AlO_2^- and PO_2^+ units, and resulting in a completely neutral lattice. Incomplete substitution of Si by P led to silicoaluminophosphates (SAPOs),⁸⁵ with cation-exchange abilities. Recently, research has focused on the incorporation of neighbor elements of Si and Al - typically Ga and Ge - leading to the first chiral germanosilicate ITQ-37.⁸⁶

3.2.2. Synthesis

Before the first industrial zeolite synthesis accomplished by Barrer in 1948,⁷² first attempts focused on mimicking the geologic conditions involving high temperatures ($T > 200\text{ }^\circ\text{C}$) and pressures ($P > 100\text{ bar}$).⁸⁷ In the late 1940's, systematic syntheses performed on large-scale

⁸² Wadlinger, R. L.; Kerr, G. T.; Rosinski, E. J. US Patent 3,308,069, **1967**.

⁸³ Argauer, R. J.; Landolt, G. R. US Patent 3,702,886, **1972**.

⁸⁴ Wilson, S. T.; Lok, B. M.; Messina, C. A.; Cannan, T. R.; Flanigen, E. M. *J. Am. Chem. Soc.* **1982**, *104*, 1146–1147.

⁸⁵ Lok, B. M.; Messina, C. A.; Patton, R. L.; Gajek, R. T.; Cannan, T. R.; Flanigen, E. M. *J. Am. Chem. Soc.* **1984**, *106*, 6092–6093.

⁸⁶ Sun, J.; Bonneau, C.; Cantín, Á.; Corma, A.; Díaz-Cabañas, M. J.; Moliner, M.; Zhang, D.; Li, M.; Zou, X. *Nature* **2009**, *458*, 1154–1157.

⁸⁷ Davis, M. E.; Lobo, R. F. *Chem. Mater.* **1992**, *4*, 756–768.

were proposed by Milton and co-workers, who developed hydrothermal methods using aluminosilicate gels at lower temperatures (~ 100 °C) and autogenous pressures. Typically, the first syntheses of aluminum-rich zeolites A and X involved pretty much the same reagents as nowadays, that is:

- a source of silica (sodium silicate, TetraEthOxySilane TEOS, fumed silica, amorphous silica)
- a source of alumina (sodium aluminate, aluminum hydroxide, aluminum sulfate)
- water
- a mineralizer to solubilize silicate and aluminate species (alkali-metal hydroxide)
- a structure directing agent or template, around which the aluminosilicate lattice forms.

The mixture of the components gives a gel that crystallizes upon heating.

In 1961, thanks to the work of Barrer and Denny reporting the use of tetramethylammonium (TMA^+) as structure directing agents,⁸⁸ organic molecules such as alkylammonium cations allowed to synthesize ‘intermediate silica’ zeolites (*vide infra*). Indeed, the sodalite structure contains six T atoms (Si or Al) per cage, which means 3 extra framework cations when Si/Al = 1. However, because of its size, only one TMA^+ cation can enter the sodalite cage, and cannot diffuse in and out thereafter. Therefore, TMA^+ cations force sodalite cages to crystallize around them, leading to Si/Al = 5.

Until 1978, all zeolite syntheses involved the use of hydroxide ions as mineralizers in high pH (typically greater than 12) hydrothermal conversions. In 1978, Flanigen and Patton patented a procedure in which fluoride ions act as mineralizers in the synthesis of silicalite.⁸⁹ With the replacement of OH^- by F^- , crystallization can be carried out at neutral or acidic conditions. In addition, F^- form stable complexes with heteroatoms and allow for significant level of incorporation into the zeolite framework. This is particularly interesting for transition metals, which are usually not stable at high pH aqueous conditions (mononuclear iron species tend to condense to higher nuclearity, for instance). Another advantage of fluoride ions is the possibility to obtain large zeolite crystals (of high interest for adsorption/diffusion studies). By slowly dissolving the silicon source, fluoride ions change the kinetic of the crystallization.

⁸⁸ Barrer, R. M.; Denny, P. J. *J. Chem. Soc.* **1961**, 971–982.

⁸⁹ Flanigen, E. M.; Patton, R. L. U.S. Patent 4,073,865, **1978**.

With this method, Shimizu and Hamada obtained MFI zeolite (silicalite 1) crystallites up to 4 mm in size.⁹⁰

3.2.3. Acidobasic properties of zeolites

Both Lewis and Brönsted acidities occur in zeolites. Lewis acidity is provided by the counterbalancing metal cations. Brönsted acidity results either from protonation of an Al-O-Si oxygen center, or from the reaction of water with a proton or a metal center to give a hydronium ion. Since the synthesis of zeolites is usually carried out in basic conditions (*vide infra*), NH₄ exchange followed by thermal removal of ammonia are necessary to obtain this Brönsted acidity.

H-zeolites were firstly considered as superacids on the basis of the product distribution of isoalkanes cracking at 500 °C.⁹³ The results were in line with the Haag Dessau mechanism, involving the C-H and C-C bond protolysis as first activation step of the alkane. Hammett acidity and UV-spectrophotometric measurements were also carried out – even if not suitable - to prove the superacid character of certain solid acids. Nevertheless, the ability to activate hydrocarbons at lower temperatures or to replace superacids in several organic transformations remain the most representative arguments of the singular behavior of acidic zeolites compared to common acids, and this may be rationalized by confinement effects.⁹¹ According to this concept, each cavity of the zeolite framework can act as a nanoreactor, able to maximize the interaction between the reactant and a specific acidic site.

Several methods have been developed to determine the nature, number and strength of acid sites in zeolites.⁹² Nevertheless, none of them gives entire satisfaction and the lack of a solid acids scale comparable to the p*K*_a scale for aqueous solutions remains a major concern.⁹³ Usual methods of acidity characterization include solid-state IR and ¹H NMR spectroscopies, able to provide information concerning the nature and number of acid sites. Signals can be assigned either to terminal SiOH or SiOHAL groups, and to the sodalite cage or supercage in

⁹⁰ Shimizu, S.; Hamada, H. *Angew. Chem. Int. Ed.* **1999**, *38*, 2725–2727.

⁹¹ (a) Derouane, E. G. *J. Catal.* **1986**, *100*, 541–544. (b) Derouane, E. G. *J. Mol. Catal. A Chem.* **1998**, *134*, 29–45. (c) Sastre, G.; Corma, A. *J. Mol. Catal. A Chem.* **2009**, *305*, 3–7.

⁹² Farneth, W. E.; Gorte, R. J. *Chem. Rev.* **1995**, *95*, 615–635.

the case of the faujasite topology. Solid state IR is the best method to distinguish between Brönsted and Lewis acidities, *via* the adsorption of a base like pyridine. Its coordination to a Lewis or Brönsted site appears at distinct vibrational frequencies (~ 1450 and 1540 cm^{-1} , respectively).⁹⁴ Quantitative determination of site densities is possible on the basis of literature values for molar extinction coefficients in a few zeolite systems.

With the solid state IR of adsorbed pyridine, temperature program desorption (TPD) of amines is probably one of the most widely used method for assessing acidity in zeolites. It typically involves saturation of the zeolite surface with ammonia, followed by linear increase of the temperature under a flow of inert gas. The gradual desorption of ammonia can be monitored by absorption or mass spectroscopy analysis of the effluent gas. The concentration of acid sites is then inferred from the amount of ammonia desorbed at a particular temperature, while the peak desorption temperature is attributed to a certain acid strength (the higher the temperature, the higher the strength of acid site). However, careful interpretations are necessary, and require a good knowledge of the different adsorption/desorption which may occur (physically sorbed species must not be considered, for instance).

Among the other available methods, Sommer *et al.* recently reported a non-destructive protocol for the measurement of Brönsted acid sites in zeolites and various solid acids, via $\text{H}_2\text{O}/\text{D}_2\text{O}$ exchange steps.⁹⁵

Due to the higher electronegativity of silicon compared to aluminum, it is well recognized that the strongest acid sites are preferentially located at isolated AlO_4 tetrahedra, having no other AlO_4 tetrahedra as closest neighbors. This is one explanation for the usual higher catalytic activity of dealuminated Y zeolite – also called Ultra Stable Y or USY, compared to Y. The lower acid sites density is compensated by the higher acid strength of the remaining sites.⁹⁴ Dealumination is classically performed by steaming at high temperatures ($500\text{--}600\text{ }^\circ\text{C}$). The hydrolysis of Al-framework cations firstly creates AlOH species and cationic Al_xO_y clusters in the sodalite cages. Their presence nearby acidic OH groups enhances their acid strength. When Al species are removed from the framework (by acid extraction), the lattice recrystallizes, and Si ions replace the missing Al atoms, creating a $20\text{--}200\text{ \AA}$ size mesoporosity. The high catalytic activity exhibited thereafter by dealuminated zeolites was

⁹³ Olah, G. A.; Prakash, G. K. S.; Sommer, J. In *Superacids*; Wiley, New York, **1985**.

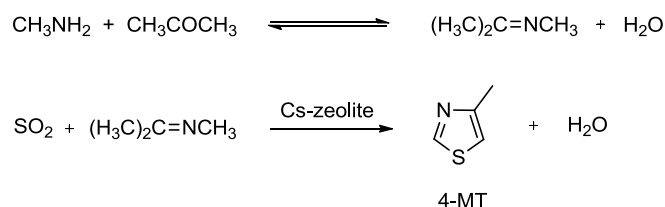
⁹⁴ Weitkamp, J. *Solid State Ionics* **2000**, *131*, 175–188.

⁹⁵ Louis, B.; Walspurger, S.; Sommer, J. *Catal. Lett.* **2004**, *93*, 81–84.

hence rationalized by a better diffusivity of the molecules into the crystalline mesopores, leading to high performance catalysts.⁸⁰

Basic zeolites can be created by introducing heavy metal cations like Rb^+ and Cs^+ . The increasing negative charge on the aluminum center is transferred to an adjacent oxygen atom, forming a basic site. Detailed studies have shown that the basicity of these zeolites may be between pyridine ($\text{p}K_{\text{b}}$ 8.8) and piperidine ($\text{p}K_{\text{b}}$ 11.12).⁹⁶

An example of basic zeolites catalysis has been developed by Merck for the synthesis of 4-methylthiazole (4-MT), a precursor of thiabendazole, a systemic fungicide.⁹⁷ The initial industrial route involving 5 steps and harmful chemicals was replaced by the direct synthesis of 4-MT from SO_2 and the imine by cesium zeolite catalysis (Scheme 12).⁹⁸



Scheme 12. Synthesis of 4-methylthiazole (4-MT) using a Cs-zeolite as catalyst

3.2.4. Main applications areas

3.2.4.1. The concept of shape selectivity

Zeolites have very high surface areas (500-700 m^2/g), mostly internal due to their microporous character. Compared to usual reaction media, cavities and pores constrain the molecules in such a way, that the product distribution deviates from the “ideal” distribution, leading to the so-called “shape-selective catalysis”.⁹⁹ This concept was introduced in 1960 by Weisz and Frillette, to account for the selective dehydration of 1-butanol over isobutanol by

⁹⁶ Corma, A.; Fornés, V.; Martín-Aranda, R. M.; García, H.; Primo, J. *Appl. Catal.* **1990**, *59*, 237–248.

⁹⁷ Gortsema, F. P.; Beshty, B.; Friedman, J. J.; Matsumoto, D.; Sharkey, J. J.; Wildman, G.; Blacklock, T. J.; Pan, S. H. Presented at the 14th Conference on Catalysis of Organic Reactions, Albuquerque, NM, **1992**.

⁹⁸ Davis, M. E. *Acc. Chem. Res.* **1993**, *26*, 111–115.

⁹⁹ Smit, B.; Maesen, T. L. M. *Nature* **2008**, *451*, 671-678.

Ca A zeolite.¹⁰⁰ Still with zeolite A (pore opening $\sim 5 \text{ \AA}$), the authors observed the selective conversion of normal paraffins over their branched isomers. These results are among the first examples of reactant selectivity, which describes the preferential adsorption of small molecules over bulky ones (Figure 5). This so-called “sieving property” of zeolites found subsequently important applications in adsorption/purification and separation. Drying of refrigerant and natural gas, and normal-isoparaffin separation (IsoSiv process) were the first major industrial applications of “sieving” zeolites, marketed by Union Carbide in the 1960’s.

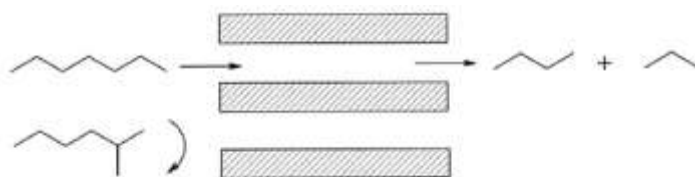


Figure 5. Illustration of the reactant shape selectivity. Branched alkanes too large to enter the zeolite pores do not react.

Besides reactant selectivity, two other types of shape selectivity occur in zeolites. Product selectivity is related to the inherent diffusivity of each product formed, and is strongly correlated to the crystal size and microporous structure of the catalyst. Typically, the desorption of bulky products is avoided by diffusion limitations, while less hindered molecules easily leave the microporous structure. The alkylation of toluene with methanol over ZSM-5 is a typical example of such selectivity.¹⁰¹ Although all xylene isomers can enter the pores of ZSM-5, diffusion measurements indicate that the diffusivity of *p*-xylene is more than 10^3 times faster than that of *m* and *o*-xylenes (Figure 6). Thus, with a ZSM-5 having appropriate crystal size ($3 \mu\text{m}$), the authors reached 97 % para selectivity for the alkylation of toluene.

¹⁰⁰ Weisz, P. B.; Frilette, V. J. *J. Phys. Chem.* **1960**, *64*, 382-382.

¹⁰¹ Chen, N. Y.; Kaeding, W. W.; Dwyer, F. G. *J. Am. Chem. Soc.* **1979**, *101*, 6783-6784.

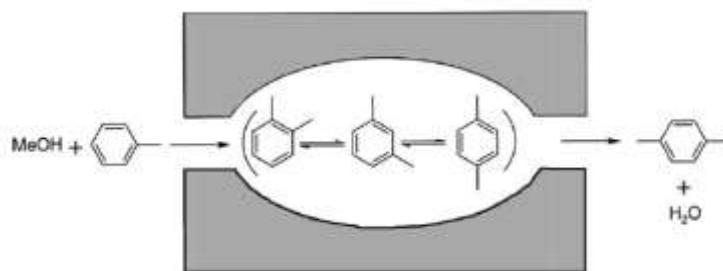


Figure 6. Illustration of the product selectivity: *p*-xylene diffuses faster than *m* and *o*-xylenes

Transition-state selectivity happens when the spatial environment around the transition state implies steric restrictions, avoiding certain configurations. This phenomenon was first proposed by Csicsery for the disproportionation of dialkylbenzenes.¹⁰² Contrary to the results with X and Y zeolites, in the reaction over mordenite symmetrical trialkylbenzenes were not present in the product distribution (Figure 7).

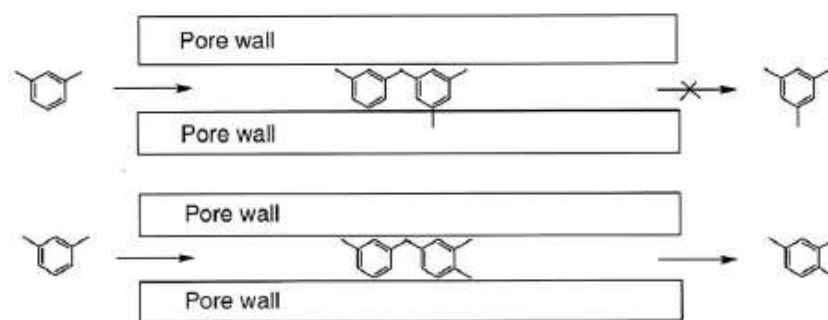


Figure 7. Illustration of the transition-state selectivity

However, symmetrical trialkylbenzenes could be successfully formed by isomerization of the other trialkylbenzene isomers. The authors suggested that the formation of the large 1,1-diphenylalkane intermediate by transalkylation required more space than available.

Due to this particular property of shape-selectivity, zeolites have found wide applications in catalysis and cover a large panel of transformations, from inorganic to the synthesis of fine chemicals. The first applications exploited the acid character of Y zeolites for the conversion of large and small hydrocarbons into high octane compounds. Since then, zeolites have been applied for the construction of more complex organic molecules including aromatics and heterocycles, among others.

¹⁰² (a) Csicsery, S. M. *J. Catal.* **1970**, *19*, 394-397. (b) Csicsery, S. M. *J. Catal.* **1971**, *23*, 124-130.

3.2.4.2. Acidic zeolites *versus* Superacids in heterogeneous catalysis

Our interest in zeolites and solid acids in general came with the development of environmental concerns along with the concept of green chemistry introduced in the 1990's (*vide infra*). In collaboration with the group of Pr. Jean Sommer, specialized in the activation of hydrocarbons by superacids, our group firstly started to work on organic transformations catalyzed by acidic zeolites. The replacement of superacids by solid acids was highly desirable from practical and environmental standpoints. Indeed, at the end of the 20th century, superelectrophilic activation and resulting dicationic intermediates were suggested in a range of organic reactions including hydroalkylation of aromatics such as the condensation of benzaldehyde with benzene,¹⁰³ the cyclization of phenyl vinyl ketones into 1-indanones,¹⁰⁴ or the selective C-C double bond hydrogenation of α,β -unsaturated ketones.¹⁰⁵ However, these methods suffered from several drawbacks, notably handling of harmful strong acids, often used in large excess, and not recyclable. Sommer *et al.* demonstrated that zeolites, and notably H-USY, were able to replace efficiently the usual superacids in all these transformations, although an excess of acidic sites was necessary to promote the reactions.¹⁰⁶ As an example, H-USY and H-ZSM5 were investigated in the reaction of α,β -unsaturated carboxylic acids with benzene derivatives. Triflic acid (Hammett acidity H_0 -14.1) was known to afford 1-indanones *via* a one pot cycliacarylation cascade.¹⁰⁷ While H-USY proved to be very efficient in the same reaction pathway, H-ZSM5 induced an unexpected decarboxylation process leading to 1,1-diarylethanes (Scheme 13).¹⁰⁸

¹⁰³ Koltunov, K. Y.; Walspurger, S.; Sommer, J. *Catal. Lett.* **2004**, *98*, 89–94.

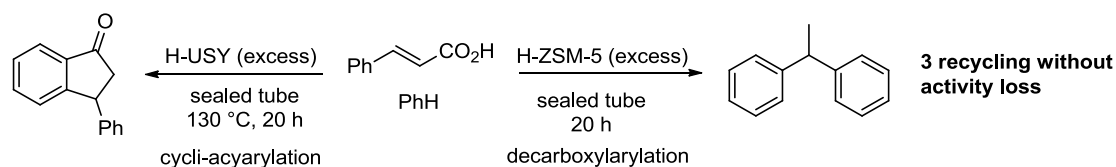
¹⁰⁴ Koltunov, K. Y.; Walspurger, S.; Sommer, J. *Tetrahedron Lett.* **2005**, *46*, 8391–8394.

¹⁰⁵ Koltunov, K. Y.; Walspurger, S.; Sommer, J. *J. Mol. Catal. A Chem.* **2006**, *245*, 231–234.

¹⁰⁶ Koltunov, K. Y.; Walspurger, S.; Sommer, J. *Chem. Commun.* **2004**, 1754–1755.

¹⁰⁷ (a) Prakash, G. K. S.; Yan, P.; Török, B.; Olah, G. A. *Catal. Lett.* **2003**, *87*, 109–112. (b) Rendy, R.; Zhang, Y.; McElrea, A.; Gomez, A.; Klumpp, D. A. *J. Org. Chem.* **2004**, *69*, 2340–2347.

¹⁰⁸ Chassaing, S.; Kumarraja, M.; Pale, P.; Sommer, J. *Org. Lett.* **2007**, *9*, 3889–3892.

Scheme 13. Reaction of α,β -unsaturated carboxylic acids with benzene derivatives

The zeolite nature proved also critical in the previously reported cyclization of arylvinylketones,¹⁰⁴ showing different reactivity depending on the substitution of the starting material.¹⁰⁹ Interesting solvents effects were also demonstrated on this reaction.¹¹⁰

3.2.4.3. Metal-doped zeolites as heterogeneous catalysts for organic transformations

*Copper zeolites*¹¹¹

Ion exchange properties of zeolites constitute an easy way to modulate their reactivity. It is possible to introduce almost any cation by simple soaking zeolites into an ion-containing aqueous solution. NH_4 exchange is for instance the most straightforward method to give hydrothermally prepared Na zeolites their Brønsted acid character. Cu^{II} -zeolites have hence been prepared since the 1960's by this method,¹¹² and used in environmental applications

¹⁰⁹ Sani Souna Sido, A.; Chassaing, S.; Pale, P.; Sommer, J. *Appl. Catal. A Gen.* **2008**, *336*, 101–108.

¹¹⁰ Sani Souna Sido, A.; Chassaing, S.; Kumarraja, M.; Pale, P.; Sommer, J. *Tetrahedron Lett.* **2007**, *48*, 5911–5914.

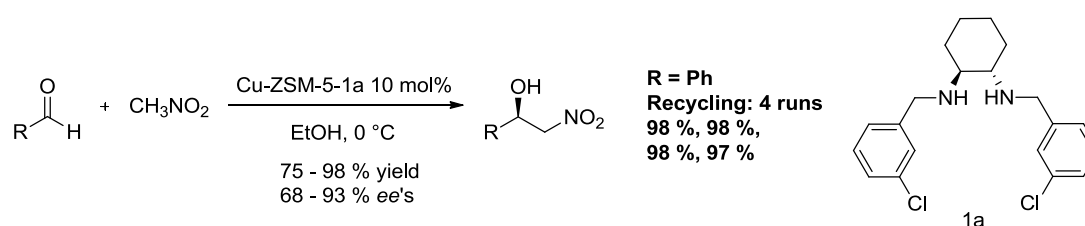
¹¹¹ For recent reviews on organic reactions catalyzed by copper(I)-zeolites, see: (a) Chassaing, S.; Alix, A.; Boningari, T.; Sido, K. S. S.; Keller, M.; Kuhn, P.; Louis, B.; Sommer, J.; Pale, P. *Synthesis* **2010**, 1557–1567. (b) Chassaing, S.; Alix, A.; Olmos, A.; Keller, M.; Sommer, J.; Pale, P. *Z. Naturforsch. B* **2010**, *65*, 783–790.

For recent characterizations of copper zeolites, see: (c) Lamberti, C.; Turnes Palomino, G.; Bordiga, S.; Berlier, G.; D'Acapito, F.; Zecchina, A. *Angew. Chem., Int. Ed.* **2000**, *39*, 2138–2141. (d) Turnes Palomino, G.; Bordiga, S.; Zecchina, A.; Marra, G. L.; Lamberti, C. *J. Phys. Chem. B* **2000**, *104*, 8641–8651. (e) Lamberti, C.; Bordiga, S.; Bonino, F.; Prestipino, C.; Berlier, G.; Capello, L.; D'Acapito, F.; Llabre's i Xamena, F. X.; Zecchina, A. *Phys. Chem. Chem. Phys.* **2003**, *5*, 4502–4509. (f) Prestipino, C.; Capello, L.; D'Acapito, F.; Lamberti, C. *Phys. Chem. Chem. Phys.* **2005**, *7*, 1743–1746. (g) Berthomieu, D.; Delahay, G. *Catal. Rev.* **2006**, *48*, 269–313.

¹¹² Nicula, A.; Stamires, D.; Turkevich, J. *J. Chem. Phys.* **1965**, *42*, 3684–3692.

such as NO_x reduction,^{111g} and other redox processes like methane oxidation,¹¹³ or phenol hydroxylation.¹¹⁴

A few applications of Cu^{II}-zeolites to organic synthesis have been reported, notably for the preparation of α -amino ketones from silyl enol ethers,¹¹⁵ the aziridination of styrene,¹¹⁶ or the amination of aryl halides.¹¹⁷ Recently, efforts have been directed toward asymmetric heterogeneous catalysis by the incorporation of chiral ligands in Cu^{II} zeolites. A diamine-Cu^{II} complex been incorporated in a mesoporous ZSM-5 for the asymmetric Henry reaction, affording β -nitroalcohols in high yields and *ee*'s (Scheme 14).¹¹⁸



Scheme 14. Asymmetric Henry reaction catalyzed by a Cu^{II} complex incorporated in a ZSM-5

Cu^{II}-bis(oxazoline) complexes have also been encapsulated into Y and USY for the cyclopropanation of styrene with ethyl diazoacetate.¹¹⁹

¹¹³ Vanelderen, P.; Hadt, R. G.; Smeets, P. J.; Solomon, E. I.; Schoonheydt, R. A.; Sels, B. F. *J. Catal.* **2011**, *284*, 157–164.

¹¹⁴ Wang, J.; Park, J.-N.; Jeong, H.-C.; Choi, K.-S.; Wei, X.-Y.; Hong, S.-I.; Lee, C. W. *Energ. Fuel.* **2004**, *18*, 470–476.

¹¹⁵ Phukan, P.; Sudalai, A. *Indian J. Chem. B* **2001**, *40B*, 515–517.

¹¹⁶ (a) Gullick, J.; Taylor, S.; Kerton, O.; McMorn, P.; King, F.; Hancock, F. E.; Bethell, D.; Page, P. C. B.; Hutchings, G. J. *Catal. Lett.* **2001**, *75*, 151–154. (b) Taylor, S.; Gullick, J.; McMorn, P.; Bethell, D.; Page, P. C. B.; Hancock, F. E.; King, F.; Hutchings, G. J. *J. Chem. Soc., Perkin Trans. 2* **2001**, 1714–1723. (c) Gullick, J.; Taylor, S.; McMorn, P.; Bethell, D.; Bulman-Page, P. C.; Hancock, F. E.; King, F.; Hutchings, G. J. *J. Mol. Catal. A Chem.* **2002**, *182-183*, 571–575. (d) Taylor, S.; Gullick, J.; Galea, N.; McMorn, P.; Bethell, D.; Bulman Page, P. C.; Hancock, F. E.; King, F.; Willock, D. J.; Hutchings, G. J. *Top. Catal.* **2003**, *25*, 81–88. (e) Gullick, J.; Ryan, D.; McMorn, P.; Bethell, D.; King, F.; Hancock, F.; Hutchings, G. *New J. Chem* **2004**, *28*, 1470–1478.

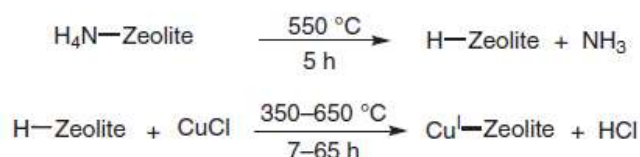
¹¹⁷ Patil, N. M.; Gupte, S. P.; Chaudhari, R. V. *Appl. Catal. A Gen.* **2010**, *372*, 73–81.

¹¹⁸ Khan, N.-u. H.; Ansari, M. B.; Prasetyanto, E. A.; Jin, H.; Park, S.-E. *Tetrahedron Asymmetry* **2011**, *22*, 117–123.

¹¹⁹ Silva, A. R.; Albuquerque, H.; Fontes, A.; Borges, S.; Martins, A.; Carvalho, A. P.; Pires, J. *Ind. Eng. Chem. Res.* **2011**, *50*, 11495–11501.

On the other hand, because of the poor solubility of Cu^{I} salts in aqueous solution, Cu^{I} -zeolites were first obtained indirectly by ionic exchange with a copper(II) salt followed by reduction with CO or H_2 at high temperatures.¹²⁰ Other methods based on the reaction of H-zeolites and gaseous copper(I) chloride were reported thereafter.¹²¹

Based on these results, we developed at the laboratory a two-step synthesis of Cu^{I} -zeolites from commercial NH_4 forms (Equation 4).^{111a}



Equation 4. Preparation of Cu^{I} -zeolites by solid exchange

Calcination at 550 °C for 5 hours led to the elimination of gaseous ammonia and provided the Brönsted acidic zeolite. The latter was then ground with solid CuCl and heated under nitrogen flow for 3 days at 350 °C. X-Ray powder Diffraction (XRD) and elemental analysis coupled with Scanning Electron Microscopy (SEM) confirmed the retention of the zeolite framework and the incorporation of copper. Various contact times and temperatures were screened in order to define the best conditions. Those parameters proved critical toward the crystallinity of the framework, as well as the Cu loading. 48 hours at 350 °C resulted in 86% crystallinity and 80% Cu loading (20% remaining protons), while 15 hours at 650 °C reduced crystallinity to 65% but provided complete Cu exchange (no Brönsted acid sites left).¹²²

Recently a Cu^{I} -Y zeolite has been prepared by heating a mixture of CuCl_2 with H-Y zeolite at high temperature.¹²³ Upon heating, CuCl_2 decomposed into Cl_2 , which rapidly escaped, and CuCl, which reacted with the H-zeolite to afford the final Cu^{I} -Y. This catalyst and Cu^{I} -

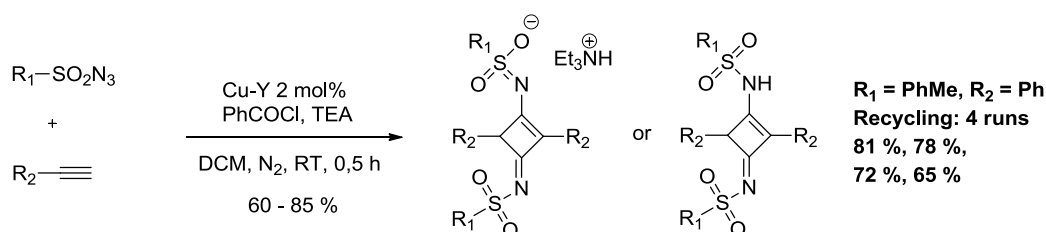
¹²⁰ Kazansky, V. B.; Pidko, E. A. *Catal. Today* **2005**, *110*, 281–293. (c) Taylor, S.; Gullick, J.; Galea, N.; McMorn, P.; Bethell, D.; Bulman Page, P. C.; Hancock, F. E.; King, F.; Willock, D. J.; Hutchings, G. J. *Top. Catal.* **2003**, *25*, 81–88.

¹²¹ (a) Spoto, G.; Bordiga, S.; Scarano, D.; Zecchina, A. *Catal. Lett.* **1992**, *13*, 39–44. (b) Drake, I. J.; Zhang, Y.; Briggs, D.; Lim, B.; Chau, T.; Bell, A. T. *J. Phys. Chem. B* **2006**, *110*, 11654–11664.

¹²² Kuhn, P.; Pale, P.; Sommer, J.; Louis, B. *J. Phys. Chem. C* **2009**, *113*, 2903–2910.

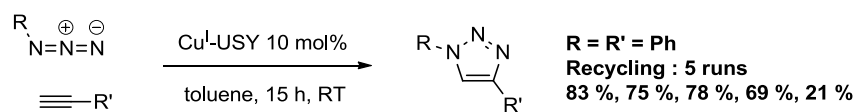
¹²³ Li, Z.; Wang, R.-Y.; Zheng, H.-Y.; Xie, K.-C. *Fuel* **2010**, *89*, 1339–1343.

zeolites prepared by other methods proved efficient toward the oxidative carbonylation of methanol into dimethyl carbonate.¹²⁴ Cu^I-zeolites have also been used for the desulfurization of commercial liquid fuels¹²⁵, and recently, in an original [3+2]/[2+2] cycloaddition cascade of sulfonyl azides and terminal alkynes, affording bis-*N*-sulfonylcyclobutenes (Scheme 15).¹²⁶



Scheme 15. [3+2]/[2+2] cycloaddition cascade of sulfonyl azides and terminal alkynes

This reaction is the logical continuation of the work initiated by Pale & Sommer. Indeed, they reported in 2007 the first application of Cu^I-zeolites to an organic transformation, the well-known Huisgen [3+2]-cycloaddition (Scheme 16).¹²⁷



Scheme 16. Cu^I-USY catalyzed Huisgen [3+2]-cycloaddition

Cu^I-USY proved to be the most efficient catalyst, affording regioselectively 1,4-disubstituted 1,2,3-triazoles. Subsequently, the method was extended to azides and alkynes derived from carbohydrates and aminoacids, and proceeded very well despite the prominent size of these molecules.¹²⁸ Variants of the cycloaddition, carried out in one pot from multicomponents

¹²⁴ (a) Drake, I. J.; Zhang, Y.; Briggs, D.; Lim, B.; Chau, T.; Bell, A. T. *J. Phys. Chem. B* **2006**, *110*, 11654–11664. (b) Zhang, Y.; Briggs, D. N.; De Smit, E.; Bell, A. T. *J. Catal.* **2007**, *251*, 443–452. (c) Rebmann, G.; Keller, V.; Ledoux, M. J.; Keller, N. *Green Chem.* **2008**, *10*, 207–213.

¹²⁵ Hernandez-Maldonado, A. J.; Yang, R. T. *Ind. Eng. Chem. Res.* **2003**, *42*, 3103–3110.

¹²⁶ Namitharan, K.; Pitchumani, K. *Org. Biomol. Chem.* **2012**, *10*, 2937–2941.

¹²⁷ (a) Chassaing, S.; Kumarraja, M.; Sani Souna Sido, A.; Pale, P.; Sommer, J. *Org. Lett.* **2007**, *9*, 883–886. (b) Chassaing, S.; Sido, A. S. S.; Alix, A.; Kumarraja, M.; Pale, P.; Sommer, J. *Chem. Eur. J.* **2008**, *14*, 6713–6721.

¹²⁸ Alix, A.; Chassaing, S.; Pale, P.; Sommer, J. *Tetrahedron* **2008**, *64*, 8922–8929.

were also proposed thereafter.¹²⁹ In the same context, Cu^I-USY was also applied to the [3+2] cycloaddition of pyrazol-3-one ylides with alkynes,¹³⁰ in the 3-component synthesis of propargylamines,¹³¹ and in the homocoupling of alkynes.¹³² All these reactions belong to the ‘zeo-click concept’, formulated by analogy with the philosophy developed by Sharpless in 2001. Thanks to metal-doped zeolites, we aim to design straightforward, simple, safe and green syntheses of molecules. Cycloadditions, couplings, cascades and multicomponents reactions are step and atom economical transformations that perfectly comply with this objective.

Scandium zeolites

Recently, Pale *et al.* also investigated scandium zeolites as Lewis acid heterogeneous catalysts in several organic reactions. In contrast with copper zeolites, these solids had not been well studied so far. As early as 1980, Selim *et al.* reported the synthesis of Sc^{III}-Y by successive ion-exchanges with ScCl₃.¹³³ The catalytic activity of the so-prepared solid was further assessed in the cracking of *n*-octane and cumene, and these are pretty much the only applications for which this type of zeolite was evaluated. One attempt to prepare Sc-ZSM-5 by hydrothermal method with fluoride ions was also reported.¹³⁴

In the same way as for Cu^I, Pale *et al.* successfully introduced Sc^{III} in the zeolite framework by solid exchange between scandium triflate and H-USY. Complete characterization of this solid was carried out and, in order to establish structure-activity relationships, the potential of Sc^{III}-USY was assessed in the Aza Diels-Alder [4+2] cycloaddition of alkenes and *N*-arylimines (Scheme 17).¹³⁵

¹²⁹ (a) Beneteau, V.; Olmos, A.; Boningari, T.; Sommer, J.; Pale, P. *Tetrahedron Lett.* **2010**, *51*, 3673–3677. (b) Boningari, T.; Olmos, A.; Reddy, B. M.; Sommer, J.; Pale, P. *Eur. J. Org. Chem.* **2010**, 6338–6347.

¹³⁰ Keller, M.; Sido, A. S. S.; Pale, P.; Sommer, J. *Chem. Eur. J.* **2009**, *15*, 2810–2817.

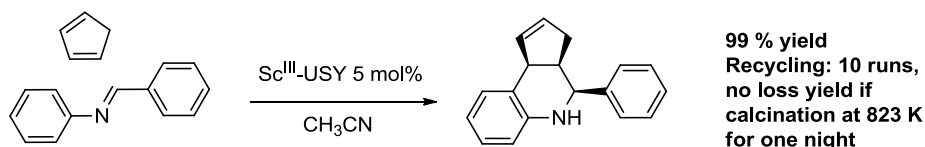
¹³¹ Patil, M. K.; Keller, M.; Reddy, B. M.; Pale, P.; Sommer, J. *Eur. J. Org. Chem.* **2008**, 4440–4445.

¹³² (a) Kuhn, P.; Alix, A.; Kumarraja, M.; Louis, B.; Pale, P.; Sommer, J. *Eur. J. Org. Chem.* **2009**, 423–429. (b) Kuhn, P.; Pale, P.; Sommer, J.; Louis, B. *J. Phys. Chem. C* **2009**, *113*, 2903–2910.

¹³³ Selim, M. M.; El-Shobaky, G. A.; Badran, A. *Surf. Technol.* **1980**, *11*, 47–54.

¹³⁴ Brigden, C. T.; Thompsett, D.; Williams, C. D. *Dalton Trans.* **2004**, 2829–2830.

¹³⁵ (a) Olmos, A.; Rigolet, S.; Louis, B.; Pale, P. *J. Phys. Chem. C* **2012**, *116*, 13661–13670. (b) Olmos, A.; Sommer, J.; Pale, P. *Chem. Eur. J.* **2011**, *17*, 1907–1914.



Scheme 17. Sc^{III}-USY catalyzed Aza Diels-Alder [4+2] cycloaddition

The results demonstrated that at high scandium loading, zeolites were less efficient catalysts. In contrast, 2 or 5 mol% Sc-USY afforded tetrahydroquinolines in high yields. These observations suggested that more dissipated Lewis acid sites and maybe higher Brønsted sites density favor the reaction.

In addition to these results, Sc^{III}-USY was also reported as Lewis acid heterogeneous catalyst in the imino-Diels-Alder¹³⁶ and Mukaiyama¹³⁷ reactions.

Palladium and others

Besides scandium and copper, palladium exchanged zeolites have been widely studied since the 1980's, owing to the importance of coupling reactions in organic synthesis. Bifunctional palladium-copper zeolites successfully worked as heterogeneous catalysts in the Wacker process.¹³⁸ Palladium¹³⁹ and bifunctional palladium-basic zeolites¹⁴⁰ were reported for the Heck reaction. Suzuki¹⁴¹ coupling and copper free palladium zeolites for the Sonogashira¹⁴² coupling were also investigated.

Isolated examples of organic reactions promoted by other transition-metal doped zeolites such as zinc,¹⁴³ or gold¹⁴⁴ can be found in the literature.

¹³⁶ Olmos, A.; Louis, B.; Pale, P. *Chem. Eur. J.* **2012**, *18*, 4894–4901.

¹³⁷ Olmos, A.; Alix, A.; Sommer, J.; Pale, P. *Chem. Eur. J.* **2009**, *15*, 11229–11234.

¹³⁸ (a) Elleuch, B.; Naccache, C.; Ben Taarit, Y. *Stud. Surf. Sci. Catal.* **1984**, *19*, 139–145. (b) Espeel, P. H.; De Peuter, G.; Tielen, M. C.; Jacobs, P. A. *J. Phys. Chem.* **1994**, *98*, 11588–11596.

¹³⁹ (a) Djakovitch, L.; Heise, H.; Kohler, K. *J. Organomet. Chem.* **1999**, *584*, 16–26. (b) Djakovitch, L.; Koehler, K. *J. Mol. Catal. A Chem.* **1999**, *142*, 275–284. (c) Dams, M.; Drijkoningen, L.; Pauwels, B.; Van Tendeloo, G.; De Vos, D. E.; Jacobs, P. A. *J. Catal.* **2002**, *209*, 225–236.

¹⁴⁰ Corma, A.; Garcia, H.; Leyva, A.; Primo, A. *Appl. Catal. A Gen.* **2003**, *247*, 41–49.

¹⁴¹ (a) Corma, A.; Garcia, H.; Leyva, A. *Appl. Catal. A Gen.* **2002**, *236*, 179–185. (b) Artok, L.; Bulut, H. *Tetrahedron Lett.* **2004**, *45*, 3881–3884.

¹⁴² (a) Djakovitch, L.; Rollet, P. *Adv. Synth. Catal.* **2004**, *346*, 1782–1792. (b) Djakovitch, L.; Rollet, P. *Tetrahedron Lett.* **2004**, *45*, 1367–1370.

¹⁴³ Maggi, R.; Bosica, G.; Gherardi, S.; Oro, C.; Sartori, G. *Green Chem.* **2005**, *7*, 182–184.

Silver zeolites

Ag cluster containing zeolites have been widely studied because of the catalytic activity of this type of material in processes such as the oxidation of ethylene, or the photochemical cleavage of H₂O in H₂ and O₂.¹⁴⁵ These Ag cluster zeolites are formed after reduction of Ag⁺ cations either upon heating/dehydration, by reaction with reductive agents (H₂), or by sorption of metal atom.¹⁴⁶ Upon dehydration, auto-reduction to small clusters was detected already at 300 °C. Ag⁺ cations may be reduced by water oxygens or oxygens of the zeolite framework, and the concentration of the clusters seems correlated to the dehydration time and temperature.¹⁴⁷ The so-formed Ag⁰ particles migrate from the surface and interact with Ag⁺ cations to create cationic silver clusters, trapped in sodalite cages.¹⁴⁸ Kevan *et al.* reported that in partially hydrated Y, Ag⁰ was located at the center of the β-cage, and coordinated to four water molecules (Figure 8).¹⁴⁹

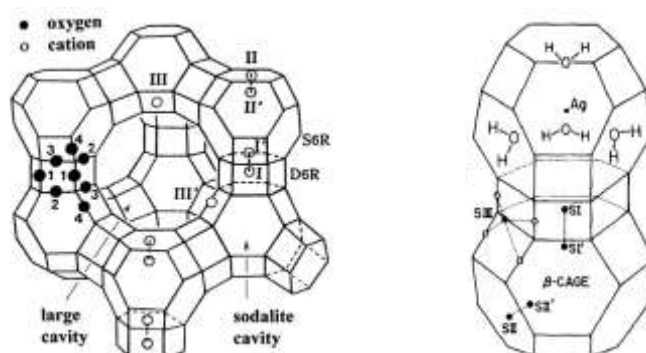


Figure 8. Location of the cations in the structure of zeolite X (on the left). Zoom on two sodalite cavities or β-cages containing Ag⁰ (on the right).

Interestingly, the interaction of large Ag clusters with ethylene tends to be more Van der Waals than molecular, compared to small Ag clusters.

¹⁴⁴ Neatu, F.; Li, Z.; Richards, R.; Toullec, P. Y.; Genet, J.-P.; Dumbuya, K.; Gottfried, J. M.; Steinrueck, H.-P.; Parvulescu, V.; Michelet, V. *Chem. Eur. J.* **2008**, *14*, 9412–9418.

¹⁴⁵ Sun, T.; Seff, K. *Chem. Rev.* **1994**, *94*, 857–870.

¹⁴⁶ Jeong, M. S.; Kim, Y.; Seff, K. *J. Phys. Chem.* **1993**, *97*, 10139–10143.

¹⁴⁷ Lee, S. H.; Kim, Y.; Seff, K. *Micropor. Mesopor. Mat.* **2000**, *41*, 49–59.

¹⁴⁸ Sambasivan, S.; Fischer, D. A.; DeKoven, B. M.; Kuperman, A. *Adv. Mater.* **2000**, *12*, 1809–1813.

¹⁴⁹ Narayana, N.; Kevan, L. *J. Chem. Phys.* **1982**, *76*, 3999–4005.

Recently, the crystal structure of an ethylene sorbed complex in fully oxidized and hydrated Ag-X was determined.¹⁵⁰ The authors investigated the effect of sorption on the cations positions, and observed that a part of the cations lying at site II slightly moved into the supercage, so as to better coordinate to ethylene molecules (Figure 8).

Ag-zeolites exhibit remarkable luminescent properties,¹⁵¹ and find applications in several photochemical reactions such as the photodecomposition of organic compounds,¹⁵² notably pesticides,¹⁵³ or the photocatalytic decomposition of NO_x.¹⁵⁴ Silver containing zeolites are used for their antibacterial properties against various infectious agents,¹⁵⁵ and in food packaging.¹⁵⁶

Their molecular sieve properties are also exploited for the adsorption of hydrogen sulfide¹⁵⁷ or the separation of ethylene/ethane mixtures.¹⁵⁸

In organic synthesis however, applications of silver zeolites remained very limited until now. AgNaY were reported for several glycosylations,¹⁵⁹ although not involved in a catalytic

¹⁵⁰ (a) Choi, E. Y.; Kim, S. Y.; Kim, Y.; Seff, K. *Micropor. Mesopor. Mat.* **2003**, *62*, 201–210. (b) Lee, Y. M.; Choi, S. J.; Kim, Y.; Seff, K. *J. Phys. Chem. B* **2005**, *109*, 20137–20144.

¹⁵¹ De Cremer, G.; Antoku, Y.; Roeffaers, M. B. J.; Sliwa, M.; Van Noyen, J.; Smout, S.; Hofkens, J.; De Vos, D. E.; Sels, B. F.; Vosch, T. *Angew. Chem., Int. Ed.* **2008**, *47*, 2813–2816.

¹⁵² Tayade, R. J.; Suroolia, P. K.; Lazar, M. A.; Jasra, R. V. *Ind. Eng. Chem. Res.* **2008**, *47*, 7545–7551.

¹⁵³ Kanan, M. C.; Kanan, S. M.; Austin, R. N.; Patterson, H. H. *Environ. Sci. Technol.* **2003**, *37*, 2280–2285.

¹⁵⁴ Ju, W.-S.; Matsuoaka, M.; Iino, K.; Yamashita, H.; Anpo, M. *J. Phys. Chem. B* **2004**, *108*, 2128–2133.

¹⁵⁵ (a) Krishnani, K. K.; Zhang, Y.; Xiong, L.; Yan, Y.; Boopathy, R.; Mulchandani, A. *Bioresour. Technol.* **2012**, *117*, 86–91. (b) Lalueza, P.; Carmona, D.; Monzon, M.; Arruebo, M.; Santamaria, J. *Micropor. Mesopor. Mat.* **2012**, *156*, 171–175. (c) Moeretoe, T.; Hoeiby-Pettersen, G. S.; Halvorsen, C. K.; Langsrud, S. *Food Control* **2012**, *28*, 118–121.

¹⁵⁶ (a) Quintavalla, S.; Vicini, L. *Meat Science* **2002**, *62*, 373–380. (b) Lee, J.; Lee, Y.-H.; Jones, K.; Sharek, E.; Pascall, M. A. *Int. J. Food Sci. Technol.* **2011**, *46*, 2382–2386.

¹⁵⁷ Sung, C.-Y.; Al Hashimi, S.; McCormick, A.; Tsapatsis, M.; Cococcioni, M. *J. Phys. Chem. C* **2012**, *116*, 3561–3575.

¹⁵⁸ Aguado, S.; Bergeret, G.; Daniel, C.; Farrusseng, D. *J. Am. Chem. Soc.* **2012**, *134*, 14635–14637.

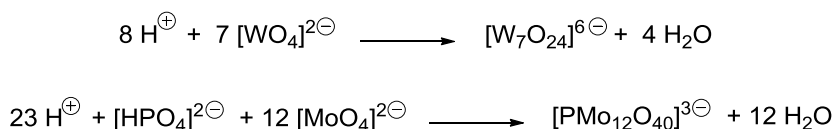
¹⁵⁹ (a) Garegg, P. J.; Koepper, S.; Ossowski, P.; Thiem, J. *J. Carbohydr. Chem.* **1986**, *5*, 59–65. (b) Finch, P.; Siriwardena, A. H. *Glycoconj. J.* **1989**, *6*, 477–488. (c) Thomas, R. L.; Sarkar, A. K.; Kohata, K.; Abbas, S. A.; Matta, K. L. *Tetrahedron Lett.* **1990**, *31*, 2825–2828. (d) Olsson, L.; Kelberlau, S.; Jia, Z. J.; Fraser-Reid, B. *Carbohydr. Res.* **1998**, *314*, 273–276. (e) Ruiz, M. C. d. R.; Amer, H.; Stanetty, C.; Beseda, I.; Czollner, L.; Shah, P.; Jordis, U.; Kueenburg, B.; Classen-Houben, D.; Hofinger, A.; Kosma, P. *Carbohydr. Res.* **2009**, *344*, 1063–1071.

process, and as true heterogeneous catalyst in a three component synthesis of propargylamines.¹⁶⁰

3.3. Polyoxometalates

3.3.1. Topology and main families

Polyoxometalate chemistry is a key emerging area of interest, whose early bases date back from the 19th century. At that time, Berzelius, Werner and Pauling, considered as the fathers of this field, experimented the tendency of early transition metals (Mo^{VI} , W^{VI} , V^{V}) to form polyoxoanions in aqueous solutions (Equation 5).¹⁶¹



Equation 5. Formation of phosphomolybdates and tungstates in aqueous solutions

Subsequently, polyoxometalates were intensively studied and described. Werner¹⁶² and Pauling¹⁶³ were the first to imagine structures based on face and edge-sharing polyhedra, or corner-sharing octahedra, respectively.

In 1933, Keggin settled these hypotheses and solved the structure of the heteropolyacid $[\text{H}_3\text{PW}_{12}\text{O}_{40}] \cdot 5 \text{H}_2\text{O}$ (latter corrected in $6 \text{H}_2\text{O}$) by monocrystal X-ray diffraction (Figure 9).¹⁶⁴

¹⁶⁰ Maggi, R.; Bello, A.; Oro, C.; Sartori, G.; Soldi, L. *Tetrahedron* **2008**, *64*, 1435–1439.

¹⁶¹ Pope, M. T.; Müller, A. *Angew. Chem. Int. Ed.* **1991**, *30*, 34–48.

¹⁶² Werner A. *Neuere Anschauungen auf dem Gebiete der Anorganischen Chemie*; Braunschweig, **1905**.

¹⁶³ Pauling, L. *J. Am. Chem. Soc.* **1929**, *51*, 2868–2880.

¹⁶⁴ Keggin, J. F. *Nature* **1933**, *131*, 908–909.

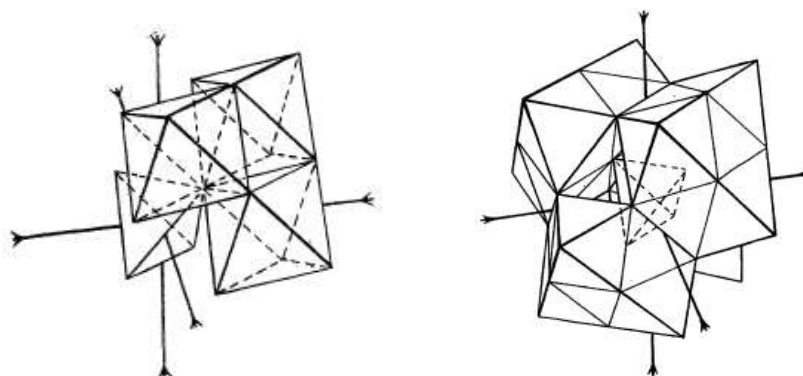


Figure 9. Representation of the $\text{PW}_{12}\text{O}_{40}^{3-}$ anion by Keggin in 1933 (on the right). On the left, the arrangement of 3 WO_6 octahedra relative to the central PO_4^{3-} tetrahedron.

However, it was not until the development of modern instrumentation and analytical methods in the early 1970's, that real progresses were made concerning the elucidation of the polyoxometalates structure. Since then, the chemistry of these materials rapidly expanded, and this is mainly due to the numerous fields of action they offer.

Polyoxometalates – commonly called POMs - are a large family of metal oxygen clusters $(\text{MO}_x)_n$. M are called “*addenda* atoms” and refer to early transition metals in their high oxidation state (typically Mo^{6+} , W^{6+} , V^{5+} , and less commonly Nb^{5+} , Ta^{5+} , Re^{7+} , I^{7+}) with $x = 4-7$. The limited number of polyniobates, tantalates and chromates is due to the inability of these elements to adopt various oxygen coordination numbers in aqueous solutions. Nb and Ta are always 6-coordinate, Cr is 4-coordinate. In contrast, V, Mo and W can accommodate 5, 6 or even 7 oxo ligands.

POMs can possibly include in their framework one or several internal heteroatoms (P and Si are the most common but over 60 heteroelements are known). This category of POMs is called heteropolyanions, opposed to isopolyanions, which do not contain any heteroatom. Heteropolyanions constitute by far the most studied subset of POMs, owing to their robust structure compared to isopolyanions. The Keggin $[\text{XM}_{12}\text{O}_{40}]^{n-}$ and the Wells-Dawson $[\text{X}_2\text{M}_{18}\text{O}_{62}]^{n-}$ structures (where $X = \text{W}$ or Mo , tetrahedrally coordinated) are the most common heteropolyanions, extensively studied for their catalytic properties. In the Keggin structure, the central heteroatom X is tetrahedrally coordinated to 4 oxygen atoms, and caged by 12 MO_6 octahedra building blocks, linked with each other by bridging oxygen atoms. The Wells-Dawson structure consists in a dimer of 2 lacunary Keggin units, each missing 3 octahedra (Figure 10).

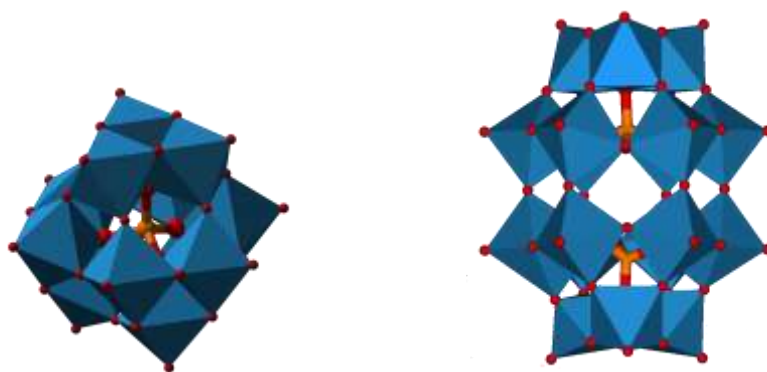


Figure 10. The Keggin $[XM_{12}O_{40}]^{n-}$ (on the left) and the Wells-Dawson $[X_2M_{18}O_{62}]^{n-}$ structures (on the right). MO_6 blue octahedra surrounding the central yellow heteroatom(s) X. Oxygen atoms are red.

An important subset of heteropolyanions is the molybdenum blue and brown clusters $[X_aM_n^{VI}M_m^V]$ (Figure 11).¹⁶⁵ Their discovery is very old but their structure was only solved in 1995 by Müller. He reported a high-nuclearity $\{Mo_{154}\}$ cluster with a ring topology that crystallized from a solution of molybdenum blue.¹⁶⁶ By changing the reaction conditions he obtained the formation of a $\{Mo_{132}\}$ spheric cluster.¹⁶⁷

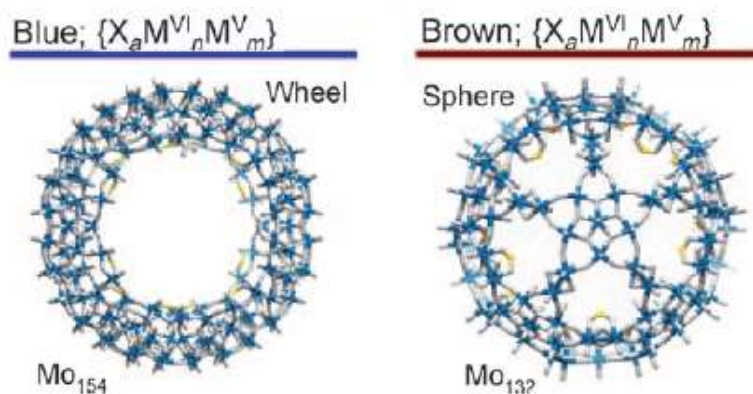


Figure 11. Molybdenum blue and brown clusters.

This class of highly reduced POMs clusters is an emerging area finding most applications in nanosciences.

¹⁶⁵ Long, D.-L.; Tsunashima, R.; Cronin, L. *Angew. Chem. Int. Ed.* **2010**, *49*, 1736–1758.

¹⁶⁶ Müller, A.; Krickemeyer, E.; Meyer, J.; Bögge, H.; Peters, F.; Plass, W.; Diemann, E.; Dillinger, S.; Nonnenbruch, F.; Randerath, M.; Menke, C. *Angew. Chem. Int. Ed.* **1995**, *34*, 2122–2124.

¹⁶⁷ Müller, A.; Krickemeyer, E.; Bögge, H.; Schmidtman, M.; Peters, F. *Angew. Chem. Int. Ed.* **1998**, *37*, 3359–3363.

3.3.2. Synthesis of POMs

In aqueous solutions, transition metals can coordinate to aqua (H_2O), hydroxo (OH^-) or oxo (O_2^-) ligands. In their high oxidation state however, they tend to form stable complexes with the corresponding highly charged oxo ligands O_2^- . Upon acidification, condensation of different oxo anions occurs and leads to the formation of M-O-M bridges. The coordination number of addenda atoms increases and condensed structures appear (Figure 12).¹⁶⁸

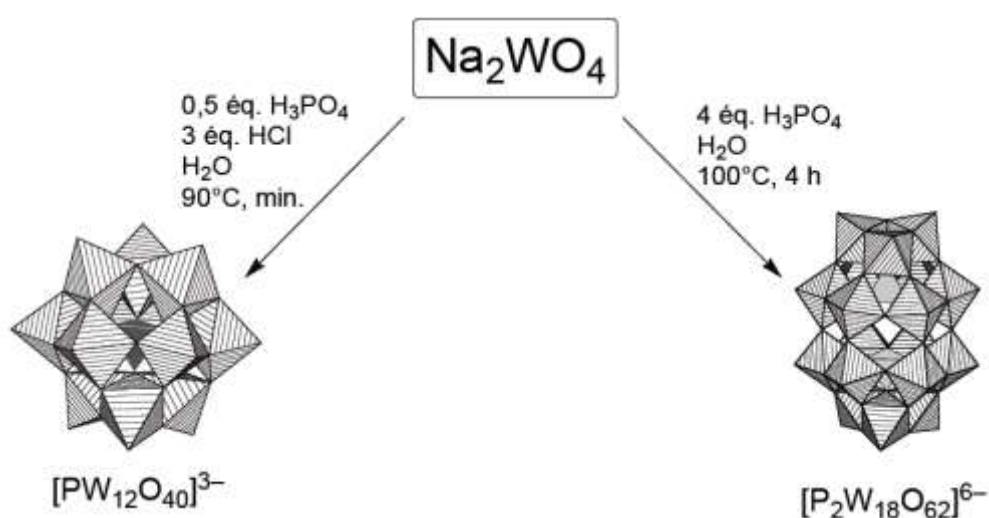


Figure 12. Examples of reaction conditions to synthesize Keggin or Dawson HPAs.

By fine tuning of different factors, i. e. stoichiometry, solvent, pH, temperature, concentration, counterions, one can obtain tailor made structures of polyoxometalates.¹⁶⁹ Heteropolyacids (HPAs) are the conjugated acids of heteropolyanions. They are usually prepared by the ‘etherate method’ of Drechsel.¹⁷⁰ The addition of ether to a strongly acidic aqueous solution of the POM forms a system of three layers, with ether on top, then an aqueous layer and at the bottom, a saturated solution of the acid in ether, the etherate. The latter is then decomposed in water and crystallized.

¹⁶⁸ Hasenkopf, B. *Front. Biosci.* **2005**, *10*, 275–287.

¹⁶⁹ (a) Contant, R.; Hervé, G. *Rev. Inorg. Chem.* **2002**, *22*, 2, 63–111. (b) Klemperer, W. G. *Inorg. Synth.* **1990**, *27*, 71–135.

¹⁷⁰ Drechsel, E. *Ber. Dtsch. Chem. Ges.* **1887**, *20*, 1452–1455.

3.3.3. Highlights on the structures of heteropolyanions

To get a better idea of the behavior of polyoxometalates, especially in catalysis, it is important to distinguish the different structural levels they provide. The primary structure is the large polyanion (Keggin, Dawson, *etc.*), in other words the arrangement of the MO_x polyhedra around the heteroatom(s). The secondary structure defines the 3-dimensionnal arrangement of the polyanion with the counterions (protons, metallic cations) and water molecules, often coming from crystallization. Finally, the tertiary structure represents the way nanoparticles of the secondary structure assemble into particles, and is characterized by different factors: size of the particles, distribution of the protons, pore structures (Figure 13).¹⁷¹

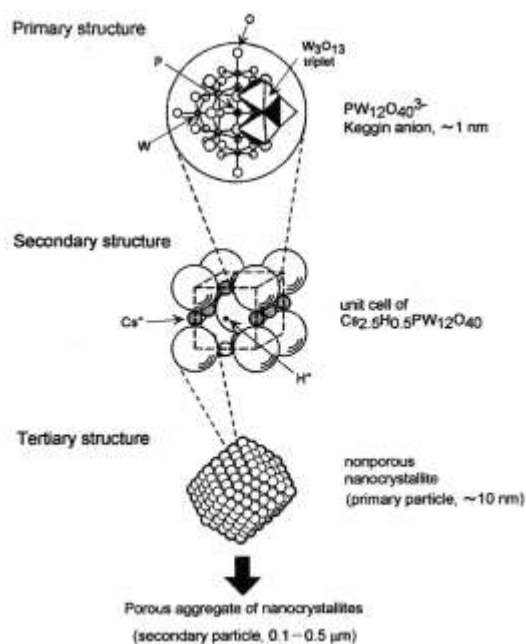


Figure 13. Hierarchic structures of $\text{Cs}_{2.5}\text{H}_{0.5}\text{PW}_{12}\text{O}_{40}$.

In the structure, highly charged addenda atoms create dipole attractions toward their adjacent unshared oxygen atoms. The attraction is stronger for terminal oxygens, owing to their higher polarizability compared to internal ones. The availability of empty d -orbitals of transition metals allows significant $p\pi$ - $d\pi$ overlap, which leads to shorter $\text{M-O}_{\text{terminal}}$ bonds (often double bonds), and longer *trans* M-O bonds.¹⁷² For instance, W-O bonds for terminal oxygens *versus*

¹⁷¹ Mizuno, N.; Misono, M. *Chem. Rev.* **1998**, *98*, 199–218.

¹⁷² Borrás-Almenar, J. J.; Coronado, E.; Müller, A.; Pope, M. T. *Polyoxometalate Molecular Science*; Kluwer Academic Publishers, Dordrecht, NATO Science Series, II: Mathematics, Physics and Chemistry, **2003**.

peripheral oxygens usually range from 0.7 to 1.0 Å.¹⁷³ This structural modification is called the octahedral distortion. Since terminal oxygens are strongly polarized toward the interior of the structure, they are relatively indisposed to attach protons. Hence, the O-H interaction is very weak, and this accounts for the characteristic strong acidity of HPAs.

3.3.4. Acid and redox properties of HPAs

HPAs are pure Brønsted acids, much stronger than the usual inorganic acids such as HCl, H₂SO₄, HNO₃ (Table 7), and stronger than other solid acids such as SiO₂-Al₂O₃, or H-X and H-Y zeolites.

Table 7. Dissociation constants of most common HPAs in acetone solution.¹⁷²

	p <i>K</i> ₁	p <i>K</i> ₂	p <i>K</i> ₃
H₃PW₁₂O₄₀	1,6	3,0	4,0
H₄SiW₁₂O₄₀	2,0	3,6	5,3
H₃PMo₁₂O₄₀	2,0	3,6	5,3
H₄SiMo₁₂O₄₀	2,1	3,9	5,9
H₂SO₄	6,6		
HCl	4,3		
HNO₃	9,4		

Although not perfectly viable, Hammett acidity measurements were carried out and suggested that H₃PW₁₂O₄₀ was a superacid.¹⁷¹ Temperature Programmed Desorption (TPD) of pyridine and ammonia more clearly demonstrated that H₃PW₁₂O₄₀ was a stronger acid than SiO₂-Al₂O₃ and H-ZSM-5, but weaker than SO₄²⁻/ZrO₂.¹⁷⁴

As a result of the strong acidity of HPAs, the corresponding heteropolyanions have therefore weak Brønsted basicity, and are considered as soft bases, due to their low charge density and high polarizability. The localization of acid sites in HPAs has been studied by various

¹⁷³ Baker, L. C. W.; Glick, D. C. *Chem. Rev.* **1998**, 98, 3–50.

¹⁷⁴ (a) Misono, M.; Mizuno, N.; Katamura, K.; Kasai, A.; Konishi, Y.; Sakata, K.; Okuhara, T.; Yoneda, Y. *Bull. Chem. Soc. Jpn.* **1982**, 55, 400–406. (b) Okuhara, T.; Nishimura, T.; Watanabe, H.; Misono, M. *J. Mol. Catal.* **1992**, 74, 247–256.

methods. X-ray and neutron diffraction studies on the hexahydrated form of the Keggin HPA ($\text{H}_3\text{PW}_{12}\text{O}_{40}$), suggested that all terminal oxygen atoms were hydrogen-bonded to $[\text{H}_2\text{OHOH}_2]^+$ cations. Consequently, 3 protons were attached to the heteropolyanion (Figure 14).

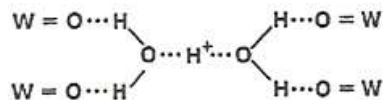


Figure 14. Protons sites in hexahydrated form.

In the dehydrated form, the localization of the protons remains controversial.¹⁷¹ X-ray and neutron diffractions of the solid state showed that most often, protons are attached to bridging oxygen atoms. Although they are less accessible than terminal ones, they are more basic. Concerning the behavior of HPAs in solution, pH-dependency of ^{17}O NMR chemical shifts afforded the same conclusions.¹⁷² Based on IR studies, Mizuno *et al.* assumed that protons migrated from terminal oxygens onto bridging ones upon dehydration above 373 K.¹⁷⁵

Due to the high oxidation state of *addenda* atoms (Mo^{VI} , W^{VI} , V^{V}), polyoxometalates exhibit oxidative properties. The stability of the reduced species and the reversibility of the reduction depend on the nature of the POM.¹⁶¹

3.3.5. Modifications of POMs

The formation of heteropolyanions by self-assembly of different oxo anions assumes that the coordination bonds (MOM bridges) can reversibly be cleaved. In fact, all heteropoly species can be degraded in strong basic conditions. The mechanism of the degradation involves attack by hydroxide ions and modification of the metal's coordination number.¹⁷³ These processes are now well understood and controlled (partial) degradation conditions have been set up in order to obtain the so-called lacunary species. Lacunary structures in the strict sense are obtained after removal of one or more *addenda* atom(s). Further grafting of different species led to the creation of novel classes of tailor made “functionalized polyoxometalates”. Among this very large family, one can distinguish different cases, not all actually deriving from a lacunary POM:

¹⁷⁵ Lee, K. Y.; Mizuno, N.; Okuhara, T.; Misono, M. *Bull. Chem. Soc. Jpn.* **1989**, 62, 1731–1739.

- Replacement of an oxo ligand by another element attached to an organic chain, for instance, the introduction of RN_2^- imido ligand instead of O_2^- .
- Grafting of an organic chain to an oxo ligand, which becomes an alkoxo ligand.
- Insertion of an organometallic chain into a lacunary structure, either directly, or indirectly by introducing the metal first, and subsequently grafting an organic ligand.

3.3.6. Applications

The versatile properties of polyoxometalates, including their structural diversity, acidity, and redox properties have opened up a large field of applications,¹⁷⁶ ranging from materials science,¹⁷⁷ magnetism,¹⁷⁸ photochemistry,¹⁷⁹ pharmacology¹⁸⁰ and catalysis. We will try to get a quick overview of the latter area, with an emphasis on recent applications of HPA and their salts in organic synthesis.

An interesting property of polyoxometalate is their ability to solubilize in a wide range of solvents - from water to hydrocarbons, depending precisely on the counterion nature.¹⁶¹ For this reason, they can be used either as homogeneous catalysts,¹⁸¹ or heterogeneous catalysts.¹⁷¹

The catalytic applications of polyoxometalates are mainly driven by their inherent acidic and redox properties. According to Mizuno *et al.*,¹⁷¹ different types of heterogeneous catalysis occur in POMs:

- Surface-type catalysis, in which the reaction rate is proportional to the surface area. Isomerization of olefins over $\text{H}_3\text{PMO}_{12}\text{O}_{40}$ is a typical example of such catalysis.¹⁸²
- Bulk-type catalysis, also called ‘pseudoliquid’ catalysis. Reactants are adsorbed in solid bulk (interpolyanion space) and react. The reaction rate depends on the volume or weight of

¹⁷⁶ Katsoulis, D. E. *Chem. Rev.* **1998**, *98*, 359–388.

¹⁷⁷ (a) Coronado, E.; Gómez-García, C. J. *Chem. Rev.* **1998**, *98*, 273–296. (b) Klemperer, W. G.; Wall, C. G. *Chem. Rev.* **1998**, *98*, 297–306.

¹⁷⁸ Müller, A.; Peters, F.; Pope, M. T.; Gatteschi, D. *Chem. Rev.* **1998**, *98*, 239–272.

¹⁷⁹ (a) Papaconstantinou, E. *Chem. Soc. Rev.* **1989**, *18*, 1–31. (b) Yamase, T. *Chem. Rev.* **1998**, *98*, 307–326.

¹⁸⁰ Rhule, J. T.; Hill, C. L.; Judd, D. A.; Schinazi, R. F. *Chem. Rev.* **1998**, *98*, 327–358.

¹⁸¹ (a) Hill, C. L.; Prosser-McCartha, C. M. *Coord. Chem. Rev.* **1995**, *143*, 407–455. (b) Weinstock, I. A. *Chem. Rev.* **1998**, *98*, 113–170.

¹⁸² Misono, M.; Konishi, Y.; Furuta, M.; Yoneda, Y. *Chem. Lett.* **1978**, *7*, 709–712.

catalyst. The synthesis of MTBE from isobutylene and methanol, catalyzed by the Dawson HPA $\text{H}_6\text{P}_2\text{W}_{18}\text{O}_{62}$ is a good example, the latter being much more active than $\text{SO}_4^{2-}/\text{ZrO}_2$, $\text{SiO}_2\text{-Al}_2\text{O}_3$, and H-ZSM-5.¹⁸³

In analogy to the shape selectivity of microporous zeolites, shape selective adsorption occurs in polyoxometalates. Okuhara et al. demonstrated that depending on the Cs/H ratio of different cesium-exchanged heteropolyacids, molecules of different sizes reacted more or less efficiently. $\text{Cs}_{2.2}\text{H}_{0.8}\text{PW}_{12}\text{O}_{40}$ catalyzed the dehydration of 2-hexanol (molecular size 0.50 nm) and the decomposition of isopropyl acetate (0.50 nm), but not cyclohexyl acetate (0.60 nm) and 1,3,5-trimethylbenzene (0.75 nm). In contrast, $\text{Cs}_{2.5}\text{H}_{0.5}\text{PW}_{12}\text{O}_{40}$ was efficient in all reactions.¹⁸⁴

Due to their solubility in polar solvents, heteropolyacids have been grafted on different solid supports, especially silica gel¹⁸⁵ and zirconia,¹⁸⁶ and used as recyclable heterogeneous catalysts in various organic reactions. Several examples also described the use of non-supported HPAs, either as heterogeneous catalysts in apolar solvents, or as homogeneous catalysts recovered by precipitation at the end of the reaction.¹⁸⁷

¹⁸³ (a) Shikata, S.; Okuhara, T.; Misono, M. *J. Mol. Catal. A Chem.* **1995**, *100*, 49–59. (b) Shikata, S.; Nakata, S.-i.; Okuhara, T.; Misono, M. *J. Catal.* **1997**, *166*, 263–271.

¹⁸⁴ Okuhara, T.; Nishimura, T.; Misono, M. *Chem. Lett.* **1995**, *24*, 155–156.

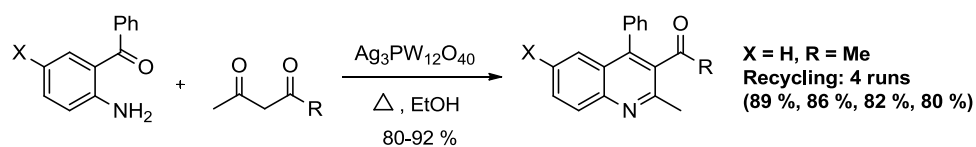
¹⁸⁵ (a) Jafari, A. A.; Mahmoudi, H.; Mirjalili, B. F. *J. Iran. Chem. Soc.* **2011**, *8*, 851–856. (b) Aliyan, H.; Fazaeli, R.; Naghash, H. J.; Massah, A. R.; Momeni, A. R.; Iravani, Z. *Heteroat. Chem.* **2009**, *20*, 325–331.

¹⁸⁶ (a) Pathan, S.; Patel, A. *RSC Adv.* **2012**, *2*, 116–120. (b) Naik, M. A.; Samantaray, S.; Mishra, B. G. *J. Cluster Sci.* **2011**, *22*, 295–307. (c) Satam, J. R.; Parghi, K. D.; Jayaram, R. V. *Catal. Commun.* **2008**, *9*, 1071–1078. (d) Mohammadpoor-Baltork, I.; Moghadam, M.; Tangestaninejad, S.; Mirkhani, V.; Hojati, S. F. *Polyhedron* **2008**, *27*, 750–758. (e) Firouzabadi, H.; Iranpoor, N.; Jafari, A. A.; Jafari, M. R. *J. Mol. Catal. A Chem.* **2006**, *247*, 14–18. (f) Kozhevnikova, E. F.; Quartararo, J.; Kozhevnikov, I. V. *Appl. Catal., A* **2003**, *245*, 69–78. (g) Meuzelaar, G. J.; Maat, L.; Sheldon, R. A. *Catal. Lett.* **1998**, *56*, 49–51.

¹⁸⁷ (a) Allameh, S.; Heravi, M. M.; Hashemi, M. M.; Bamoharram, F. F. *Chin. Chem. Lett.* **2011**, *22*, 131–134. (b) Hekmatshoar, R.; Sadjadi, S.; Sadjadi, S.; Heravi, M. M.; Beheshtiha, Y. S.; Bamoharram, F. F. *Synth. Commun.* **2010**, *40*, 1708–1716. (c) Giri, B. Y.; Devi, B. L. A. P.; Lakshmi, K. V.; Prasad, R. B. N.; Lingaiah, N.; Prasad, P. S. S. *Synth. Commun.* **2006**, *36*, 3797–3801.

HPA salts, i.e. cesium,¹⁸⁸ ammonium¹⁸⁹ and several transition metal salts have also been employed as catalysts in organic synthesis.

Silver doped HPAs proved to be efficient heterogeneous catalysts in various reactions,¹⁹⁰ notably in the Friedländer quinoline synthesis (Scheme 18).¹⁹¹



Scheme 18. Ag-POM catalyzed Friedländer quinoline synthesis by Yadav et al.

Isolated examples of copper,¹⁹² iron¹⁹³ and samarium-exchanged¹⁹⁴ HPAs were also reported.

Through another approach, Malacria et al. investigated the use of hybrid POMs, obtained by modification of a lacunary structure, as heterogeneous catalysts for various reactions. Notably, they reported the grafting of a lanthanide complex on a lacunary Dawson heteropolyanion, for application as Lewis heterogeneous catalyst in Mannich type and 3-component reactions (Scheme 19).¹⁹⁵

¹⁸⁸ (a) Firouzabadi, H.; Jafari, A. A. *Curr. Org. Chem.* **2008**, *12*, 233-256. (b) Kozhevnikova, E. F.; Quartararo, J.; Kozhevnikov, I. V. *Appl. Catal., A* **2003**, *245*, 69-78.

¹⁸⁹ (a) Giri, B. Y.; Devi, B. L. A. P.; Gangadhar, K. N.; Lakshmi, K. V.; Prasad, R. B. N.; Lingaiah, N.; Prasad, P. S. S. *Synth. Commun.* **2007**, *37*, 2331-2336. (b) Giri, B. Y.; Devi, B. L. A. P.; Lakshmi, K. V.; Prasad, R. B. N.; Lingaiah, N.; Prasad, P. S. S. *Synth. Commun.* **2006**, *36*, 3797-3801.

¹⁹⁰ (a) Yadav, J. S.; Reddy, B. V. S.; Praveenkumar, S.; Nagaiah, K.; Lingaiah, N.; Saiprasad, P. S. *Synthesis* **2004**, 901-904. (b) Yadav, J. S.; Reddy, B. V. S.; Sridhar, P.; Reddy, J. S. S.; Nagaiah, K.; Lingaiah, N.; Saiprasad, P. S. *Eur. J. Org. Chem.* **2004**, 552-557. (c) Reddy, K. M.; Babu, N. S.; Suryanarayana, I.; Prasad, P. S. S.; Lingaiah, N. *Tetrahedron Lett.* **2006**, *47*, 7563-7566. (d) Lingaiah, N.; Babu, N. S.; Reddy, K. M.; Prasad, P. S. S.; Suryanarayana, I. *Chem. Commun.* **2007**, 278-279. (e) Yadav, J. S.; Reddy, B. V. S.; Purnima, K. V.; Jhansi, S.; Nagaiah, K.; Lingaiah, N. *Catal. Commun.* **2008**, *9*, 2361-2364.

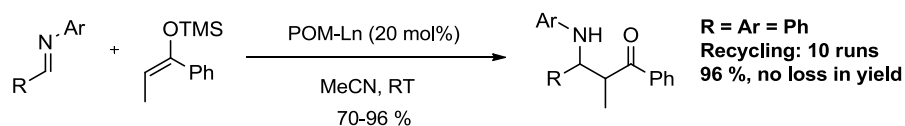
¹⁹¹ Yadav, J. S.; Reddy, B. V. S.; Sreedhar, P.; Rao, P. S.; Nagaiah, K. *Synthesis* **2004**, 2381-2385.

¹⁹² (a) Yadav, J. S.; Reddy, B. V. S.; Purnima, K. V.; Nagaiah, K.; Lingaiah, N. *J. Mol. Catal. A Chem.* **2008**, *285*, 36-40. (b) Pasha, N.; Babu, N. S.; Venkateswara Rao, K. T.; Prasad, P. S. S.; Lingaiah, N. *Tetrahedron Lett.* **2009**, *50*, 239-242.

¹⁹³ Venkateswara Rao, K. T.; Sai Prasad, P. S.; Lingaiah, N. *J. Mol. Catal. A Chem.* **2009**, *312*, 65-69.

¹⁹⁴ Kumar, C. R.; Jagadeeswaraiyah, K.; Prasad, P. S. S.; Lingaiah, N. *ChemCatChem* **2012**, *4*, 1360-1367.

¹⁹⁵ Boglio, C.; Lemiere, G.; Hasenknopf, B.; Thorimbert, S.; Lacote, E.; Malacria, M. *Angew. Chem. Int. Ed.* **2006**, *45*, 3324-3327.



Scheme 19. Ln-POM catalyzed Mannich-type reaction by Malacria et al.

More recently, they were able to cyclize sensitive allenols in soft buffering conditions, by grafting a gold complex on a Dawson α_1 -organotin-substituted polyoxotungstate (already functionalized POM).¹⁹⁶

4. Objectives of the thesis

4.1. Development of heterogeneous procedures catalyzed by metal-doped solids

In order to tackle the environmental issues encountered in the modern chemical industry, the first objective of this Ph.D. thesis is the development of environmental friendly procedures for fine organic synthesis, based on the use of recyclable catalysts.

Transition-metal catalysis has gained widespread use in the total synthesis of complex natural molecules of biological interest, and in the development of practical methodologies to access such products. However, a large part of the homogeneous catalysts employed in these transformations rely on the use of expensive ligands and transition-metals which can not be recovered and recycled at the end of the reaction. To solve this problem, we aimed to design heterogeneous catalysts combining the advantages of recyclable solid supports and the ability of several metallic cations to promote organic transformations. We hope that such metal-doped solids will gain larger application in fine organic synthesis.

To better comply with the principles of green chemistry, we will focus on transformations that are atom economic and convergent. For each targeted reaction, we will try to design the most suitable metal-doped heterogeneous catalyst, and demonstrate its advantages compared to homogeneous catalysts such as ease of handling, efficiency and of course, recyclability.

¹⁹⁶ Dupre, N.; Brazel, C.; Fensterbank, L.; Malacria, M.; Thorimbert, S.; Hasenknopf, B.; Lacote, E. *Chem. Eur. J.* **2012**, *18*, 12962–12965.

4.2. Comprehension of the mechanisms of hydrocarbon conversion

Whereas the transition from homogeneous to heterogeneous catalysis remains difficult to adopt in fine organic chemistry and total synthesis of complex molecules, recyclable solid acids have been used extensively since the 1950's in most of the important petrochemical processes such as hydrocarbon cracking, reforming or hydroisomerization. However, the understanding of the mechanisms of alkane activation over solid acids such as zeolites has always represented a challenge for the scientific community. Although a lot of work has already been accomplished in this field, several questions are still a matter of debate. The second objective of this Ph.D. thesis is to shed light on one of these issues. The reaction of ^2H and ^{13}C labeled isobutanes over acidic zeolite will be studied by *in situ* NMR. We hope that the determination of the energetic parameters of the reaction will help us to get insight concerning the mechanism of the hydride transfer, a process which plays a major role in the conversion of hydrocarbons over solid acids.

Chapter 2 :

Activation of small alkanes on solid acids :
study of the hydride transfer reaction by
isotopic exchange between ^2H - and ^{13}C -
labeled isobutanes

1. *Mechanisms of hydrocarbon conversion on solid acids : an overview*

Despite the recent efforts to develop new renewables energies, hydrocarbons contained in raw oil constitute up to now – and still for several years, the first energy resource in the world. In addition, saturated hydrocarbons represent the main feedstock for key unsaturated building blocks of organic synthesis, i. e. ethylene, propylene and benzene. In order to transform the inert starting hydrocarbons into valuable products, petrochemical processes such as cracking, reforming or hydroisomerization used to employ drastic conditions, namely high temperatures and pressures, as well as strong acids (HF, H₂SO₄).¹⁹⁷ To better comply with the green chemistry principles, solid acids such as zeolites progressively replaced the harmful liquid superacids in petrochemical transformations.¹⁹⁸ Not only easy to handle and safe, they can also be recovered and recycled several times, which goes towards more sustainable processes. Looking at the economic importance of the reactions we just mentioned, every improvement that can be brought in this field seems particularly useful. The extension of the catalyst lifetime and the minimization of the side products are part of this objective, for instance. Understanding the mechanisms of hydrocarbon conversion is a difficult challenge which attracted the attention of chemists for a long time.^{197,199} Although many theoretical and experimental studies have been carried out, several aspects of this issue remain fuzzy and any insight would certainly help to progress in the right direction.

1.1. Hydrocarbon cracking: an illustration of the early issues concerning the first step of alkane conversion

Among all the oil refining steps, hydrocarbon cracking (nowadays called Fluid Catalytic Cracking or FCC) is the most important process and, as such, has received the highest interest regarding the elucidation of its mechanism.²⁰⁰ Other processes such as isomerization or alkylation involve the same type of reactivity and thus, FCC serves as a basis for the understanding of these reactions. Typically, FCC enables to convert high-molecular weight

¹⁹⁷ (a) Pines, H. *The Chemistry of Catalytic Hydrocarbon Conversion*; Academic Press, New York, NY, 1981.

(b) Olah, G. A.; Molnar, A. *Hydrocarbon Chemistry*; J. Wiley, New York, NY, 1995.

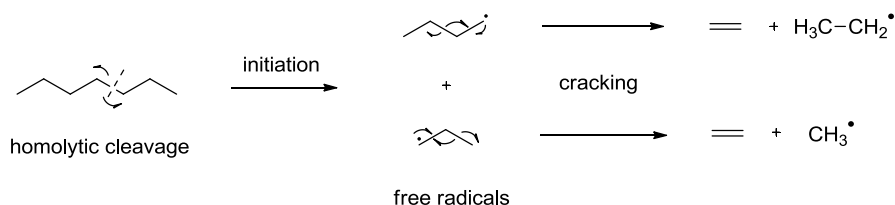
¹⁹⁸ Corma, A. *Chem. Rev.* **1995**, *95*, 559–614.

¹⁹⁹ Sommer, J.; Jost, R.; Hachoumy, M. *Catal. Today* **1997**, *38*, 309–319.

hydrocarbon fractions of crude oil to smaller and more valuable products such as gasoline, olefinic gases, and small alkanes like butane and propane.

Alkane cracking is a chain reaction and as such, includes 3 main steps: initiation, propagation and termination. The process is usually carried out at high temperature and utilizes USY-zeolite as solid acid catalyst. Studies have demonstrated that the product distribution is time dependent, with a distinction between the initial time of the cracking and what is called steady state.²⁰⁰ These observations suggested that several mechanisms were involved.

Thermal cracking is now well established as one of the possible reaction pathways, proceeding *via* homolytic cleavage and free radical intermediates, but significant only at high temperatures (> 800 K) (Scheme 20).²⁰¹



Scheme 20. Thermal cracking *via* homolytic cleavage and free radical intermediates.

Main products range typically from C1 to C4 with ethylene as the smallest hydrocarbon.

In addition to this thermal process, two different catalytic cycles have been suggested for hydrocarbon cracking, both proceeding *via* carbenium intermediates.

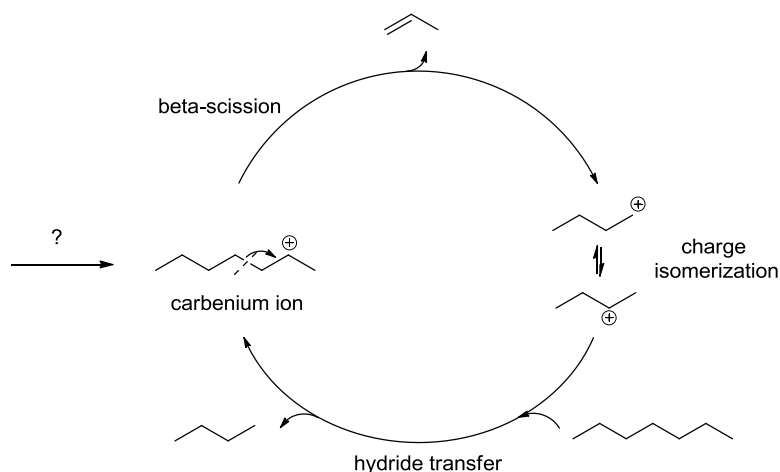
The oldest mechanism or classical catalytic cracking dates back from the 1930's with the work of Whitmore,²⁰² and later Greensfelder.²⁰³ It assumes the existence of a carbenium ion which undergoes cracking through β -scission of a C-C bond, β to the carbenium center (Scheme 21).

²⁰⁰ (a) Dupain, X.; Makkee, M.; Moulijn, J. A. *Appl. Catal. A Gen.* **2006**, 297, 198–219. (b) Corma, A.; Orchillés, A. V. *Microporous Mesoporous Mater.* **2000**, 35–36, 21–30.

²⁰¹ Kotrel, S.; Knözinger, H.; Gates, B. C. *Microporous Mesoporous Mater.* **2000**, 35–36, 11–20.

²⁰² Whitmore, F. C.; Church, J. M. *J. Am. Chem. Soc.* **1932**, 54, 3710–3714.

²⁰³ Greensfelder, B. S.; Voge, H. H.; Good, G. M. *Ind. Eng. Chem.* **1949**, 41, 2573–2584.



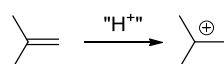
Scheme 21. Reaction mechanism of the classical catalytic cracking.

This scission generates an alkene and a smaller primary carbenium ion, which isomerizes into a more stable secondary or tertiary carbenium ion. Hydride transfers from heavy alkanes yield light alkanes and regenerate a long chain carbenium ion, which maintains the catalytic cycle. The olefin can either isomerize or be protonated by the catalyst and crack further.

It is worth mentioning that the smallest hydrocarbon obtained by this mechanism is propane, since β -scission of light alkanes ($< C_6$) requires the formation of high energy primary carbenium ions. Consequently, classical catalytic cracking is more selective to gasoline (typically C5-C12) than thermal cracking.

Although correct at first sight, this mechanism did not allow to account for complex product distribution of cracking, notably products lighter than C3 molecules. The other issue that remained fuzzy was the formation of the initial carbenium species or activation step of the alkane. Several suggestions were put forward:

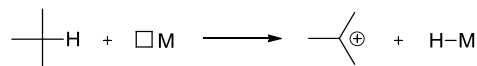
- Carbenium would be formed by protonation of alkenes, which could either stem from impurities in the feed, or derive from free radicals thermal cracking (providing sufficient temperature) (Scheme 22).



Scheme 22. Carbenium formed by protonation of alkenes.

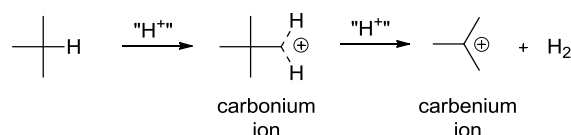
- It has been proposed that carbenium ions could be obtained from hydride abstraction by Lewis acid sites of the catalyst (Scheme 23). However, the lack of experimental proofs

confirming this hypothesis, as well as unfavorable thermodynamic conditions – unstable and weak M-H bond in acid conditions compared to strong C-H alkane bonds of ~ 100 kcal.mol⁻¹ – discredited this suggestion.¹⁹⁹



Scheme 23. Hydride abstraction by Lewis acid sites of the catalyst.

- The catalyst would protonate alkanes to form carbonium ions (Scheme 24), precursors of carbeniums, following the concept of σ -basicity proposed by Olah in 1972.²⁰⁴



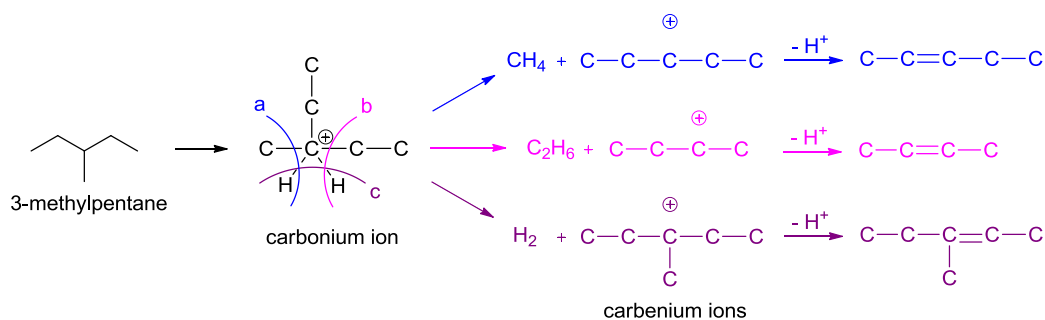
Scheme 24. Protonation of the alkane by the catalyst.

In 1984, Haag and Dessau were the first to establish the parallel with the reactivity of alkanes in liquid superacids and to propose a mechanism related to the concept of σ -basicity.²⁰⁵ Prior to their presentation, only few reports mentioned this possibility,²⁰⁶ which was not seriously considered. The Haag-Dessau mechanism came out after looking at the product distribution of *n*-hexane and 3-methylpentane cracking catalyzed by solid acids (H-USY, H-ZSM-5, silica-alumina) at 623-823 K.²⁰⁵ Formation of light products such as dihydrogen, methane and ethane could not be explained by the classical cracking mechanism. Haag and Dessau proposed that acid catalysts protonated hydrocarbons at the most substituted position to give pentacoordinated carbonium intermediates, which collapsed to provide carbenium ions and small alkanes. They imagined several splitting possibilities, yielding different pairs of carbenium/alkane or carbenium/dihydrogen (Scheme 25).^{200b}

²⁰⁴ Olah, G. A. *Angew. Chem., Int. Ed.* **1973**, *12*, 173–212.

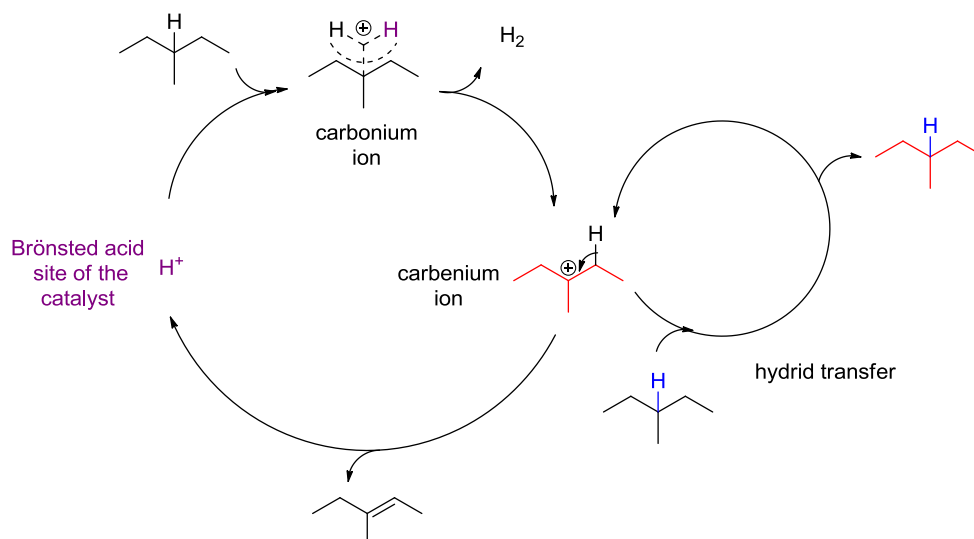
²⁰⁵ Haag, W.O.; Dessau, R.M. In *Proceedings of the 8th International Congress on Catalysis*, July 2-6, Berlin, 1984, Vol. 2, 305–315.

²⁰⁶ Bloch, H. S.; Pines, H.; Schmerling, L. *J. Am. Chem. Soc.* **1946**, *68*, 153–153.



Scheme 25. Splitting possibilities for the cracking of 3-methylpentane.

Contrary to the classical viewpoint in which one carbenium ion allows several turnovers of the catalytic cycle, in the Haag-Dessau mechanism, the protonation by the catalyst is necessary for each turnover (Scheme 26).



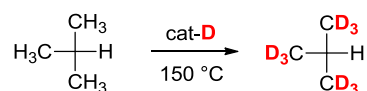
Scheme 26. Haag-Dessau reaction mechanism.

However, it is well accepted that this mechanism is mostly significant during the initial stages of cracking. Indeed, alkenes formed throughout the cycle can be protonated much easily than initial paraffins. In addition, hydride transfer is also a more favorable process than the protonation of alkanes by catalytic sites. Thus, both low concentrations of alkenes and paraffins are necessary for this protolytic cracking to be significant. At high conversion level the classical cracking is assumed to prevail.

1.2. The emergence of H/D exchange studies

When the protolytic cracking mechanism was proposed by Haag and Dessau, it was underlined that although consistent with Olah's hydrocarbons chemistry in superacids, the main difference between the two was the large temperature gap.²⁰⁷ Whereas homogeneous reactions of Olah occurred at or near room temperature in strong acidic media, hydrocarbons cracking over acidic zeolites required more than several hundreds of degrees Kelvin (typically $473 \text{ K} < T < 673 \text{ K}$). Therefore, it was assumed that those temperatures were necessary to compensate the lower acid strength of solid acids.

In fact, recent studies showed that exchanges between small alkanes and solid acids took place even at room temperature.²⁰⁸ To demonstrate such reactions, isotopic labeling of catalyst and/or hydrocarbon remains one of the most useful and practical tool, enabling to follow at an early stage the interaction between the two entities, involving notably fast hydron exchanges. This method, combined with the huge progress achieved in high-field multinuclear NMR, MAS-NMR, FT-IR, UV-vis and MS techniques have made H/D exchange studies methods of choice to demonstrate the mechanisms of hydrocarbon conversion. As early as 1950, Hindin et al. reported the regioselective H/D exchange between isobutane and a deuterated silica alumina catalyst at $150 \text{ }^\circ\text{C}$, using mass spectroscopy (Scheme 27).²⁰⁹



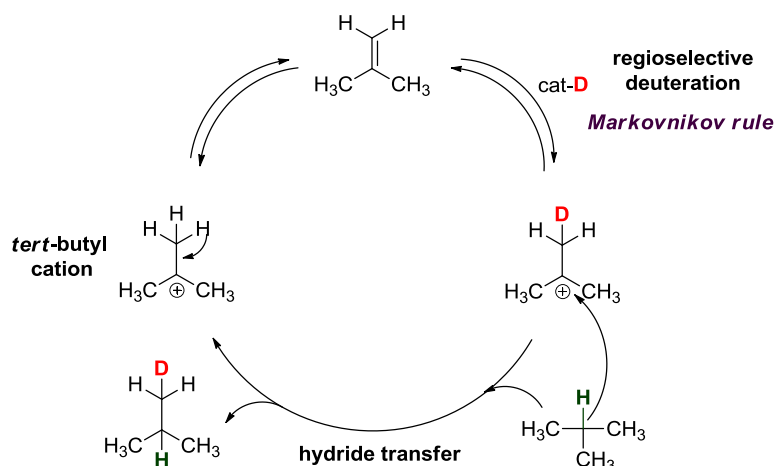
Scheme 27. Regioselective H/D exchange between isobutane and a deuterated silica alumina.

As reaction mechanism, they suggested the existence of a *tert*-butyl cation in equilibrium with isobutene, which would be regioselectively deuterated by the catalyst at the methyl positions, according to the Markovnikov rule. Desorption of the deuterated cation would then be performed by hydride transfer from an isobutane molecule, giving back the *tert*-butyl cation (Scheme 28).

²⁰⁷ Hall, W. K.; Lombardo, E. A.; Engelhardt, J. J. *Catal.* **1989**, *115*, 611–615.

²⁰⁸ (a) Truitt, M. J.; Toporek, S. S.; Rovira-Truitt, R.; White, J. L. *J. Am. Chem. Soc.* **2006**, *128*, 1847–1852. (b) Sani Souna Sido, A.; Barbiche, J.; Sommer, J. *Chem. Commun.* **2010**, *46*, 2913–2914. (c) Sani Souna Sido, A.; Walspurger, S.; Barbiche, J.; Sommer, J. *Chem.--Eur. J.* **2010**, *16*, 3215–3221.

²⁰⁹ Hindin, S. G.; Mills, G. A.; Oblad, A. G. *J. Am. Chem. Soc.* **1951**, *73*, 278–281.



Scheme 28. Reaction mechanism proposed for the regioselective H/D exchange.

Hindin et al. noticed the similarity of their results with the work of Otvos et al., who previously reported the same regioselectivity for the exchange between isobutane and deuterated sulfuric acid.²¹⁰

1.2.1. About the nature of the reaction intermediates

Although carbocationic species have been recognized for a long time as reaction intermediates in acid catalyzed hydrocarbon transformations,²¹¹ their formation as well as their true nature are still debated. Up to now, only particularly stabilized carbenium ions such as cyclic alkenyl²¹² or aromatic derivatives²¹³ could be detected by spectroscopic techniques. Therefore, carbenium ions derived from hydrocarbons are better considered transient species in the zeolite framework (Scheme 29, right). Several studies demonstrated that actual intermediates may be in fact more stable alkoxy species, covalently bound to the framework

²¹⁰ Otvos, J. W.; Stevenson, D. P.; Wagner, C. D.; Beeck, O. *J. Am. Chem. Soc.* **1951**, 73, 5741–5746.

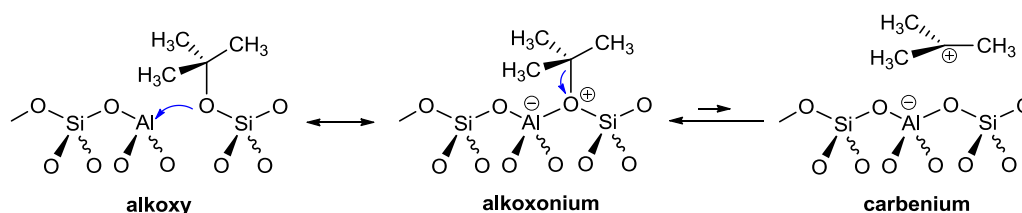
²¹¹ (a) Nenitzescu, C. D.; Cantuniari, I. P. *Ber. Dtsch. Chem. Ges.* **1933**, 66, 1097–1100. (b) Nenitzescu, C. D.; Drăgan, A. *Ber. Dtsch. Chem. Ges.* **1933**, 66, 1892–1900.

²¹² (a) Yang, S.; Kondo, J. N.; Domen, K. *J. Phys. Chem. B* **2001**, 105, 7878–7881. (b) Yang, S.; Kondo, J. N.; Domen, K. *Catal. Today* **2002**, 73, 113–125.

²¹³ Bjørgen, M.; Bonino, F.; Kolboe, S.; Lillerud, K.-P.; Zecchina, A.; Bordiga, S. *J. Am. Chem. Soc.* **2003**, 125, 15863–15868.

bridging oxygens (Scheme 29, left).²¹⁴ However, this topic is still a matter of debate, as shown by recent calculations indicating that the *tert*-butyl cation may be an actual reaction intermediate, more stable than its *tert*-butoxide counterpart, depending on the zeolite structure and on the temperature.²¹⁵

Equilibrium between alkoxides and carbenium ions has not been clearly demonstrated so far (Scheme 29), but is supported by theoretical calculations,²¹⁶ as well as various transformations, such as the Koch reaction,²¹⁷ the Friedel-Crafts acylation of alkenes,²¹⁸ or the halogen switch reaction.²¹⁹



Scheme 29. Alkoxy, alkoxonium and carbenium species as possible reaction intermediates.

Sommer et al. recently brought evidence for the existence of carbenium ions as reaction intermediates in a H/D exchange study between 2-methylpentane and deuterated isobutane over H-USY zeolite at room temperature.^{208b} By *ex situ* NMR spectroscopy, they were able to observe a redistribution of deuterium over the two isoalkanes, showing an equilibrium between the starting mixture of 2-methylpentane/deuterated isobutane and the so-formed deuterated 2-methylpentane/isobutane (Scheme 30).

²¹⁴ (a) Haw, J. F.; Nicholas, J. B.; Xu, T.; Beck, L. W.; Ferguson, D. B. *Acc. Chem. Res.* **1996**, *29*, 259–267. (b) Aronson, M. T.; Gorte, R. J.; Farneth, W. E.; White, D. *J. Am. Chem. Soc.* **1989**, *111*, 840–846.

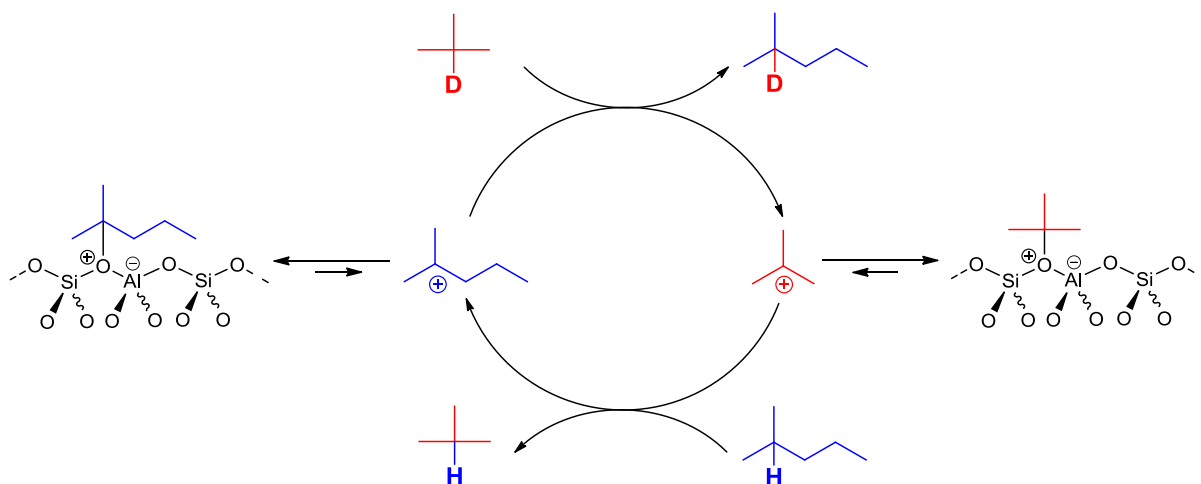
²¹⁵ Tuma, C.; Sauer, J. *Angew. Chem., Int. Ed.* **2005**, *44*, 4769–4771.

²¹⁶ Boronat, M.; Viruela, P. M.; Corma, A. *J. Am. Chem. Soc.* **2004**, *126*, 3300–3309.

²¹⁷ Stepanov, A. G.; Luzgin, M. V.; Romannikov, V. N.; Zamaraev, K. I. *J. Am. Chem. Soc.* **1995**, *117*, 3615–3616.

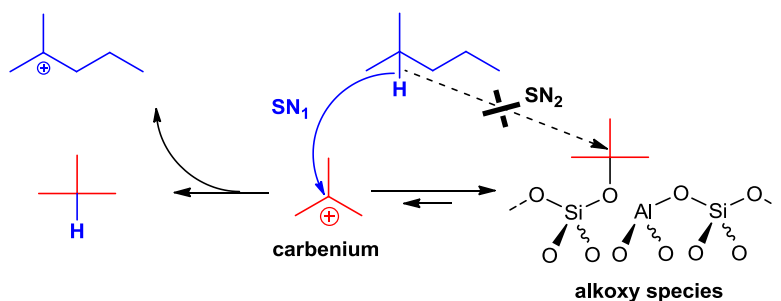
²¹⁸ Luzgin, M. V.; Romannikov, V. N.; Stepanov, A. G.; Zamaraev, K. I. *J. Am. Chem. Soc.* **1996**, *118*, 10890–10891.

²¹⁹ Franco, M.; Rosenbach, N.; Ferreira, G. B.; Guerra, A. C. O.; Kover, W. B.; Turci, C. C.; Mota, C. J. A. *J. Am. Chem. Soc.* **2008**, *130*, 1592–1600.



Scheme 30. Hydride transfer between 2-methylpentane and isobutane by Sommer et al.

The deuteride and hydride transfer reaction leading to the formation of deuterated 2-methylpentane and isobutane was rationalized by the existence of carbenium ions as reaction intermediates. Indeed, even if alkoxides are considered the most stable species, it is reasonably not possible to perform a $\text{S}_{\text{N}}2$ reaction on such sterically hindered tertiary centers (Scheme 31).



Scheme 31. Necessity of carbeniums as reaction intermediates in the hydride transfer process.

Therefore, the authors suggested that a small fraction of carbenium ions must be present to enable the hydride transfer.

1.2.2. Direct exchange versus carbenium type mechanism

Further to the early study of Hindin et al., numerous research groups investigated the reaction of small alkanes ranging from C1 to C7 over various deuterated acid catalysts such as zeolites,²²⁰ heteropolyacids²²¹ or sulfated zirconias.²²²

While branched alkanes reacted well at temperatures as low as room temperature, linear ones remained unreactive. Whatever the solid acid and the branched alkane, exchange always occurred at the hydrons vicinal to the branching, as found initially by Hindin and co-workers.²⁰⁹

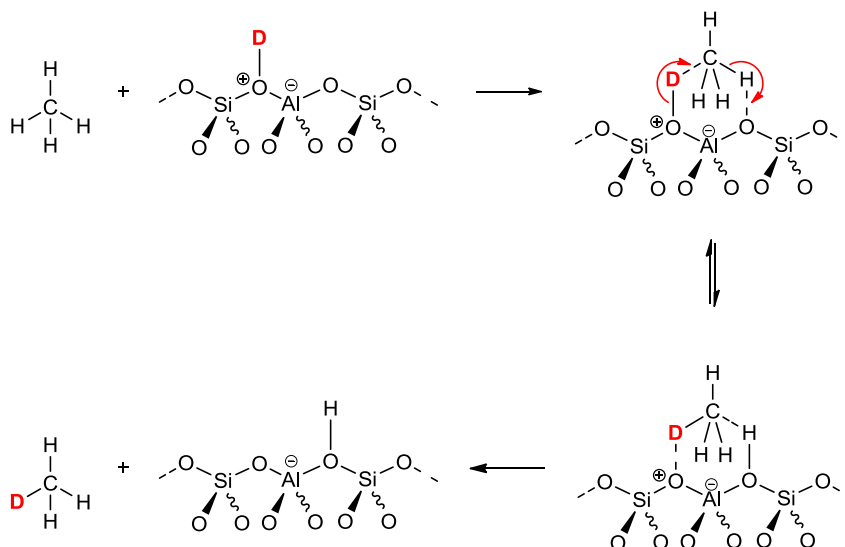
In the case of methane, ethane and neopentane, which cannot give an olefin by deprotonation, higher temperatures were required for the exchange to take place. Similarly, other linear alkanes exchanged hydrons at temperatures higher than 150 °C. To account for these observations, numerous experimental studies as well as theoretical calculations were carried out and proposed a concerted mechanism involving a pentacoordinated carbon similar to a carbonium ion as transition state (Scheme 32).^{220e,223}

²²⁰ (a) Mota, C. J. A.; Martins, R. L. *J. Chem. Soc., Chem. Commun.* **1991**, 0, 171–173. (b) Mota, C. J. A.; Nogueira, L.; Kover, W. B. *J. Am. Chem. Soc.* **1992**, *114*, 1121–1123. (c) Sommer, J.; Hachoumy, M.; Garin, F.; Barthomeuf, D.; Vedrine, J. *J. Am. Chem. Soc.* **1995**, *117*, 1135–1136. (d) Engelhardt, J.; Hall, W. K. *J. Catal.* **1995**, *151*, 1–9. (e) Schoofs, B.; Martens, J. A.; Jacobs, P. A.; Schoonheydt, R. A. *J. Catal.* **1999**, *183*, 355–367. (f) Schoofs, B.; Schuermans, J.; Schoonheydt, R. A. *Microporous Mesoporous Mater.* **2000**, *35–36*, 99–111.

²²¹ Essayem, N.; Coudurier, G.; Vedrine, J. C.; Habermacher, D.; Sommer, J. *J. Catal.* **1999**, *183*, 292–299.

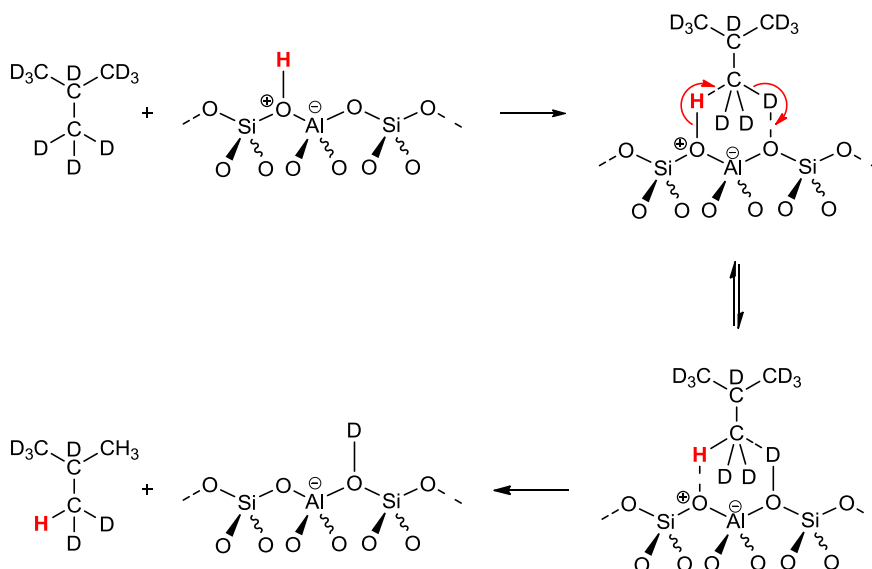
²²² (a) Hua, W.; Sassi, A.; Goepfert, A.; Taulelle, F.; Lorentz, C.; Sommer, J. *J. Catal.* **2001**, *204*, 460–465. (b) Haouas, M.; Walspurger, S.; Taulelle, F.; Sommer, J. *J. Am. Chem. Soc.* **2004**, *126*, 599–606. (c) Sommer, J.; Habermacher, D.; Hachoumy, M.; Jost, R.; Reynaud, A. *Appl. Catal. A Gen.* **1996**, *146*, 193–205.

²²³ (a) Vollmer, J. M.; Truong, T. N. *J. Phys. Chem. B* **2000**, *104*, 6308–6312. (b) Lercher, J. A.; Santen, R. A.; Vinek, H. *Catal. Lett.* **1994**, *27*, 91–96. (c) Narbeshuber, T. F.; Stockenhuber, M.; Brait, A.; Seshan, K.; Lercher, J. A. *J. Catal.* **1996**, *160*, 183–189. (d) Stepanov, A. G.; Arzumanov, S. S.; Luzgin, M. V.; Ernst, H.; Freude, D.; Parmon, V. N. *J. Catal.* **2005**, *235*, 221–228. (e) Esteves, P. M.; Nascimento, M. A. C.; Mota, C. J. A. *J. Phys. Chem. B* **1999**, *103*, 10417–10420.



Scheme 32. Direct exchange of methane over acidic zeolite : reaction mechanism

For branched alkanes which undergo a regioselective H/D exchange exclusively at the methyl groups, this mechanism was also suggested by some authors.^{208a,223e-224} Notably, White et al. observed this regioselective exchange between perdeuterated isobutane and H-ZSM-5 at room temperature (Scheme 33).^{208a,224}

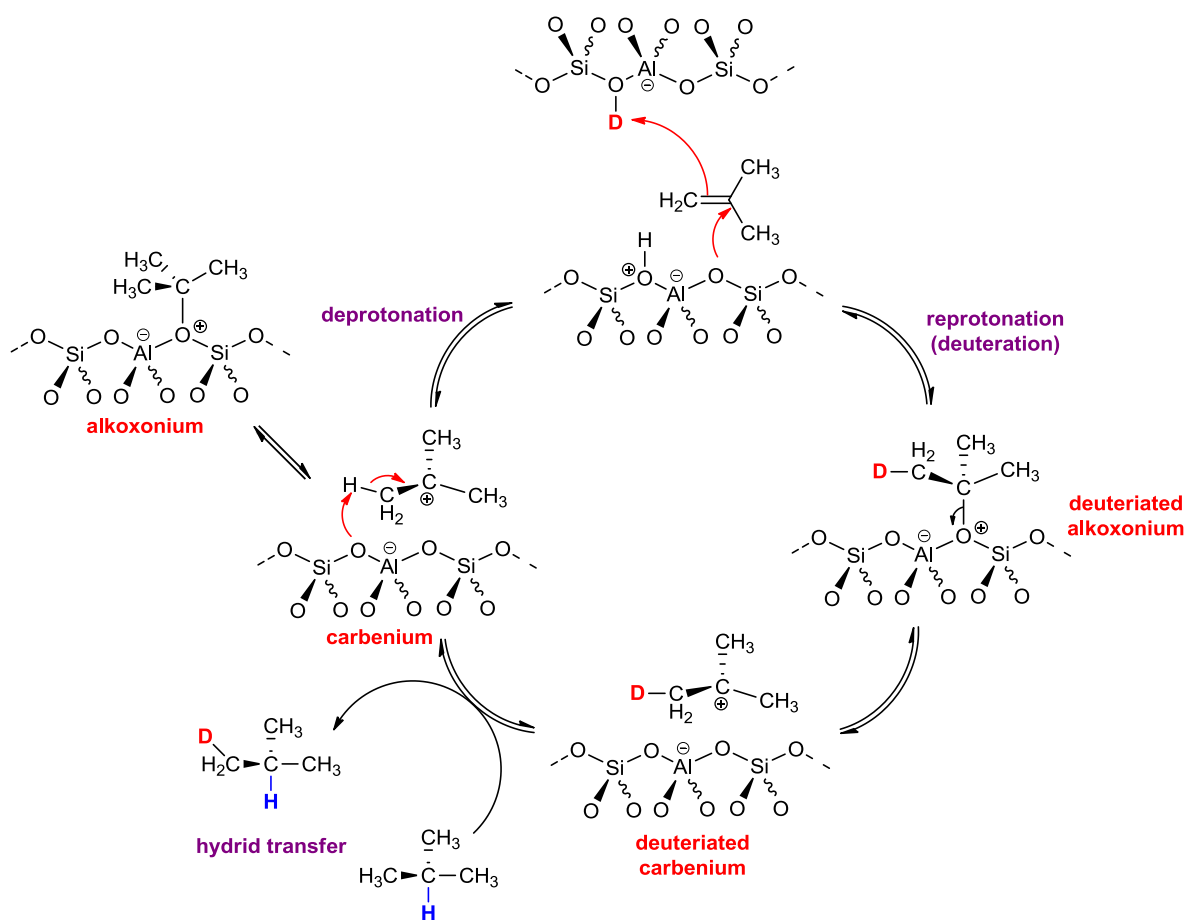


Scheme 33. Direct exchange proposed for isobutane over acidic zeolite.

They rationalized the regioselectivity by the better accessibility of the methyl groups toward the catalyst surface, compared to the methine one. However, it was argued that isobutane was

²²⁴ Sremaniak, L. S.; Whitten, J. L.; Truitt, M. J.; White, J. L. *J. Phys. Chem. B* **2006**, *110*, 20762–20764.

not a representative example. Indeed, the regioselectivity is the same whether it is based on the accessibility of the methyl substituents or on the deuteration of alkene intermediates according to the Markovnikov rule. To make this issue clear, Sommer et al. reinvestigated H/D exchanges at room temperature between various types of alkanes and deuterated zeolites.^{208b-c} All isoalkanes underwent exchanges exclusively next to the tertiary center. Linear alkanes such as *n*-butane or *n*-hexane remained untouched. As already proposed by Hindin et al.,²⁰⁹ they suggested a carbenium type mechanism, accounting for the regioselectivity observed by the involvement of alkene intermediates (Scheme 34).



Scheme 34. Reaction mechanism *via* carbenium intermediates.

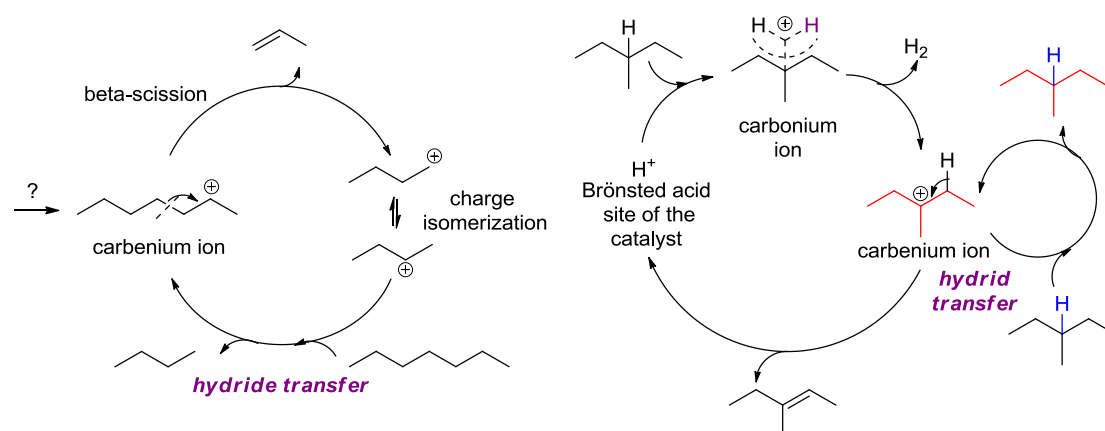
Finally, the work of Sommer et al. enabled to demonstrate that the regioselectivity was better correlated to the inherent reactivity of isoalkanes than to the accessibility of the protons toward the catalyst surface.

To sum up, both carbonium and carbenium related mechanisms are involved in the activation of small alkanes over solid acids. The existence of both species as reaction intermediates in the gas phase has been supported by quantum chemical calculations, if only their positive

charge is not easily accessible from the catalyst surface.²²⁵ For isoalkanes, reactive at room temperature, the carbenium type mechanism is the most viable possibility, based on the regioselectivity of the exchange. In the particular case of methane, ethane and neopentane, which only possess primary hydrogens, only direct exchanges *via* carbonium type intermediates can be considered, but require high temperatures to occur. For linear alkanes, activated at temperatures higher than 150 °C, probably both mechanisms are involved.

2. Focus on an important step of alkane conversion: the hydride transfer reaction

Hydride transfer is a reaction involved in most of the solid acids catalyzed petrochemical processes. As previously mentioned in the case of hydrocarbon cracking, whatever the mechanism, classical or protolytic, hydride transfer enables the desorption of the alkane. At the same time, it ensures the propagation of the reaction by regenerating a carbocationic intermediate, which maintains the catalytic cycle (Scheme 35).

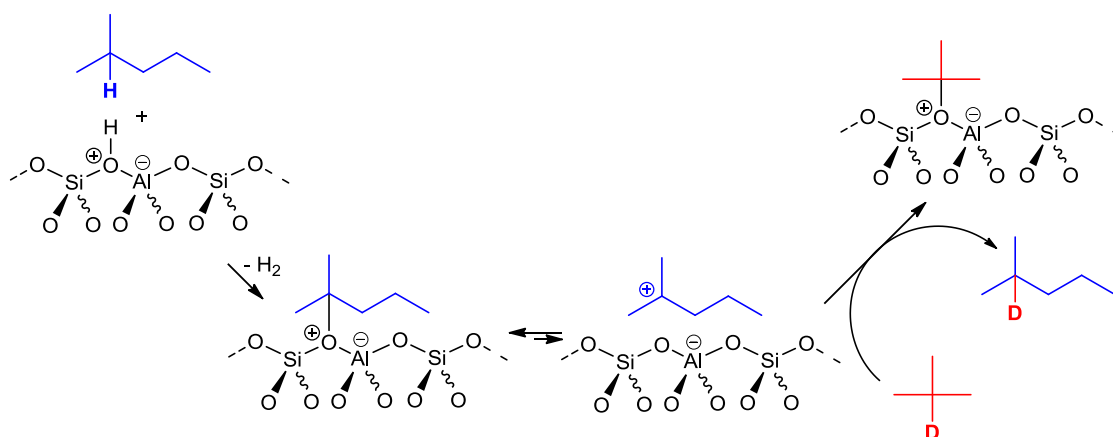


Scheme 35. Classical (left) and protolytic (right) cracking mechanisms involving hydride transfer.

Consequently, it seems essential to shed light on the mechanism of hydride transfer between carbenium ions and saturated hydrocarbons. However, under the drastic industrial conditions, the reaction is too fast to be studied. So far, there has been a lot of experimental studies of the

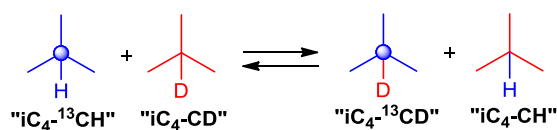
²²⁵ Boronat, M.; Corma, A. *Appl. Catal. A Gen.* **2008**, 336, 2–10.

hydride transfer process in the gas phase.²²⁶ Theoretical investigations based on density functional theory calculations and the *ab initio* MP2 method were also reported.²²⁷ Following the work of Sommer et al. who experimentally evidenced this bimolecular process by *ex situ* NMR using 2-methylpentane and deuterated isobutane (Scheme 36),^{208b} we were interested in determining the energetic and kinetic parameters of such a process.



Scheme 36. Hydride transfer between 2-methylpentane & isobutane studied by Sommer et al.

To achieve this goal, we intended to monitor by *in situ* MAS-NMR the H/D exchange occurring between ¹³C and ²H labeled isobutanes in the presence of H-USY zeolite. Similar to the exchange between 2-methylpentane and deuterated isobutane (Scheme 36),^{208b} we expected to observe the hydridee/protide transfer between the two alkanes, leading to the presence of four isotopologs at equilibrium (Scheme 37).



Scheme 37. Objective : the hydride transfer study between ¹³C and ²H labeled isobutanes.

It is noteworthy to mention that such exchange was already studied by mass spectroscopy in the presence of concentrated sulfuric acid.²²⁸ If successful, this experiment should enable to

²²⁶ Meot-Ner, M. In *Gas-Phase Ion Chemistry*; Bowers, M. T., Ed., Academic: New York, 1979; Vol. 1.

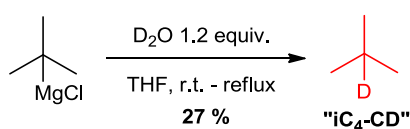
²²⁷ Boronat, M.; Viruela, P.; Corma, A. *J. Phys. Chem. B* **1997**, *101*, 10069–10074.

²²⁸ Beeck, O.; Otvos, J. W.; Stevenson, D. P.; Wagner, C. D. *J. Chem. Phys.* **1949**, *17*, 418–419.

determine for the first time the activation energy of the hydride transfer of isobutane, by direct experimental measurement.

2.1. Preparation of ^{13}C and ^2H labeled isobutanes

Isobutane-2- d_1 ($\text{iC}_4\text{-CD}$) has been already synthesized many times from Grignard reagents in view of H/D exchange studies.^{210,229} Based on a procedure reported by Sassi et al.,²³⁰ we prepared it in one step by addition of deuterium oxide to a commercial solution of *tert*-butylmagnesium chloride in THF (Scheme 38).



Scheme 38. Preparation of ^2H labeled isobutane.

With a boiling point of $-11.7\text{ }^\circ\text{C}$, the so-formed isobutane was recovered at the outlet of the condenser by condensation in a cold trap at $-117\text{ }^\circ\text{C}$ (mixture of ethanol and liquid nitrogen). In order to remove possible traces of isobutene formed by the competing elimination reaction, bromine was added to the trap, and the resulting gas was bubbled through two traps containing an aqueous solution of $\text{Na}_2\text{S}_2\text{O}_3$. The purified gas was finally recovered in a ball-shape glassware containing brine. Thanks to this method, the gas can be stored at ambient pressure, which is constantly maintained by addition or removal of brine. Moreover, the gas is easily available for analysis or further reaction through rubber septum.

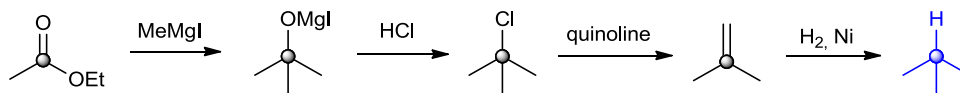
Concerning the synthesis of isobutane-2- C^{13} ($\text{iC}_4\text{-}^{13}\text{CH}$), there was only one precedent in the literature, dating back from 1950.²³¹ The procedure started from toxic ^{13}C labeled potassium cyanide, and required 6 steps in 28 % overall yield. Nevertheless, the end of the synthesis (Scheme 39) highlighted that ethyl acetate-2- C^{13} could be a suitable starting material for the preparation of isobutane-2- C^{13} . Actually, it turned out to be the cheapest commercially available candidate for the synthesis. The methodology used by Wagner et al. (Scheme 39)²³¹

²²⁹ Wagner, C. D.; Stevenson, D. P. *J. Am. Chem. Soc.* **1950**, *72*, 5785.

²³⁰ Sassi, A.; Goepfert, A.; Sommer, J.; Esteves, P. M.; Mota, C. J. *J. Labelled Compd. Radiopharm.* **1999**, *42*, 1023–1030.

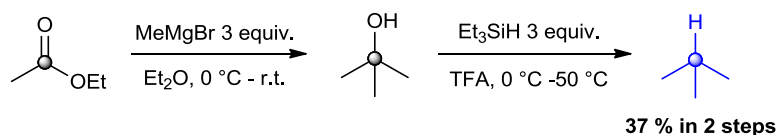
²³¹ Wagner, C. D.; Stevenson, D. P.; Otvos, J. W. *J. Am. Chem. Soc.* **1950**, *72*, 5786–5786.

relied on two successive additions of a Grignard reagent to ethyl acetate-2- C^{13} , leading after treatment with HCl to *tert*-butyl chloride-2- C^{13} . Elimination in the presence of quinoline followed by hydrogenation of isobutene-2- C^{13} finally yielded isobutane-2- C^{13} .



Scheme 39. Preparation of ^{13}H labeled isobutane by Wagner et al. in 1950.

We optimized this sequence and obtained the ^{13}C labeled alkane in two steps. Similar to the strategy of Wagner et al., we isolated *tert*-butyl alcohol-2- C^{13} after addition of 3 equivalents of a solution of methylmagnesium bromide in diethyl ether. Direct reduction of the alcohol to isobutane-2- C^{13} was then achieved by treatment with 3 equivalents of triethylsilane in trifluoroacetic acid (Scheme 40).



Scheme 40. Our improved preparation of ^{13}H labeled isobutane.

The reduction of various functional groups and notably alcohols into alkanes by organosilanes has been known for a long time.²³² The reaction proceeds best with secondary, tertiary or benzylic alcohols, which can lead to stabilized carbenium ions. Typical conditions employ trifluoroacetic acid which plays the role of catalyst and triethylsilane as hydride donor, due to its ease of handling and reactivity.^{232a,d}

Purification similar to isobutane-2- d_1 , including addition of bromine and bubbling through aqueous and organic solutions was necessary to remove traces of side products and achieve high purity of the gas. To finish, both gases were frozen in cold traps at -196 °C (liquid nitrogen) and pumped under vacuum in order to discard the presence of air.

Quantification of the ratio isobutane/air by comparison with a sample of commercial isobutane using GC analysis revealed a value of 93 % for $i\text{C}_4\text{-}^{13}\text{CH}$ and 99 % for $i\text{C}_4\text{-CD}$.

²³² (a) Carey, F. A.; Tremper, H. S. *J. Am. Chem. Soc.* **1968**, *90*, 2578–2583. (b) West, C. T.; Donnelly, S. J.; Kooistra, D. A.; Doyle, M. P. *J. Org. Chem.* **1973**, *38*, 2675–2681. (c) Mayr, H.; Dogan, B. *Tetrahedron Lett.* **1997**, *38*, 1013–1016. (d) Carey, F. A.; Tremper, H. S. *J. Org. Chem.* **1971**, *36*, 758–761.

The isotopic purity of each labeled isobutane was further assessed by analysis of their ^1H NMR spectrum using the DMfit program. Figure 15 shows the ^1H NMR spectrum (black) in the methyl and methine ranges of $i\text{C}_4\text{-}^{13}\text{CH}$ in $\text{C}_2\text{Cl}_4\text{D}_2$ as solvent. The peak at 1.56 ppm is due to the presence of water in the solvent. The signals related to $i\text{C}_4\text{-}^{13}\text{CH}$ and their corresponding J -patterns are reported on the blue spectrum. Non-labeled isobutane $i\text{C}_4\text{-CH}$, present as isotopic impurity, is visible in the methine range (green spectrum). From these data the ratio $i\text{C}_4\text{-}^{13}\text{CH}/i\text{C}_4\text{-CH}$ has been assessed to 98/2.

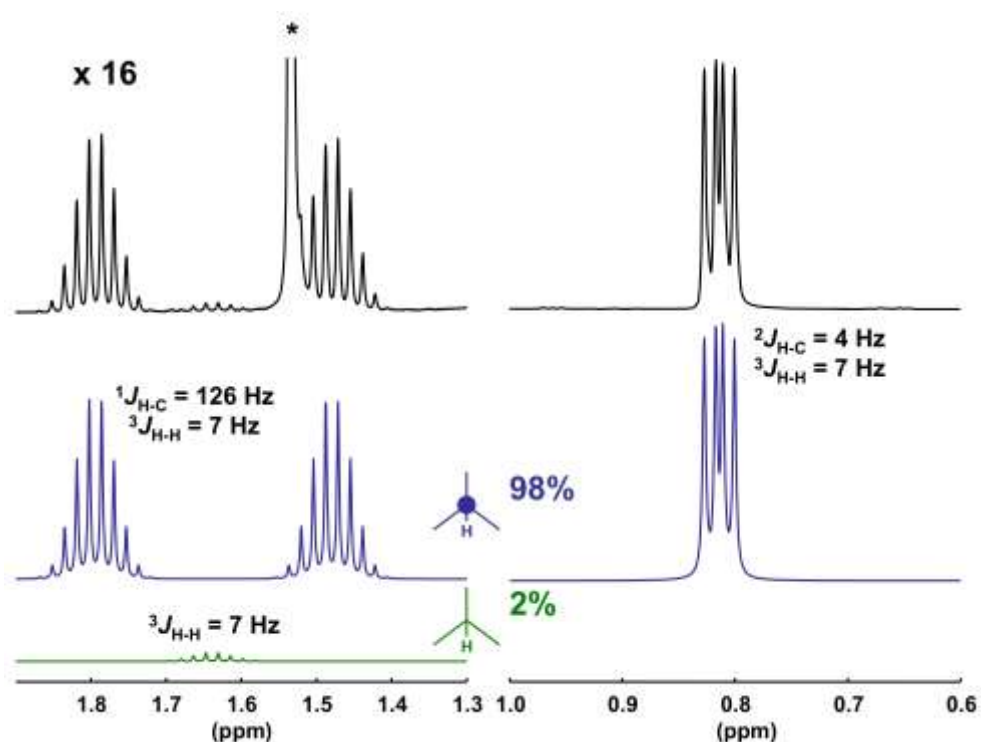


Figure 15. Experimental ^1H NMR spectrum (black) in the methyl and methine ranges of $i\text{C}_4\text{-}^{13}\text{CH}$ in $\text{C}_2\text{Cl}_4\text{D}_2$. “*” is due to some water present in the solvent. Calculated J -patterns for $i\text{C}_4\text{-}^{13}\text{CH}$ (blue) and $i\text{C}_4\text{-CH}$ (green) present as isotopic impurity are shown.

^1H NMR spectra of $i\text{C}_4\text{-CD}$ in $\text{C}_2\text{Cl}_4\text{D}_2$ as solvent is reported in Figure 16 (black). A similar analysis has been performed, revealing that 8 % of isobutane $i\text{C}_4\text{-CH}$ was present as isotopic impurity.

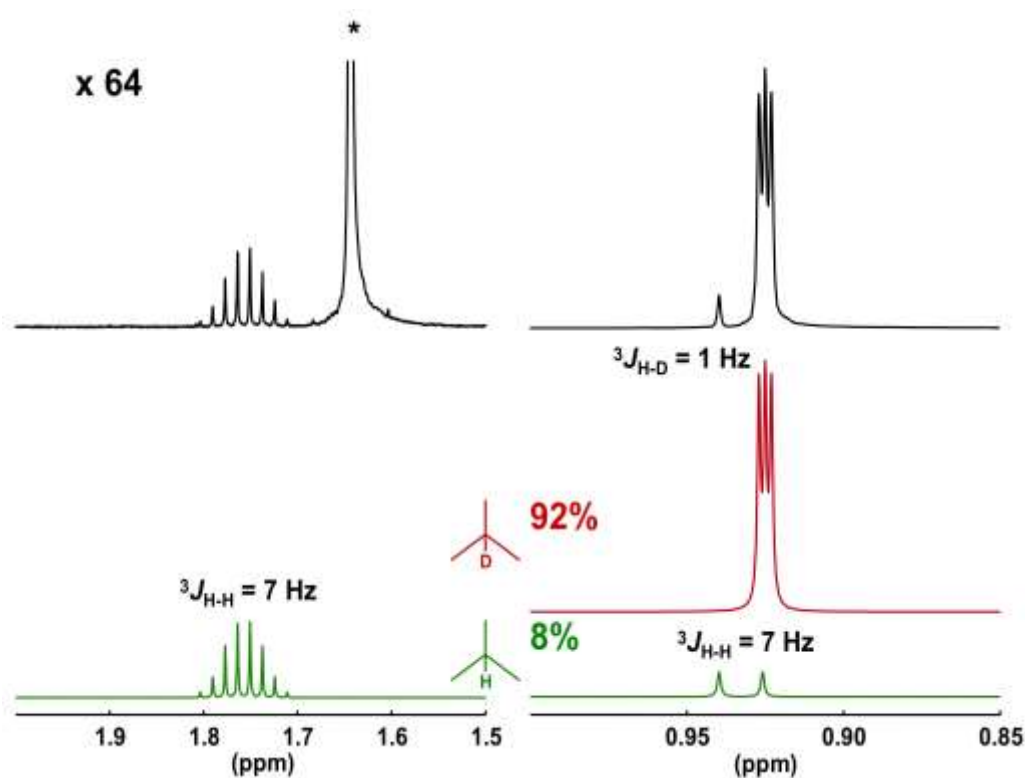


Figure 16. Experimental ${}^1\text{H}$ NMR spectrum (black) in the methyl and methine ranges of iC_4-CD in $C_2Cl_4D_2$. “*” is due to some water present in the solvent. Calculated J -patterns for iC_4-CH (red) and iC_4-CD (green) present as isotopic impurity are shown.

In the end, both isobutane-2- d_1 and isobutane-2- C^{13} were successfully prepared in a straightforward manner, in modest yield but sufficient amount and purity to be used further in the hydride transfer reaction. A 50/50 mixture of the two gases was prepared to this purpose. Based on the ${}^1\text{H}$ NMR spectrum of the mixture, the DMfit program calculated a final composition $iC_4-^{13}CH:iC_4-CD:iC_4-CH$ of 42:53:5.

2.2. The hydride transfer study: experimental results

Specific homemade device was used to activate the catalyst, load the mixture of gases and seal the 4 mm NMR rotor without exposure to the ambient atmosphere prior to each experiment. Around 65 mg of H-USY zeolite (Si/Al = 11; 4.33 mmol H acid/g)²³³ was first dried in oven at 250 °C for 54 h and subsequently outgassed under vacuum ($< 10^{-7}$ mbar) at room temperature for 3 h. After activation, the amount of H-USY was reduced to 50 mg. After introduction of 0.5 mL of the 50/50 gaseous mixture $iC_4-^{13}CH/iC_4-CD$ (0.4 mmol iC_4/g)

in the rotor containing activated H-USY, the hydride transfer between the two isotopologs was directly monitored by *in situ* ^1H and $^{13}\text{C}\{^1\text{H}\}$ MAS NMR spectroscopy. 5 kinetic experiments were carried out at $T = 297\text{ K}$, 307 K , 312 K , 317 K and 327 K , and recorded each time by ^1H and $^{13}\text{C}\{^1\text{H}\}$ detection, either direct or *via* inept transfer (DEPT45).

Each detection mode possesses its own advantages and drawbacks. ^1H NMR exhibits high sensitivity but in the present study, suffered from the overlap of the H-USY silanol signals with the $i\text{C}_4\text{-}^{13}\text{CH}/i\text{C}_4\text{-}^{13}\text{CD}$ methine signals. Indeed, USY exhibits 3 broad signals at $\delta = 1.6$, $2.7\text{--}2.8$, and $4.4\text{--}5.0$ ppm, attributed to the silanol group SiOH, Brønsted protons SiOHAl in large cavities, and SiOHAl in hexagonal prism units, respectively (Figure 17).²³⁴

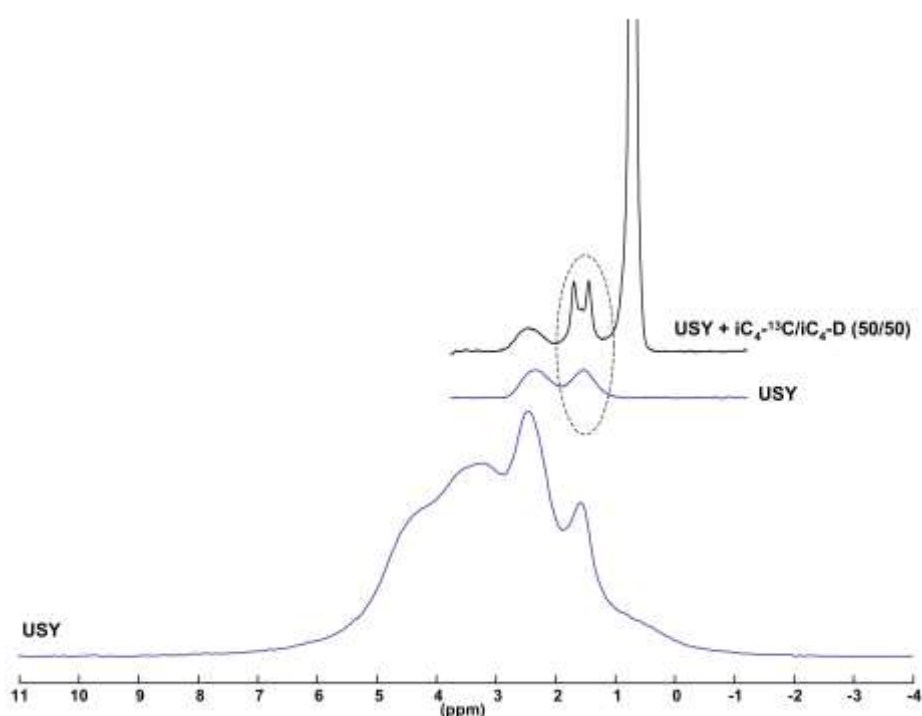


Figure 17. Experimental ^1H NMR spectra of H-USY zeolite (blue), and the 50/50 gaseous mixture $i\text{C}_4\text{-}^{13}\text{CH}/i\text{C}_4\text{-}^{13}\text{CD}$ adsorbed on H-USY (black).

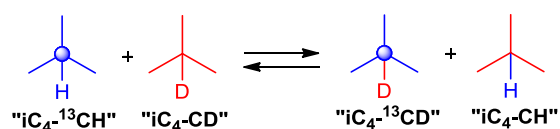
On the other hand, $^{13}\text{C}\{^1\text{H}\}$ direct detection exhibits good resolution but low sensitivity. The $^{13}\text{C}\{^1\text{H}\}$ detection *via* inept transfer (DEPT45) enables to overcome this, by providing a high sensitivity to carbon signals carrying protons. However, this method results in only partial information: the ^{13}C labeled carbon of $i\text{C}_4\text{-}^{13}\text{CH}$ will be observed but not the one of $i\text{C}_4\text{-}^{13}\text{CD}$.

²³³ Haouas, M.; Fink, G.; Taulelle, F.; Sommer, J. *Chem.--Eur. J.* **2010**, *16*, 9034–9039.

²³⁴ (a) Brunner, E. *J. Mol. Struct.* **1995**, *355*, 61–85. (b) Kao, H.-M.; Grey, C. P. *J. Phys. Chem.* **1996**, *100*, 5105–5117.

In the end, ^1H and ^{13}C NMR proved complementary since the former allowed the observation of $i\text{C}_4\text{-}^{13}\text{CH}$ consumption and simultaneous $i\text{C}_4\text{-CH}$ formation, while the latter enabled to follow the conversion of $i\text{C}_4\text{-}^{13}\text{CH}$ into $i\text{C}_4\text{-}^{13}\text{CD}$.

The four isotopologs (Scheme 27) were differentiated by ^1H , ^2H and ^{13}C NMR, thanks to the different scalar coupling between the various nuclei, i.e., $^1J(^{13}\text{C}\text{-}^1\text{H})$ and $^1J(^{13}\text{C}\text{-}^2\text{H})$.



Scheme 27. Expected equilibrium between the different isotopologs.

In the proton observation, the main information was found in the methine range, where the resolution was higher than those of the methyl groups. Indeed, although both $i\text{C}_4\text{-}^{13}\text{CH}$ and $i\text{C}_4\text{-CH}$ methines resonated at the same chemical shift (1.6 ppm), they could be distinguished because the former appeared as a doublet ($^1J_{\text{C-H}}$) and the latter as a singlet. The situation is better illustrated in Figure 18, which shows the stack plot ^1H NMR spectra of the H/D exchange performed at 312 K over a period of 64 h. The expansion in the methine range highlights the decrease of the $i\text{C}_4\text{-}^{13}\text{CH}$ doublet with simultaneous increase of the $i\text{C}_4\text{-CH}$ singlet.

In the proton decoupled carbon observation, the main signal arised from the ^{13}C labeled carbon, which appeared as a singlet at 23.3 ppm for $i\text{C}_4\text{-}^{13}\text{CH}$ and as a triplet ($^1J_{\text{C-D}}$) at 22.8 ppm for $i\text{C}_4\text{-}^{13}\text{CD}$. Initially, we observed the singlet of the ^{13}C labeled carbon of $i\text{C}_4\text{-}^{13}\text{CH}$, which progressively decreased over time to the expense of the 1:1:1 triplet related to the ^{13}C labeled carbon bound to deuterium in produced $i\text{C}_4\text{-}^{13}\text{CD}$ (Figure 19). The evolution of both ^1H and ^{13}C NMR spectra perfectly represented the H/D exchange process, which took place between the ^{13}C - and D-labeled isobutanes.

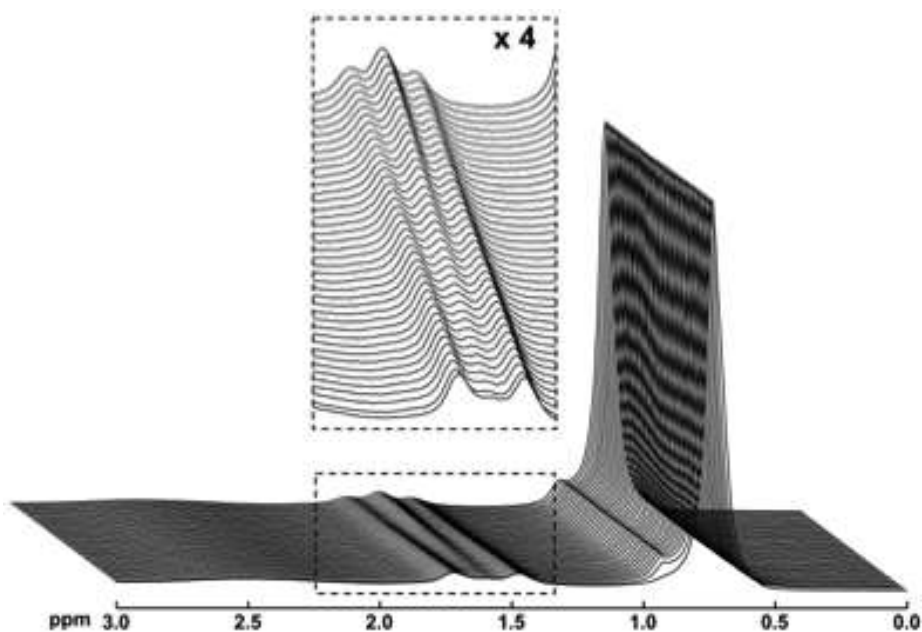


Figure 18. Stack plot ^1H NMR spectra of the H/D exchange between $i\text{C}_4\text{-}^{13}\text{CH}$ and $i\text{C}_4\text{-CD}$ at 312 K over a period of 64 h.

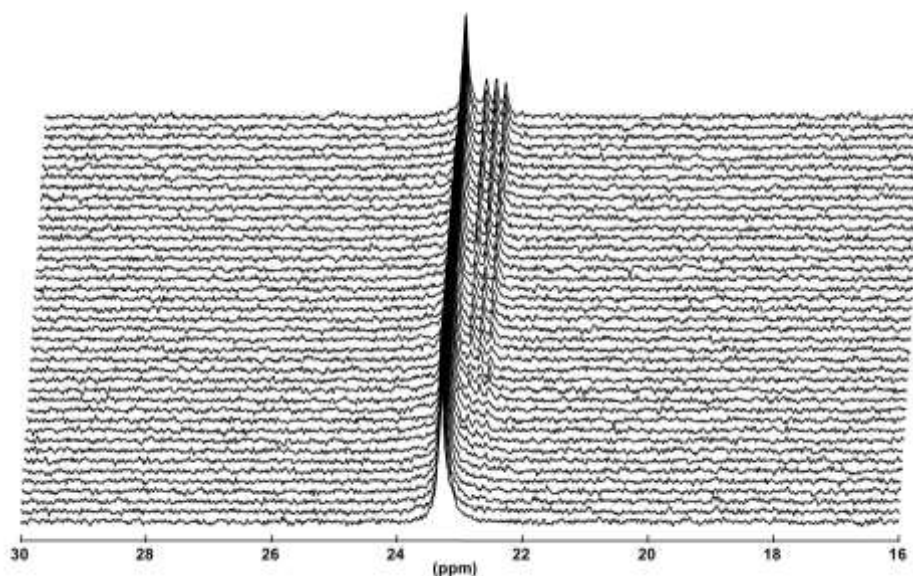


Figure 19. Stack plot $^{13}\text{C}\{^1\text{H}\}$ NMR spectra of the H/D exchange between $i\text{C}_4\text{-}^{13}\text{CH}$ and $i\text{C}_4\text{-CD}$ at 312 K over a period of 64 h.

2.3. The hydride transfer study: interpretation of the results

Spectral decomposition was necessary to provide the magnitude of the resonances. As an example, ^1H NMR spectra were decomposed as depicted in Figure 20. The green resonance area A1-4 represented the methyl protons of the four isotopologs. The pink areas B1 and B2

corresponded to the methine protons of $iC_4\text{-}^{13}CH$ and $iC_4\text{-}CD$, respectively. For the simulation of each spectrum it was considered that, whatever the reaction time, the ratio $A1\text{-}4/(B1 + B2)$ had to be equal to 18. In order to fulfill this condition, the C2 area corresponding to the silanol groups of H-USY was fixed.

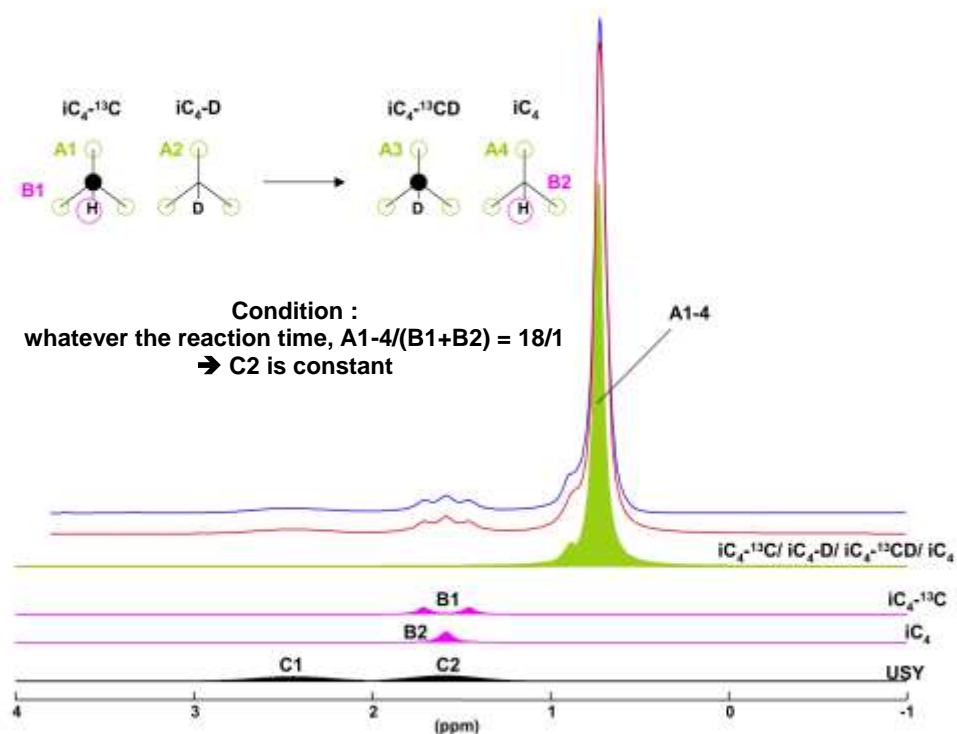


Figure 20. Experimental (blue) and calculated (red) 1H MAS NMR spectra of the 50:50 mixture of $iC_4\text{-}^{13}CH:iC_4\text{-}CD$ adsorbed on USY zeolite.

Then, intensities related to each compound and corresponding to their concentrations were plotted as a function of time for each experiment (each temperature). For example, the intensities of the methine protons in 1H NMR spectra provided the consumption of $iC_4\text{-}^{13}CH$, and the formation of $iC_4\text{-}CH$, depicted in Figure 21 (filled and open circles, respectively).

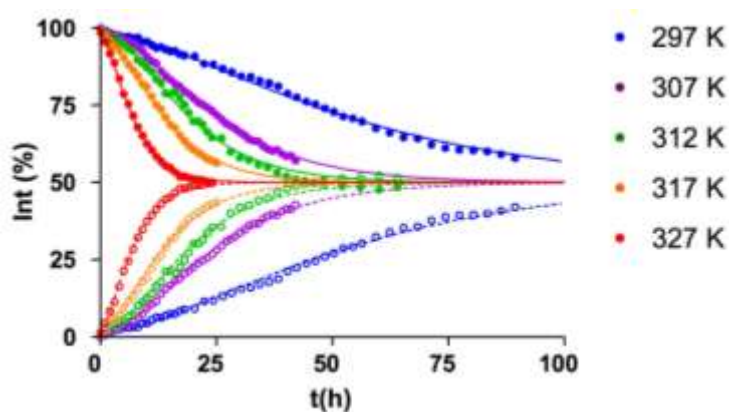


Figure 21. Kinetics of H/D exchange between $iC_4-^{13}CH$ and iC_4-CD on USY zeolite: methine 1H NMR signal area of $iC_4-^{13}CH$ (filled circles) and iC_4-CH (open circles) as a function of time at various temperatures.

From the latter graph it can be noticed that the consumption of $iC_4-^{13}CH$ and the formation of iC_4-CH were S-shaped, which suggested a complex behavior with two H/D exchange regimes. From this, we assumed that the reaction involved two consecutive steps and an intermediate species, as schematically represented in Figure 22.

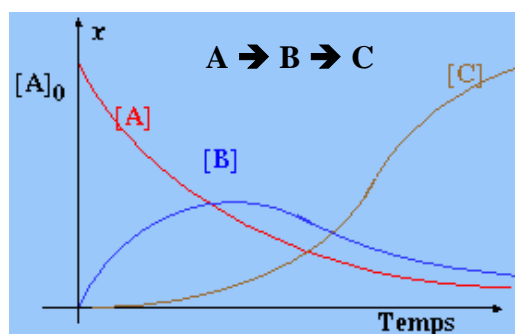
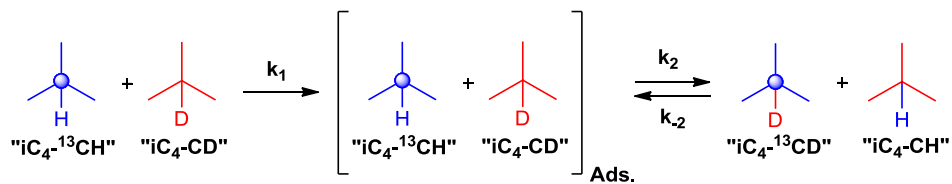


Figure 22. Schematic representation of the consumption of $iC_4-^{13}CH$ (A+B) and formation of iC_4-CD (C).

Consequently, the H/D exchange may be described as follows: the formation of the reactive intermediates in a first place, and the hydridee exchange *via* framework-solvated carbocationic intermediates in a second place (Scheme 41).^{208b} The first step can be interpreted as an induction period necessary to create the active species,^{208a,222b,235} probably adsorbed at the surface of the active site of the catalyst.²³⁶

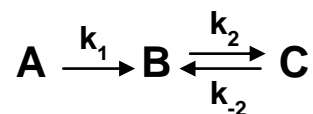
²³⁵ Arzumanov, S. S.; Stepanov, A. G.; Freude, D. *J. Phys. Chem. C* **2008**, *112*, 11869–11874.

²³⁶ Bučko, T.; Benco, L.; Hafner, J.; Ángyán, J. G. *J. Catal.* **2007**, *250*, 171–183.



Scheme 41. Interpretation of the experimental results : a two steps reaction

According to Scheme 41, data analysis was performed using a two consecutive steps model, taking into account this adsorption phenomenon (Equation 6).



Equation 6. Two consecutive steps model used for the interpretation.

From this equation, we were able to deduce the analytic expressions of the concentrations of A, B and C, assuming first-order reactions and $k_2 = k_{-2}$:

$$\begin{array}{l}
 \text{i)} \quad -\frac{d[A]}{dt} = [A]k_1 \\
 \text{ii)} \quad \frac{d[B]}{dt} = [A]k_1 - [B]k_2 + [C]k_{-2} \\
 \text{iii)} \quad [A] + [B] + [C] = a
 \end{array}$$

$$\begin{array}{l}
 \text{i)} \quad -\frac{d[A]}{dt} = [A]k_1 \\
 \quad \quad -\frac{d[A]}{[A]} = k_1 dt \\
 \quad \quad \ln[A] = -k_1 t + \text{Cte} \\
 \quad \quad \text{For } t=0, [A] = a \\
 \quad \quad \text{Cte} = \ln a \\
 \quad \quad \ln[A] = -k_1 t + \ln a \\
 \quad \quad \boxed{[A] = ae^{-k_1 t}}
 \end{array}$$

$$\text{ii) } \frac{d[B]}{dt} = [A]k_1 - [B]k_2 + [C]k_{-2}$$

$$\text{If } k_2 = k_{-2}$$

$$\frac{d[B]}{dt} = [A]k_1 + ([C] - [B])k_2$$

$$[C] = a - [A] - [B]$$

$$\frac{d[B]}{dt} = [A]k_1 + (a - [A] - 2[B])k_2$$

$$\frac{d[B]}{dt} = (k_1 - k_2)[A] + k_2a - 2k_2[B]$$

$$\frac{d[B]}{dt} = (k_1 - k_2)ae^{-k_1t} + k_2a - 2k_2[B]$$

$$\frac{d[B]}{dt} + 2k_2[B] = (k_1 - k_2)ae^{-k_1t} + k_2a$$

$$\frac{d[B]}{dt} e^{2k_2t} + 2k_2[B]e^{2k_2t} = (k_1 - k_2)ae^{-k_1t}e^{2k_2t} + k_2ae^{2k_2t}$$

$$\frac{d([B]e^{2k_2t})}{dt} = (k_1 - k_2)ae^{(2k_2 - k_1)t} + k_2ae^{2k_2t}$$

$$[B]e^{2k_2t} = \frac{k_1 - k_2}{2k_2 - k_1} \cdot ae^{(2k_2 - k_1)t} + \frac{a}{2}e^{2k_2t} + Cte$$

$$t = 0, [B] = 0$$

$$Cte = -a \left(\frac{k_1 - k_2}{2k_2 - k_1} + \frac{1}{2} \right) = \frac{-ak_1}{2(2k_2 - k_1)}$$

$$[B] = \frac{a}{2} \left(\frac{2k_1 - 2k_2}{2k_2 - k_1} \cdot e^{-k_1t} - \frac{k_1}{2k_2 - k_1} \cdot e^{-2k_2t} + 1 \right)$$

$$\text{iii) } [A] + [B] = \frac{a}{2} \left(\frac{2k_1 - 2k_2}{2k_2 - k_1} \cdot e^{-k_1t} - \frac{k_1}{2k_2 - k_1} \cdot e^{-2k_2t} + 1 \right) + ae^{-k_1t}$$

$$[A] + [B] = \frac{a}{2} \left(\frac{2k_2}{2k_2 - k_1} \cdot e^{-k_1t} - \frac{k_1}{2k_2 - k_1} \cdot e^{-2k_2t} + 1 \right)$$

$$[C] = a - ([A] + [B]) = \frac{a}{2} \left(\frac{-2k_2}{2k_2 - k_1} \cdot e^{-k_1t} + \frac{k_1}{2k_2 - k_1} \cdot e^{-2k_2t} + 1 \right)$$

Finally, since NMR cannot distinguish between the adsorbed and desorbed state corresponding to A and B, the expressions of the concentrations or intensities for the consumed and produced isobutanes can be written as follows:

$$\text{Consumption of the reactants (A+B): } I = \frac{I_0}{2} \left(\frac{2k_2}{2k_2 - k_1} \cdot e^{-k_1(t+t_0)} - \frac{k_1}{2k_2 - k_1} \cdot e^{-2k_2(t+t_0)} + 1 \right)$$

$$\text{Formation of the products (C): } I = \frac{I_0}{2} \left(\frac{-2k_2}{2k_2 - k_1} \cdot e^{-k_1(t+t_0)} + \frac{k_1}{2k_2 - k_1} \cdot e^{-2k_2(t+t_0)} + 1 \right)$$

Equation 7. Calculated concentrations for the simulation of the experimental curves.

where $I_0 = a$ is the starting amount of protons in the methine position or ^{13}C labeled carbon (100%) for ^1H or ^{13}C detection respectively, and t_0 is the offset time to compensate the delay from the origin of the kinetics. Simulations of the experimental curves (superimposed to the experimental data in Figure 21) using Equation 7 allowed to determine the rate constants k_1 and k_2 of both steps, i.e., ‘adsorption’ and H/D exchange.

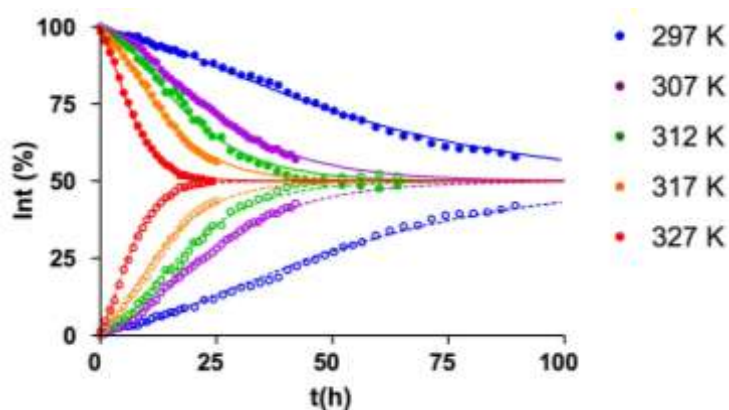


Figure 21. Kinetics of H/D exchange between $i\text{C}_4\text{-}^{13}\text{CH}$ and $i\text{C}_4\text{-CD}$ on USY zeolite: methine ^1H NMR signal area of $i\text{C}_4\text{-}^{13}\text{CH}$ (filled circles) and $i\text{C}_4\text{-CH}$ (open circles) as a function of time at various temperatures. Full lines represent the corresponding simulated intensities.

From the Arrhenius equation (Equation 8), we were able to deduce the apparent activation energy of the hydride transfer between $i\text{C}_4\text{-}^{13}\text{CH}$ and $i\text{C}_4\text{-CD}$, *via* the corresponding Arrhenius plots (Equation 8, Figure 23), where A is the pre-exponential factor and R the gas constant.

$$k = Ae^{-\frac{E_a}{RT}}$$

$$\ln(k) = \ln(A) - \frac{E_a}{RT}$$

Equation 8. Arrhenius equation (left) and equation of the Arrhenius plot (right).

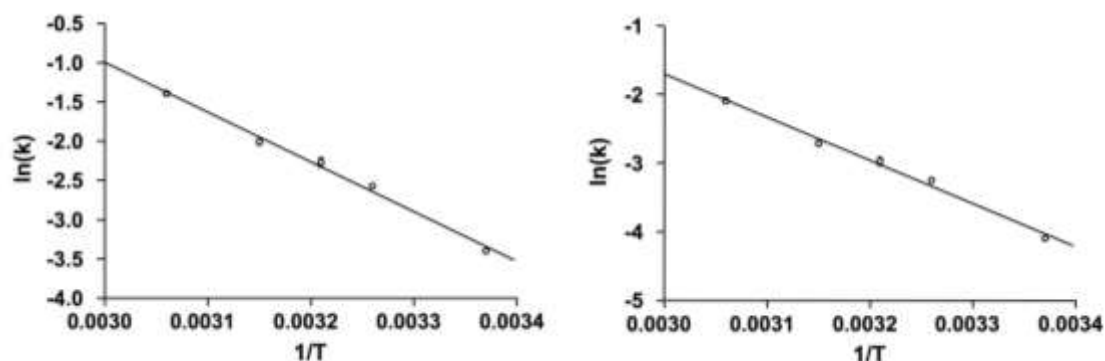


Figure 23. Arrhenius plots of k_1 (left) and k_2 (right) related to ^1H NMR data.

The rate constant values k_1 and k_2 for ^1H and ^{13}C NMR, as well as the corresponding apparent activation energy are reported in Table 8. The values of k_1 were found systematically twice those of k_2 , which suggested that stationary H/D exchange regime took place once intermediate species become prominent. Consequently, Arrhenius plots of k_1 and k_2 (Figure 23) provided the same apparent activation energy value. In addition, ^1H and ^{13}C NMR afforded comparable results within experimental error, confirming that both measurements were related to the same process (Table 8).

Table 8. Calculated rate constants k_1 and k_2 obtained from fitting the experimental ^1H and ^{13}C NMR data using Equation 7 and the corresponding apparent activation energy for the hydride transfer.

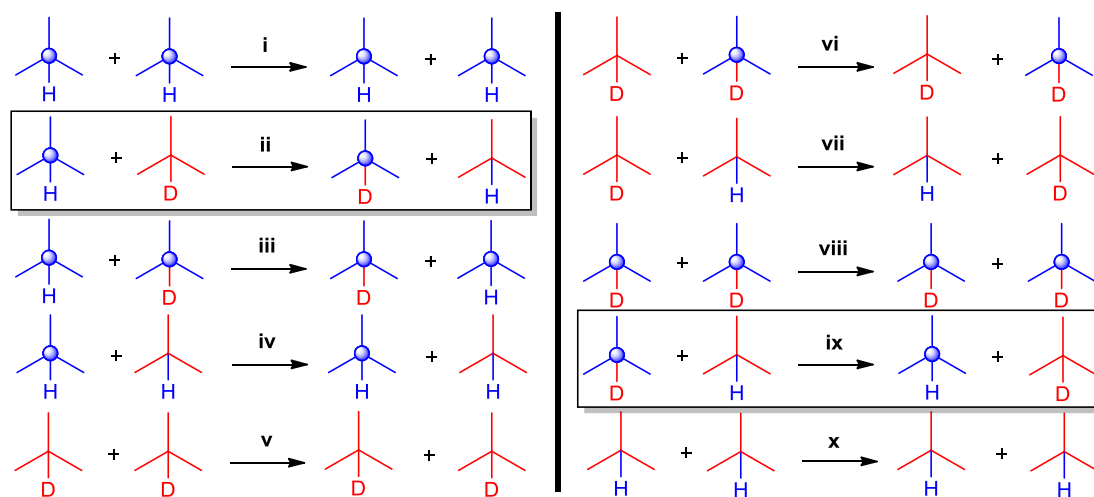
T (K)	$k_1 (10^{-3} \text{ h}^{-1})$		$k_2 (10^{-3} \text{ h}^{-1})$		$E_a (\text{kJ}\cdot\text{mol}^{-1})$	
	^1H	^{13}C	^1H	^{13}C	^1H	^{13}C
297	33.5 ± 0.8	31.5 ± 1.4	16.8 ± 0.4	15.7 ± 0.7		
307	76.9 ± 1.4	69.1 ± 2.8	38.6 ± 0.7	34.5 ± 1.4		
312	103.2 ± 6.7	91.3 ± 5.0	51.3 ± 3.3	46.2 ± 2.6	52 ± 1	56 ± 1
317	133.4 ± 5.4	118.3 ± 5.3	66.7 ± 2.7	59.1 ± 2.6		
327	248.1 ± 6.4	275.5 ± 20.3	124.0 ± 3.2	137.9 ± 10.2		

When comparing the values of the rate constant k_2 related to the hydride transfer process with the values obtained for the “classic” H/D exchange between hydrocarbon and zeolite,^{222b} it turns out that k_2 values are five times lower (Table 9).

Table 9. Comparison of the activation energy and rate constant values at different temperatures between the present hydride transfer study and the H/D exchange between perdeuterated 2-methylpentane and H-USY.

	$iC_4\text{-}^{13}CH/iC_4\text{-}CD$	deuterated 2-MP/ H-USY ^{222b}	ratio
$K_{297} (h^{-1})$	0.016	0.083	5
$K_{307} (h^{-1})$	0.036	0.164	5
$K_{317} (h^{-1})$	0.061	0.363	6
$E_a (kJ.mol^{-1})$	52	58	1

This difference can be accounted for the “isotopic dilution” (50:50 $^{13}C:^{12}C$ and $^2H:^1H$ in methine position) occurring in the present hydride transfer study. The $k_2/K_{\text{classic H/D}}$ ratio of 1/5 is due to the probability of 1/5 to observe the expected hydride transfer process in our NMR experiments. Indeed, among the ten possible bimolecular reactions between the four isotopologs (Scheme 42), only two involving distinct 2H and ^{13}C labeled molecules could be actually distinguished by NMR.



Scheme 42. Representation of the ten possible bimolecular reactions between the four isotopologs. Only the two framed could be observed by NMR.

Therefore, the actual k_2 rate constant of the hydride transfer process should be 5 times higher, which results in values very close to those calculated for the classic H/D exchange in the same

temperature range (Table 9).^{222b} This result suggested that both exchanges are related to a common process. In addition, the activation energy of 52-56 kJ/mol calculated here for the hydride transfer between labeled isobutanes is comparable to typical activation energies of H/D exchanges between zeolites and hydrocarbons operating *via* carbenium intermediates.^{208a,222a,233,237} It is known that in comparison, mechanisms involving pentavalent carbonium ion type intermediates, as for methane or ethane, require much higher activation energy (> 100 kJ/mol).²³⁸

In summary, we were able to observe the hydride transfer reaction between ¹³C and ²H labeled isobutanes by *in situ* MAS NMR at room temperature. Experimental results showing an apparent slow reaction enabled to distinguish two consecutive steps, involving the formation of intermediate adsorbed species in a first place and subsequent hydride transfer. The rate constant and activation energy values of the process were in perfect concordance with those of classical exchanges between zeolites and hydrocarbons involving carbenium type mechanisms. These results represent the first direct measurement of the kinetic and energetic parameters of such a reaction, and provided further evidence of the involvement of carbenium intermediates *via* indirect elimination/addition reactions for the activation of branched alkanes over acidic zeolites.

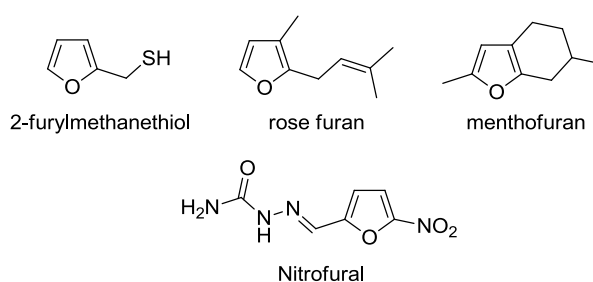
²³⁷ Sommer, J.; Habermacher, D.; Jost, R.; Sassi, A.; Stepanov, A. G.; Luzgin, M. V.; Freude, D.; Ernst, H.; Martens, J. *J. Catal.* **1999**, *181*, 265–270.

²³⁸ (a) Kramer, G. J.; van Santen, R. A. *J. Am. Chem. Soc.* **1995**, *117*, 1766–1776. (b) Kramer, G. J.; van Santen, R. A.; Emeis, C. A.; Nowak, A. K. *Nature* **1993**, *363*, 529–531.

Chapter 3 :
Silver(I)-heteropolyacids as “green”
catalysts for the synthesis of furans from
alkynyloxiranes

1. Furans: utility and accessibility

Furans are important compounds in organic chemistry, occasionally found in natural sources such as plants and microorganisms. Some natural products containing a furan ring exhibit an intense odor, such as 2-furylmethanethiol, a component of coffee aroma, rose furan, a component of rose oil, or menthofuran, contained in peppermint oil (Scheme 43).²³⁹ Some furan derivatives, such as the antibiotic Nitrofurantoin, have shown bactericidal activity, and are used against infectious diseases (Scheme 43).²³⁹ Consequently, furans are particularly useful in the flavors and fragrances as well as in the pharmaceutical industry.

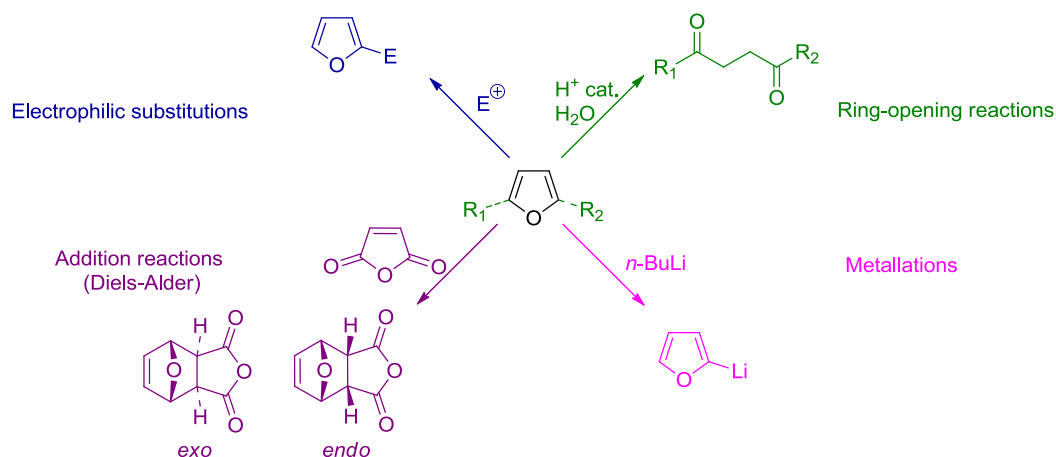


Scheme 43. Important furan compounds in the fragrances and the pharmaceutical industry.

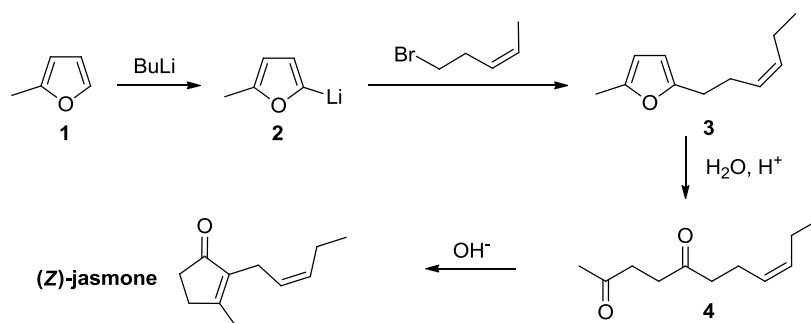
Due to their ability to undergo various transformations such as addition reactions (Diels-Alder), electrophilic substitutions, metallations, or ring opening reactions, furans have found considerable importance as synthetic intermediates and represent key building blocks in organic synthesis (Scheme 44).²³⁹⁻²⁴⁰ As an example, the (*Z*)-jasmonone fragrance has been synthesized in four steps from methylfuran.²³⁹ Metallation, alkylation, and ring opening of the furan moiety constituted the three first steps of the synthesis. The so-obtained 1,4 diketone **4** was finally converted to (*Z*)-jasmonone by a base-catalyzed intramolecular aldol condensation (Scheme 45).

²³⁹ Eicher, T.; Hauptmann S. *The Chemistry of Heterocycles*, 2nd ed.; Wiley-VCH: Weinheim, 2003.

²⁴⁰ Lipshutz, B. H. *Chem. Rev.* **1986**, *86*, 795–819.



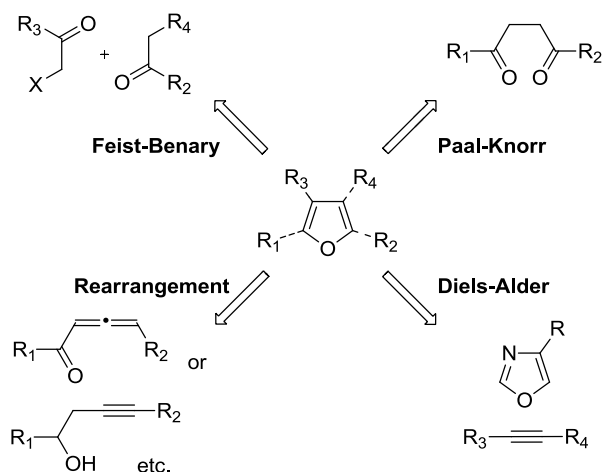
Scheme 44. Main reactivity of the furan building block.

Scheme 45. Synthesis of (*Z*)-jasmone from methylfuran.

Among the standard reactions used to access furan derivatives, the Paal-Knorr synthesis provides 2,5-disubstituted furans through acid-catalyzed cyclodehydration of 1,4-dicarbonyl compounds (Scheme 46). Another well-known reaction is the Feist-Benary synthesis, occurring in the presence of a base. Aldol addition of a β -keto carboxylic ester to an α -halocarbonyl compound, followed by cyclocondensation leads to 2,3,4-trisubstituted furans (Scheme 46).

A less trivial alternative to access the furan unit is the Diels-Alder reaction of oxazoles with activated alkynes.²⁴¹ The first “classical” [4+2] cycloaddition is followed by a [4+2] cycloreversion, thermodynamically favored by the formation of stable nitriles, along with the desired furan (Scheme 46).

²⁴¹ Hou, X. L.; Cheung, H. Y.; Hon, T. Y.; Kwan, P. L.; Lo, T. H.; Tong, S. Y.; Wong, H. N. C. *Tetrahedron* **1998**, *54*, 1955–2020.



Scheme 46. Main synthetic approaches toward furan derivatives.

Finally, the rearrangement of allene or alkyne derivatives catalyzed by transition metals is probably the most convergent and straightforward route for the synthesis of furans (Scheme 46).²⁴¹⁻²⁴² Mercury,²⁴³ palladium,²⁴⁴ platinum²⁴⁵ and more recently gold catalysts²⁴⁶ were already explored for this type of cyclization. The latter was usually preferred over the others due to its non-toxicity, mildness and tolerance toward numerous functional groups.

2. Precedents for the rearrangement of allenes and alkyne derivatives to furans by silver(I) catalysis

Compared to the numerous versions catalyzed by palladium²⁴¹⁻²⁴² or gold,²⁴⁶ only two procedures developed by Marshall proposed the use of less expensive silver salts as catalysts, for the rearrangement of allene or alkyne derivatives to furans. The first one described the cyclization of allenones catalyzed by AgNO_3 in acetone (Scheme 47).²⁴⁷

²⁴² Gilchrist, T. L. *J. Chem. Soc., Perkin Trans. 1* **2001**, 2491–2515.

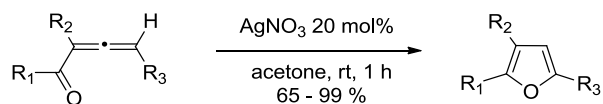
²⁴³ Miller, D. *J. Chem. Soc. C* **1969**, 12–15.

²⁴⁴ Minami, I.; Yuhara, M.; Watanabe, H.; Tsuji, J. *J. Organomet. Chem.* **1987**, 334, 225–242.

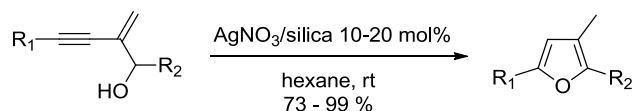
²⁴⁵ Nakamura, I.; Mizushima, Y.; Yamamoto, Y. *J. Am. Chem. Soc.* **2005**, 127, 15022–15023.

²⁴⁶ (a) Krause, N.; Winter, C. *Chem. Rev.* **2011**, 111, 1994–2009. (b) Hashmi, A. S. K.; Schwarz, L.; Choi, J.-H.; Frost, T. M. *Angew. Chem. Int. Ed.* **2000**, 39, 2285–2288.

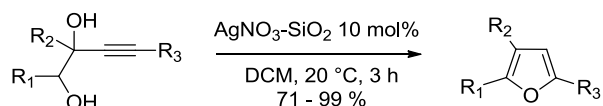
²⁴⁷ (a) Marshall, J. A.; Robinson, E. D. *J. Org. Chem.* **1990**, 55, 3450–3451. (b) Marshall, J. A.; Wang, X. J. *J. Org. Chem.* **1991**, 56, 960–969. (c) Marshall, J. A.; Bartley, G. S. *J. Org. Chem.* **1994**, 59, 7169–7171.

Scheme 47. AgNO₃ catalyzed cyclization of allenones proposed by Marshall et al.

Although mild and efficient, this method employed not readily available allenones as starting materials. For this reason, Marshall explored the conversion of more accessible β -alkynyl allylic alcohols. Interestingly, AgNO₃ supported on silica gel turned out to be the best catalytic system, promoting the reaction very rapidly in hexane (Scheme 48).²⁴⁸

Scheme 48. Heterogeneous version starting from β -alkynyl allylic alcohols.

According to the authors, the catalyst could even be recycled, at least one time, with or without a slight decrease in yield and reaction rate depending on the substrate. Cyclization of alkyne 1,2-diols based on these conditions revealed that despite leaching of silver salts in the reaction medium, the catalyst retained approximately the same activity for three successive runs (Scheme 49).²⁴⁹



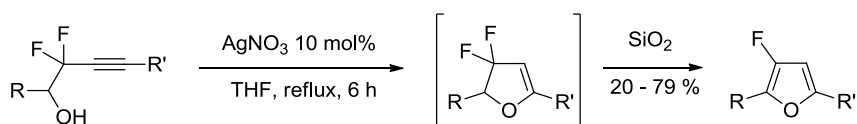
Scheme 49. Cyclization of alkyne 1,2-diols based on the conditions of Marshall et al.

Non supported silver nitrate proved also effective in THF for the cyclization of *gem*-difluorohomopropargyl alcohols in 3,3-difluoro-4,5-dihydrofurans, which yielded the corresponding 3-fluorinated furan upon treatment with silica gel (Scheme 50).²⁵⁰

²⁴⁸ Marshall, J. A.; Sehon, C. A. *J. Org. Chem.* **1995**, *60*, 5966–5968.

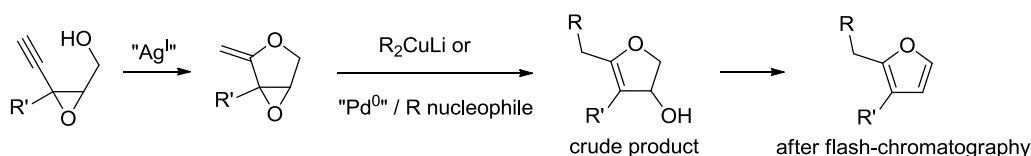
²⁴⁹ Hayes, S. J.; Knight, D. W.; Menzies, M. D.; O'Halloran, M.; Tan, W.-F. *Tetrahedron Lett.* **2007**, *48*, 7709–7712.

²⁵⁰ Arimitsu, S.; Hammond, G. B. *J. Org. Chem.* **2007**, *72*, 8559–8561.



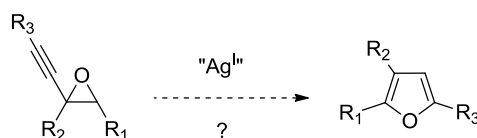
Scheme 50. AgNO₃ catalyzed cyclization of *gem*-difluorohomopropargyl alcohols.

In 1987, our group proposed a two-step approach to furans and dihydrofurans, based on the cyclization of epoxyalkynols catalyzed by silver salts, followed by nucleophilic addition mediated by organocuprates or palladium(0) catalysts (Scheme 51).²⁵¹



Scheme 51. Two-step approach to furans from epoxyalkynols by Pale et al.

It was subsequently envisioned that a one-pot cycloisomerization of alkynyl epoxides assisted by silver(I) catalysts alone could be possible, and deserved to be investigated (Scheme 52).



Scheme 52. Envisioned one-pot cycloisomerization of alkynyl epoxides.

Actually, this type of rearrangement has been already studied with various transition metal catalysts such as mercury,²⁴³ palladium,²⁵² molybdenum,²⁵³ ruthenium,²⁵⁴ gold²⁵⁵ and platinum.²⁵⁶ The molybdenum and ruthenium variants were though limited to starting materials bearing terminal alkynes, due to the formation of a vinylidene intermediate in the course of the reaction. The SmI₂/Pd^{II} system proposed by Aurecochea et al. was also limited by the nature of the substrate and required the elimination of a leaving group at the

²⁵¹ Dalla, V.; Pale, P. *Tetrahedron Lett.* **1996**, 37, 2781–2784.

²⁵² Aurecochea, J. M.; Solay-Ispizua, M. *Heterocycles*, **1994**, 37, 223–226.

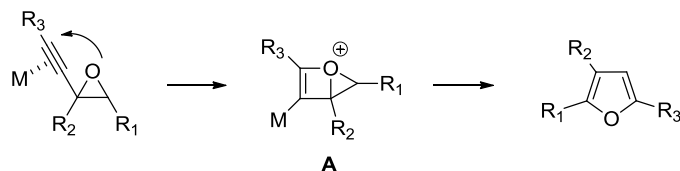
²⁵³ McDonald, F. E.; Schultz, C. C. *J. Am. Chem. Soc.* **1994**, 116, 9363–9364.

²⁵⁴ Lo, C.-Y.; Guo, H.; Lian, J.-J.; Shen, F.-M.; Liu, R.-S. *J. Org. Chem.* **2002**, 67, 3930–3932.

²⁵⁵ Hashmi, A. S. K.; Sinha, P. *Adv. Synth. Catal.* **2004**, 346, 432–438.

²⁵⁶ Yoshida, M.; Al-Amin, M.; Matsuda, K.; Shishido, K. *Tetrahedron Lett.* **2008**, 49, 5021–5023.

propargylic position to be effective.²⁵⁷ Concerning the rearrangement catalyzed by late transition metals, Hg, Au, and Pt, “direct” cyclizations proceeding through the bicyclic intermediate **A** were always proposed as reaction mechanisms (Scheme 53).^{255-256,258-259}



Scheme 53. Classical reaction mechanism involving a « direct cyclization ».

Most of these procedures were more effective with hydrated catalysts,²⁵⁸ or in the presence of water^{243,256,259} or free alcohols.^{243,255,255,258} However, none of the above-mentioned versions seriously considered the influence of this factor on the reaction efficiency. Based on these observations, and with no precedent mentioning the use of silver salts, Blanc et al. embarked on this direction and investigated the silver(I)-catalyzed rearrangement of alkyneoxiranes in the presence or not of alcohols.²⁶⁰ The addition of methanol as nucleophile dramatically increased the conversion of the alkyneoxirane (Table 10). Indeed, running the reaction in dichloromethane alone with silver triflate as catalyst resulted in poor yield of furan (entry 1), while in the presence of methanol, 73 % yield was obtained (entry 2).

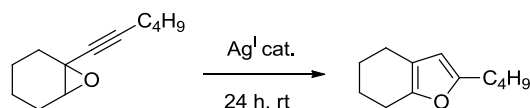
It is noteworthy that increasing or decreasing the reaction temperature did not improve the yield, and was on the contrary deleterious. As suspected from oxirane opening by the added methanol, bulkier alcohols were less efficient compared to the latter.

²⁵⁷ Aurrecochea, J. M.; Perez, E.; Solay, M. *J. Org. Chem.* **2001**, *66*, 564–569.

²⁵⁸ Shu, X.-Z.; Liu, X.-Y.; Xiao, H.-Q.; Ji, K.-G.; Guo, L.-N.; Qi, C.-Z.; Liang, Y.-M. *Adv. Synth. Catal.* **2007**, *349*, 2493–2498.

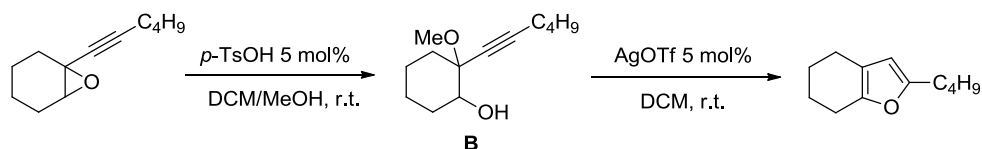
²⁵⁹ (a) Ji, K.-G.; Shen, Y.-W.; Shu, X.-Z.; Xiao, H.-Q.; Bian, Y.-J.; Liang, Y.-M. *Adv. Synth. Catal.* **2008**, *350*, 1275–1280. (b) Dai, L.-Z.; Shi, M. *Tetrahedron Lett.* **2008**, *49*, 6437–6439.

²⁶⁰ (a) Blanc, A.; Tenbrink, K.; Weibel, J.-M.; Pale, P. *J. Org. Chem.* **2009**, *74*, 4360–4363. (b) Blanc, A.; Tenbrink, K.; Weibel, J.-M.; Pale, P. *J. Org. Chem.* **2009**, *74*, 5342–5348.

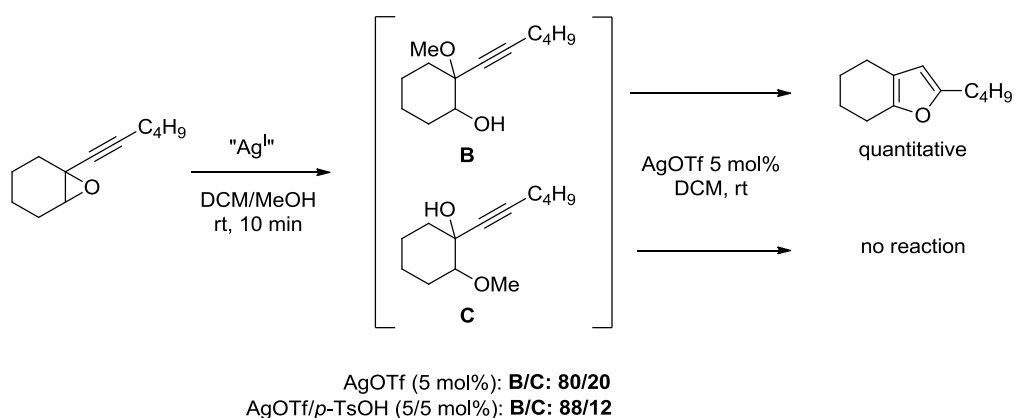
Table 10. Reaction conditions for the rearrangement of alkynyloxirane in furan.²⁶⁰

Entry	Catalyst (mol %)	Solvent	Furan yield (%)
1	AgOTf (5)	DCM	20
2	AgOTf (5)	DCM/MeOH (9/1)	73
3	AgOTf/ <i>p</i> -TsOH (5)/(5)	DCM/MeOH (9/1)	80

With the same idea, several cocatalysts were screened to facilitate the oxirane opening. Silver triflate combined with *p*-toluenesulfonic acid afforded the best results (entry 3). Actually, the oxirane opening product **B** could be isolated by running the reaction with the acid alone, and then cyclized in the presence of silver triflate (Scheme 54).

Scheme 54. Control experiment enabling to isolate the intermediate **B**.

Further NMR monitoring of the reaction in the presence of AgOTf alone or both catalysts showed that after 10 min, 2 regioisomeric products **B** and **C** resulting from oxirane opening were actually formed (Scheme 55).

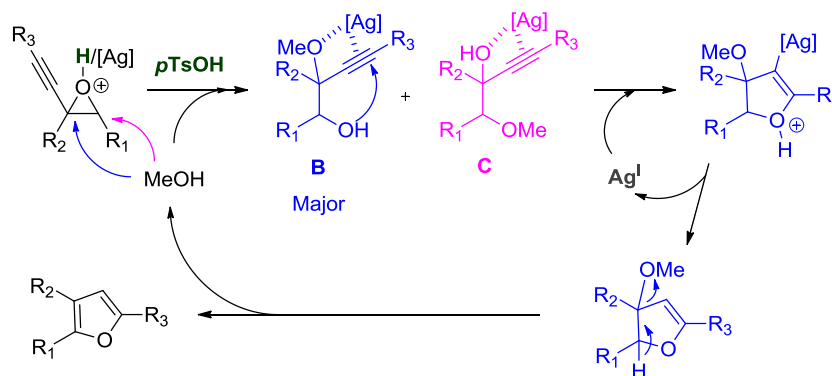
Scheme 55. Control experiments enabling to detect the formation of regioisomers **B** and **C**.

The regioisomer **B** resulting from a S_N2 at the propargylic position was the major one in both cases. However the presence of the Brønsted acid clearly favored the opening at this position,

increasing the **B/C** ratio from 80/20 to 88/12. In sharp contrast with isomer **B**, the regioisomer **C** did not react further in the presence of silver triflate.

These results provided evidence that the mechanism involved a cascade of events promoted by an external hydroxy nucleophile, including possible traces of water, and not a direct cyclization proceeding through the bicyclic intermediate **A**, as proposed in the previous Au^{255,258,259} and Pt-catalyzed²⁵⁶ variants (Scheme 53).

Instead, the mechanism of the silver catalyzed version involves the nucleophilic attack of methanol on the oxirane, favored by coordination of *p*-TsOH on the latter (Scheme 56). Naturally this opening can also be promoted by the Lewis acidic silver(I) ion, in the absence of other acid catalyst. Two regioisomers **B** and **C** are formed subsequently.



Scheme 56. Reaction mechanism proposed by Blanc et al.

The major regioisomer **B** easily cyclizes upon activation of the triple bond by the silver catalyst, affording a vinylic silver species. After protodemetalation, and subsequent elimination of methanol, the 2,3,5-trisubstituted furan is finally recovered.

3. *Silver(I)-heteropolyacids as bifunctional heterogeneous catalysts for the rearrangement of alkyloxiranes into furans*

In order to shift from homogeneous to heterogeneous catalysis, we wondered if we could replace the combination of silver triflate and *p*-toluene sulfonic acid by a unique bifunctional solid including both a metal and Brønsted acidity. The so-catalyzed transformation would constitute a green alternative to the method already developed in our group for the cycloisomerization of alkyloxiranes into furans.

With their tunable properties, heteropolyacids (HPA) seemed particularly suitable for this purpose. It is well-known that HPA exhibit strong Brønsted acidity, superior to the common liquid acids (Chapter I, Table 7). Moreover, metal salts of HPA, notably Cs salts of Keggin anions have been prepared for a long time by ionic exchange.²⁶¹ Indeed, protons in the secondary structure can be easily replaced by other cations without affecting the primary Keggin structure. Usually, when large counterions are introduced (NH_4^+ , Cs^+), the resulting POMs exhibit different properties from the parent HPA. They become insoluble in water, and possess higher surface areas due to the appearance of a micro/mesoporous tertiary structure.²⁶² For example, the surface area of $\text{H}_3\text{PW}_{12}\text{O}_{40}$ is $5 \text{ m}^2/\text{g}$, whereas for $\text{Cs}_{2.5}\text{H}_{0.5}\text{PW}_{12}\text{O}_{40}$ and $\text{Cs}_3\text{PW}_{12}\text{O}_{40}$ it increases to 135 and $156 \text{ m}^2/\text{g}$, respectively.²⁶³ It is noteworthy that Okamoto et al. prepared $\text{Ag}_3\text{PW}_{12}\text{O}_{40}$ by ionic exchange and classified the dodecahedral particles obtained as non-porous single crystals.²⁶⁴ In any case, we thought that the controlled and partial substitution of protons by silver cations in heteropolyacids would allow to design tailor made catalysts, exhibiting dual properties (metallic and acidic) in a single structure. Therefore, we chose to investigate the use of Ag-H-POMs in the rearrangement of alkynyloxiranes.

3.1. Preparation of the bifunctional Ag-H-POMs

In order to assess the influence of the Ag/H ratio on the cycloisomerization, we attempted to prepare a series of silver dodecatungstosilicic acid salts (Ag-H-POMs) $\text{Ag}_x\text{H}_{4-x}\text{SiW}_{12}\text{O}_{40}$ where $x = 1, 2, 3, 4$ by the conventional ion exchange method.²⁶¹ Through addition of the appropriate amount of silver nitrate to an aqueous solution of the commercial silicotungstic acid $\text{H}_4\text{SiW}_{12}\text{O}_{40}$, partial or complete substitution of protons by silver cations was achieved, in quantitative yields (Equation 9).²⁶⁵

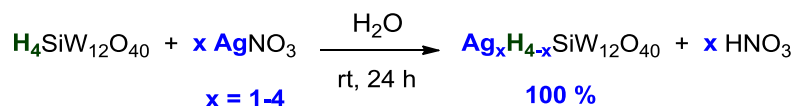
²⁶¹ Tatematsu, S.; Hibi, T.; Okuhara, T.; Misono, M. *Chem. Lett.* **1984**, 865–868.

²⁶² (a) Soled, S.; Miseo, S.; McVicker, G.; Gates, W. E.; Gutierrez, A.; Paes, J. *Catal. Today* **1997**, *36*, 441–450. (b) Ito, T.; Inumaru, K.; Misono, M. *J. Phys. Chem. B* **1997**, *101*, 9958–9963. (c) Mizuno, N.; Misono, M. *Chem. Lett.* **1987**, *16*, 967–970.

²⁶³ Lee, K. Y.; Misono, M. In *Preparation of Solid Catalysts*; Wiley-VCH Verlag GmbH, **2008**; 240–261.

²⁶⁴ Okamoto, K.; Uchida, S.; Ito, T.; Mizuno, N. *J. Am. Chem. Soc.* **2007**, *129*, 7378–7384.

²⁶⁵ Borghèse, S.; Blanc, A.; Pale, P.; Louis, B. *Dalton Trans.* **2011**, *40*, 1220–1223.



Equation 9. Preparation of bifunctional Ag-H-POMs by substitution of the parent HPA.

3.2. Characterization of the Ag-H-POMs catalysts

The chemical composition and the structure of the so-obtained Ag-H-POMs were subsequently ascertained by several physico-chemical techniques. All Ag-H-POMs exhibited infrared bands at similar frequencies, close to those of silicotungstic acid (Table 11).²⁶⁵

The FT-IR bands of Ag₃HSiW₁₂O₄₀ (Figure 24) and all other Ag-H-POMs were in accordance with the characteristic bands of a Keggin structure,²⁶⁶ and were assigned as follows: ν_s (W-O_d), 1020-1012 cm⁻¹, ν_{as} (W-O_d), 975-963 cm⁻¹, ν_{as} (Si-O_a), 908-904 cm⁻¹, ν_{as} (W-O_b-W), 880-870 cm⁻¹, ν_{as} (W-O_c-W), 742-728 cm⁻¹ (Figure 25). The bands located between 1621-1607 cm⁻¹ and 3500-2500 cm⁻¹ corresponded to the presence of water in the coordination sphere.²⁶⁷

Table 11. Wavelengths of maximum absorbance (ν_{max}) of the synthesized Ag-H-POMs.

Ag-H-POM	IR (neat) ν_{max} (cm ⁻¹)
H ₄ SiW ₁₂ O ₄₀	742, 880, 908, 975, 1020, 1617, 2500–3500 (broad)
AgH ₃ SiW ₁₂ O ₄₀	733, 874, 904, 964, 1018, 1621, 2500–3500 (broad)
Ag ₂ H ₂ SiW ₁₂ O ₄₀	733, 870, 904, 963, 1015, 1607, 2500–3500 (broad)
Ag ₃ HSiW ₁₂ O ₄₀	735, 870, 905, 963, 1012, 1610, 2500–3500 (broad)
Ag ₄ SiW ₁₂ O ₄₀	728, 872, 904, 965, 1012, 1610, 2500–3500 (broad)

²⁶⁶ (a) Rocchiccioli-Deltcheff, C.; Fournier, M.; Franck, R.; Thouvenot, R. *Inorg. Chem.* **1983**, *22*, 207–216. (b) Thouvenot, R.; Fournier, M.; Franck, R.; Rocchiccioli-Deltcheff, C. *Inorg. Chem.* **1984**, *23*, 598–605.

²⁶⁷ Mothe-Esteves, P.; Maciel Pereira, M.; Arichi, J.; Louis, B. *Cryst. Growth Des.* **2010**, *10*, 371–378.

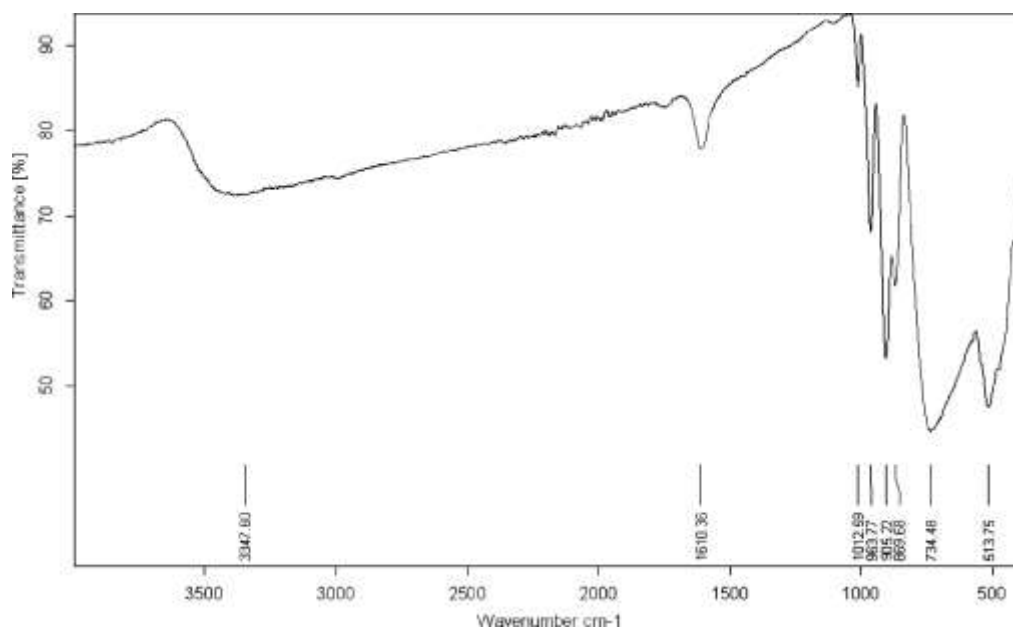


Figure 24. FT-IR spectrum of $\text{Ag}_3\text{HSiW}_{12}\text{O}_{40}$.

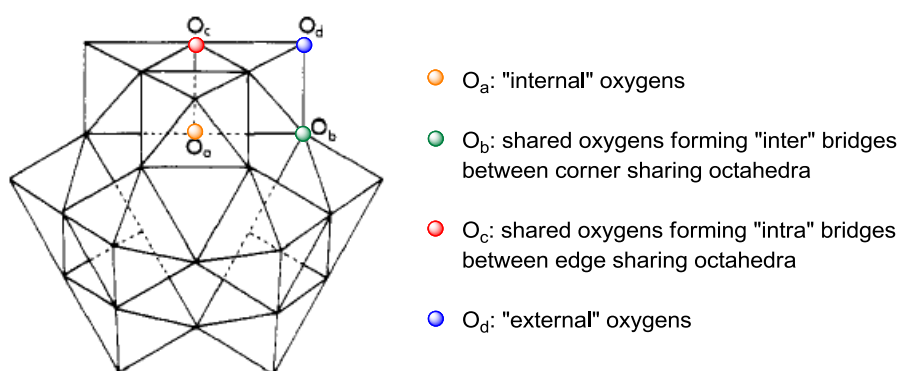


Figure 25. Localization of the different types of oxygen atoms in the Keggin structure, in connection with the FT-IR assignments.

The structure of the Ag-H-POMs was further analyzed by powder X-Ray Diffraction (XRD),²⁶⁸ which confirmed that the materials exhibited the characteristic (220), (310), (222), (400), (411), (420), (332) and (510) reflections derived from the bodycentered cubic secondary structure of the parent $\text{H}_4\text{SiW}_{12}\text{O}_{40}$.²⁶⁹ It is well-known that the replacement of protons by silver cations in HPA results in a decrease of the lattice parameter a_0 , and thus to a

²⁶⁸ Borghèse, S.; Louis, B.; Blanc, A.; Pale, P. *Catal. Sci. Technol.* **2011**, *1*, 981–986.

²⁶⁹ Pesaresi, L.; Brown, D. R.; Lee, A. F.; Montero, J. M.; Williams, H.; Wilson, K. *Appl. Catal. A Gen.* **2009**, *360*, 50–58.

contracted unit cell.²⁷⁰ This is usually showed by a shift toward higher 2θ diffraction angles, as can be seen from the refinement of the dominant 25,5-26,5° reflection in the XRD pattern of the present Ag-H-POMs (Figure 26). The latter also indicates that each $\text{Ag}_x\text{H}_{4-x}\text{SiW}_{12}\text{O}_{40}$ was made of a single crystalline phase, as found previously for $x \geq 1$.^{270a,c}

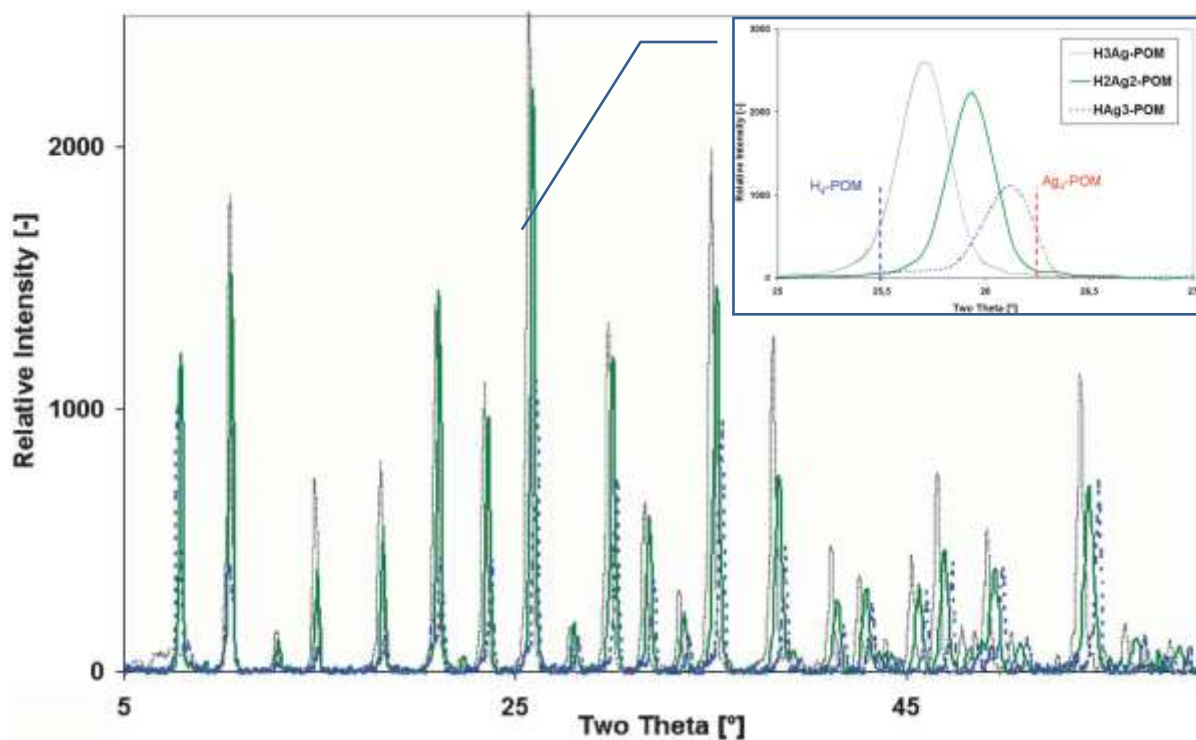


Figure 26. XRD patterns of $\text{Ag}_x\text{H}_{4-x}\text{SiW}_{12}\text{O}_{40}$, $x = 1-3$.

Scanning Electron Microscopy (SEM) gave insight into the morphology of the crystals, showing that Ag-H-POMs formed dodecahedral particles of about 10 μm in size (Figure 27).²⁶⁸ This morphology is characteristic of this type of material and was already reported for silver and other salts of HPA.²⁶⁴

²⁷⁰ (a) Haber, J.; Pamin, K.; Matachowski, L.; Napruszewska, B.; Połtowicz, J. *J. Catal.* **2002**, *207*, 296–306. (b) Parent, M. A.; Moffat, J. B. *Langmuir* **1996**, *12*, 3733–3739. (c) Zieba, A.; Matachowski, L.; Gurgul, J.; Bielańska, E.; Drelinkiewicz, A. *J. Mol. Catal. A Chem.* **2010**, *316*, 30–44.

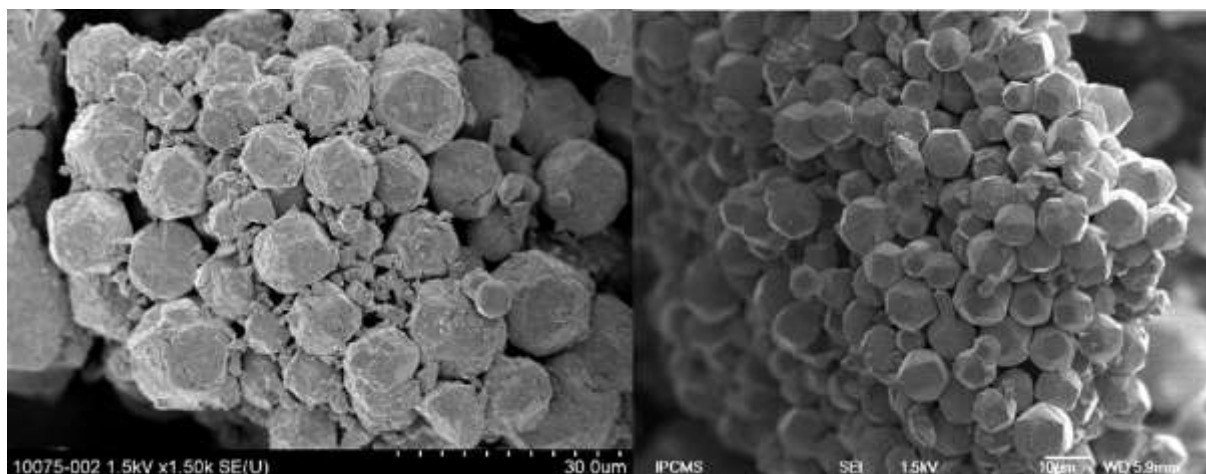


Figure 27. SEM images of $\text{Ag}_2\text{H}_2\text{SiW}_{12}\text{O}_{40}$ (left) and $\text{Ag}_4\text{SiW}_{12}\text{O}_{40}$ (right).

The elemental composition of each Ag-H-POM was obtained by EDX analysis coupled to SEM. Statistical EDX-mapping confirmed the homogeneous distribution of Ag, Si, O and W atoms throughout the material (Figure 28).²⁶⁸

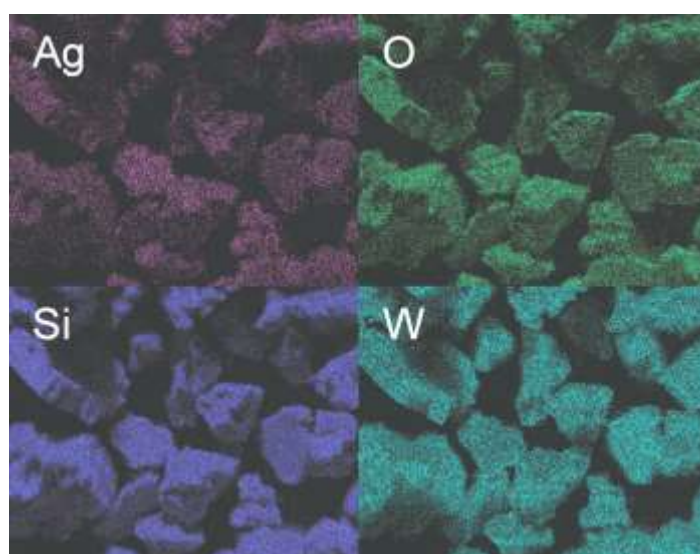


Figure 28. EDX mapping performed on $\text{Ag}_2\text{H}_2\text{SiW}_{12}\text{O}_{40}$.

The expected stoichiometry of each Ag-H-POM was ascertained from the W/Ag and Ag/Si atomic ratios calculated by EDX analysis.²⁶⁵ The amount of protons per catalyst was also determined experimentally by our H/D exchange technique.⁹⁵ From these results, we were able to calculate the number of protons per Keggin unit for each POM. All these data (Table 12) were in agreement with the expected values and confirmed that the proton-silver exchange occurred properly.

Table 12. Chemical composition of $\text{Ag}_x\text{H}_{4-x}\text{SiW}_{12}\text{O}_{40}$.

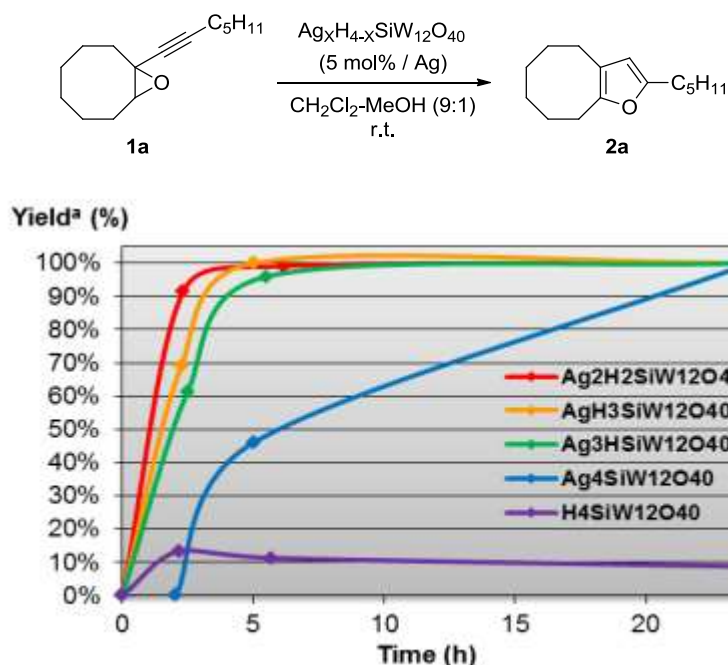
$\text{Ag}_x\text{H}_{4-x}\text{SiW}_{12}\text{O}_{40}$	W/Ag ^a	Ag/Si ^a	Brønsted acidity ^b	H ^c
x = 0	-	-	1,43	4,1
x = 1	12	1	0,94	2,8
x = 2	6	2	0,65	1,9
x = 3	4	3	0,39	1,2
x = 4	3	4	0	0

^a [atomic%] (EDX). ^b [mmol H⁺/g] (H/D isotope exchange). ^c Calculated H⁺ number per Keggin unit [-]

3.3. Screening of reaction conditions using Ag-H-POMs catalysts

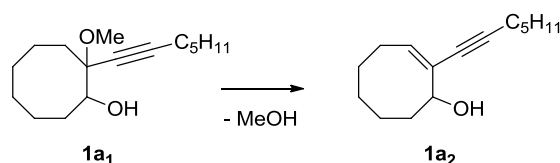
After the complete characterization of our Ag-H-POMs, we embarked on the screening of reaction conditions and evaluated the potential of each catalyst toward the cycloisomerization of alkyloxiranes to furans.²⁶⁸ The cyclooctane derivative **1a** was chosen as model substrate and submitted to the conditions set up earlier by Blanc et al.,²⁶⁰ namely 5 mol% catalyst (calculated to have 5 mol% silver(I)) in a 9:1 mixture of dichloromethane/methanol at room temperature (Figure 29).

Figure 29. Screening of reaction conditions for the rearrangement of alkyloxirane **1a** catalyzed by Ag-H-POMs.



^a Yields of **2a** were calculated from ¹H NMR integration relative to naphthalene as an internal standard.

Catalysis by pure silicotungstic acid $\text{H}_4\text{SiW}_{12}\text{O}_{40}$ (5 mol% of protons) afforded a maximum of 10 % yield of furan, the major product being the oxirane opening product at the propargylic position **1a₁** (60 %), along with the product resulting from the elimination of methanol **1a₂** (27 %) (Scheme 57).



Scheme 57. Elimination of methanol on regioisomer **1a₁** leading to enyne **1a₂**.

As expected, the presence of silver within the catalyst enabled the quantitative formation of furan after 24 h. Nevertheless, with the non-acidic $\text{Ag}_4\text{SiW}_{12}\text{O}_{40}$, the rearrangement of **1a** occurred slowly, and required 24 h to be complete. On the other hand, the three bifunctional Ag-H-POMs catalyzed the reaction very rapidly, achieving a complete conversion after only 5 h. Among the Ag-H-POMs, $\text{Ag}_2\text{H}_2\text{SiW}_{12}\text{O}_{40}$ proved to be the best catalyst, affording 92 % yield of furan after 2 h, against 61 and 69 % for $\text{Ag}_3\text{HSiW}_{12}\text{O}_{40}$ and $\text{AgH}_3\text{SiW}_{12}\text{O}_{40}$, respectively. These results indicated that the most suitable Ag/H ratio for the reaction was 1, and confirmed the necessity of both silver(I) and protons to quickly afford high yields, as already noticed in the homogeneous version of the reaction.²⁶⁰ In addition, the development of these new heterogeneous conditions highlighted the influence of the Brønsted acidity on the reaction rate, the latter being lowered down if the catalyst contains too many or not enough acidic sites.

It is noteworthy that silver salts of tungstophosphoric acid seemed to be as efficient as their silico counterparts, since the transformation of **1a** catalyzed by 5 mol% of $\text{Ag}_{2.5}\text{H}_{0.5}\text{PW}_{12}\text{O}_{40}$ afforded 70 % yield of furan after 24 h (isolated yield).

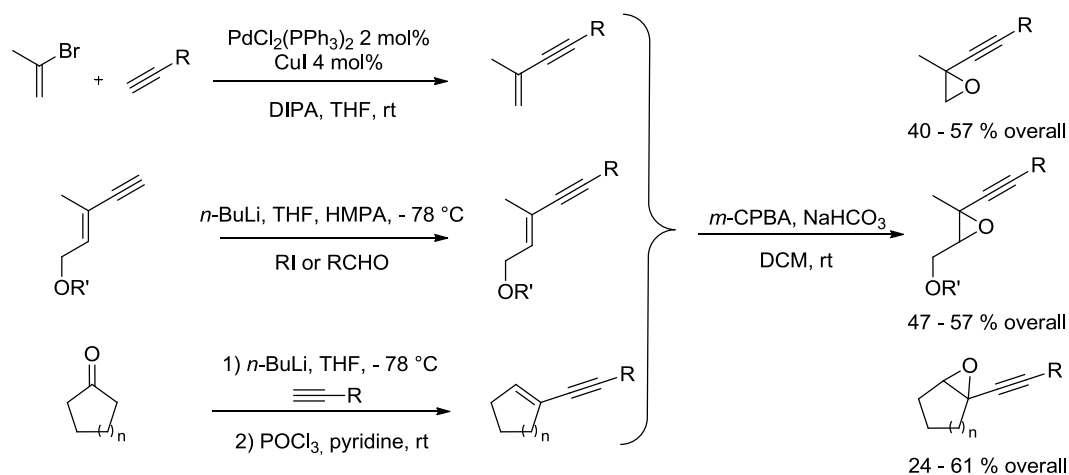
As expected after the introduction of silver cations in HPA, the resulting Ag-H-POMs were insoluble in the reaction medium (dichloromethane/methanol: 9/1). In order to discard the possibility of silver leaching during the reaction, $\text{Ag}_2\text{H}_2\text{SiW}_{12}\text{O}_{40}$ was stirred for 24 h in a mixture of dichloromethane/methanol (9/1), and after filtration of the catalyst, the alkynyloxirane **1a** was added to the filtrate. No conversion was observed, which confirmed the heterogeneous nature of the Ag-H-POM catalyzed reaction.

3.4. Scope of the Ag-H-POMs catalyzed rearrangement of alkyloxiranes

In order to assess the scope of the reaction, a series of alkyloxiranes was prepared and submitted to the best catalyst $\text{Ag}_2\text{H}_2\text{SiW}_{12}\text{O}_{40}$. Each time it was possible, the yield and reaction time were compared with the results in homogeneous conditions.²⁶⁸ Alkyloxiranes were basically synthesized by *m*-CPBA epoxidation of the corresponding enynes, obtained either from Sonogashira cross-coupling or dehydration of the precursor alcohol (Scheme 58).²⁶⁰ The alkyloxirane was obtained according to the procedure reported by Andersson.²⁷¹

The size of the ring joined to the epoxide, as well as the alkyne substituents were varied, in order to assess their influence on the reaction.

Under both homogeneous and heterogeneous conditions, the eight and seven-membered furans (Table 13, entries 1, 2, 3) were very quickly obtained in high yields, whatever the functional group at the alkyne (simple alkyl chain or benzyl). In contrast, for the six-membered ring **2d** (entry 4), a different behavior was observed depending on the reaction conditions. With $\text{Ag}_2\text{H}_2\text{SiW}_{12}\text{O}_{40}$ as catalyst, only 40 % of furan was formed after 24 h, against 80 % for the combination of silver triflate and *p*-TsOH.



Scheme 58. Synthetic pathways to alkyloxiranes carrying various functional groups.

Looking for an explanation to this unexpected result, we examined in details the product distribution obtained at the beginning of the reaction. ^1H NMR monitoring revealed that after

²⁷¹ Södergren, M. J.; Alonso, D. A.; Bedekar, A. V.; Andersson, P. G. *Tetrahedron Lett.* **1997**, 38, 6897–6900.

ten minutes, the ratio between the two oxirane opening products (**B**:**C**, Scheme 56) was 50:50 under heterogeneous conditions, against 88:12 under homogeneous conditions. Since only isomer **B** seemed to cyclize according to the results of Blanc et al.,^{260b} the maximum yield that could be obtained with $\text{Ag}_2\text{H}_2\text{SiW}_{12}\text{O}_{40}$ was thus 50 %.

In their homogeneous version, Blanc et al. suggested that the furan **2e** (entry 5) was not obtained, probably because of the formation of alkynylsilver.²⁶⁰ In the present case, NMR monitoring confirmed the opening of the epoxide at the propargylic position only (isomer **B**), but the resulting alcohol did not evolve further, even under reflux, which may also be related to the formation of alkynylsilver.

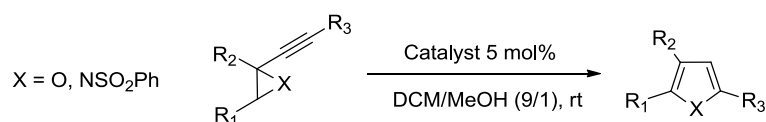
Only 7 % yield of the five-membered furan **2f** (entry 6) was detected by NMR, along with degradation and a 50:50 ratio of opening products after 2 h. This result was in agreement with the homogeneous version, in which only traces of furan were observed.

After this evaluation of cyclic derivatives, the preparation of furans carrying a free or protected hydroxyl group in position 2 and an alkyl chain in position 5 was examined (entries 7, 8, 9). Epoxide **1h** carrying a benzyl protecting group is the only one that had been previously evaluated, mostly yielding degradation under homogeneous conditions. In the presence of $\text{Ag}_2\text{H}_2\text{SiW}_{12}\text{O}_{40}$, the NMR seemed to confirm the opening of the epoxide after 2 h, but except for degradation, no evolution to the expected furan was detected, even after 24 h.

The same epoxide carrying a free hydroxyl in position 2 (entry 7) was clearly too reactive and degraded rapidly in the reaction conditions. When the alcohol was protected by a silyl group (entry 9), the transformation was not easier. NMR revealed that the TBS group was not stable in the present conditions and started to decompose already after 1.5 h. Thus, even if the addition of methanol actually happened according to NMR, the subsequent cyclization did not take place.

Interestingly, when the hydroxyl group was carried by the alkyne (entry 10), the cycloisomerization became possible. 41 % of furan **2j** was obtained after 1.5 h, and this yield did not increase with longer reaction times, suggesting a limitation induced by the free alcohol. Indeed, when the latter was protected by a pivaloyl group (entry 11), the yield increased to 70 %, the competition with methanol being no longer possible. These results were in total agreement with the observations made in homogeneous conditions, affording 52 and 81 % yield in comparable reaction times for the furan **2j** and **2k**, respectively.

Table 13. Scope of the rearrangement of alkynyloxiranes to furans.



Entry	Alkynyloxiranes or Alkynylaziridines	Furans or Pyrroles	Ag ₂ H ₂ SiW ₁₂ O ₄₀ ^a		AgOTf/ <i>p</i> TsOH ^b		
			yield ^c (%)	time (h)	yield ^d (%)	time (h)	
1		1a	2a	92	2	92	3
2		1b	2b	89	1,75	90	1,75
3		1c	2c	84	5	72	3
4		1d	2d	40	24	80	24
5		1e	2e	- ^e	48	- ^e	72
6		1f	2f	7 ^e	2,5	Traces	24
7		1g	2g	- ^e	24	x	x
8		1h	2h	- ^e	24	- ^e	24
9		1i	2i	- ^e	24	x	x
10		1j	2j	41	1,5	52	2
11		1k	2k	70	24	81	16
12		1l	2l	50	36 ^f	56	16
13		1m	2m	51 ^g	48	61 ^g	16 ^f

^a 5 mol%/Ag. ^b 5 mol% of each catalyst. ^c Yields of **2a** were calculated from ¹H NMR integration relative to naphthalene as an internal standard. ^d Isolated yields. ^e Degradation occurred leading to unidentified by-products. ^f Reaction run at reflux. ^g 10 mol% catalyst.

The acetoxyated alkynyloxirane **1l** was converted to the furan **2l** in 50 % yield after 24 h at 40 °C. The same result as Blanc et al. on this type of substrate was observed in our case,²⁷² involving the nucleophilic substitution of methanol and elimination of the acetyl group.

Finally, the alkynylaziridine **1m** was successfully rearranged into the corresponding pyrrole, by using 10 mol% $\text{Ag}_2\text{H}_2\text{SiW}_{12}\text{O}_{40}$. Longer reaction times were necessary to complete the transformation. Slightly higher yield (61 %) was afforded in homogeneous conditions by running the reaction at reflux.

To sum up concerning the scope of this rearrangement of alkynyloxiranes into furans, the bifunctional heterogeneous catalyst $\text{Ag}_2\text{H}_2\text{SiW}_{12}\text{O}_{40}$ was globally as efficient in terms of yields, reaction rates, and tolerance toward functional groups as the combination of AgOTf and *p*-TsOH, except for isolated examples such as cyclohexane derivative **1d**. In some cases (**1d**, **1f**), the formation of nearly equal amounts of the two epoxide opening products seemed to be the main cause for lowered reaction yields.

3.5. Recycling of the catalyst

The last factor we examined was the recyclability of the catalyst, using our model substrate **1a**. At the end of each reaction, $\text{Ag}_2\text{H}_2\text{SiW}_{12}\text{O}_{40}$ was recovered, washed with *n*-pentane and dried 5 min at 110 °C before being reengaged. Four successive runs could be achieved with no significant decrease in yields, affording after 24 h 100 %, 100 %, 96 % and 79 % respectively (Figure 30). However, the NMR monitoring revealed that the reaction rate started to fall off at the first recycling, requiring 24 h of reaction to reach finally satisfying yields.

²⁷² Blanc, A.; Alix, A.; Weibel, J.-M.; Pale, P. *Eur. J. Org. Chem.* **2010**, 1644–1647.

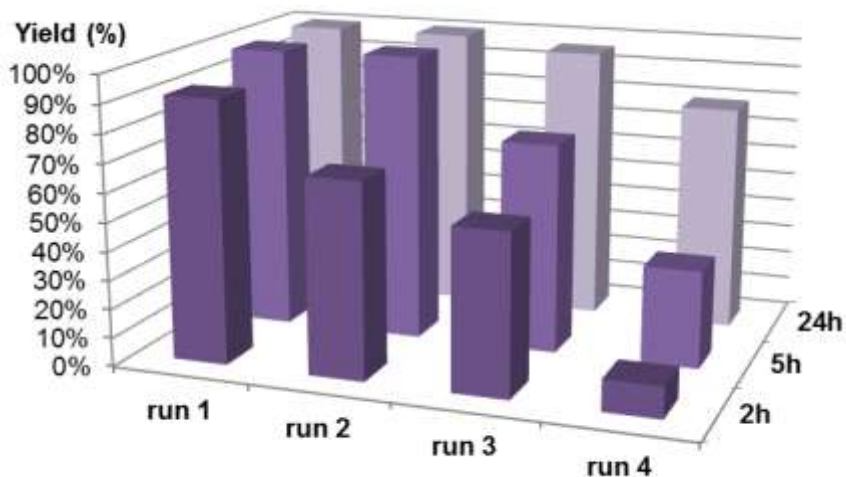
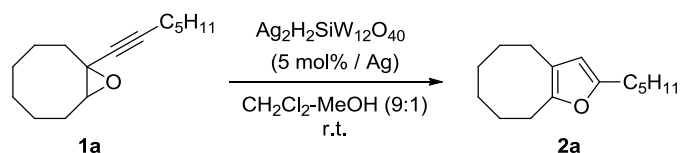


Figure 30. Recycling tests of $\text{Ag}_2\text{H}_2\text{SiW}_{12}\text{O}_{40}$ in the rearrangement of alkynyloxirane **1a**.

From a structural point of view, powder XRD of the catalyst after the first run confirmed the retention of the Keggin unit (Figure 31). Except for slight variations in the relative intensities, the main peaks corresponding to the strongest reflections were still present after one run. The only major difference was the very broad peak at 7.9° , which could be interpreted as a beginning of amorphization of the catalyst.²⁷³ The latter amorphization could be an indication of the deactivation of the Ag-H-POM.

Besides, SEM imaging showed slight external modifications of the material and EDX-mapping revealed a less homogeneous distribution of silver throughout the catalyst. The latter observation suggested that the POM stoichiometry would rather tend to a combination of Ag_3H , Ag_2H_2 and AgH_3 , which would account for the lower rates of cyclization after successive recycling.

In the light of these results, the influence of calcination time and temperature on the catalyst activity after recycling certainly deserves to be investigated more in depth. Organic matter deposit and coke formation in the material could obviously disturb the regular proceeding of the reaction.

²⁷³ (a) Hamed, M. N. H. *J. Appl. Sci. Res.* **2010**, *6*, 8, 1218–1239. (b) Marosi, L.; Escalona Platero, E.; Cifre, J.; Otero Arean, C. *J. Mater. Chem.* **2000**, *10*, 1949–1955.

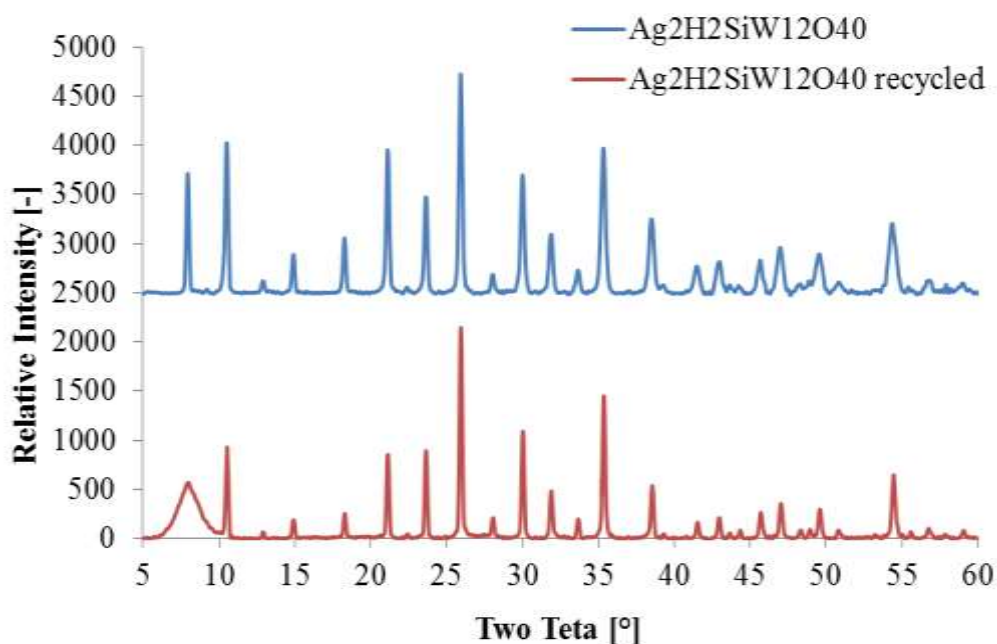


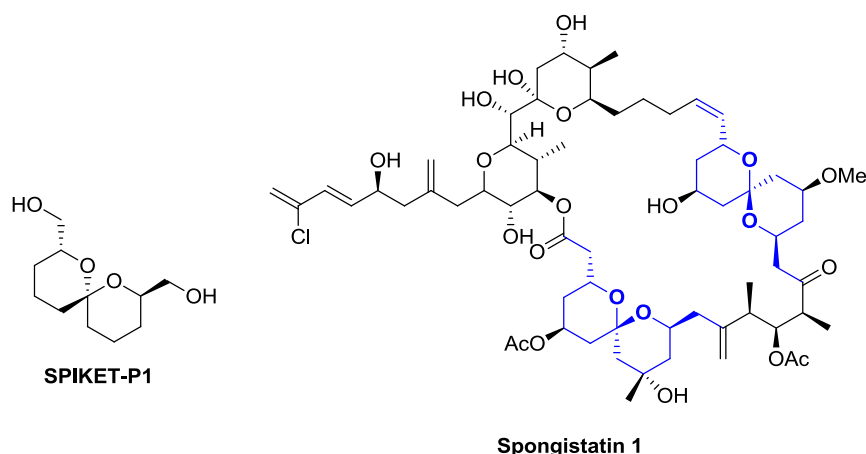
Figure 31. XRD patterns of $\text{Ag}_2\text{H}_2\text{SiW}_{12}\text{O}_{40}$ before and after one recycling.

Finally, the development of this new heterogeneous pathway to 2,3,5-trisubstituted furans through the cycloisomerization of alkynyloxiranes was successfully achieved by bifunctional silver acidic polyoxometalates. $\text{Ag}_2\text{H}_2\text{SiW}_{12}\text{O}_{40}$ possessing a 1:1 ratio of silver cations/protons proved to be the most active catalyst for the reaction. Compared to the homogeneous conditions employing a combination of AgOTf and $p\text{-TsOH}$, the bifunctional catalyst exhibited a similar behavior in terms of yields, reaction rates and tolerance towards functional groups. Moreover, it was possible to recycle the catalyst at least 3 times without significant yield decrease. The influence of calcination time and temperature on the catalyst activity after recycling should be studied in more details in the future to improve the catalyst recyclability. The present successful work suggests that other bi- or multifunctional POMs supporting attractive transition metals should be designed for targeted reactions, and contribute in this way to the development of greener procedures in organic synthesis.

Chapter 4 :
Synthesis of ketals and spiroketals by Ag-
zeolite catalyzed dihydroalkoxylation of
alkynediols

1. The spiroketal moiety: importance and accessibility

Acetal and especially spiroketal motifs are present in a number of natural molecules found in insects, plants, bacterial and marine sources.²⁷⁴ Spiroketal consist of two oxygenated rings connected to each other by a single spiro carbon atom. Most of the natural products containing these structures exhibit biological activities.^{274a,274e} In addition, the spiroketal ring system is a well-recognized pharmacophore in drug discovery.²⁷⁵ As a consequence, the design of efficient and practical methodologies to access spiroketals has attracted the attention of synthetic chemists more particularly.^{274f-276} The efforts directed to this end have enabled to point out unnatural simple candidates of biological interest.^{274e,275} As an example, SPIKET-P1 has been identified as a potent pharmacophore of spongistatin 1, a marine natural product exhibiting notably high cytotoxic activity against cancer cell lines (Scheme 59).²⁷⁷



Scheme 59. Unnatural spiroketal SPIKET-P1 (left) and natural product spongistatin 1 (right).

²⁷⁴ (a) Parkes, K. E. B.; Pattenden, G. *Tetrahedron Lett.* **1986**, 27, 1305–1308. (b) Aho, J. E.; Pihko, P. M.; Rissa, T. K. *Chem. Rev.* **2005**, 105, 4406–4440. (c) Fletcher, M. T.; Kitching, W. *Chem. Rev.* **1995**, 95, 789–828. (d) Perron, F.; Albizati, K. F. *Chem. Rev.* **1989**, 89, 1617–1661. (e) Milroy, L.-G.; Zinzalla, G.; Loiseau, F.; Qian, Z.; Prencipe, G.; Pepper, C.; Fegan, C.; Ley, S. V. *ChemMedChem* **2008**, 3, 1922–1935. (f) Sperry, J.; Wilson, Z. E.; Rathwell, D. C. K.; Brimble, M. A. *Nat. Prod. Rep.* **2010**, 27, 1117–1137.





²⁷⁵ Zinzalla, G.; Milroy, L.-G.; Ley, S. V. *Org. Biomol. Chem.* **2006**, 4, 1977–2002.

²⁷⁶ (a) Palmes, J. A.; Aponick, A. *Synthesis* **2012**, 44, 3699–3721. (b) Coric, I.; List, B. *Nature* **2012**, 483, 315–319. (c) Boivin, T. L. B. *Tetrahedron* **1987**, 43, 3309–3362. (c) Ley, S. V.; Milroy, L.-G.; Myers, R. M. *Product Class 9: Spiroketal*, In *Science of Synthesis*, Vol. 29; Warriner, S., Ed.; Georg Thieme: Stuttgart, **2007**, 613.

²⁷⁷ (a) Huang, H.; Mao, C.; Jan, S.-T.; Uckun, F. M. *Tetrahedron Lett.* **2000**, 41, 1699–1702. (b) Sharma, A.; Iyer, P.; Gamre, S.; Chattopadhyay, S. *Synthesis* **2004**, 1037–1040.

When embarking on the synthesis of spiroketal derivatives it is necessary to consider the stereochemical issues associated with this class of compounds.^{276a,276c} Due to the possible rotation of the rings around the acetal carbon, spiroketals can exhibit various conformations. Usually, in the most thermodynamically stable form, the two C-O bonds are in axial orientation to each other, in order to maximize the number of anomeric interactions. Indeed, the overlap between the axial lone pair of oxygens and the corresponding antibonding σ^* -orbital of the axial C-O bond results in an energetic stabilization, estimated at approximately 1.4-2.4 kcal/mol per anomeric interaction.²⁷⁸ Illustration of the situation is given in Table 14 using the 6,6-spiroketal core. The latter can exhibit four conformations, but the most stable is the diaxial configuration that accumulates two anomeric interactions.^{276a,276c} To each stereoisomer is attributed a specific E/Z nomenclature.

Table 14. Configuration and stereochemistry in spiroketals.

				
Configuration	diaxial	axial-equatorial	axial-equatorial	equatorial-equatorial
Anomeric effects	2	1	1	0
Stereochemistry	(E,E)	(Z,E)	(E,Z)	(Z,Z)

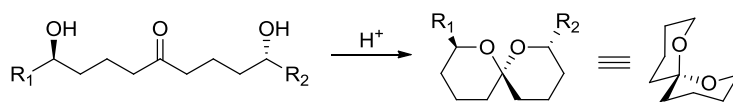
Of course, the presence of substituents on the rings leading to steric interactions, chelations or hydrogen bondings also has an influence on the global stability and relative configuration of the spiro compound.^{276a,276c} However, anomeric effect can often help to predict the stereochemical result of spiroketalization reactions.

1.1. Traditional approaches toward spiroketal moieties

Among the various synthetic strategies employed to reach attractive spiroketal targets,²⁷⁶ the most widespread method is the acid-catalyzed dehydration of dihydroxy ketones (Scheme 60).^{276a,276c,279}

²⁷⁸ (a) Deslongchamps, P.; Rowan, D. D.; Pothier, N.; Sauvé, G.; Saunders, J. K. *Can. J. Chem.* **1981**, *59*, 1105–1121. (b) Descotes, G.; Lissac, M.; Delmau, J.; Duplan, J. *C. R. Acad. Sci. Ser. C*, **1968**, *267*, 1240–1241.

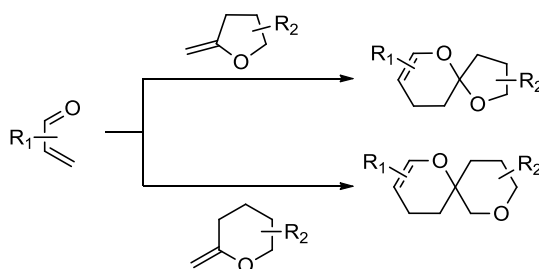
²⁷⁹ Mead, K. T.; Brewer, B. N. *Curr. Org. Chem.* **2003**, *7*, 227–256.



Scheme 60. Example of acid-catalyzed dehydration of dihydroxy ketone.

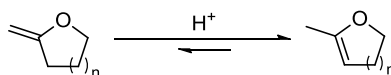
This methodology is effective for the preparation of most spiroketal-containing natural products, whose stereochemistry is mainly governed by anomeric effects.

Hetero-Diels-Alder (HDA) based approaches have shown to be efficient and convergent methods to access alternative spiroketal structures,²⁸⁰ containing a double bond which can be further manipulated. One of the advantages of this method is the possibility to easily access diverse scaffolds through the choice of appropriate reaction partners. As illustrated in Scheme 61, the [4+2]-cycloaddition between enone/enal moieties and α -methylene pyran or furan derivatives provides either 6,5 or 6,6-spiroketal.



Scheme 61. Hetero-Diels-Alder approach to spiroketals.

The main limitation of HDA-based syntheses of spiroketals is the tendency of the dienophile *exocyclic* double bond to isomerize into the corresponding *endocyclic* product, even under mild acid conditions (Scheme 62).

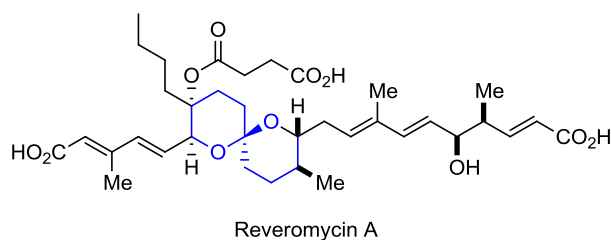


Scheme 62. Isomerization of the dienophile under acid conditions.

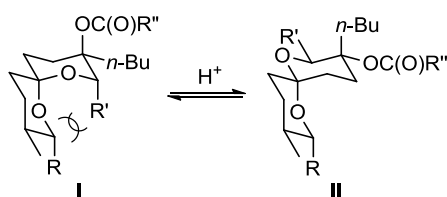
In terms of stereoselectivity, HDA reaction is a good alternative to the cyclization of dihydroxy ketones as it often favors the formation of kinetic *versus* thermodynamic products. Typical illustration of this issue has been highlighted in the total synthesis of reveromycin A

²⁸⁰ Rizzacasa, M. A.; Pollex, A. *Org. Biomol. Chem.* **2009**, *7*, 1053–1059.

(Scheme 63), a natural product exhibiting notably antifungal and antitumor activity.²⁸¹ It is known that the 6,6-spiroketal core of the molecule is particularly prone to isomerization under acidic conditions, due to a steric interaction involving the axial C19 side chain (Scheme 64). The isomerization of I to II enables to remove the latter constraint but at the same time costs one favorable anomeric effect, which results in a small energy difference between the two conformers.



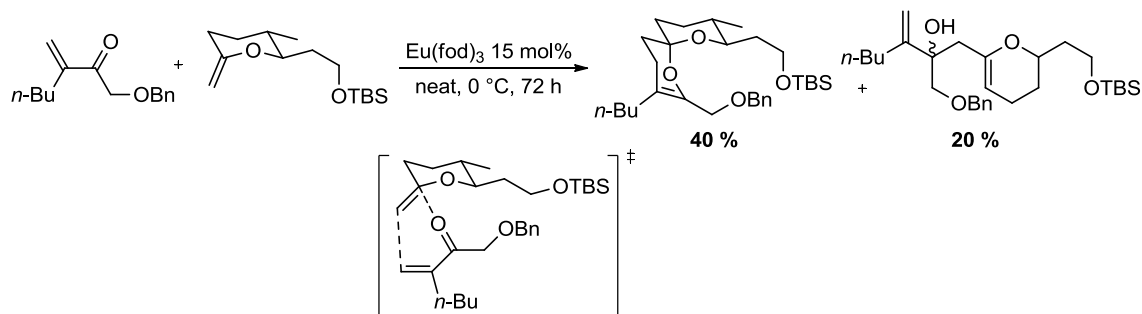
Scheme 63. Structure of the reveromycin A including a 6,6-spiroketal core.



Scheme 64. Isomerization of the 6,6-spiroketal core under acid conditions.

Consequently, classical approaches based on thermodynamic conditions such as the cyclization of dihydroxy ketone derivatives resulted in mixtures of the two compounds. Rizzacasa managed to solve this issue using a kinetically stereocontrolled HDA reaction.²⁸¹ $\text{Eu}(\text{fod})_3$ was found to be the most effective catalyst to promote the [4+2]-cycloaddition, which proceeded best without any solvent. Under these conditions, the desired spiroketal was obtained as a single isomer (Scheme 65). The modest 40 % yield of the reaction was notably accounted for the formation of a side Ene-reaction product in 20 %.

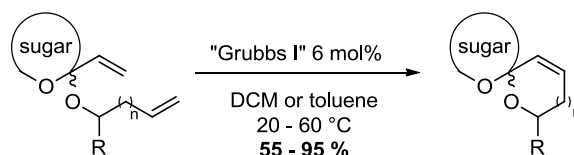
²⁸¹ El Sous, Mariana; Ganame, D.; Zanatta, S.; Rizzacasa, M. A. *ARKIVOC* **2006**, *vii*, 105–119.



Scheme 65. Synthesis of the kinetic spiroketal under the conditions of Rizzacasa et al.

1.2. Recent strategies based on C=C bond creation

Less conventional strategies based on the creation of C=C instead of C-O bonds under transition-metal catalysis have also been applied to the preparation of attractive spiroketal targets. Ring closure metathesis (RCM) of alkenes or enynes belongs to these recent methodologies. One of the first examples of this type of synthesis has been reported by van Boom and co-workers in 1998.²⁸² They successfully prepared anomeric and non-anomeric spiroketals by ring-closure-metathesis of alkene derivatives in the presence of Grubbs's first generation catalyst. The reaction proceeded with retention of configuration at the ketal carbon (Scheme 66).

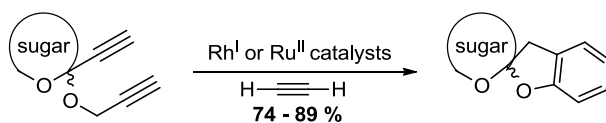


Scheme 66. Ring closure metathesis (RCM) of alkenes for the synthesis of spiroketals.

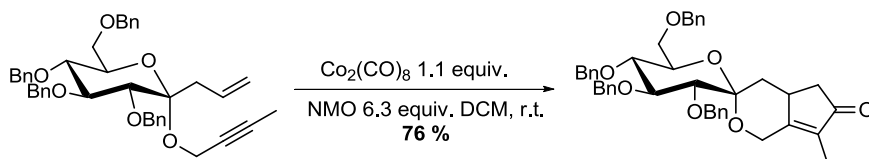
Ring rearrangement strategies based on the creation of carbon-carbon bonds have also been used to prepare more complex spiroketal-fused tricyclic structures. Illustrative examples include the [2+2+2] cycloaddition of C-alkynyl carbohydrate derivatives with acetylene

²⁸² (a) van Hooft, P. A. V.; Leeuwenburgh, M. A.; Overkleeft, H. S.; van der Marel, G. A.; van Boeckel, C. A. A.; van Boom, J. H. *Tetrahedron Lett.* **1998**, *39*, 6061–6064. (b) van Hooft, P. A. V.; El Oualid, F.; Overkleeft, H. S.; van der Marel, G. A.; van Boom, J. H.; Leeuwenburgh, M. A. *Org. Biomol. Chem.* **2004**, *2*, 1395–1403.

(Scheme 67),²⁸³ or the Pauson-Khand reaction of ketal enynes (Scheme 68),²⁸⁴ which respectively provided access to benzene- and cyclopentenone-fused spiroketal moieties.



Scheme 67. [2+2+2] cycloaddition of C-alkynyl carbohydrate derivatives with acetylene.



Scheme 68. Pauson-Khand reaction giving cyclopentenone-fused spiroketal moieties.

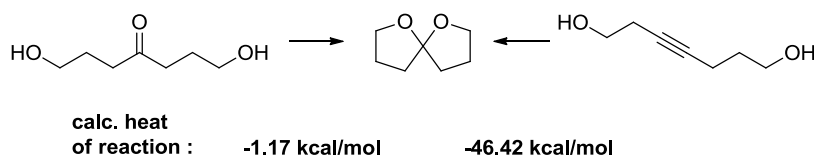
1.3. The dihydroalkoxylation of alkynediols

The development of transition-metal catalysis during the second half of the 20th century has enabled the diversification of the methodologies to access spiroketals. As demonstrated in the precedent paragraph, novel and original strategies based on the creation of carbon-carbon bonds have started to emerge, providing interesting alternatives to the traditional approaches requiring acidic conditions. Very recently, the expansion of gold and other late transition-metal catalysis has accompanied the development of a very attractive spiroketalization method, which is the dihydroalkoxylation of alkynediols. Similar to the traditional dehydration of dihydroxy ketones, this strategy produces spiroketals through the creation of two C-O bonds, but is comparatively more exothermic (Scheme 69),²⁸⁵ and atom economic.

²⁸³ (a) McDonald, F. E.; Zhu, H. Y. H.; Holmquist, C. R. *J. Am. Chem. Soc.* **1995**, *117*, 6605–6606. (b) Yamamoto, Y.; Hashimoto, T.; Hattori, K.; Kikuchi, M.; Nishiyama, H. *Org. Lett.* **2006**, *8*, 3565–3568.

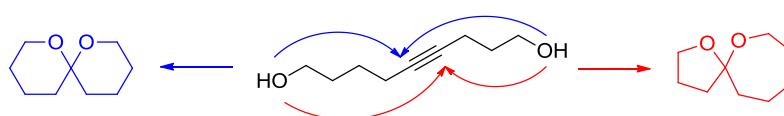
²⁸⁴ Leeuwenburgh, M. A.; Appeldoorn, C. C. M.; van Hooft, P. A. V.; Overkleeft, H. S.; van der Marel, G. A.; van Boom, J. H. *Eur. J. Org. Chem.* **2000**, *2000*, 873–877.

²⁸⁵ Tlais, S. F.; Dudley, G. B. *Beilstein J. Org. Chem.* **2011**, *7*, 570–577.



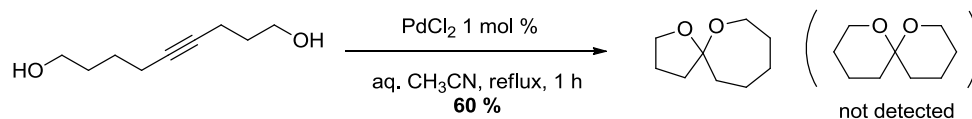
Scheme 69. Dehydration of dihydroxy ketones vs dihydroalkoxylation of alkyne diols.

In addition, non-polar alkynes are relatively inert toward a number of reaction conditions compared to the corresponding ketones. On the other hand, the use of alkyne diols induces regiochemistry issues, as the double cyclization can possibly occur at both carbons of the triple bond (Scheme 70).

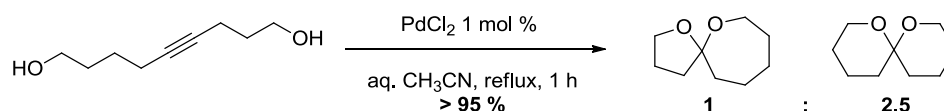


Scheme 70. Regiochemistry issues in the dihydroalkoxylation of alkyne diols.

The first investigations of this methodology were reported by Utimoto in 1983.²⁸⁶ In the presence of 1 mol % PdCl₂ or PdCl₂(PhCN)₂, he observed the smooth conversion of various alkyne diols into the corresponding spiroketals (Scheme 71).

Scheme 71. PdCl₂ catalyzed spiroketalization by Utimoto.

Although the reaction proceeded in satisfying yields, the regioselectivity was difficult to control. Indeed, using the same conditions, De Brabander reported a different selectivity for the cyclization of 4-nonyne-1,9-diol (Scheme 72).²⁸⁷



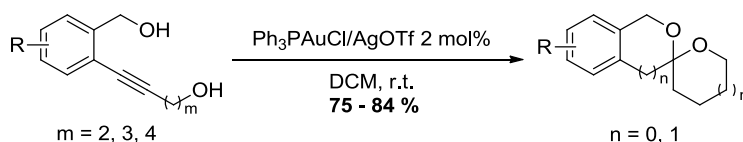
Scheme 72. Control experiments about the regioselectivity by De Brabander et al.

²⁸⁶ Utimoto, K. *Pure Appl. Chem.* **1983**, *55*, 1845–1852.

²⁸⁷ Liu, B.; De Brabander, J. K. *Org. Lett.* **2006**, *8*, 4907–4910.

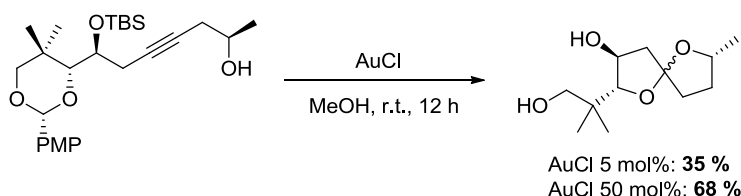
In order to address this regioselectivity concern, De Brabander and co-workers studied the hydroalkoxylation of monoprotected alkyndiols in the presence of Au^I, Au^{III}, Pd^{II} and Pt^{II} catalysts.²⁸⁷ A Zeise's dimer [Cl₂Pt(CH₂=CH₂)]₂ proved to be an efficient and selective catalyst, favoring 6-*exo* over 7-*endo* and 6-*endo* over 5-*exo* cyclization pathways. In contrast, PdCl₂(PhCN)₂ and the combination of MeAuPPh₃ and AgPF₆ tended to favor 5-*exo* over 6-*endo* cyclization mode.

Recent studies confirmed that gold salts were efficient catalysts for the dihydroalkoxylation of alkyndiols. Zhang and co-workers successfully prepared a series of 5,6-aromatic spiroketals including the bisbenzannelated core of rubromycins, using a combination of Ph₃PAuCl and AgOTf in dichloromethane (Scheme 73).²⁸⁸



Scheme 73. Gold-catalyzed dihydroalkoxylation of alkyndiols by Zhang et al.

Dudley and co-workers reported the synthesis of 5,5-spiroketal derivatives in the presence of AuCl in methanol.²⁸⁹ The protection of one hydroxyl functional group as an acetal favored the desired 5-*endo*-dig attack of the other hydroxyl in a first place (Scheme 74). In a second place, the Lewis acidity of AuCl promoted the hydrolysis of the PMP acetal, leading to the expected 5-*exo*-trig cyclization. In addition, the cleavage of the silyl ether also occurred under the reaction conditions.



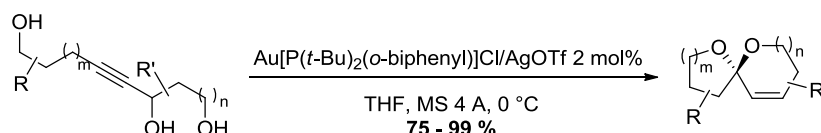
Scheme 74. Gold-mediated synthesis of 5,5-spiroketal derivatives by Dudley et al.

²⁸⁸ Zhang, Y.; Xue, J.; Xin, Z.; Xie, Z.; Li, Y. *Synlett* **2008**, 940–944.

²⁸⁹ Tlais, S. F.; Dudley, G. B. *Beilstein J. Org. Chem.* **2011**, *7*, 570–577.

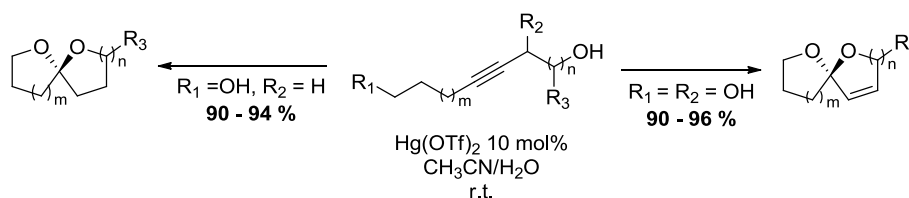
However, high catalyst loading (50 mol%) was necessary to reach satisfying yields. As a reason for this, the authors underlined the instability of gold(I) chloride in methanol.

Aponick and co-workers reported a variant of this type of spiroketalization, starting from monopropargylic triols.²⁹⁰ They obtained monounsaturated spiroketals in good yields using a combination of Au[P(*t*-Bu)₂(*o*-biphenyl)]Cl and AgOTf (Scheme 75).



Scheme 75. Spiroketals from monopropargylic triols by Aponick et al.

Similar spiroketalization of monopropargylic triols was found to be effective in the presence of 10 mol% mercury(II) triflate in aqueous acetonitrile at room temperature.²⁹¹ Deslongchamps and co-workers successfully prepared both monounsaturated and saturated spiroketals in high yields and short reaction times under these conditions (Scheme 76). Interestingly, this catalytic system seemed to favor 6-*exo*-dig over 7-*endo*-dig or 5-*endo*-dig cyclization pathways.



Scheme 76. Mercury(II)-catalyzed synthesis of spiroketals by Deslongchamps & co-workers.

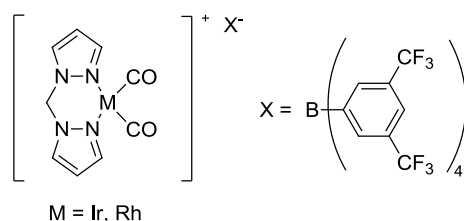
In addition to Au^I, Au^{III}, Pd^{II} and Pt^{II} and Hg^{II} catalytic systems, Messerle proposed the Rh^I and Ir^I catalyzed hydroalkoxylation of alkyndiols.²⁹² A screening of ligands and counterions

²⁹⁰ Aponick, A.; Li, C.-Y.; Palmes, J. A. *Org. Lett.* **2009**, *11*, 121–124.

²⁹¹ Ravindar, K.; Reddy, M. S.; Deslongchamps, P. *Org. Lett.* **2011**, *13*, 3178–3181.

²⁹² (a) Messerle, B. A.; Vuong, K. Q. *Pure Appl. Chem.* **2006**, *78*, 385–390. (b) Messerle, B. A.; Vuong, K. Q. *Organometallics* **2007**, *26*, 3031–3040. (c) Selvaratnam, S.; Ho, J. H. H.; Huleatt, P. B.; Messerle, B. A.; Chai, C. L. L. *Tetrahedron Lett.* **2009**, *50*, 1125–1127. (d) Ho, J. H. H.; Hodgson, R.; Wagler, J.; Messerle, B. A. *Dalton Trans.* **2010**, *39*, 4062–4069.

revealed that $\text{Rh}(\text{bpm})(\text{CO})_2\text{BAr}^{\text{F}}_4$ and $[\text{Ir}(\text{bpm})(\text{CO})_2]\text{BAr}^{\text{F}}_4$ were the most efficient catalysts (Scheme 77).

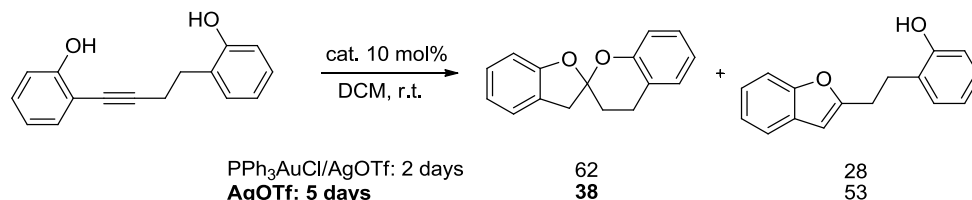


Scheme 77. $\text{Rh}(\text{bpm})(\text{CO})_2\text{BAr}^{\text{F}}_4$ and $[\text{Ir}(\text{bpm})(\text{CO})_2]\text{BAr}^{\text{F}}_4$ complexes.

Provided sufficient temperature (≥ 100 °C), aliphatic and aromatic alkynediols were converted into the expected spiroketals using 1 mol% catalyst. The efficiency of the reaction seemed dependent on the size of the ring formed, the iridium(I) complex favoring [5,5]-spiroketals, while the rhodium(I) catalyst better promoted [6,6]-bicycles.

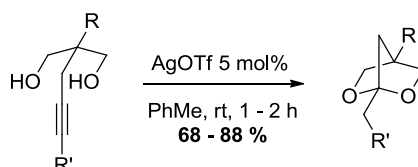
1.4. The silver(I)-catalyzed cycloisomerization of alkynols and alkynediols

Despite their ability to activate alkynes toward nucleophilic substitution, silver(I) salts were so far never reported as catalysts for the spiroketalization of alkynediols. Most of the time, they were only used as co-catalysts in combination with gold salts, to generate more active gold species. However, when developing their gold-catalyzed methodology toward the bisbenzannelated core of rubromycin,²⁸⁸ Zhang and co-workers noticed that AgOTf alone was able to promote the spiroketalization, although in lower yield and longer reaction time (Scheme 78).



Scheme 78. AgOTf catalyzed synthesis of the bisbenzannelated core of rubromycin.

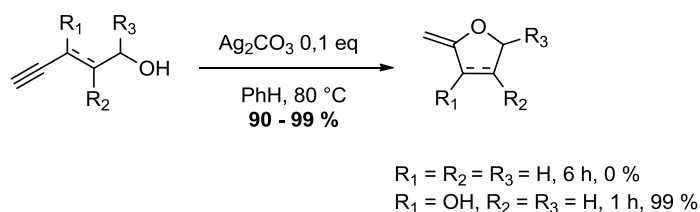
Interestingly, Lee and co-workers also described the utilization of silver triflate as catalyst for the preparation of bridged bicyclic ketals from alkyne diols (Scheme 79).²⁹³



Scheme 79. AgOTf catalyzed synthesis of bridged bicyclic ketals from alkyne diols.

The authors found that the moderate reactivity of silver(I) was actually more appropriate for the reaction than the conditions previously reported by Genêt et al.,²⁹⁴ i.e. gold(I) or (III) chloride in methanol, which finally proved less selective. All substrates were converted in 1 to 2 h at 25 °C to the corresponding ketals in high yields.

In addition, the silver(I)-catalyzed hydroalkoxylation of acetylenic alcohols to α -methylene oxanes and oxolanes has been reported by Pale and co-workers in 1987.²⁹⁵ The cyclization proved to be highly regioselective, yielding exclusively *exo*-cyclic enol ethers in the presence of 10 mol% silver carbonate in toluene (Scheme 80).



Scheme 80. Silver(I)-catalyzed hydroalkoxylation of acetylenic alcohols by Pale et al.

Interestingly, when oxygenated substituents and particularly electron-donating ones were present at the propargylic position, the cyclization rate dramatically increased (Scheme 80).²⁹⁶ In that case, the coordination of silver(I) to the triple bond was probably reinforced by hyper conjugation of the adjacent C-O bond, rendering the subsequent cyclization easier. Although

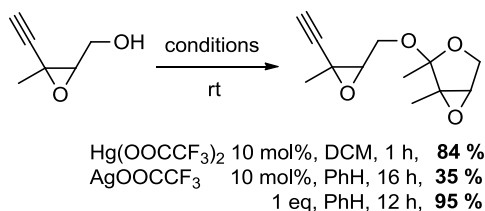
²⁹³ Oh, C. H.; Yi, H. J.; Lee, J. H. *New J. Chem* **2007**, *31*, 835–837.

²⁹⁴ Antoniotti, S.; Genin, E.; Michelet, V.; Genet, J.-P. *J. Am. Chem. Soc.* **2005**, *127*, 9976–9977.

²⁹⁵ (a) Pale, P.; Chuche, J. *Tetrahedron Lett.* **1987**, *28*, 6447–6448. (b) Pale, P.; Chuche, J. *Eur. J. Org. Chem.* **2000**, 1019–1025.

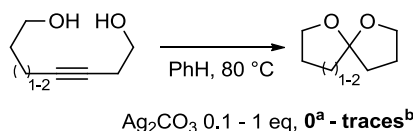
²⁹⁶ Dalla, V.; Pale, P. *New J. Chem* **1999**, *23*, 803–805.

not emphasized at that time, the screening of reaction conditions revealed that mercury and silver trifluoroacetate were able to catalyze the formation of acetal self-adducts (Scheme 81).^{295b}



Scheme 81. Formation of acetal self-adducts in the presence of AgOOCCF_3 .

However, attempts to obtain spiroketals from alkyndiols under the set up conditions remained unsuccessful (Scheme 82).



^a No conversion. ^b Some oxidation of alcohol to aldehyde occurred.

Scheme 82. Attempts to synthesize spiroketals in the presence of Ag_2CO_3 .

In light of all the results we just mentioned, further investigations seemed necessary to determine whether optimal reaction conditions based on silver(I) catalysts could be found to promote the spiroketalization of alkyndiols. In addition, the existing methodologies based on Au^{I} , Au^{III} , Pd^{II} , Pt^{II} , Hg^{II} , Rh^{I} and Ir^{I} catalytic systems suffer from the use of expensive and non-recyclable complexes, high catalyst loadings or toxic heavy metal salts in the case of Hg^{II} . Therefore, the development of a “greener procedure” with less detrimental impact on the environment would be particularly useful. To achieve this goal, we decided to investigate the potential of silver(I)-containing heterogeneous catalysts and more particularly Ag^{I} -zeolites toward the hydroalkoxylation of alkynols and alkyndiols. Indeed, we reasoned that the nanoscale environment of such porous solids could favor the cyclization of these substrates. The recent crystal structure determination of an ethylene sorbed complex on Ag-X zeolite supported our hypothesis. The structure showed that Ag^+ cations lying at sites II were able to form π -complexes with ethylene by slightly moving into the supercage (Figure 32).²⁹⁷

²⁹⁷ Lee, Y. M.; Choi, S. J.; Kim, Y.; Seff, K. *J. Phys. Chem. B* **2005**, *109*, 20137–20144.

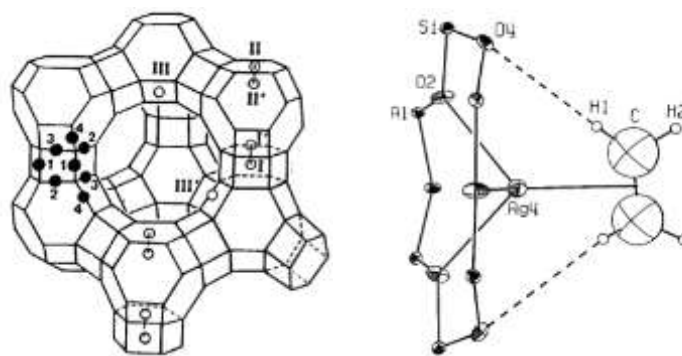
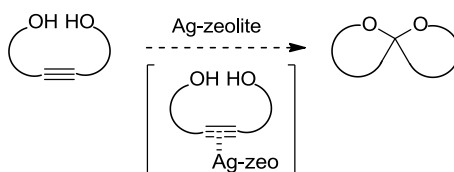


Figure 32. Schematic representation of oxygen (•) and silver (○) atoms location in Ag–X zeolite (left). Part of X-ray structure of an ethylene sorbed Ag-X zeolite showing the π -complex formed around tetrahedral Ag⁺ ion (right).

These results suggested that similar coordination of Ag⁺ ions with alkynes could possibly occur at least in the faujasite-type zeolites (X or Y) exhibiting large cages. A ring closure proceeding *via* this type of π -complex intermediate should thus be possible (Scheme 83).



Scheme 83. Proposed cyclization of alkyndiols in the presence of Ag-doped zeolites.

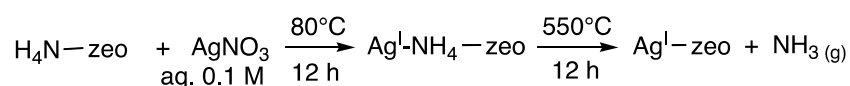
2. Ag^I-zeolite catalyzed cycloisomerization of alkynols and alkyndiols

2.1. Preparation of silver-doped zeolites

In order to study more in depth the influence of the zeolite environment on the reaction, we prepared a series of silver(I)-zeolites exhibiting various topologies and pore diameters. Silver(I)-zeolites were synthesized according to classical ion-exchange procedures reported in the literature.²⁹⁸ Typically, a parent zeolite (NH₄ or Na form) was added to an aqueous solution of silver nitrate (0,1 M). The resulting suspension was stirred in the dark at 80 °C for

²⁹⁸ (a) Narayana, N.; Kevan, L. *J. Chem. Phys.* **1982**, *76*, 3999–4005. (b) Boddenberg, B.; Burmeister, R. *Zeolites* **1988**, *8*, 480–487. (c) Hutson, N. D.; Reisner, B. A.; Yang, R. T.; Toby, B. H. *Chem. Mater.* **2000**, *12*, 3020–3031.

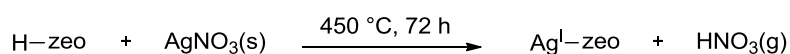
12 h. After cooling, filtration, and washing with distilled water, the resulting powder was dried for 24 h at 110 °C. To maximize the silver content in the material, a second ion-exchange can be carried out thereafter in the same conditions. Finally, Ag-NH₄-zeolites were calcinated at 550 °C for 12 h, in order to remove gaseous ammoniac and recover the Ag-H-form of the material (Equation 10).



Equation 10. Preparation of Ag-doped zeolites by ion-exchange.

In the end, Ag-USY, Ag-Na-Y, Ag-β, Ag-MOR and Ag-ZSM-5 could be prepared by the ion-exchange method.

Due to the success previously met with Cu^I-¹¹¹ and Sc^{III}-zeolites,¹³⁵⁻¹³⁷ we also attempted to prepare – for the first time – Ag-zeolites by solid exchange. As an example, the parent H-USY was ground with an appropriate amount of silver nitrate and the resulting solid mixture was heated at 450 °C for 3 days under N₂ flux (Equation 11). The amount of silver salt was calculated to replace 20 % of the acidic sites of H-USY.



Equation 11. Preparation of Ag-doped zeolites by solid-exchange.

Elimination of gaseous nitric acid accompanied the sublimation of silver nitrate, whose decomposition is supposed to occur at 440 °C.

2.2. Characterization of the materials

After the preparation of the Ag-zeolite catalysts, further characterization was performed in order to get insight concerning the structure and composition of the materials.

The silicon, aluminum and silver contents of several zeolites were established by elemental analysis and are reported in Table 15. From these values, the Si/Al ratio and silver loading per gramm of zeolite could be calculated. Surprisingly, Ag-USY prepared by one or two ionic exchanges exhibited approximately the same Ag loading, with 0.86 and 1.02 mmol Ag/g,

respectively. The silver content of Ag-USY prepared by solid-exchange was slightly lower (0.73 mmol Ag/g) and inferior to the theoretical loading (0.94 mmol Ag/g). After two ion-exchanges, Ag-NaY exhibited more than twice the Ag content of Ag-USY (2.29 mmol Ag/g). This difference may be correlated to the number of exchangeable sites in each zeolite. This number is lower in USY, owing to the removal of framework aluminum species when USY is prepared from Y. At the opposite, Ag-ZSM5 exhibited half the Ag content of Ag-USY, as suspected from its low exchange capacity (Si/Al = 17).

Table 15. Elemental analysis of several Ag-zeolites.

Ag-zeolite	preparation	Si [w%]	Al [w%]	Ag [w%]	Si/Al ^a	Ag [mmol/g] ^b
Ag-USY	1 ion-exch.	29.56	9.65	9.33	3.06	0.86
Ag-USY	2 ion-exch.	28.75	9.49	10.96	3.03	1.02
Ag-USY	sol.-exch.	27.8	9.21	7.88	3.02	0.73 ^c
Ag-NaY	2 ion-exch.	18.81	6.84	24.7	2.75	2.29
Ag-ZSM5	2 ion-exch.	38.89	2.31	5.25	16.84	0.49

^a Calculated Si/Al ratio from Si and Al w% values. ^b Calculated silver loading per gramm of zeolite from Al w% values. ^c Theoretically 0.94 mmol Ag/g were expected (amount of AgNO₃ used in the synthesis).

Calculated Si/Al ratios of USY zeolites indicated that the chemical composition of the material was conserved whatever the preparation method.

Powder X-Ray Diffraction (XRD) patterns of parent H-USY and Ag-USY after two ion-exchanges are shown in Figure 33. The similarity between the two diffractograms revealed that no significant structural modification occurred during the ionic exchange, preserving the faujasite structure. A slight variation in the peak intensities of the (331), (220) and (311) reflections was detected, which is usually correlated to the location of the cations.²⁹⁹ In H-USY, the order and difference in peak intensities was as follows: $I_{331} > I_{220} > I_{311}$. After two ion-exchanges, the intensities got closer to: $I_{331} \gg I_{220} \sim I_{311}$. This variation could be attributed to a redistribution of the countercations in the zeolite framework.³⁰⁰

²⁹⁹ Salavati-Niasari, M. *Polyhedron* **2009**, 28, 2321–2328.

³⁰⁰ Ferreira, L.; Fonseca, A. M.; Botelho, G.; Aguiar, C. A.; Neves, I. C. *Microporous Mesoporous Mater.* **2012**, 160, 126–132.

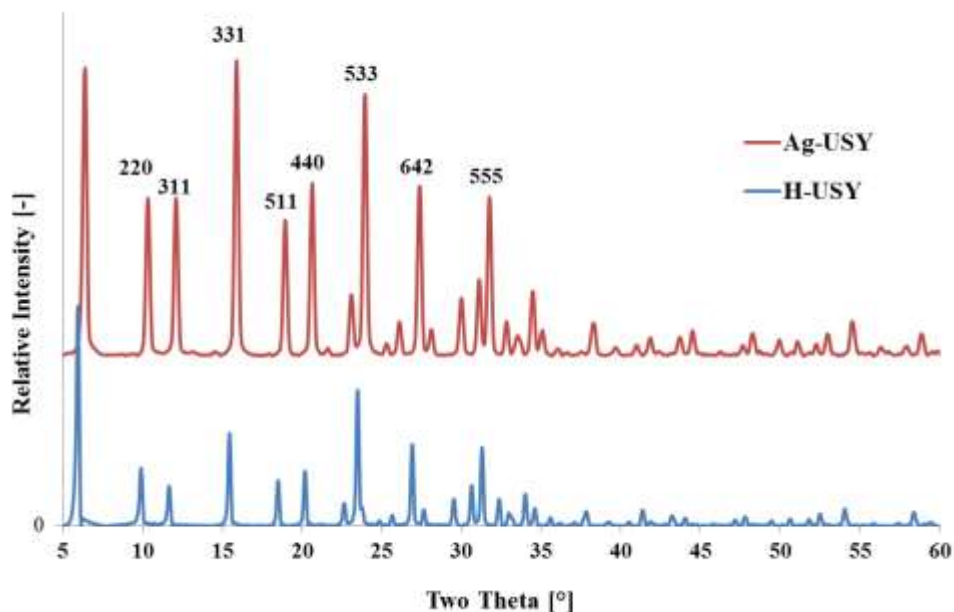


Figure 33. Powder XRD patterns of H-USY and Ag-USY prepared by two cationic exchanges.

The presence of the characteristic peaks of metallic silver at 38.12° and 44.28° were not clearly detected,³⁰¹ suggesting that the low silver content of the so-prepared Ag-USY (11 w% by elemental analysis) favored dispersed metallic species in the zeolite structure.

Scanning Electron Microscopy (SEM) provided information concerning the morphology of the crystals. In concordance with powder-XRD, the micrographs confirmed that USY remained crystalline after two ion exchanges (Figure 34). The crystals obtained formed regular particles, characteristic of the faujasite structure.^{300,302} In addition, EDX-analysis coupled to SEM confirmed that the Ag content of Ag-USY prepared by two ion-exchanges was around 10-13 w%, which is consistent with the value determined by elemental analysis (11 w%, Table 15).

³⁰¹ Concepción-Rosabal, B.; Rodríguez-Fuentes, G.; Bogdanchikova, N.; Bosch, P.; Avalos, M.; Lara, V. H. *Microporous Mesoporous Mater.* **2005**, *86*, 249–255.

³⁰² Lopes, A. C.; Silva, M. P.; Gonçalves, R.; Pereira, M. F. R.; Botelho, G.; Fonseca, A. n. M.; Lanceros-Mendez, S.; Neves, I. C. *J. Phys. Chem. C* **2010**, *114*, 14446–14452.

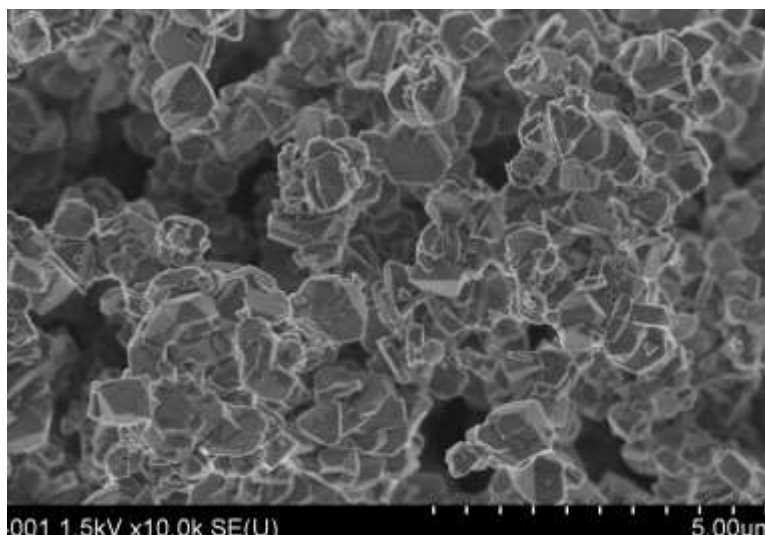


Figure 34. SEM micrograph of Ag-USY prepared by 2 ion-exchanges.

X-ray Photoelectron Spectroscopy (XPS) analysis was performed to get insight concerning the chemical state of silver at the surface of the material.

Figure 35 shows the high resolution spectrum of Ag-USY in the Ag 3d region. Whatever the preparation method, solid or ion-exchange, we observed two main peaks centered at 369.5 and 375.5 eV corresponded to the binding energies (BE) of Ag 3d_{5/2} and Ag 3d_{3/2}, respectively.

The peak surface areas are correlated to the amount of silver at the surface of the material. From these spectra, it can be inferred that Ag-USY prepared by two ion-exchanges exhibits a higher silver content at the surface compared to Ag-USY prepared by solid-exchange. These results are consistent with elemental analysis, which indicated a silver content of 1.02 and 0.73 mmol/g, for two ion-exchanges and solid-exchange, respectively.

Binding energy values depend on the chemical state of the atom but also on its local physical and chemical environment. Atoms of higher positive oxidation state exhibit higher binding energy. It is also known that BE tend to shift to higher values in the Y-zeolite environment.³⁰³ In the present case, the collected values suggested that silver species may be in the +1 oxidation state at the surface of the zeolite,³⁰⁴ in agreement with the results of powder-XRD. Indeed, for metallic silver (Ag⁰), BE are known to be around 368.3 eV and 374.3 eV for Ag

³⁰³ Barr, T. L. *Appl. Surf. Sci.* **1983**, *15*, 1–35.

³⁰⁴ (a) Mun, S. H.; Kang, S. W.; Cho, J.-S.; Koh, S.-K.; Kang, Y. S. *J. Membr. Sci.* **2009**, *332*, 1–5. (b) Liu, N.; Gong, M.; Zhang, P.; Li, L.; Li, W.; Lee, R. *J. Mater. Sci.* **2011**, *46*, 3162–3168. (c) Huo, H.; Su, H.; Jiang, W.; Tan, T. *Biochem. Eng. J.* **2009**, *43*, 2–7.

$3d_{5/2}$ and Ag $3d_{3/2}$, respectively.³⁰⁵ We observed a positive BE chemical shift of 1.2 eV from theoretical Ag⁰ to Ag-USY, which may partly result from the Y zeolite environment. In addition, a binding energy of 369.4 eV for the Ag $3d_{5/2}$ of Ag-NaY was previously reported and is consistent with our result.³⁰⁶

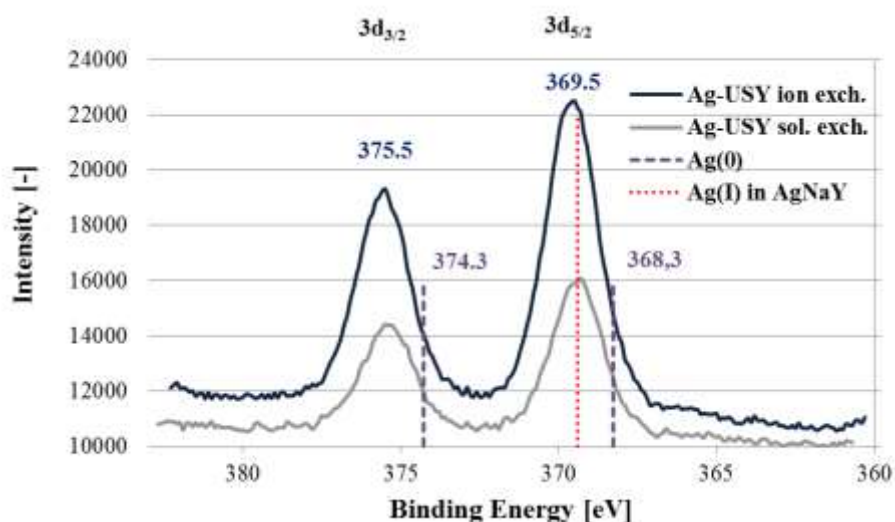


Figure 35. High resolution X-ray Photoelectron spectrum of the Ag 3d region of Ag-USY prepared by 2 ionic exchanges and solid exchange. Theoretical values of Ag⁰ (purple dotted lines), and an experimental value for Ag^I in AgNaY (red dotted line) are reported.

2.3. Influence of the zeolite topology on the hydroalkoxylation of alkynols

With these Ag-zeolites in hands, we first assessed the influence of their topology and pore dimensions on the hydroalkoxylation of simple commercial 4-pentyn-1-ol **3a** (Table 16). Experiments were carried out at *isoweight* of catalyst. Indeed, from a “green chemistry” and economical point of view, it can be interesting to identify the type of zeolite that requires the lowest amount of material to efficiently promote the reaction.

³⁰⁵ (a) Shin, H. S.; Choi, H. C.; Jung, Y.; Kim, S. B.; Song, H. J.; Shin, H. J. *Chem. Phys. Lett.* **2004**, *383*, 418–422. (b) Liu, N.; Gong, M.; Zhang, P.; Li, L.; Li, W.; Lee, R. *J. Mater. Sci.* **2011**, *46*, 3162–3168. (c) Anson, A.; Maham, Y.; Lin, C. C. H.; Kuznicki, T. M.; Kuznicki, S. M. *J. Nanosci. Nanotechnol.* **2009**, *9*, 3134–3137. (d) Zhang, C.; Yang, Q.; Zhan, N.; Sun, L.; Wang, H.; Song, Y.; Li, Y. *Colloids Surf., A* **2010**, *362*, 58–64.

³⁰⁶ Takahashi, A.; Yang, R. T.; Munson, C. L.; Chinn, D. *Ind. Eng. Chem. Res.* **2001**, *40*, 3979–3988.

To our delight, in the presence of each Ag-zeolite the reaction produced the acetal **4a**, resulting from the tandem cyclization/hydroalkoxylation of **3a**, as previously reported with Rh^I and Ir^I complexes.³⁰⁷

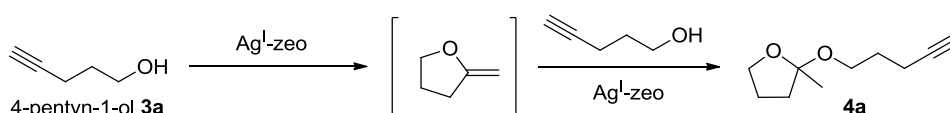
Table 16. Isoweight comparison of Ag-zeolites for the cycloisomerization of 4-pentyn-1-ol.

4-pentyn-1-ol **3a** (200 mg) $\xrightarrow[\text{neat, rt, 24 h}]{\text{Ag}^{\text{I}}\text{-zeo, 55 mg}}$ **4a**

Entry	Ag-zeolite	Topology	Pore diameter	Yield (%)
1	H-USY	cage-type	7.4 x 7.4 Å	0 ^a
2	Ag-USY sol. ^b	cage-type	7.4 x 7.4 Å	26 ^c
3	Ag-USY 1 imp. ^d	cage-type	7.4 x 7.4 Å	75 ^c
4	Ag-USY 2 imp. ^e	cage-type	7.4 x 7.4 Å	85 ^c
5	Ag-NaY 2 imp. ^f	cage-type	7.4 x 7.4 Å	0 ^a
6	Ag-β 1 imp.	channel-type	7.6 x 6.4 Å 5.5 x 5.5 Å	40 ^g
7	Ag-ZSM-5 1 imp.	channel-type	5.1 x 5.5 Å 5.3 x 5.6 Å	18 ^g
8	Ag-MOR 1 imp.	channel-type	6.5 x 7.0 Å 2.6 x 5.7 Å	15 ^g

^a No conversion. ^b Ag-USY prepared by solid exchange, 0.73 mmol Ag/g. ^c Isolated yield. ^d Ag-USY prepared by one ion-exchange, 0.86 mmol Ag/g. ^e Ag-USY prepared by 2 ion-exchanges, 1.02 mmol Ag/g. ^f Ag-NaY prepared by 2 ion-exchanges, 2.29 mmol Ag/g. ^g Yields assessed from ¹H NMR of the crude.

The reaction was regioselective, since 5-*exo*-dig cyclization exclusively occurred, as previously reported by Pale and co-workers under silver catalysis.²⁹⁵ However, in contrast, the α-methylene oxolane intermediate could not be detected or isolated, and the second hydroalkoxylation directly took place to yield acetal **4a** (Scheme 84). The same regioselectivity was also observed by Messerle and co-workers with Rh^I and Ir^I catalysts.³⁰⁷



Scheme 84. Double hydroalkoxylation of 4-pentyn-1-ol leading to an acetal self-adduct.

The purely acidic H-USY, used as reference, did not give any transformation while all Ag-doped zeolites gave the ketal cycloisomerization in low to high yields (Table 16). These results confirmed the necessity of silver(I) to promote the transformation (entry 1). Medium-

³⁰⁷ Elgafi, S.; Field, L. D.; Messerle, B. A. *J. Organomet. Chem.* **2000**, 607, 97–104.

pores zeolites exhibiting one-dimensional (entry 8) or interconnected channels (entries 6 and 7) afforded poor yields of acetals. By comparison, the cage-type USY seemed more efficient. However, the preparation method proved critical, as only Ag-USY prepared by ionic exchange provided high yields of acetals (entries 3-4 *versus* 2). Further characterization of Ag-USY prepared by solid exchange has to be performed to determine the origin of its lower activity. Since elemental analysis and XPS did not show any irregularity in the chemical composition or chemical state of silver, the difference may rather be correlated to the structure and/or morphology of the material.

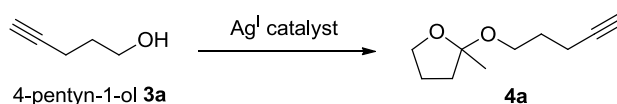
With the same large pore diameters but free of Brønsted acid sites, Ag-NaY was not able to promote any conversion of 4-pentyn-1-ol, contrary to Ag-USY zeolites prepared by ion or solid exchange (entry 5). Despite the structural variations accompanying the synthesis of USY from Y, such as the creation of mesoporosity, the absence of conversion with Ag-NaY should not be attributed to the porosity, since zeolites with small pores proved that they were able to catalyze the reaction. In addition, at isoweight of catalyst, Ag-NaY exhibits twice the silver loading of Ag-USY. The lack of Brønsted acidity in Ag-NaY is thus the most likely explanation for the absence of reaction. An additional experiment in the presence of Ag-(H)-Y would allow to shed light on this issue.

2.4. Screening of reaction conditions for the cyclization of alkynols

Having identified Ag-USY prepared by 2 ion-exchanges as a promising catalyst for the reaction, we examined various factors which may influence the result of the tandem cyclization/hydroalkoxylation, and we compared other types of catalysts, in order to set up appropriate reaction conditions (Table 17).

Control experiments using the conditions of Pale and co-workers²⁹⁵ confirmed that the zeolite medium was not necessary to catalyze the ketal formation. Indeed, contrary to what Pale and co-workers reported,^{295b} the acetal **4a** could be isolated in 65 % yield after 11 h at 80 °C in the presence of 2 mol% silver carbonate in toluene (entry 1). Surprisingly, in the absence of solvent, Ag₂CO₃ was also able to promote the reaction, although in low yield (entry 2).

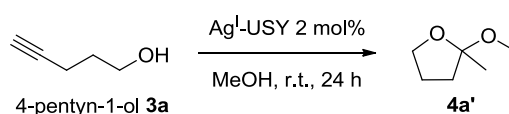
At room temperature with 2 mol % Ag-USY, 24 h seemed necessary to complete the reaction (entries 3-4). Higher temperature dramatically increased the reaction rate (entry 5) but also proved deleterious (entry 6). Lower catalytic charge resulted in incomplete conversion (entry 9).

Table 17. Screening of reaction conditions for the cycloisomerization of 4-pentyn-1-ol **3a**.

Entry	Ag-catalyst	Ag (mol%)	Solvent	T (°C), t (h)	Yield (%)
1	Ag ₂ CO ₃	2	PhMe	r.t. – 80 °C, 11 h	65
2	Ag ₂ CO ₃	2	neat	r.t. – 80 °C, 24 h	13 ^a
3	Ag-USY 2 imp. ^b	2	neat	r.t., 24 h	85
4	“	“	neat	r.t., 16 h	77
5	“	“	neat	50 °C, 1 h	63
6	“	“	neat	80 °C, 3 h	17
7	“	“	MeOH (1 eq.)	r.t., 24 h	77
8	“	“	MeOH (4 eq.)	r.t., 24 h	62
9	“	1	neat	r.t., 24 h	62
10	Ag ₂ H ₂ SiW ₁₂ O ₄₀	2	neat	r.t., 4 h	24
11	“	2	DCM	r.t., 4 h	60
12	“	2	DCM	r.t., 24 h	61
13	“	5	DCM	r.t., 24 h	24 ^c
14	Ag ₃ HSiW ₁₂ O ₄₀	2	DCM	r.t., 24 h	27
15	Ag ₄ SiW ₁₂ O ₄₀	2	DCM	r.t., 24 h	33 ^d
16	“	5	DCM	r.t., 24 h	62

^a Assessed from ¹H NMR of the crude, 87 % starting material. ^b Ag^I-USY prepared by 2 ion-exchanges, 1.02 mmol Ag/g. ^c Degradation of the acetal occurred. ^d Conversion assessed by TLC < 50 %.

In the presence of methanol (entries 7-8), the latter was incorporated in place of 4-pentyn-1-ol, leading to 2-methoxy-2-methyltetrahydrofuran **4a'** (Scheme 85). It is noteworthy that the yield of acetal was higher at lower concentrations of methanol (1 *versus* 4 equivalents). Similar tandem cycloisomerizations/hydroalkoxylations in the presence of external alcohol nucleophiles were already reported with Pt^{II},²⁸⁷ Au^I,³⁰⁸ Rh^I and Ir^I catalysts.³⁰⁷

Scheme 85. 2-methoxy-2-methyltetrahydrofuran **4a'** obtained in the presence of methanol.

Following our results in the rearrangement of alkynyloxiranes under Ag-H-POMs catalysis (*cf.* Chapter III), we were also interested in exploring the potential of silver heteropolyacids toward this tandem cyclization/hydroalkoxylation. The Ag-POMs prepared for the rearrangement of alkynyloxiranes to furans were thus compared to Ag-USY. Without any

³⁰⁸ Belting, V.; Krause, N. *Org. Lett.* **2006**, *8*, 4489–4492.

solvent, $\text{Ag}_2\text{H}_2\text{SiW}_{12}\text{O}_{40}$ seemed not particularly stable and only 24% yield of acetal could be isolated from the dark sticky mixture formed after 4 h (entry 10). Since the Ag-POM catalyzed rearrangement of alkynyloxiranes was efficient in dichloromethane, this solvent was then investigated. As expected, under these conditions the yield increased to 60 % after 4 h (entry 11). Longer reaction times were not beneficial, and higher catalytic charge proved deleterious, as degradation of the acetal partly occurred after 24 h with 5 mol% $\text{Ag}_2\text{H}_2\text{SiW}_{12}\text{O}_{40}$ (entry 13 *versus* 12).

As already noticed in the rearrangement of alkynyloxiranes, the Ag/H ratio seemed particularly influential on the reaction. Indeed, 2 mol% $\text{Ag}_3\text{HSiW}_{12}\text{O}_{40}$ or $\text{Ag}_4\text{SiW}_{12}\text{O}_{40}$ afforded roughly 30 % yield, compared to the 60 % obtained with $\text{Ag}_2\text{H}_2\text{SiW}_{12}\text{O}_{40}$ (entries 14 and 15 *versus* 12). In the case of $\text{Ag}_4\text{SiW}_{12}\text{O}_{40}$, the conversion was low according to thin layer chromatography. When the catalytic charge was raised to 5 mol%, a 62 % yield was finally reached, and no significant acetal degradation was observed (entry 16).

In summary, the results showed that silver(I) alone was able to promote the tandem cyclization/hydroalkoxylation (Ag_2CO_3 , Ag_4 -POM), but an appropriate concomitant acidity clearly increased the efficiency of the reaction. This acidity can be brought either by residual protons in Ag-doped zeolites or by an appropriate Ag-H-POM. On the other hand, too much acidity proved deleterious to the acetal moiety, as one would expect from an acid labile ketal functional group.

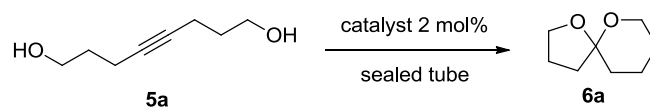
2.5. Screening of reaction conditions for the dihydroalkoxylation of alkyne diols

In complement to this study, a screening of catalysts and reaction conditions was also performed on the dihydroalkoxylation of alkyne diols (Table 18). Model substrate chosen for this purpose was oct-4-yn-1,8-diol **5a**, available in 3 steps from but-2-yn-1,4-diol.³⁰⁹

³⁰⁹ von Hirschheydt, T.; Wolfart, V.; Gleiter, R.; Irngartinger, H.; Oeser, T.; Rominger, F.; Eisentrager, F. *J. Chem. Soc., Perkin Trans. 2* **2000**, 175–183.

Table 18. Screening of reaction conditions for the dihydroalkoxylation of oct-4-yn-1,8-diol

5a.



Entry	Ag-catalyst	Solvent	T (°C), t (h)	Yield (%)
1	Ag ₂ CO ₃	neat	r.t. – 95 °C, 24 h	0 ^a
2	H-USY	neat	r.t. – 95 °C, 24 h	0 ^a
3	Ag-ZSM-5 ^b	neat	r.t. – 95 °C, 22 h	16 ^c
4	Ag-USY sol. ^d	neat	r.t. – 95 °C, 24 h	54 ^e
5	Ag-USY 2 imp. ^f	neat	r.t. – 95 °C, 24 h	83
6	Ag-NaY ^g	neat	95 °C, 21 h	79 ^h
7	Ag-USY w. EFAL ⁱ	neat	95 °C, 21 h	73
8	Ag-USY 2 imp. ^f	pentane	60 °C, 22 h	15
9	“	Et ₂ O	95 °C, 20 h	47
10	“	CH ₂ Cl ₂	95 °C, 20 h	20
11	“	CH ₃ CN	95 °C, 24 h	27
12	“	MeOH	95 °C, 22 h	78
13	Ag ₂ H ₂ SiW ₁₂ O ₄₀	neat	95 °C, 7 h	45
14	“	MeOH	95 °C, 24 h	79 ^j
15	Ag ₄ SiW ₁₂ O ₄₀	neat	95 °C, 7 h	71
16	“	MeOH	95 °C, 24 h	80 ^j

^a No conversion. ^b Ag-ZSM-5 prepared by 2 ion-exchanges, 0.49 mmol Ag/g. ^c 84 % of recovered starting material. ^d Ag-USY prepared by solid exchange, 0.73 mmol Ag/g. ^e 33 % of recovered starting material. ^f Ag-USY prepared by two ion-exchanges, 1.02 mmol Ag/g. ^g Ag-NaY prepared by 2 ion-exchanges, 2.29 mmol Ag/g. ^h with 5 mol% Ag-NaY. ⁱ Ag-USY prepared by 2 ion-exchanges, without Extra-Framework Aluminum species (EFAL), 1.16 mmol Ag/g. ^j Yields assessed by ¹H NMR of the crude.

Without any solvent, silver carbonate alone or purely acidic H-USY were not able to promote any transformation, at room temperature or at 95 °C (entries 1-2). In the presence of 2 mol% silver-zeolites, the cycloisomerization occurred but required heating at 95 °C (reaction in sealed tube). Moreover, the reaction efficiency was highly dependent on the zeolite structure. With interconnected channels of medium diameters (5.1 x 5.5 and 5.3 x 5.6 Å), Ag-ZSM-5 afforded only 16 % of spiroketal **6a**, and most of the starting material was recovered (entry 3). In contrast, with its large spherical pores (7.4 x 7.4 Å), Ag-USY was more active as catalyst, but its efficiency depended on the preparation method. Indeed, as in the ketal formation from 4-pentyn-1-ol, Ag-USY prepared by solid exchange was less efficient, providing the expected spiroketal in 54 %, against 83 % yield for Ag-USY prepared by two ion-exchanges (entries 4 and 5). Contrary to the result obtained with 4-pentyn-1-ol, Ag-NaY was as efficient in the spiroketalization of **9a** as the Ag-USY containing Brönsted acid sites. This result suggested that the presence of Brönsted acidity was not decisive for the reaction.

It is known that the dealumination process performed at high temperature to synthesize USY from Y zeolite leads to the creation of Extra-Framework Aluminum species (EFAL). In some cases it was shown that the removal of EFAL produced more active catalysts.³¹⁰ Several suggestions have been put forward, and notably, the creation of strong Brønsted acid sites.^{310a} The removal of EFAL particles that would block a fraction of the micropores of USY has also been proposed as an explanation for the enhanced activity,³¹¹ but has not been unambiguously demonstrated.^{310a} In order to determine the effect of EFAL on the dihydroalkoxylation of oct-4-yn-1,8-diol, we decided to prepare a EFAL-free Ag-USY. The removal of EFAL was carried out according to reported procedures,^{310b} by refluxing H-USY in a solution of ethylenediaminetetraacetic acid (disodium salt: Na₂H₂-EDTA) at 335 K for 24 h. EDTA is a hexadentate ligand known for its ability to bind metal ions such as Al³⁺. The resulting EFAL-free Na-USY was then ion-exchanged with a solution of ammonium nitrate, to obtain the EFAL-free NH₄-USY. Subsequent silver-doping was performed by usual ion-exchange (two times). Ag-USY without EFAL was still active as catalyst, leading to the expected spiroketal in similar yield compared to the regular Ag-USY (entry 7). This result suggested a minor role of EFAL on the cyclization.

Although the reaction perfectly proceeded without solvent, it could be necessary to find one for the transformation of solid starting materials with high melting points. In this context, a rapid screening was carried out using the best catalyst Ag-USY. The reaction did not proceed very well in apolar *n*-pentane, and barely more in polar aprotic solvents such as dichloromethane and acetonitrile (entries 10-11). Curiously, almost 50 % yield was reached in diethyl ether, and more interestingly, the transformation proceeded very well in polar protic methanol, affording a 78 % yield of spiroketal, without any side product or intermediate related to the incorporation of the latter.

Silver HPA were also investigated and compared to Ag-USY for this dihydroalkoxylation of alkynediols. Without solvent, the reaction was stopped after 7 hours, due to the formation of dark viscous mixtures, as observed with 4-pentyn-1-ol. Nevertheless, the reaction yielded 45 % and 71 % of the expected spiroketal **6a**, with Ag₂H₂SiW₁₂O₄₀ and Ag₄SiW₁₂O₄₀, respectively. This difference might be accounted for the sensitivity and decomposition of spiroketal under strong acid conditions, as observed for acetal **4a** derived from 4-pentyn-1-ol.

³¹⁰ (a) Katada, N.; Kageyama, Y.; Takahara, K.; Kanai, T.; Begum, H. A.; Niwa, M. *J. Mol. Catal. A Chem.* **2004**, *211*, 119–130. (b) Xu, B.; Bordiga, S.; Prins, R.; van Bokhoven, J. A. *Appl. Catal., A* **2007**, *333*, 245–253.

³¹¹ Kuehne, M. A.; Kung, H. H.; Miller, J. T. *J. Catal.* **1997**, *171*, 293–304.

The use of methanol as solvent was investigated due to the interesting result obtained with Ag-USY (entry 12). Indeed, in that case, the reaction proved as effective with both catalysts, affording 80 % of spiroketal after 24 h.

In summary, the results demonstrated that silver(I) alone (Ag-NaY, Ag₄-POM) was able to promote the spiroketalization of alkynediols. Contrary to the tandem cycloisomerization/hydroalkoxylation of 4-pentyn-1-ol, the presence of Brønsted acidity in the catalyst did not seem to particularly favor the spiroketalization. In both reactions, Ag-USY prepared by ion exchange proved to be a very efficient catalyst, able to promote complete transformations without any solvent.

2.6. Scope of the Ag-USY catalyzed cyclization of alkynols and alkynediols

With a suitable catalyst in hand, we prepared a series of alkynols and alkynediols, in order to determine the scope of this ketal and spiroketal synthesis.

The hydroalkoxylation of alkynols **3a-e** proved regioselective (Table 19), occurring exclusively in a 5-*exo*-dig pathway, and despite the possibility of 6-*endo*-dig ring closure. The same regioselectivity was already reported with Rh^I and Ir^I catalytic systems,²⁹² notably.

The formation of the 6-membered oxane **4b** from commercial 5-hexyn-1-ol **3b** was slightly more difficult than its 5-membered counterpart, and required a slight heating at 35 °C to be effective (entry 2).

The conversion of (*Z*)-2,3-epoxy-3-methylpent-4-ynol **3c**, readily prepared by *m*-CPBA epoxidation of (*Z*)-3-methylpent-2-en-4-ynol, remained very limited under the set up conditions. The starting material being solid until 40 °C, heating was necessary in the absence of solvent. After 24 h at 80 °C, the expected acetal **4c** was recovered in only 8 %, along with degradation. By comparison, the EFAL-free Ag-USY provided approximately twice the yield of acetal.³¹² In methanol, no conversion could be observed after 24 h at room temperature. However, upon heating at 95 °C, the corresponding acetal **4c'** could be detected and isolated in 16 % yield after 4 h. The low yields obtained with this substrate may be attributed to the sensitivity of the intermediate α -methylene oxolane, especially in the presence of Brønsted acid catalysts. It is noteworthy that the same compound reacted efficiently under the

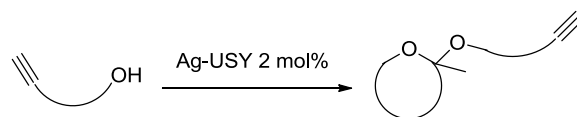
³¹² (a) Katada, N.; Kageyama, Y.; Takahara, K.; Kanai, T.; Begum, H. A.; Niwa, M. *J. Mol. Catal. A Chem.* **2004**, *211*, 119–130. (b) Xu, B.; Bordiga, S.; Prins, R.; van Bokhoven, J. A. *Appl. Catal., A* **2007**, *333*, 245–253.

conditions of Pale et al.²⁹⁵ (10 mol% Ag₂CO₃, benzene, 80 °C, 1 h), giving quantitatively the corresponding 2-methylene oxolane.

Similarly, no conversion could be observed in the reaction of *trans*-2-propargyl cyclohexanol **3d** at room temperature (entry 5). Heating at 95 °C for 24h only resulted in poor conversion or degradation. Under the conditions of Pale,²⁹⁵ this substrate could be converted but required 1 equivalent of silver carbonate, along with heating at 80 °C for 6 h. Moreover, the product was too sensitive to be isolated and was only identified by ¹H NMR after reaction in deuterated benzene.

To our delight, in the presence of Ag-USY the commercial 4-pentynoic acid yielded the expecting lactone **4e** and the ketone **4e'**, resulting from hydrolysis of its acetylenic end. The two products were isolated in a global 57 % yield, with a 38:62 ratio in favor of the ketone **4e'**.

Table 19. Scope of the Ag-USY catalyzed hydroalkoxylation of acetylenic alcohols.

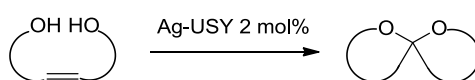


Entry	Alkynol	Acetal	Solvent	T (°C), t (h)	Yield (%)
1	3a	4a	-	r.t., 24 h	85
2	3b	4b	-	35 °C, 24 h	68
3	3c	4c	-	80 °C, 24 h	8 (19 ^a)
4	3c	4e'	MeOH	r.t.- 95 °C, 4 h	16
5	3d	4d	-	r.t. - 95 °C, 24 h	0 ^b
6	3e	4e	-	80 °C, 24 h	57 (38:62)
		4e'			

^a Run with 2 mol% Ag-USY without EFAL. ^b Incomplete conversion and degradation occurred.

A panel of aliphatic and aromatic alkynediols was then submitted to Ag-USY, due to the high synthetic interest of the potential fused bicyclic ketals and spiroketals (Table 20). In all cases, heating at 95 °C was necessary, as found in the screening of reaction conditions. Linear alkynediols **5a** and **5b** were converted into the corresponding spiroketals **6a**, **6b** and **6b'** in high yields, without solvent and in the presence of only 2 mol% Ag-USY. In the case of **5b**, selectivity in favor of the spiro[5.5]- or [4.6]ketal was not clearly observed, both being obtained in a ratio of (42:58). This result only suggested a slight preference for the 5-*exo* + 7-*endo* pathway compared to the 6-*endo* + 6-*exo* alternative.

Table 20. Scope of the Ag-USY catalyzed dihydroalkoxylation of alkynediols.



Entry	Alkynediol	Acetal or Spiroketal	Solvent	T (°C), t (h)	Yield (%)
1	5a	6a	-	95 °C, 24 h	83
2	5b	6b 6b'	-	95 °C, 24 h	86 (42:58)
3	5c	6c	-	95 °C, 22 h	21 ^a (80:20)
4	5c	6c'	PhMe	110°C, 24 h	46 (66:34)
5	5c	6c	MeOH	95 °C, 2 h	70 ^a (41:59)
6	5d	6d	-	95 °C, 24 h	51 ^a (17:83)
7	5d	6d'	-	95 °C, 24 h	47 ^c (12:88)
8	5d	6d 6d'	MeOH	95 °C, 2 h	85 (10:90)
9	5e	6e	-	95 °C, 24 h	16 ^a
10	5e	6e	PhMe	110°C, 24 h	18
11	5e	6e	MeOH	95 °C, 2 h	88 ^a
12	5f	6f	MeOH	95 °C, 24 h	47 ^a (74 ^b)
13	5f	6f			81 ^c
14	5g	6g	-	80 °C, 23 h	81
15	5h	6h	-	95 °C, 52 h	65
16	5h	6h	-	95 °C, 7 h	73 ^a

^a Run with 5 mol% Ag-USY. ^b Run with 5 mol% Ag-USY without EFAL. ^c Run with 10 mol% Ag-USY.

A series of aromatic alkynediols was examined afterwards. Under the usual reaction conditions, conversions remained incomplete, with yields ranging between 16 and 51 %

(entries 3, 6 and 9). Since alkynediol **5e** was solid at room temperature, we suspected that in the absence of solvent, the viscosity of the reaction mixtures could limit the diffusion of the substrates in the zeolite. However, the use of toluene to increase the solubility did not allow to reach complete conversions (entries 4 and 10).

Higher catalyst loading proved also ineffective (entry 7 *versus* 6). Therefore, with the results of solvents screening in mind (Table 18), we decided to attempt the cyclizations in methanol. Indeed, under these conditions we were very pleased to observe high yields and very fast transformations, complete in only a couple of hours (entries 5, 8 and 11). Due to a short acetylenic chain, alkynediol **5c** afforded a mixture of spiro[4.4]ketal **6c** and monocyclized enol ether **6c'** in a 41:59 ratio. Interestingly, without methanol, the selectivity was reversed, in favor of **6c** (80:20). It is worth noting that **5c** yielded the same mixture of compounds with similar selectivity under rhodium or iridium catalysis.²⁹² On the other hand, the PPh₃AuCl/AgOTf combination exclusively afforded the spiro[4.4]ketal **6c**.²⁸⁸

Spiro[4.5]ketals **6d** and **6d'** were both obtained from 5-[(2-hydroxymethyl)phenyl]pent-4-yn-1-ol, with a large regioselectivity in favor of **6d'** (> 20:80), whatever the conditions, with or without methanol. The same alkynediol gave a 50:50 or 37:63 ratio in the presence of rhodium and iridium complexes,²⁹² against 60:40 with gold catalyst.²⁸⁸

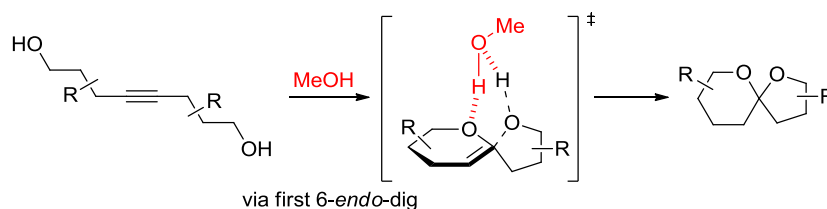
Despite its similarity with **5b**, which gave a mixture of regioisomers, 6-[(2-hydroxymethyl)phenyl]hex-5-yn-1-ol **5e** yielded the spiro[5.5]ketal **6e** exclusively, as found in other transition metal catalyzed homogeneous versions.^{288,292}

Interestingly, the large and rigid bisbenzannelated alkynediol **5f** could also be cyclized to the corresponding spiro[5.6]ketal **6f**. With 5 mol% Ag-USY, conversion was not complete, yielding a moderate 47 % yield. Again, Ag-USY without EFAL proved to be more effective, giving a 73 % yield for the same catalyst loading. It is worth noting that 10 mol% Ag-USY allowed to reach 81 % of the spiroketal **6f**.

The Ag-USY catalyzed dihydroalkoxylation of alkynediols was also efficient in the preparation of fused bicyclic ketals such as **6g** and **6h**, obtained respectively in 81 and 65 % yield with only 2 mol% catalyst, without solvent. Long reaction time was necessary for **6g** but could be drastically reduced with higher catalyst loading (entry 16 *versus* 15). The access to these hexahydrofurofuran and pyran motifs is very interesting as they can be found in a number of natural and bioactive compounds.³¹³

³¹³ (a) Wu, X. Y.; Liu, X. H.; Lin, Y. C.; Luo, J. H.; She, Z. G.; Houjin, L.; Chan, W. L.; Antus, S.; Kurtan, T.; Elsässer, B.; Krohn, K. *Eur. J. Org. Chem.* **2005**, 2005, 4061–4064. (b) Rosselli, S.; Maggio, A.; Piozzi, F.;

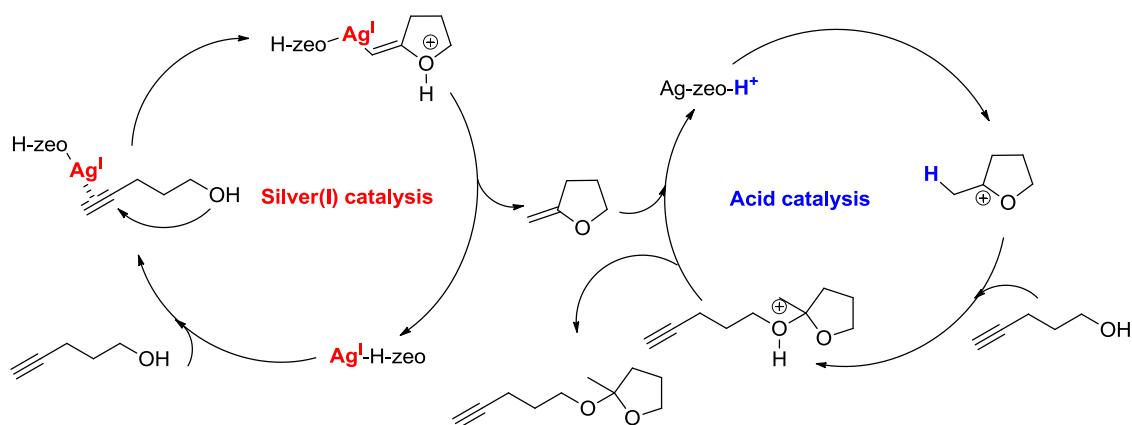
represented example, we suggested the formation of a 6-*endo*-dig intermediate, which would undergo 5-*exo*-trig ring closure in a second place, through the assistance of methanol hydrogen bonding. However, the reversed cyclization order (5-*exo*-dig then 6-*endo*-trig) could also be imagined.



Scheme 88. Possible accelerating effect by hydrogen bonding in presence of methanol.

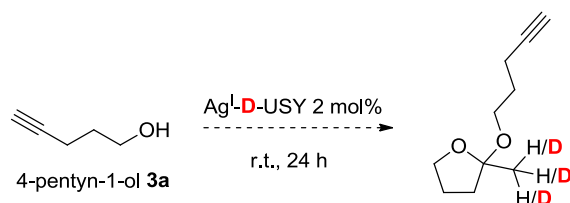
Concerning the reaction mechanism, based on the screening of catalysts (Table 16, Table 17 and Table 18), the tandem cycloisomerization/hydroalkoxylation of alkynols seemed to be favored by a silver(I) and concomitant Brønsted acid catalysis. Indeed, the reaction did not work with the Brønsted acid free Ag-NaY zeolite, and required higher catalyst loading to reach satisfying yield with Ag₄SiW₁₂O₄₀. Therefore, the following reaction mechanism using 4-pentyn-1-ol as an example could be proposed (Scheme 89). The first 5-*exo*-dig ring closure would be performed under silver(I) catalysis. The coordination of silver(I) to the triple bond makes the latter very prone to nucleophilic attack from the internal hydroxyl functional group. This step would release a reactive α -methylene oxolane intermediate after protodemetalation. In a second catalytic cycle, a Brønsted acid site of the Ag-doped zeolite would protonates the double bond. Nucleophilic attack of an external alkynol molecule on the resulting tertiary carbocation would give the expected acetal, after regeneration of the Brønsted acid site.

Indeed, in the absence of such acid catalyst, the Lewis acidity of silver(I) should also be able to catalyze this second hydroalkoxylation, although less efficiently. The same type of mechanism has already been proposed for similar reaction under gold/acid catalysis.³⁰⁸ In the absence of acid co-catalyst, the authors could only detect the formation of an *endo*-cyclization product, whereas the addition of *p*-toluene sulfonic acid led to the acetal.



Scheme 89. Proposed reaction mechanism for the dihydroalkoxylation of acetylenic alcohols.

An additional experiment with a deuterated Ag-USY zeolite catalyst should help to confirm or not this mechanism. The formation of acetal containing deuterium at the methyl position would bring evidence that the acid sites of the catalyst are able to protonate the intermediate oxolane (Scheme 90).

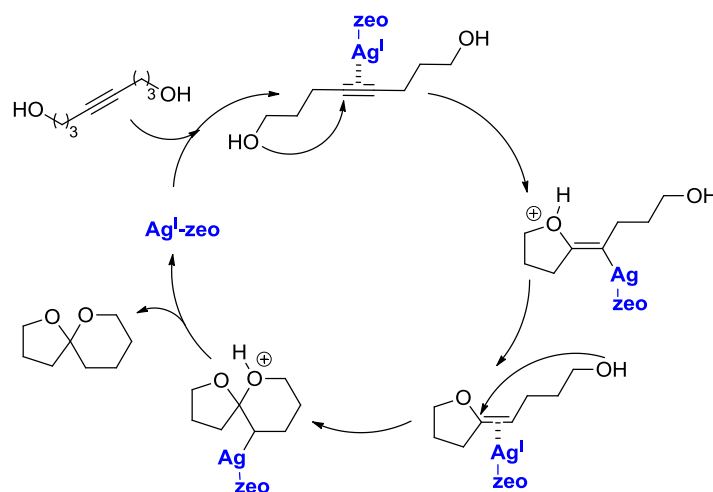


Scheme 90. Proposed control experiment to shed light on the reaction mechanism.

On the other hand, the screening of reaction conditions for the dihydroalkoxylation of alkyndiols suggested that the presence of Brønsted acidity had no significant effect on the reaction (Table 18). Indeed, Ag-NaY, Ag₂H₂SiW₁₂O₄₀ and Ag₄SiW₁₂O₄₀ were as efficient as the best catalyst Ag-USY. The use of methanol dramatically accelerated the reaction rate and enabled the conversion of aromatic alkyndiols, relatively inert in the absence of solvent.

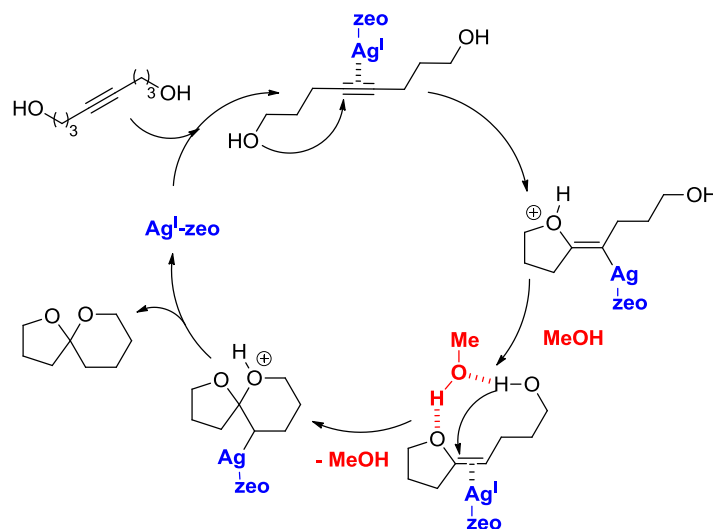
Based on these observations, we can distinguish two possibilities. For the conversion of aliphatic alkyndiols, effective without solvent, a mechanism based on silver(I) catalysis only can be proposed (Scheme 91). Once coordinated to a silver ion anchored in the zeolite pores, the alkyne would undergo nucleophilic addition of one of its terminal hydroxyl groups, leading to an alkylidene oxygenated heterocycle. It is noteworthy that this type of intermediate has been isolated (**6c'**), starting from the alkyndiol **5c**, which supports this hypothesis (Table 20, entries 3, 4 and 5). Still coordinated to the silver zeolite, this enol ether

would then undergo a second nucleophilic addition of the remaining hydroxyl group, providing the corresponding ketal.



Scheme 91. Proposed reaction mechanism for the neat synthesis of spiroketals.

For the reactions carried out in methanol, we could assume a second hydroalkoxylation assisted by hydrogen bonding, once the enol ether has formed (Scheme 92).



Scheme 92. Proposed reaction mechanism in the presence of MeOH.

2.8. Recyclability of Ag-USY

After the evaluation of the scope of this cyclization of alkynols and alkynediols, we finally investigated the recyclability of Ag-USY. It is worth mentioning that no leaching of silver was detected when the cyclization was performed in methanol. To check this hypothesis, Ag-

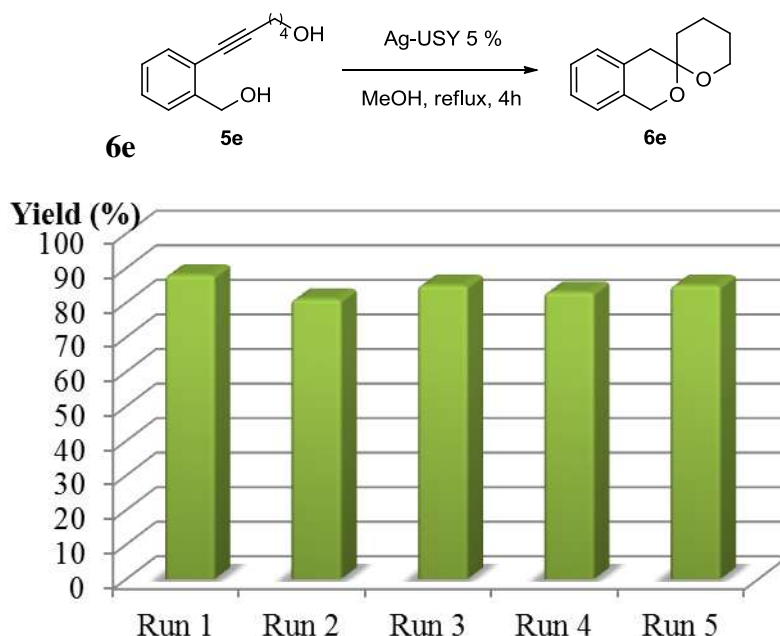
USY was stirred in MeOH at reflux for 24 h. After filtration of the catalyst, alkyndiol **5e** was added but no conversion could be detected after 4 h at 85 °C.

In a first attempt to recycle the heterogeneous catalyst, Ag-USY was simply filtered over Nylon® membrane after reaction, washed with methanol and dried for 6 h at 110 °C. Unfortunately, this ‘soft’ post-treatment seemed not sufficient and the activity of the catalyst dramatically dropped already at the second run. ¹H NMR showed after 24 h that only traces of product were present, the starting material remaining almost entirely untouched.

Therefore, in a second attempt, the brown powder recovered after filtration was washed with methanol, briefly dried at 110 °C and then calcinated at 550 °C overnight, which gave back to Ag-USY its native white color.

Interestingly, this calcination proved to be very beneficial and allowed Ag-USY to keep its activity for at least 5 runs without decrease in yield (88 %, 81 %, 85 %, 83 %, 85 %) or necessity of longer reaction time (Figure 36).

Figure 36. Recycling of Ag-USY in the cyclization of alkyndiol **5e** to spiro[5.5]ketal



3. Conclusion

In this study, we have developed a novel heterogeneous route for the tandem cyclization/hydroalkoxylation of alkynols and the double cyclization of alkyndiols to acetals, bicyclic ketals and spiroketals. Ag-USY prepared by ionic exchanges proved to be the best catalyst for these transformations. Moreover, this zeolite was effective at low silver loading

(2-5 mol%) and in the absence of solvent. Provided calcination between each run, the catalyst could be recycled without activity loss for at least 5 successive reactions.

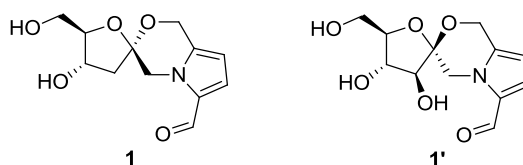
This study constitutes the first spiroketalization strategy mediated by silver(I), and the first access to spiroketals *via* heterogeneous catalysis. Compared to other transition metal catalyzed spiroketalizations, using gold or rhodium for instance, different regioselectivities were noticed, and interestingly, spiroketalizations were dramatically accelerated in the presence of methanol as solvent. As suggested by previous studies, hydrogen-bonding catalysis could be responsible for this acceleration. In the future, isotopic labeling experiments have to be carried out to confirm the proposed reaction mechanisms.

Chapter 5 :
Toward the total synthesis of acortatatin A,
using a Ag^I-catalyzed spiroketalization
strategy

1. *Acortatarin A: a natural product of biological interest*

Due to our successful preparation of spiroketal motifs from alkyne diols under heterogeneous catalysis with silver(I) zeolites, we have tried to extend this methodology to the synthesis of more complex natural products exhibiting a biological activity. In this context, we became interested in the acortatarin family of natural products, very recently isolated (cf. below) and for which, no total synthesis had been reported when we have started this work (see below).

In 2010, Hou and co-workers reported two novel spiroalkaloids **1** and **1'** (Scheme 93), isolated from the rhizome (roots of the plant) of *Acorus tatarinowii* Schott (Araceae).³¹⁵ Simultaneously, Zhang and co-workers reported the same spiroketal compound as **1**, isolated from bee-collected *Brassica campestris* (rapeseed) pollen.³¹⁶ Hou and Zhang named the spiroketal **1** respectively as acortatarin A and pollenopyrroside B, but only the former name remained afterwards.



Scheme 93. Acortatarin A/pollenopyrroside B (left) and acortatarin B (right).

Acortatarin A exhibit a unique tricyclic structure constituted of a sugar-morpholine fused spiroketal core, joined to a 2-formyl-pyrrole unit (Scheme 93). Interestingly, the rhizome of *A. tatarinowii* and the *B. campestris* pollen were both used in traditional Chinese medicine, respectively for treating central nervous system disorders,³¹⁵ and for strengthening the body's resistance against disease.³¹⁶ Up to date, proteins, polysaccharides, fatty acids and flavonoids have been identified in bee collected *B. campestris* pollen, conferring to the latter a wide range of biological activities, notably for the treatment of prostatitis, as antioxidant or antitumor agent.³¹⁶ On the other hand, plants from the genus *Acorus* are known to contain

³¹⁵ (a) Tong, X.-G.; Zhou, L.-L.; Wang, Y.-H.; Xia, C.; Wang, Y.; Liang, M.; Hou, F.-F.; Cheng, Y.-X. *Org. Lett.* **2010**, *12*, 1844–1847. (b) Tong, X.-G.; Zhou, L.-L.; Wang, Y.-H.; Xia, C.-F.; Wang, Y.; Liang, M.; Hou, F.-F.; Cheng, Y.-X. *Org. Lett.* **2011**, *13*, 4478.

³¹⁶ Guo, J.-L.; Feng, Z.-M.; Yang, Y.-J.; Zhang, Z.-W.; Zhang, P.-C. *Chem. Pharm. Bull.* **2010**, *58*, 983–985.

sesquiterpenoids and phenylpropanoids as major constituents.³¹⁷ Some of them possess anticonvulsive, spasmolytic, or neuroprotective effects.³¹⁷ The recently isolated acortatarins A and B were evaluated by Hou and co-workers for their potential inhibiting effect of high-glucose-induced Reactive Oxygen Species (ROS) production in renal mesangial cells.³¹⁵ ROS overproduction in renal cells is thought to be strongly related to the progression of Diabetic Nephropathy (DN), a major complication of diabetes.³¹⁸ It is known that ROS are produced by various pathways, including glucose metabolism.³¹⁹ However, the mechanism by which ROS accelerate the development of DN is still a matter of debate.³²⁰ Actually, free radicals including ROS are essential for host defense mechanisms in human body, but their overproduction leads to tissue damage and cell death.³²⁰ Usually, the right balance is achieved by the antioxidants naturally present in tissue, such as vitamins C, E or α -lipoic acid.³²⁰ Consequently, for a given molecule, the inhibition of ROS production is often associated with antioxidative properties. Hou and co-workers demonstrated that acortatarin A was able to inhibit ROS production in high-glucose-stimulated mesangial cells, in a dose- and time-dependent manner.³¹⁵ They correlated these results with an antioxidative property of acortatarin A. However, this hypothesis was later discredited by Aponick, based on electrochemical measurements (Figure 37).³²¹ The first and second oxidation potential of acortatarin A were found to be +1.74 and +1.90 V, whereas the value of common oxidants is rather below +0.70 V.³²² In addition, the results showed that the oxidation was not reversible. From these observations, the authors concluded that acortatarin A did not react with ROS as an antioxidant, but rather inhibited their production by another mechanism.

³¹⁷ (a) Ganjewala, D.; Srivastava, A. K. *Asian J. Plant Sci.* **2011**, *10*, 182–189. (b) Tong, X.-G.; Qiu, B.; Luo, G.-F.; Zhang, X.-F.; Cheng, Y.-X. *J. Asian Nat. Prod. Res.* **2010**, *12*, 438–442. (c) Tong, X.-G.; Wu, G.-S.; Huang, C.-G.; Lu, Q.; Wang, Y.-H.; Long, C.-L.; Luo, H.-R.; Zhu, H.-J.; Cheng, Y.-X. *J. Nat. Prod.* **2010**, *73*, 1160–1163.

³¹⁸ Ha, H.; Lee, H. B. *Kydney Int.* **2000**, *58*, S19–S25.

³¹⁹ (a) Lee, H. B.; Yu, M.-R.; Yang, Y.; Jiang, Z.; Ha, H. *J. Am. Soc. Nephrol.* **2003**, *14*, S241–S245. (b) Shi, X. Y.; Hou, F. F.; Niu, H. X.; Wang, G. B.; Xie, D.; Guo, Z. J.; Zhou, Z. M.; Yang, F.; Tian, J. W.; Zhang, X. *Endocrinology* **2008**, *149*, 1829–1839.

³²⁰ Rösen, P.; Nawroth, P. P.; King, G.; Möller, W.; Tritschler, H. J.; Packer, L. *Diabetes/Met. Res. Rev.* **2001**, *17*, 189–212.

³²¹ Borrero, N. V.; Aponick, A. *J. Org. Chem.* **2012**, *77*, 8410–8416.

³²² Penketh, G. E. *J. Appl. Chem.* **1957**, *7*, 512–521.

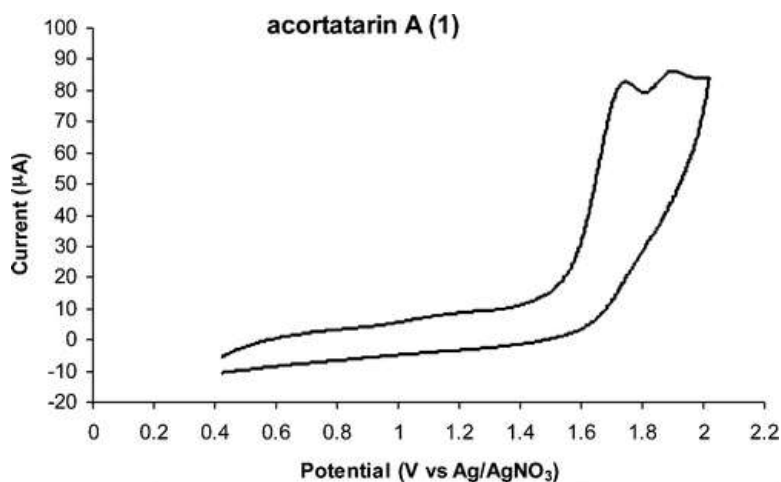


Figure 37. Voltammogram of acortatarin A in CH₃CN.

2. Previous total syntheses of acortatarin A

Soon after the identification of acortatarin, one total synthesis was reported by Jagadeesh and co-workers.³²³ Their retrosynthetic analysis was classically based on spiroketal formation from the corresponding ketone diol, **2** here, under acidic conditions (Scheme 94). The protected ketone **2** was obtained from the regioselective opening of the epoxide **5** by the 2,5-disubstituted pyrrole **3**. The latter was accessible from pyrrole **4**, while epoxide **5** was obtained after transformation of 2-deoxy-D-ribose **6**, available from the chiral pool. The synthesis required 11 steps and produced acortatarin with an overall yield of 6.4 %. It is worth noting that the spiroketalization provided a 9:1 mixture of diastereomers.

Very recently, three other total syntheses were reported. Similar to the work of Jagadeesh, Brimble et al. also proposed a synthesis based on acid mediated spiroketal formation from the protected ketone diol **7** (Scheme 95).³²⁴ The main novelty lied in the use of furan derivatives instead of very sensitive pyrroles. Following this idea, the ketone **7** was obtained from a Maillard-type reaction³²⁵ between the amino alcohol **11** and the sugar surrogate dihydropyranone **8**. The latter was available from Achmatowicz ring expansion³²⁶ of the furfuryl alcohol derivative **9**. On the other hand, the amino alcohol **11** was accessible in 7

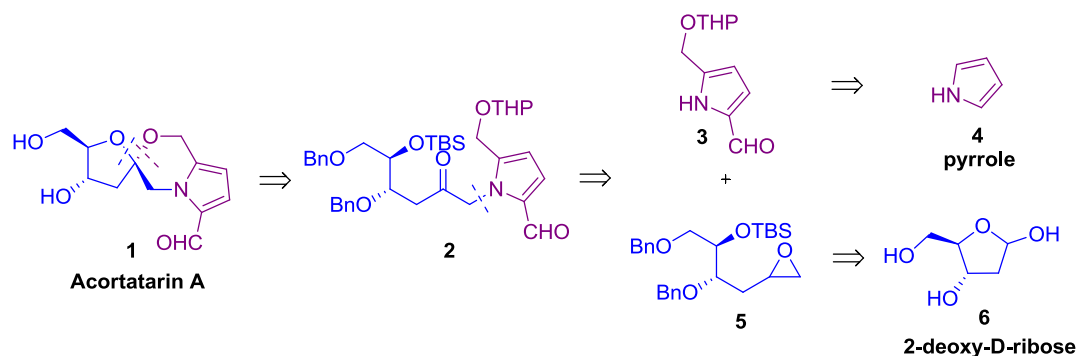
³²³ Sudhakar, G.; Kadam, V. D.; Bayya, S.; Pranitha, G.; Jagadeesh, B. *Org. Lett.* **2011**, *13*, 5452–5455.

³²⁴ Geng, H. M.; Chen, J. L.-Y.; Furkert, D. P.; Jiang, S.; Brimble, M. A. *Synlett* **2012**, *23*, 855–858.

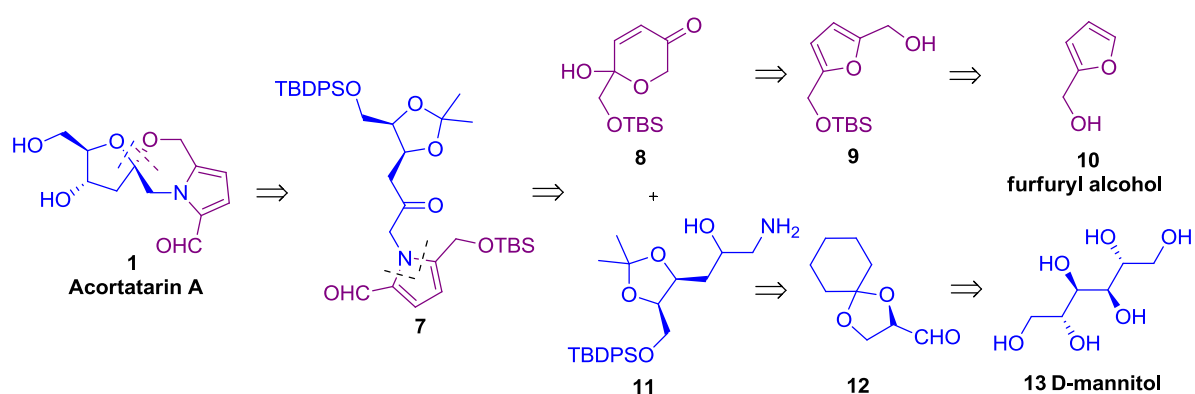
³²⁵ (a) Glomb, M. A.; Monnier, V. M. *J. Biol. Chem.* **1995**, *270*, 10017–10026. (b) Flores-Morales, P.; Gutiérrez-Oliva, S.; Silva, E.; Toro-Labbé, A. *Molecular Physics* **2009**, *107*, 1587–1596.

³²⁶ Achmatowicz Jr, O.; Bukowski, P.; Szechner, B.; Zwierzchowska, Z.; Zamojski, A. *Tetrahedron* **1971**, *27*, 1973–1996.

steps using a strategy based on diastereoselective allylation of glyceraldehyde **12**, derived from D-mannitol. This synthesis gave the natural product after 13 steps, with an overall yield of 1.7 % and a 1.5:1 diastereoselectivity.



Scheme 94. Retrosynthetic analysis of acortatarin A by Jagadeesh et al.

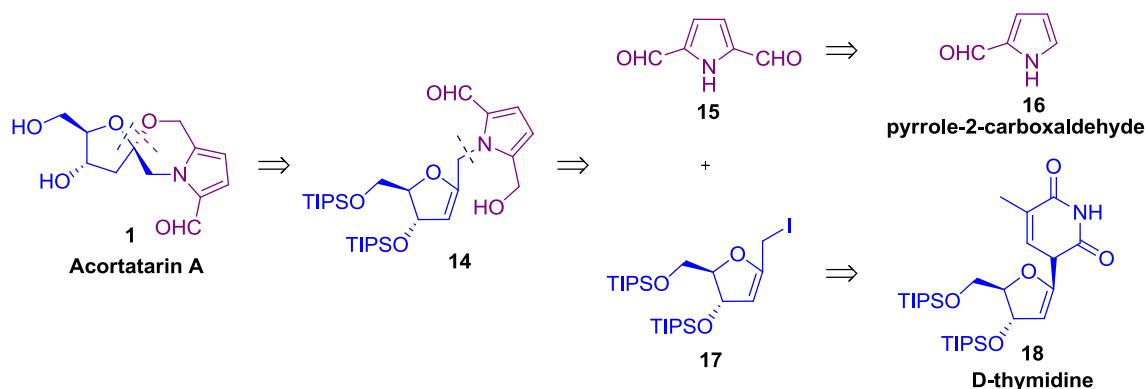


Scheme 95. Retrosynthetic analysis of acortatarin A by Brimble et al.

Due to their previous experience on the stereocontrolled synthesis of spiroketals,³¹⁴ Tan et al. reported a total synthesis of acortatarin A based on the spirocyclization of glycol **14** (Scheme 96).³²⁷ The latter intermediate was produced by *N*-alkylation of 2,5-diformyl pyrrole **15** with the ribal derivative **17**. The disubstituted pyrrole **15** was obtained in several steps from the commercially available pyrrole-2-carboxaldehyde, while ribal **17** was derived from nucleobase elimination of thymidine. This synthesis presented the advantage to be carried out in only 9 steps and 30 % overall yield from D-thymidine, with a 9:1 diastereoselectivity at the spiroketal formation step. On the other hand, it is noteworthy that the latter was performed

³²⁷ Wurst, J. M.; Verano, A. L.; Tan, D. S. *Org. Lett.* **2012**, *14*, 4442–4445.

under quite “harsh” conditions using 2 equivalents of mercury(II) acetate, and one equivalent of strong base NaHMDS.

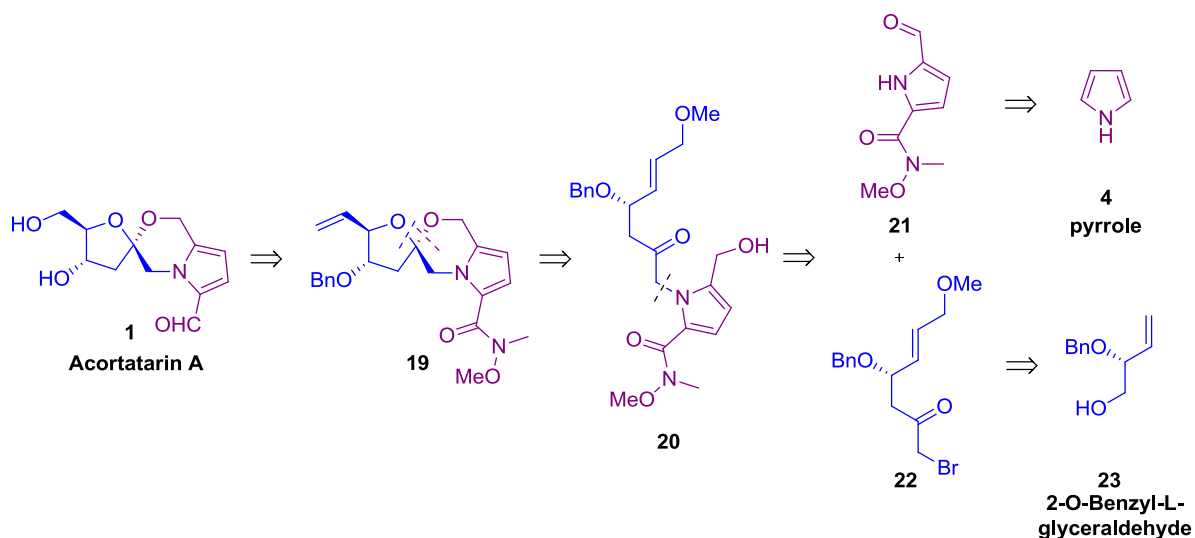


Scheme 96. Retrosynthetic analysis of acortatarin A by Tan et al.

Having recently developed a palladium(II)-catalyzed spiroketalization methodology,³²⁸⁻³²⁹ Aponick et al. applied this strategy to the synthesis of acortatarin A (Scheme 97).³²¹ Alkoxypalladation followed by elimination on ketone intermediate **20** provided the expected spiroketal **19** and created at the same time a new stereocenter, setting the vinyl group *trans* to the benzyl ether.³²⁹ According to the author, the keto-allylic intermediate **20** may be in equilibrium with its cyclic hemiketal counterpart under the reaction conditions. Similar to the synthesis of Tan et al.,³²⁷ the precursor **20** was obtained by *N*-alkylation of the 2,5-functionalized pyrrole **21** with bromoketone **22**. The latter was accessed in 7 steps from 2-*O*-benzyl-L-glyceraldehyde, while pyrrole **21** was obtained in only 2 steps from commercial pyrrole. In terms of yield and diastereoselectivity, this alternative was less efficient than the synthesis of Tan and co-workers, with a 2.5 % overall yield over 13 steps, and a 1:1 diastereoselectivity at the spirocyclization step. However, it can be noticed that the latter step was performed under palladium-catalysis with creation of a new stereocenter.

³²⁸ Palmes, J. A. Ph.D. Thesis, University of Florida, 2012.

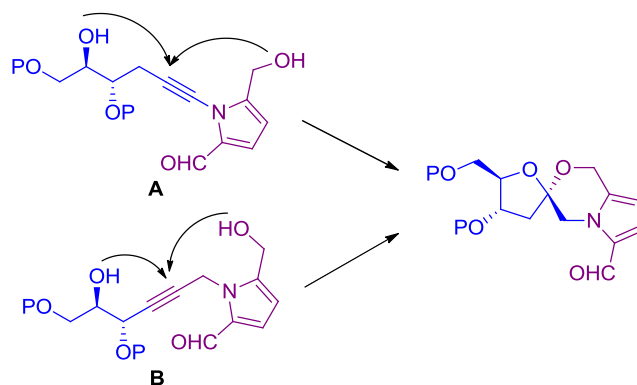
³²⁹ For leading references, see: (a) Uenishi, J. i.; Vikhe, Y. S.; Kawai, N. *Chem. Asian. J.* **2008**, *3*, 473–484. (b) Awasaguchi, K.-i.; Miyazawa, M.; Uoya, I.; Inoue, K.; Nakamura, K.; Yokoyama, H.; Kakuda, H.; Hirai, Y. *Synlett* **2010**, 2392–2396.



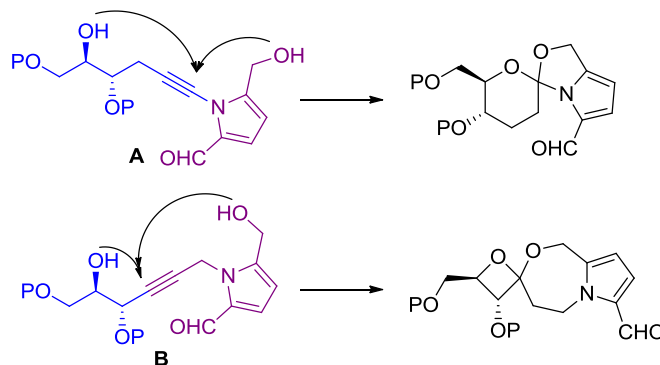
Scheme 97. Retrosynthetic analysis of acortatarin A by Aponick et al.

3. Our approach toward acortatarin A

Despite the existence of spiroketalization strategies based on the transition-metal catalyzed cycloisomerization of alkyne diols (*cf.* chapter 4), the synthesis of acortatarins using this type of methodology has not been reported so far. Consequently, we envisioned to prepare the spiroketal core of acortatarin A *via* our recently developed heterogeneous version catalyzed by Ag^I-zeolites (*cf.* chapter 4). Following this strategy, we reasoned that the spiroketal core could be accessed from two different alkyne diol intermediates, **A** or **B** (Scheme 98), both able to provide the desired spiro[4.5]ketal from [5-*exo* + 6-*endo*] or [5-*endo* + 6-*exo*] cyclizations, respectively.

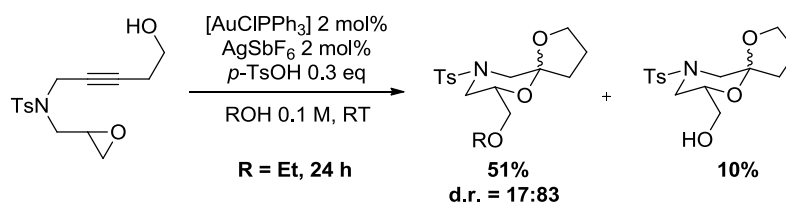
Scheme 98. [5-*exo* + 6-*endo*] or [5-*endo* + 6-*exo*] cyclization pathways toward acortatarin A.

However, in both cases, competitive [6-*endo* + 5-*exo*] and [4-*exo* + 7-*endo*] cyclizations would also be allowed, according to Baldwin rules,³³⁰ and lead to alternative spiro[4.5] and spiro[3.6]ketals, respectively (Scheme 99).



Scheme 99. Competitive cyclization pathways leading to undesired bicycles

In the literature, we found that the spiro[4.5]ketal core of acortatarin A, including the morpholine ring, has been already prepared using a gold-catalyzed intramolecular reaction of homopropargylic alcohols with epoxyalkynes (Scheme 100).³³¹ The authors found that the AuClPPh₃/AgSbF₆ combination, along with *p*-TsOH as co-catalyst gave the best result, i.e. 51 % of the desired spiroketal in a 17:83 diastereoselectivity.

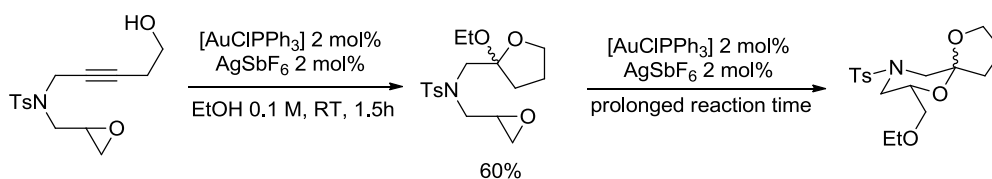


Scheme 100. Gold-catalyzed reaction yielding the spiro[4.5]ketal core of acortatarin A

Control experiments in the absence of acid co-catalyst enabled to isolate an intermediate 5-*endo*-dig cyclization product, which slowly evolved to the final spiroketal, provided longer reaction time (Scheme 101). The authors postulated a reaction mechanism proceeding *via* this oxolane intermediate, which would then undergo a second nucleophilic attack of another hydroxyl group, released after the acid or gold catalyzed epoxide opening by ethanol.

³³⁰ (a) Baldwin, J. E. *J. Chem. Soc., Chem. Commun.* **1976**, 734–736. (b) Gilmore, K.; Alabugin, I. V. *Chem. Rev.* **2011**, *111*, 6513–6556.

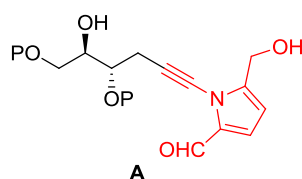
³³¹ Dai, L.-Z.; Shi, M. *Chem. Eur. J.* **2008**, *14*, 7011–7018.



Scheme 101. Control experiments showing the formation of an oxolane intermediate.

The results of Shi and co-workers³³¹ supported the transition-metal catalyzed synthesis of spiro[4.5]ketals including the morpholine ring from substrates similar to the alkyndiol **B**. Therefore, a total synthesis of acortatarin A based on this key intermediate could be envisioned.

On the other hand, the transition-metal catalyzed spiroketalization of alkyndiol intermediate **A** seemed a challenging but very interesting alternative. Indeed, this intermediate included a *N*-alkynylpyrrole functionality in its structure, which attracted our attention (Scheme 102).

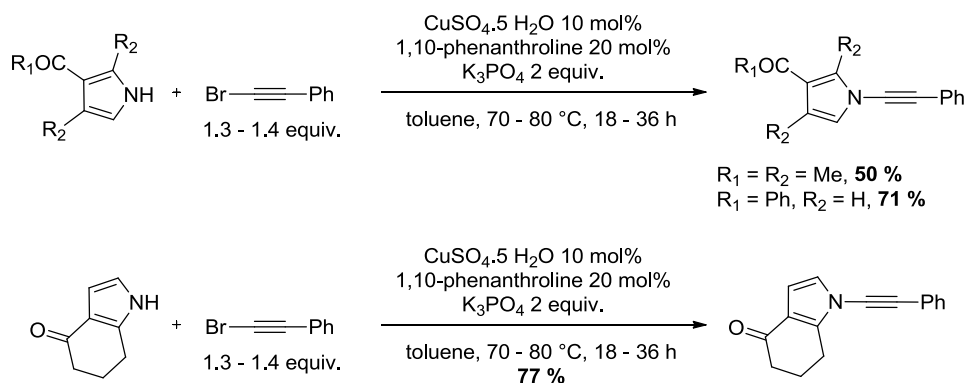


Scheme 102. Alkyndiol intermediate A including a *N*-alkynylpyrrole functionality.

With the recent development of methodologies to access ynamides,³³² we found that such *N*-alkynylpyrrole motifs have already been prepared. Notably, Hsung and co-workers reported a general method to access a variety of substituted ynamides, *via* the copper-catalyzed coupling of alkynyl bromides and *N*-nucleophiles.³³³ Vinylogous ynamides such as *N*-alkynylpyrroles could be obtained in good yields, especially those stabilized by electron-withdrawing groups (Scheme 103).

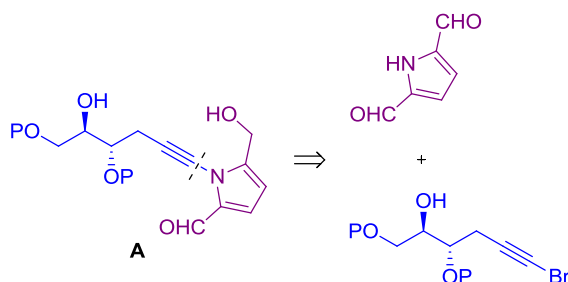
³³² (a) De Korver, K. A.; Li, H.; Lohse, A. G.; Hayashi, R.; Lu, Z.; Zhang, Y.; Hsung, R. P. *Chem. Rev.* **2010**, *110*, 5064–5106. (b) Evano, G.; Coste, A.; Jouvin, K. *Angew. Chem., Int. Ed.* **2010**, *49*, 2840–2859. (c) Evano, G.; Jouvin, K.; Coste, A. *Synthesis* **2013**, *45*, 17–26.

³³³ Zhang, Y.; Hsung, R. P.; Tracey, M. R.; Kurtz, K. C. M.; Vera, E. L. *Org. Lett.* **2004**, *6*, 1151–1154.



Scheme 103. Examples of *N*-alkynylpyrrole motifs obtained by Cu-catalyzed coupling.

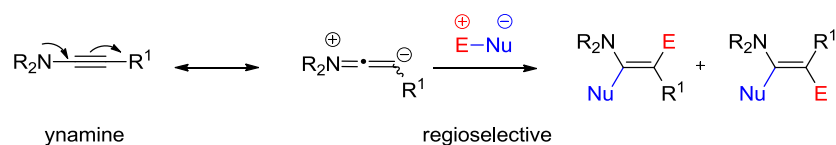
Encouraged by these results, we thought that alkyne diol intermediate **A** could be possibly obtained by coupling of the appropriate alkyne bromide and pyrrole derivatives (Scheme 104). In addition, we were attracted to the possibility of performing this reaction under heterogeneous catalysis *via* Cu^{I} -doped zeolites, in order to design as much as possible an environmental friendly total synthesis of acortatarin **A**.



Scheme 104. Possible Cu-catalyzed coupling to access the *N*-alkynylpyrrole motif of **A**.

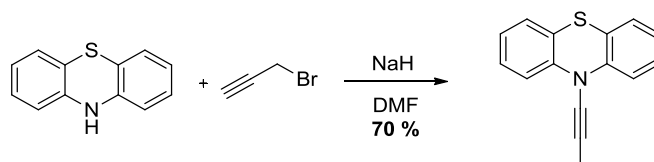
Consequently, we decided to embark on this strategy, and we proposed that acortatarin **A** was synthesized *via* a key cycloisomerization of alkyne diol **24** under Ag^{I} -zeolite catalysis (Scheme 105). The latter *N*-alkynylpyrrole derivative could be obtained by the Cu^{I} -zeolite catalyzed amidative cross-coupling between the bromoalkyne **26** and the 2,5-functionalized pyrrole **15**. The **15** and **26** building blocks could be accessed using classical organic transformations in a multi-step sequence from 2-deoxy-D-ribose and pyrrole-2-carboxaldehyde, respectively.

high reactivity combined with the possibility of regioselective transformation of this functional group (Scheme 107).



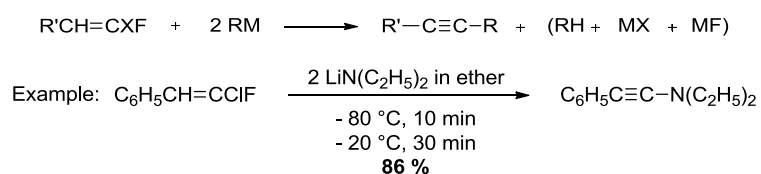
Scheme 107. Regioselectivity induced by the ynamine functional group.

The first isolated and fully characterized ynamine was reported by Zaugg et al. in 1958, from an “unusual reaction of propargyl bromide” (Scheme 108).³³⁴



Scheme 108. First synthesis of ynamine by Zaugg et al. in 1958.

Instead of the expected alkylation product *N*-(2-propynyl)phenothiazine, they isolated the isomeric counterpart *N*-(1-propynyl)phenothiazine in 70 % yield. Five years later, the first practical synthesis of ynamines was set up by Viehe (Scheme 109).³³⁵ The reaction of two equivalents of organolithium species on 1-chloro-1-fluoro alkenes yielded various heterosubstituted alkynes.



Scheme 109. First practical synthesis of ynamines by Viehe.

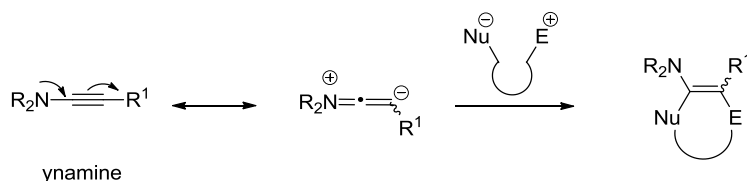
In the ensuing 20 years, the synthetic utility of ynamines was explored by various chemists.³³⁶ It was demonstrated that their singular electronic nature made them particularly prone to

³³⁴ Zaugg, H.; Swett, L.; Stone, G. *J. Org. Chem.* **1958**, *23*, 1389–1390.

³³⁵ Viehe, H. G. *Angew. Chem., Int. Ed.* **1963**, *2*, 477–477.

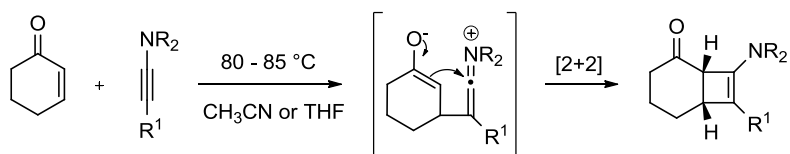
³³⁶ Zifcick, C. A.; Mulder, J. A.; Hsung, R. P.; Rameshkumar, C.; Wei, L. L. *Tetrahedron* **2001**, *57*, 7575–7606.

undergo regioselective additions in general (Scheme 107), and notably step-wise cycloadditions (Scheme 110).



Scheme 110. Cycloaddition reactions of ynamines.

As illustrated in Scheme 107 and Scheme 110, the dipolarization induced by the delocalization of the nitrogen lone pair enables to predict the regioselectivity of the addition of simple Nu^-E^+ reagents.³³⁷ Thanks to this special property of ynamines, attractive heterocyclic targets have been produced by such regioselective cycloaddition reactions. One of the most representative examples is certainly the Ficini's thermal [2+2] cycloaddition of ynamines with electron deficient alkenes, affording cyclobutenamines (Scheme 111).³³⁷

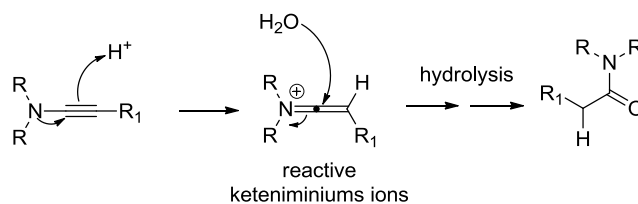


Scheme 111. Ficini's thermal [2+2] cycloaddition of ynamines.

4.2. Emergence of ynamides

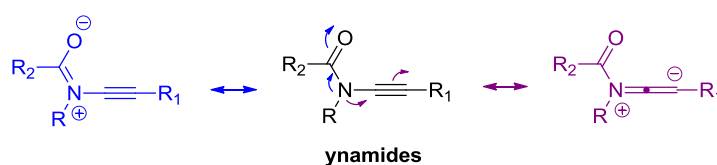
Despite these interesting results, the synthetic use of ynamines slowly ran out of steam, mainly because of their restricted accessibility and high sensitivity. The ability of the nitrogen lone pair to delocalize, at the origin of the high reactivity of ynamines, turned out to be the source of their limitation at the same time. For similar reasons, ynamines are also very sensitive to hydrolysis, as illustrated in Scheme 112.

³³⁷ Ficini, J. *Tetrahedron* **1976**, 32, 1449–1486.



Scheme 112. Sensitivity of ynamines toward hydrolysis.

Protonation of the alkyne leads to reactive keteniminiums, which upon trapping with water afford amides. As a consequence of this instability, the synthetic use of ynamines remained limited over the last 30 years. Recently, this issue was solved by the emergence of a new class of electron-deficient ynamines, called ynamides, in which the nitrogen atom is substituted by an electron-withdrawing group such as sulfonamide, imidazolidinone, oxazolidinone, lactam, etc. Due to the resonance delocalization of the nitrogen lone pair into the carbonyl oxygen of the electron-withdrawing group, the delocalization toward the alkynyl motif is greatly reduced (Scheme 113). Consequently, the presence of the electron-withdrawing group results in enhanced stability (toward hydrolysis, heating, silica gel, etc.), but maintains sufficient ynamine character to provide enhanced reactivity and regioselectivity. Ynamides thus exhibit a perfect balance between stability and reactivity.

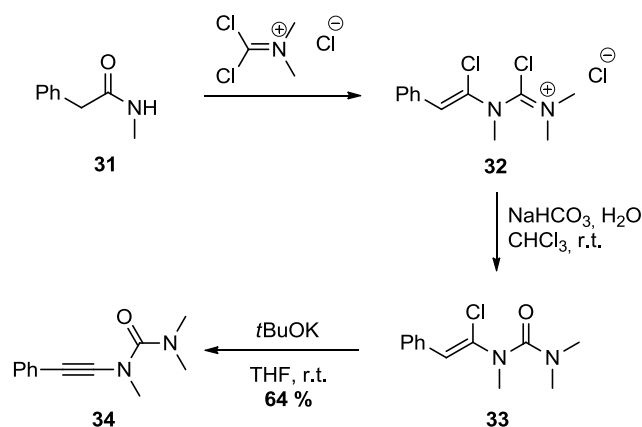


Scheme 113. Reactivity and regioselectivity in ynamides.

Thanks to these interesting properties, the chemistry of ynamides has exploded at the beginning of the 21st century, enabling transformations that were not possible with traditional ynamines. The numerous studies devoted to the preparation or transformation of this versatile functional group were recently highlighted in reviews published by major contributors of this field.³³² In particular, numerous efforts were directed toward the design of practical and efficient syntheses of ynamides.

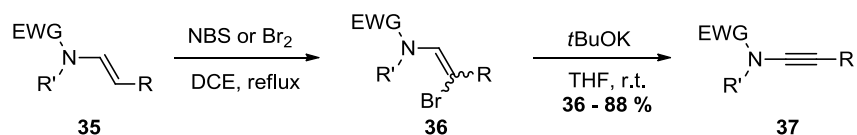
Historically, the first ynamide synthesis was reported by Viehe and co-workers in 1972 (Scheme 114).³³⁸

³³⁸ Janousek, Z.; Collard, J.; Viehe, H. G. *Angew. Chem., Int. Ed.* **1972**, *11*, 917–918.



Scheme 114. First ynamide synthesis by Viehe et al. in 1972.

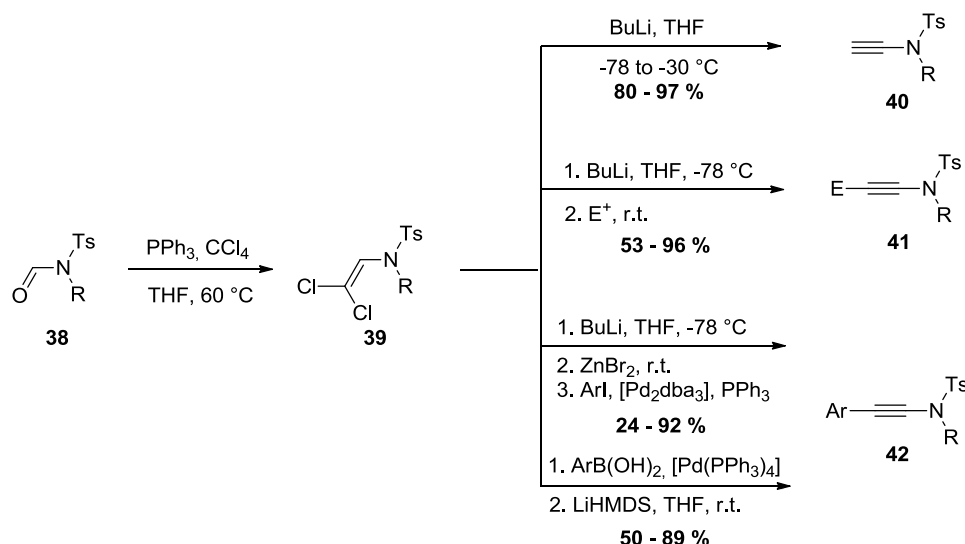
They obtained the urea derivative **34** after HCl elimination from the α -chloro-enamide **33**. The latter originated from the reaction of phosgeneiminium chloride with acetamide **31** and subsequent hydrolysis. This pioneering work has opened the way for other elimination protocols, a method extensively studied for the preparation of ynamides.³³² In this area, Hsung recently brought some improvements, notably in terms of reaction scope. Pyrrolo-, oxazolo- and imidazolidinone derived ynamides **37** were obtained from β -bromo-enamides, which can be easily accessed after bromination of the corresponding enamides **35** (Scheme 115).³³⁹



Scheme 115. Elimination protocol developed by Hsung et al.

It is worth noting that only *Z* isomers of **36** were converted to the desired ynamides. β,β -dichloroenamides **39**, prepared from the reaction of triphenylphosphine and carbon tetrachloride on formamides **38**, proved to be suitable substrates as well for these elimination protocols (Scheme 116).

³³⁹ Wei, L.-L.; Mulder, J. A.; Xiong, H.; Zifcsak, C. A.; Douglas, C. J.; Hsung, R. P. *Tetrahedron* **2001**, *57*, 459–466.

Scheme 116. Elimination protocols *via* β,β -dichloroenamides **39**

Brückner first reported their conversion to simple terminal ynamides **40** in the presence of *n*-butyl lithium at low temperature.³⁴⁰ Variants of these conditions were proposed afterwards in order to prepare functionalized ynamides. The addition of electrophiles before quenching yielded disubstituted ynamides **41**.³⁴¹ Interestingly, aryl-substituted ynamides **42** could also be prepared by introducing Negishi³⁴² or Suzuki³⁴³ coupling reactions, after of before the elimination step.

Although less efficient, another alternative for the preparation of ynamides is the isomerization of propargyl amides. As a reminder, ynamines were by chance isolated from such a transformation in 1958 (Scheme 108).³³⁴ With this strategy, Hsung and co-workers managed to prepare a series of methyl ynamides **44** in the presence of *t*BuOK in THF (Scheme 117).³⁴⁴ However, the reaction scope remained very limited, the isomerization being complete only for simple amides substrates. Amides carrying other electron withdrawing groups suffered from incomplete reaction, which stopped at the allenamide stage.³³⁹

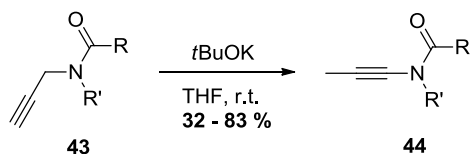
³⁴⁰ (a) Brückner, D. *Synlett* **2000**, 1402-1404. (b) Brückner, D. *Tetrahedron* **2006**, 62, 3809-3814.

³⁴¹ Rodríguez, D.; Martínez-Esperón, M. F.; Castedo, L.; Saá, C. *Synlett* **2007**, 2007, 1963-1965.

³⁴² Rodríguez, D.; Castedo, L.; Saá, C. *Synlett* **2004**, 2004, 0783-0786.

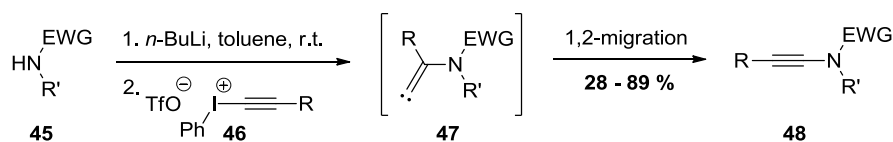
³⁴³ Couty, S.; Barbazanges, M.; Meyer, C.; Cossy, J. *Synlett* **2005**, 2005, 0905-0910.

³⁴⁴ Huang, J.; Xiong, H.; Hsung, R. P.; Rameshkumar, C.; Mulder, J. A.; Grebe, T. P. *Org. Lett.* **2002**, 4, 2417-2420.



Scheme 117. Isomerization of propargyl amide under the conditions of Hsung et al.

More popular than the isomerization of propargyl bromides, the synthesis of ynamides from alkynyliodonium salts was initiated by the work of Stang et al. on push-pull ynamines.³⁴⁵ The method was later extended to ynamides and studied in more details by Witulski et al.,³⁴⁶ as well as Imbriglio and Rainier (Scheme 118).³⁴⁷ The mechanism involves the formation of a vinylcarbene **47** after nucleophilic addition of the deprotonated amide **45** β to the iodine. The expected ynamide **48** is subsequently produced after 1,2-shift. The major limitation of this procedure is due to the starting alkynyliodonium salts, whose substitution is restricted to silyl, aromatic or electron-withdrawing groups.



Scheme 118. Synthesis of ynamides from alkynyliodonium salts.

Despite the efforts directed toward the development of practical syntheses, at the beginning of the 21st century, ynamides were still lacking a mild, direct and tolerant preparation method. In the past ten years, this situation ended with the emergence of highly efficient procedures based on copper catalysis.

The first breakthrough in this field was reported by Hsung and co-workers in 2003. Encouraged by the revival of copper catalyzed coupling reactions (*cf.* chapter I),²⁹ and following the lead of Buchwald et al. on the arylation of amides,³⁴⁸ they proposed the first

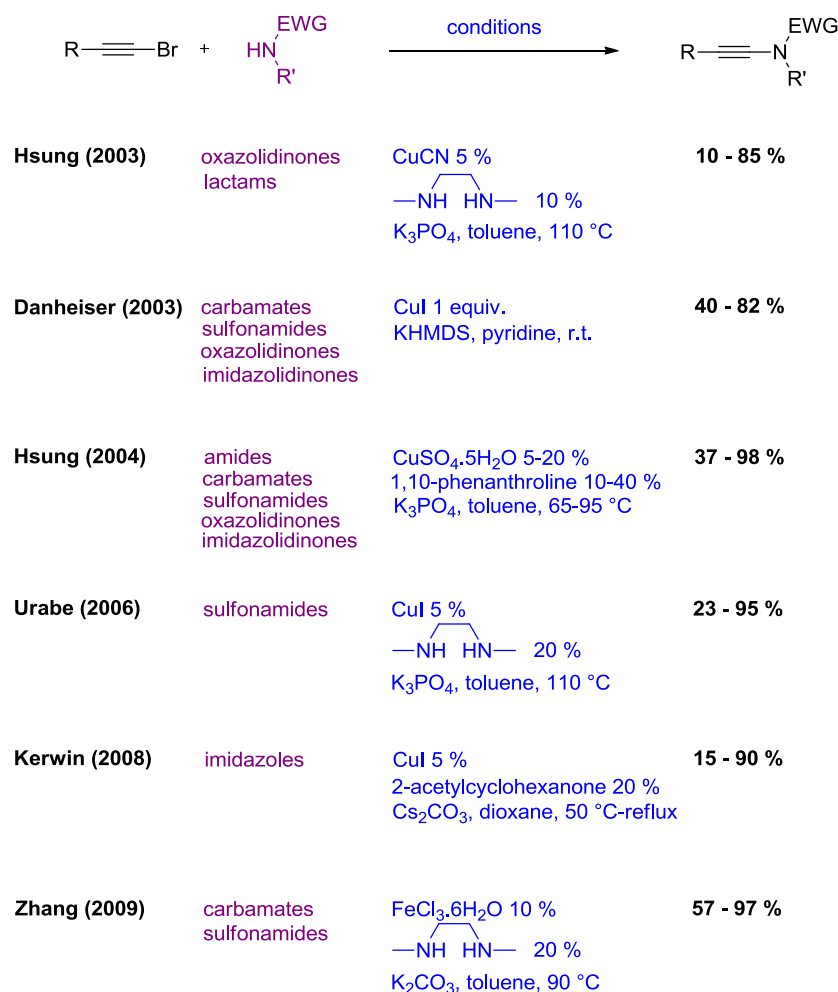
³⁴⁵ Murch, P.; Williamson, B. L.; Stang, P. J. *Synthesis* **1994**, *1994*, 1255–1256.

³⁴⁶ (a) Witulski, B.; Stengel, T. *Angew. Chem., Int. Ed.* **1998**, *37*, 489–492. (b) Witulski, B.; Stengel, T. *Angew. Chem., Int. Ed.* **1999**, *38*, 2426–2430.

³⁴⁷ (a) Rainier, J. D.; Imbriglio, J. E. *Org. Lett.* **1999**, *1*, 2037–2039. (b) Rainier, J. D.; Imbriglio, J. E. *J. Org. Chem.* **2000**, *65*, 7272–7276.

³⁴⁸ (a) Klapars, A.; Antilla, J. C.; Huang, X.; Buchwald, S. L. *J. Am. Chem. Soc.* **2001**, *123*, 7727–7729. (b) Klapars, A.; Huang, X.; Buchwald, S. L. *J. Am. Chem. Soc.* **2002**, *124*, 7421–7428.

coupling of amides and alkynyl bromides based on a CuCN/*N,N'*-dimethylethylenediamine catalytic system in the presence of K₃PO₄ as a base (Scheme 119).³⁴⁹



Scheme 119. Various versions of copper mediated coupling of amides and alkynyl bromides.

Hsung suggested that the mechanism was related to the catalytic cycle proposed by Buchwald for the *N*-arylation of amides.³⁴⁸ Despite the high temperature required for such reaction, it represented the first direct and atom economical pathway to ynamides. Oxazolidinones and lactams were efficiently converted in good yields, however amides, sulfonamides or imidazolidinones were few or not reactive at all under these conditions. In the same year, Danheiser proposed an alternative which fully complemented the Hsung's version (Scheme 119).³⁵⁰ His conditions enabled the formation of complex ynamides from a wide range of

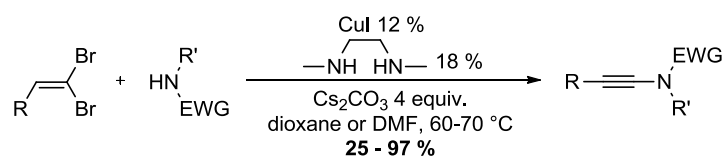
³⁴⁹ Frederick, M. O.; Mulder, J. A.; Tracey, M. R.; Hsung, R. P.; Huang, J.; Kurtz, K. C. M.; Shen, L.; Douglas, C. J. *J. Am. Chem. Soc.* **2003**, *125*, 2368–2369.

³⁵⁰ Dunetz, J. R.; Danheiser, R. L. *Org. Lett.* **2003**, *5*, 4011–4014.

amides such as carbamates, sulfonamides, oxa- and imidazolidinones at room temperature. On the other hand, stoichiometric copper iodide as well as a strong base were necessary. Subsequently, Hsung improved its first procedure with a new $\text{CuSO}_4 \cdot 5\text{H}_2\text{O}/1,10$ -phenanthroline catalytic system (Scheme 119).³³³ The latter efficiently promoted the coupling of a large variety of substrates at lower temperatures (65–95 °C), in the presence of potassium phosphate as a base. It was later shown that the quality of this base turned out to be essential for the success of the reaction.³⁵¹

Further to this pioneering work, modified conditions employing different copper source, ligand, base, and solvent were reported by other research groups (Scheme 119). The conditions were studied and adjusted for specific substrates such as sulfonamides,³⁵² or imidazoles.³⁵³ An iron-catalyzed version was also disclosed by Zhang and co-workers for the conversion of carbamates and sulfonamides.³⁵⁴

Interestingly, Evano et al. proposed the coupling of amides with alkyne precursors and other alkyne coupling partners. Depending on the available substrates, these alternatives can turn out to be very useful. With dibromoalkenes first, they proposed an efficient and rather general method using a copper iodide/*N,N'*-dimethylethylenediamine catalytic system (Scheme 120).³⁵⁵ Except for acyclic amides and ureas, most substrates were formed in good yields. The choice of the base proved crucial to avoid side-reactions between the ynamide and the starting nitrogen nucleophile.



Scheme 120. Cu-catalyzed coupling of dibromoalkenes and *N*-nucleophiles by Evano et al.

Recently, they developed a room-temperature, base-free coupling of amides with potassium alkynyltrifluoroborates (Scheme 121).³⁵⁶ The latter were obtained from a one-pot, two-step

³⁵¹ Dooleweerd, K.; Birkedal, H.; Ruhland, T.; Skrydstrup, T. *J. Org. Chem.* **2008**, *73*, 9447–9450.

³⁵² (a) Hirano, S.; Fukudome, Y.; Tanaka, R.; Sato, F.; Urabe, H. *Tetrahedron* **2006**, *62*, 3896–3916. (b) Fukudome, Y.; Naito, H.; Hata, T.; Urabe, H. *J. Am. Chem. Soc.* **2008**, *130*, 1820–1821.

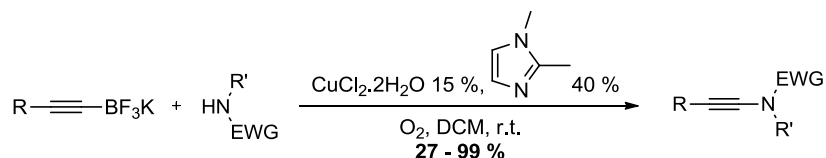
³⁵³ Laroche, C.; Li, J.; Freyer, M. W.; Kerwin, S. M. *J. Org. Chem.* **2008**, *73*, 6462–6465.

³⁵⁴ Yao, B.; Liang, Z.; Niu, T.; Zhang, Y. *J. Org. Chem.* **2009**, *74*, 4630–4633.

³⁵⁵ Coste, A.; Karthikeyan, G.; Couty, F.; Evano, G. *Angew. Chem., Int. Ed.* **2009**, *48*, 4381–4385.

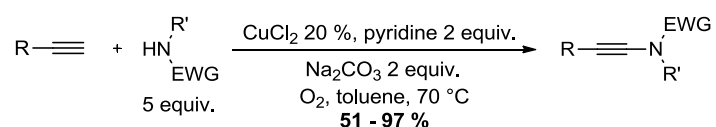
³⁵⁶ Jouvin, K.; Couty, F.; Evano, G. *Org. Lett.* **2010**, *12*, 3272–3275.

procedure from terminal alkynes. $\text{CuCl}_2 \cdot 2\text{H}_2\text{O}$ combined with 1,2-dimethylimidazole proved to be the best catalytic system, but seemed to be mostly effective on the conversion of oxazolidinones and sulfonamides.



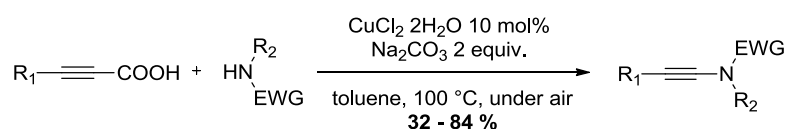
Scheme 121. Base-free coupling of amides with potassium alkynyltrifluoroborates.

Stahl and co-workers disclosed an original procedure enabling the direct coupling of terminal alkynes with amides, in the presence of oxygen as terminal oxidant (Scheme 122).³⁵⁷ A wide range of nitrogen nucleophiles were converted in very good yields. The main limitation lied in the fact that 5 equivalents of the starting amide were required to achieve these results, which was rationalized by the undesired formation of Glaser-Hay dimerized products.



Scheme 122. Direct coupling of terminal alkynes with amides by Stahl et al.

Subsequently, Jiao and co-workers also proposed an environmental friendly procedure starting from propiolic acids (Scheme 123).³⁵⁸ The aerobic oxidative amidation proceeded efficiently with only 10 mol% $\text{CuCl}_2 \cdot 2\text{H}_2\text{O}$ and two equivalents of the amide. In addition, the use of carboxylic acids as coupling partners inhibited the formation of diynes side products.



Scheme 123. Coupling of amides and propiolic acids by Jiao et al.

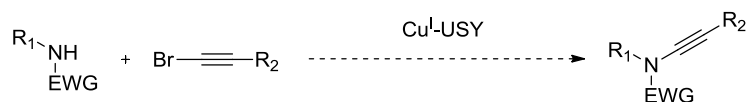
³⁵⁷ Hamada, T.; Ye, X.; Stahl, S. S. *J. Am. Chem. Soc.* **2008**, *130*, 833–835.

³⁵⁸ Jia, W.; Jiao, N. *Org. Lett.* **2010**, *12*, 2000–2003.

In summary, the recent development of copper-catalyzed amidative cross-coupling for the preparation of ynamides provided straightforward and efficient methods compared to the previous strategies, allowing the access to various substituted ynamides from simple starting materials.

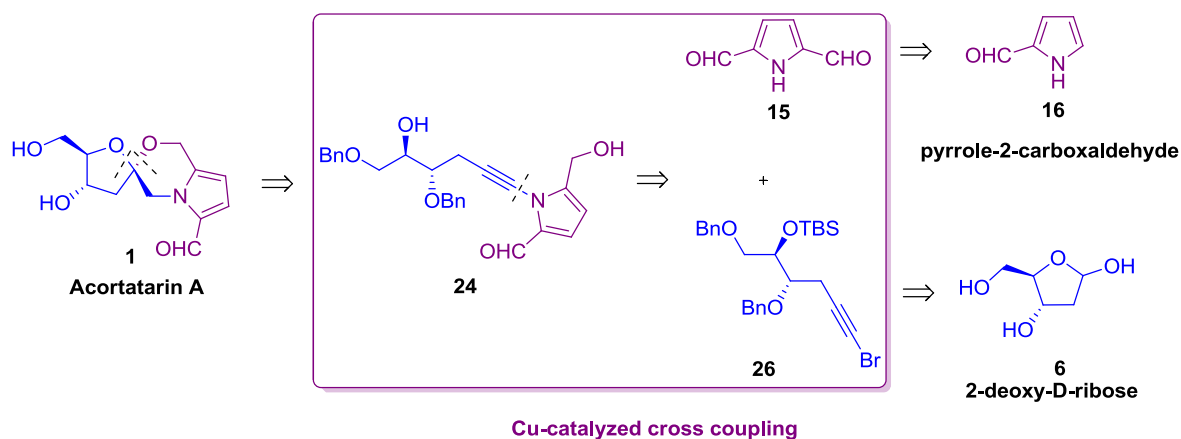
4.3. Toward a Cu-zeolite catalyzed amidative cross-coupling

Based on our previous success with Cu^{I} -USY zeolites¹¹¹ in various transformations, we decided to test its potential in this cross-coupling of *N*-nucleophiles and alkynyl bromides (Scheme 124).



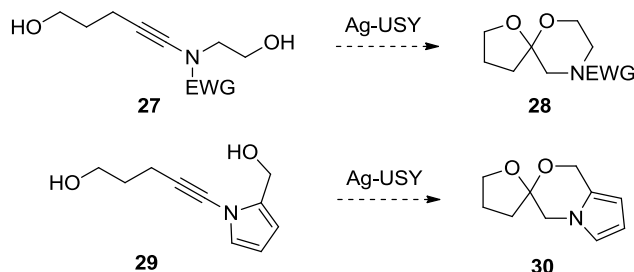
Scheme 124. Toward a Cu^{I} -USY catalyzed cross-coupling.

If successful, this may open the way for another environmental friendly ynamide synthesis, and at the same time contribute to a “greener” total synthesis of acortatarin A. As a reminder, we aimed to prepare this natural product by Ag-USY catalyzed spiroketalization of alkyne diol **24**, and we proposed to access the latter by Cu-catalyzed amidative coupling between the bromoalkyne **26** and the 2,5-diformylpyrrole **15** (Scheme 125).



Scheme 125. The Cu-catalyzed amidative coupling : a key step of the total synthesis

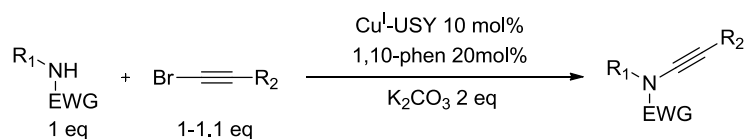
To assess the feasibility of this sequence, we decided to focus on the preparation of ynamide diols such as **27** and **29**, in view of their cyclization to the spiroketal targets **28** and **30**, model substrates of acortatarin A (Scheme 106).

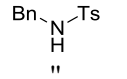
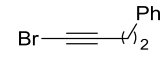
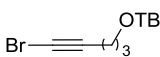
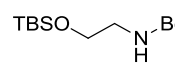
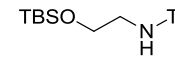
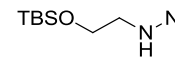
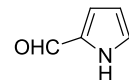
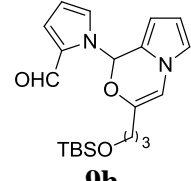


Scheme 106. Ynamide diol targets **27** and **29**, precursors of spiroketals **28** and **30**.

According to the method developed in our laboratory, Cu^I-USY zeolite was obtained from solid exchange between parent H-USY and CuCl at 350 °C for 3 days. The so-obtained zeolite was already fully characterized.¹¹¹ We decided to use the mild and tolerant conditions set up in the improved procedure of Hsung and co-workers,³³³ including 1,10-phenanthroline as ligand, K₃PO₄ or K₂CO₃ as base, in toluene at 65-110°C. The simple *N*-benzyl-4-methylbenzenesulfonamide **7a** was chosen as model *N*-nucleophile to determine the influence of several factors on the reaction efficiency and set up the reaction conditions (Table 21).

The coupling of **7a** with bromoalkyne **8a** afforded 92 % of the expected ynamide under the standard reaction conditions, i.e. after 22 h at 65 °C in toluene (entry 1). A brief screening of solvents indicated that toluene could be easily replaced by THF or even DMF if needed, both being almost equally effective under the same conditions (entries 3 and 4 *versus* 1). The reaction in dioxane gave a slightly lower yield in comparison (entry 2). The coupling of **7a** and **8b** performed at higher temperature, in refluxing toluene, enabled a faster reaction, with already 58 % of the expected ynamide after 3 h (entry 5). The conversion actually required 7 h to be complete, affording an optimum 89 % yield (entry 6). The presence of the 1,10-phenanthroline could not be avoided with Cu-USY as catalyst. In its absence, longer reaction time was not enough to bring the conversion to completion, and only 8 % of the expected ynamide could be recovered, together with the starting material (entry 7). The influence of the electron-withdrawing group on the *N*-nucleophile was also examined. Whereas the simple carbamate **7b** was almost not converted (entry 8), the tosyl and nosyl substituted amines **7c** and **7d** afforded the corresponding ynamides in high yields (entries 9 and 10).

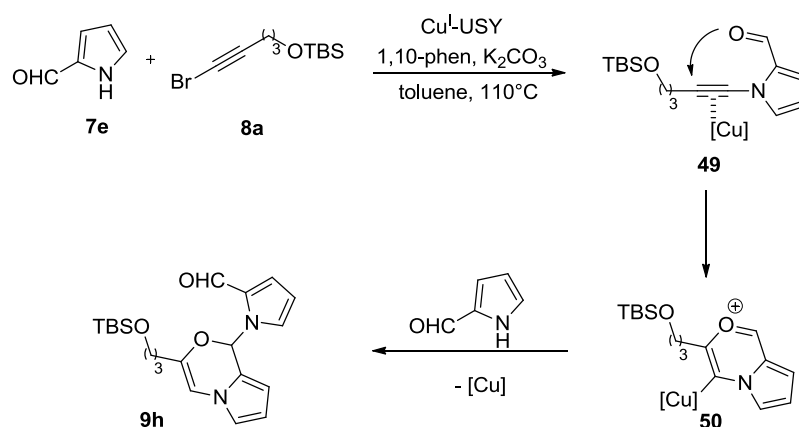
Table 21. Toward a Cu^I-USY-catalyzed amidative cross-coupling.

Entry	N-nucleophile	Alkyne	Solvent	T (°C), t (h)	Yield %
1	 7a	 8a	toluene	65 °C, 22 h	92 ^a
2	"	"	dioxane	"	82 ^a
3	"	"	THF	"	91 ^a
4	"	"	DMF	"	87 ^a
5	"	 8b	toluene	reflux, 3 h	58
6	"	"	"	reflux, 7 h	89 (85) ^b
7	"	"	"	reflux, 22 h	8 ^c
8	 7b	"	"	reflux, 24 h	traces ^d (traces) ^{b,d}
9	 7c	"	"	reflux, 5 h	74 (68) ^b
10	 7d	"	"	reflux, 24 h	91
13	 7e	"	"	110 °C, 48 h	 52 (53) ^a
14	"	"	"	"	9h 68 ^{a,e}

^a Reaction run in sealed tube. ^b With CuSO₄·5H₂O as catalyst. ^c Without 1,10-phenanthroline. ^d With K₃PO₄ instead of K₂CO₃ as a base. ^e With 2 equivalents pyrrole, 23 % of pyrrole-2-carboxaldehyde recovered.

Very interestingly, pyrrole-2-carboxaldehyde **7e** could be engaged in such coupling. A new product **9h** was isolated after 48 h at 110 °C. With 2 equivalents of pyrrole, the yield could be increased to 68 % (entry 14). Moreover, this product did not correspond to the expected *N*-alkynylpyrrole. ¹H NMR showed 7 single protons between 6 and 7 ppm, another one at 8 ppm and an aldehyde proton at 9.6 ppm, which suggested that two pyrrole units were contained in the molecule. In addition, the characteristic quaternary carbons of the alkyne around 70 and 90 ppm were no longer detected in ¹³C NMR. Instead, 3 quaternary carbons were present between 120-140 ppm. On this basis, we were able to identify the tricyclic scaffold **9h**. We assumed that this product resulted from a 3-step cascade reaction, the formation of the expected ynamide **49** being the first step (Scheme 126). A subsequent 6-*endo* cyclization induced by nucleophilic attack of the aldehyde oxygen to the alkyne, probably assisted by

copper, would lead to the bicyclic pyrrolo oxonium **50**, which could be trapped by a second pyrrole-2-carboxaldehyde molecule.

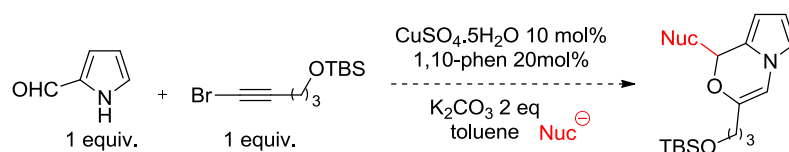


Scheme 126. Proposed reaction path to tricycle **9h**.

It is noteworthy that under the same conditions and reaction time, $\text{CuSO}_4 \cdot 5\text{H}_2\text{O}$ yielded comparable results to the copper-doped zeolite for several examples (entries 6, 8, 9 and 13), which opens the way for a green synthesis of ynamides using Cu-USY as heterogeneous catalysts.

Our attempts to trap the bicyclic pyrrolo oxonium **50** with another external nucleophile remained unsuccessful (Table 22). In the presence of 3 equivalents methanol, only **9h** could be recovered after 48 h at 95 °C (entry 1).

Table 22. Pyrrole coupling in the presence of an external nucleophile.



Entry	N-nucleophile	Alkyne	Solvent	Nuc	T (°C), t (h)	Yield %
1			toluene	MeOH, 3 equiv.	95 °C, 48 h	9h , 59
2	"	"	"	Et_3SiH , 3 equiv.	reflux, 24 h	9h ^a
3	"	"	MeOH	-	70 °C, 48 h	9h , 16 ^b

^a Detected as the major product from ^1H NMR of the crude. ^b 65 % recovered pyrrole-2-carboxaldehyde.

We also tried the coupling in the presence of triethylsilane, but again, **9h** was the major product detected by ^1H NMR of the crude reaction mixture. In a last attempt, we performed

the reaction in pure methanol, but under these conditions the conversion remained very limited (only 35%), and **9h** was the only product formed in low yield (entry 3).

This tandem cyclization/trapping process is well-known in the literature, and has been reported in various transition-metal catalyzed heterocyclizations.³⁵⁹ In particular, the work of Yamamoto and Patil on the preparation of cyclic alkenyl ethers³⁶⁰ is clearly correlated to our unexpected result. They found that *o*-alkynylbenzaldehydes could be cyclized in the presence of external alcohols and 10 mol% CuI as catalyst in DMF (Scheme 127). The authors suggested that the cyclization may be first promoted by the attack of the aldehyde oxygen to the copper-coordinated alkyne, followed by trapping of the resulting oxonium with the external alcohol.

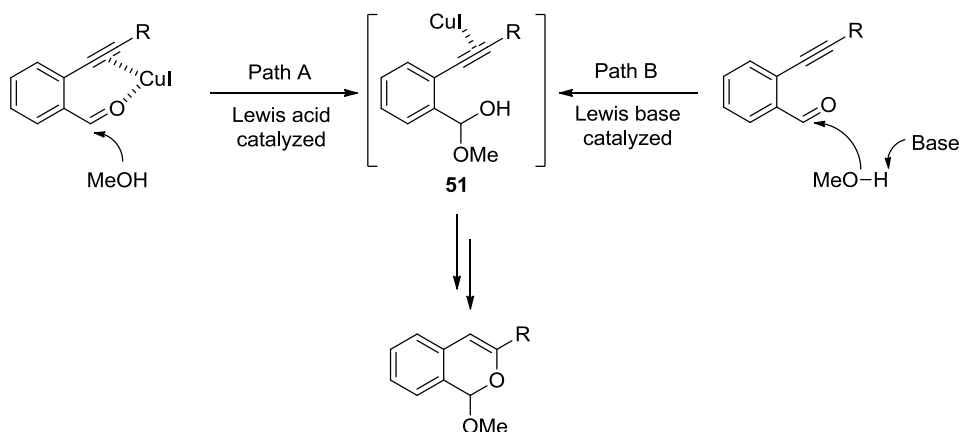


Scheme 127. Tandem cyclization/trapping process reported by Yamamoto and Patil.

They also proposed that the mechanism proceeded *via* the hemiacetal intermediate **51**, resulting either from Lewis acid or Lewis base catalysis (Scheme 128). By running the reaction in benzene instead of DMF, they showed that the desired product could not be obtained, unless 2 equivalents triethylamine were added. Based on these experiments, they concluded that the hemiacetal formation, if it ever happened, would be most certainly promoted by Lewis base catalysis.

³⁵⁹ Patil, N. T.; Yamamoto, Y. *Chem. Rev.* **2008**, *108*, 3395–3442.

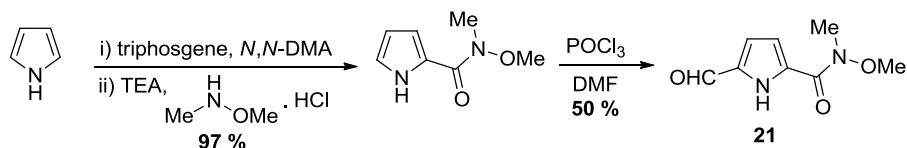
³⁶⁰ Patil, N. T.; Yamamoto, Y. *J. Org. Chem.* **2004**, *69*, 5139–5142.



Scheme 128. Reaction mechanism proposed by Yamamoto and Patil.

Yamamoto and Patil indicated that their reaction was perfectly 6-*endo*-selective, contrary to the already reported palladium-catalyzed cyclizations of alkynoic acids, mainly 5-*exo*-selective.³⁶¹

Due to the reactivity of pyrrole-2-carboxaldehyde in the coupling reaction, it could be interesting to test other pyrrole derivatives, stable enough to form the expected ynamide and less prone to cyclization. In their total synthesis of acortatarin A, Aponick and co-workers prepared the 2,5-disubstituted pyrrole **21** in 2 steps from pyrrole (Scheme 129).³²¹ After a one-pot acylation/amidation sequence, the pyrrole-2-carboxamide intermediate underwent a Vilsmeier-Haack formylation to set the aldehyde function at position 5. The Weinreb amide at position 2 should stabilize the potential ynamide formed by *N*-alkynylation of the corresponding pyrrole. Additional coupling experiments should thus be performed on both the pyrrole-2-carboxamide intermediate, and the pyrrole **21**.

Scheme 129. Synthesis of pyrrole derivative **21** by Aponick et al.

³⁶¹ (a) Bouyssi, D.; Balme, G. *Synlett* **2001**, 2001, 1191–1193. (b) Rossi, R.; Bellina, F.; Biagetti, M.; Catanese, A.; Mannina, L. *Tetrahedron Lett.* **2000**, 41, 5281–5286.

It is noteworthy that pyrroles bearing hydroxymethyl functional groups at position 2, protected or not, are particularly unstable and difficult to handle, as underlined by Aponick and co-workers.³²¹ Consequently, this precludes their potential use in the amidative coupling.

In summary, we have successfully prepared a series of ynamides by the Cu-USY catalyzed amidative coupling of alkynyl bromides and *N*-nucleophiles. The conditions developed by Hsung turned out to be suitable for the preparation of our substrates carrying two TBS protected hydroxyl ends. Comparisons on selected examples with the homogeneous conditions using CuSO₄·5H₂O as catalyst demonstrated that Cu-USY was as efficient in terms of time and reaction yield. Pyrrole-2-carboxaldehyde could even be converted to a very interesting heterocyclic precursor of acortatarin A. Using two equivalents of pyrrole, this product could be isolated in 68 % yield, although resulting from a one-pot 3-step reaction. In addition, no loss of copper species from Cu-USY seemed to occur in the reaction mixture, according to leaching tests. This promising methodology has been further studied by Matteo De Nigris during his Master II internship at the laboratory. He especially worked on the optimization of the catalyst, and on the preparation of other substrates to enlarge the scope of the reaction. In order to be more specific toward our objective, all results were not reported here.

The unexpected amidative coupling/cyclization cascade found in this section may contribute to a more direct total synthesis of acortatarin A. Indeed, two steps of the synthesis took place in one pot, *i. e.* the coupling between the alkyne derivative and the pyrrole moiety first, and then a 6-*endo* cyclization forming half of the spiroketal core in a second place, precisely leading to the desired morpholine motif.

5. *Ag-USY catalyzed spiroketalization of ynamide diols*

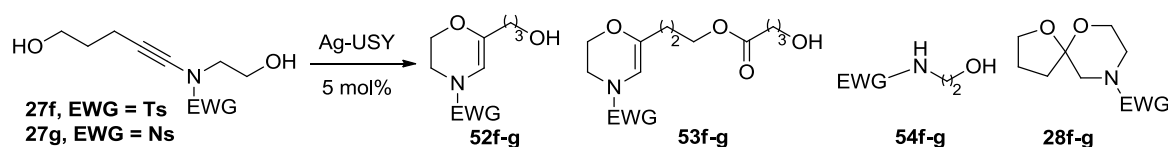
5.1. Spiroketalization of aliphatic ynamide diols

In a next step, we need to study the behavior of the so-prepared ynamide derivatives under Ag-USY catalysis, to check whether spiroketal targets **28** and **30** can be reached using this methodology (Scheme 130).

When the reaction was left for 22 h under the same conditions, **52f** and **53f** disappeared and another new product **28f** appeared. 27 % of this compound could be isolated, along with 64 % of **54f** (entry 3). Alcohol **52f** originated from the expected 6-*endo-dig* ring closure creating the morpholine unit. Compound **53f** included the same morpholine motif in its structure, but a much longer alkyl chain with an ester functional group in the middle and a terminal hydroxyl. Finally, *N*-tosylamine **54** seemed to result from the cleavage of the starting ynamide.

The reaction in methanol proceeded differently. TLC monitoring showed that alcohol **52f**, amine **54f** and spiroketal **28f** were already formed after a few hours. However, after 23 h, only 3 % of the spiroketal and 9 % of the alcohol could be isolated, the major product being the tosylamine (67 %) (entry 4). This result suggested that long reaction time at high temperature was detrimental to the spiroketal core. Ester **53f** was not detected or isolated when the reaction was run in methanol. Although less efficient, the same mechanism occurring with tosyl ynamide seemed to take place with the nosyl counterpart, forming the intermediates **52g** and **53g** first, and leading to the spiroketal only after longer reaction time (entries 5 and 6). Nosylamine **54g** was also detected after 8 and 24 h. Again, in methanol the latter was the major product, along with alcohol **52g** (entry 7).

Table 23. Ag-USY catalyzed spiroketalization of ynamide diols.

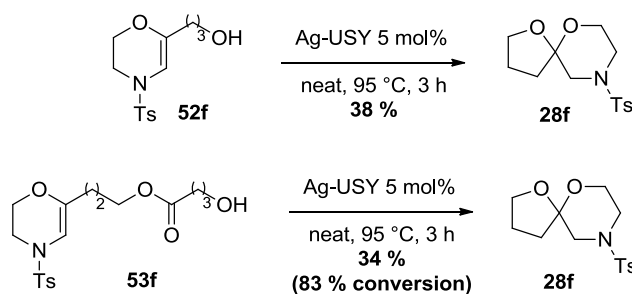


Entry	EWG	Solvent	T (°C), t (h)	52f-g	53f-g	54f-g	28f-g
1	Ts	-	95 °C, 5 h	36 %	10 %	44 %	-
2	Ts	-	95 °C, 8 h	34 %	10 %	55 %	-
3	Ts	-	95 °C, 22 h	-	-	64 %	27 %
4	Ts	MeOH	90 °C, 23 h	9 %	-	67 %	3 %
5	Ns	-	95 °C, 8 h	8 %	10 %	52 %	-
6	Ns	-	95 °C, 24 h	-	-	36 %	14 %
7	Ns	MeOH	95 °C, 24 h	17 %	-	39 %	-

^a With 10 mol% Ag-USY.

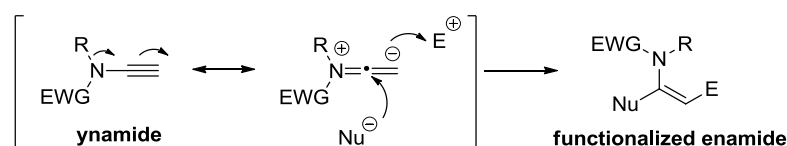
To confirm or not that morpholine derivatives **52** and **53** were actual reaction intermediates toward spiroketal **28**, they were separately placed in the presence of 5 mol% Ag-USY neat at 95 °C in a sealed tube (Scheme 132). After 3 h, TLC monitoring indicated that the reactions were nearly complete, and the expected spiroketal **28** was indeed formed as a single product. However, in both cases the yield was pretty low (34 – 38 %), as were the results of the

screening mentioned above. The only plausible explanation may be the instability of the spiroketal and its intermediates over silica gel. Nevertheless, these control experiments provided insights concerning the mechanism and confirmed that both morpholine alcohol **52** and ester **53** were reaction intermediates toward the spiroketal target **28**.



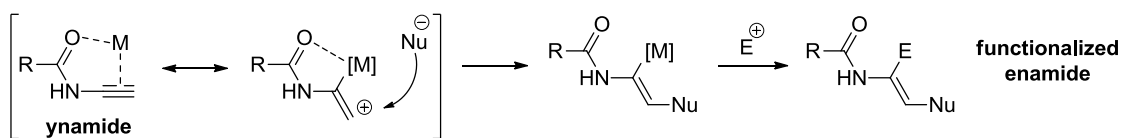
Scheme 132. Control experiments proving that **52** and **53f** are reaction intermediates.

To sum up, this short study demonstrated that spiroketals including the morpholine motif could be formed by Ag-USY catalyzed spiroketalization of ynamide diols, although in low yields. The identification of alcohol **52** and ester **53** as reaction intermediates proved that the 6-*endo* cyclization leading to the morpholine cycle occurred first in the spiroketal formation. Due to the electron-donating ability of the nitrogen atom, addition reactions to ynamides usually take place regioselectively with addition of the nucleophile α to the nitrogen, and trapping of the electrophile at the β -position (Scheme 133).



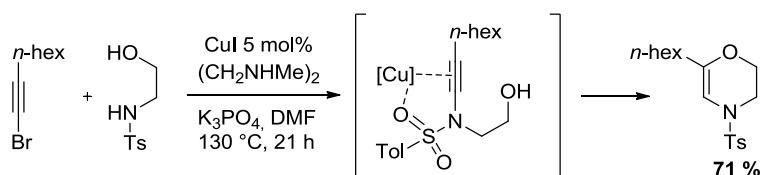
Scheme 133. Regioselectivity of addition reactions to ynamides.

However, “umpolung-type” additions of nucleophiles to ynamides have also been reported, affording the opposite regioselectivity.³³² Usually such processes are transition-metal catalyzed. Indeed, chelation of the organometallic reagent to the carbonyl or sulfonyl of the electron withdrawing group controls the regioselective addition of the nucleophile to the β -position (Scheme 134).



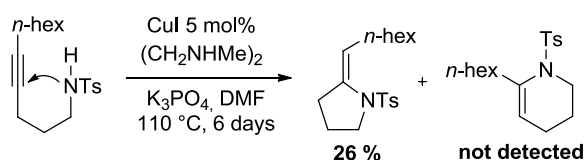
Scheme 134. “Umpolung-type” additions of nucleophiles to ynamides.

In particular, Urabe reported in 2008 the copper-catalyzed double amination of 1-bromoalkynes leading to tetrahydropyrazines.^{352b} One example with an aminoalcohol instead of a diamine led to a morpholine ring very similar to the one we obtained (Scheme 135).



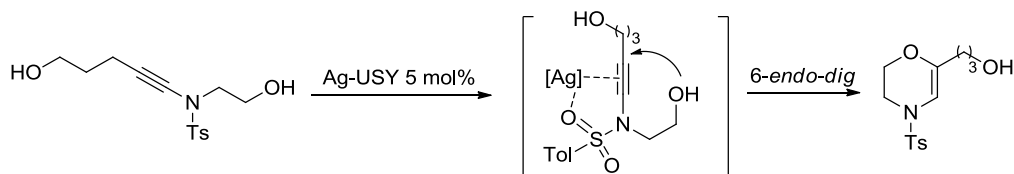
Scheme 135. Cu-catalyzed reaction of an aminoalcohol and a bromoalkyne by Urabe et al.

Alkynylation of the sulfonamide followed by intramolecular 6-*endo-dig* hydroalkoxylation were suggested as mechanism. Chelation of the copper catalyst by the sulfonyl group was assumed to play a key role in the 6-*endo* selective cyclization. Indeed, control experiment showed that simple alkynamine slowly underwent 5-*exo-dig* ring closure, the 6-*endo-dig* product being not detected (Scheme 136).



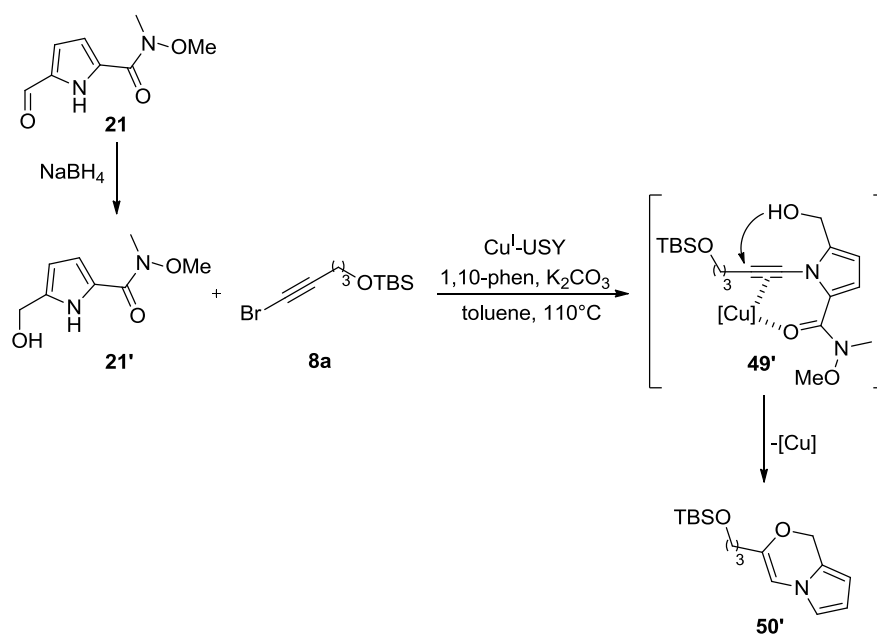
Scheme 136. Control experiment : Cu-catalyzed cyclization of an alkylamine

In our case, it is likely that the same type of chelation of the sulfonyl group to the silver metal occurred, favoring the 6-*endo-dig* ring closure in a first place (Scheme 137).



Scheme 137. Possible chelated reaction intermediate leading to morpholine-type rings.

This chelation is advantageous as it favors the regioselectivity toward the desired morpholine ring. We could also envisage taking benefit of this favorable regioselectivity in the *N*-alkynylation of pyrrole derivatives (Scheme 138). If the 2,5-disubstituted pyrrole **21'** was stable enough to be engaged in an amidative coupling with bromo alkyne partner **8a**, chelation of the copper catalyst to the Weinreb amide oxygen could in a similar fashion favor the 6-*endo-dig* cyclization of the hydroxymethyl substituent, leading to the expected bicycle **50'**.

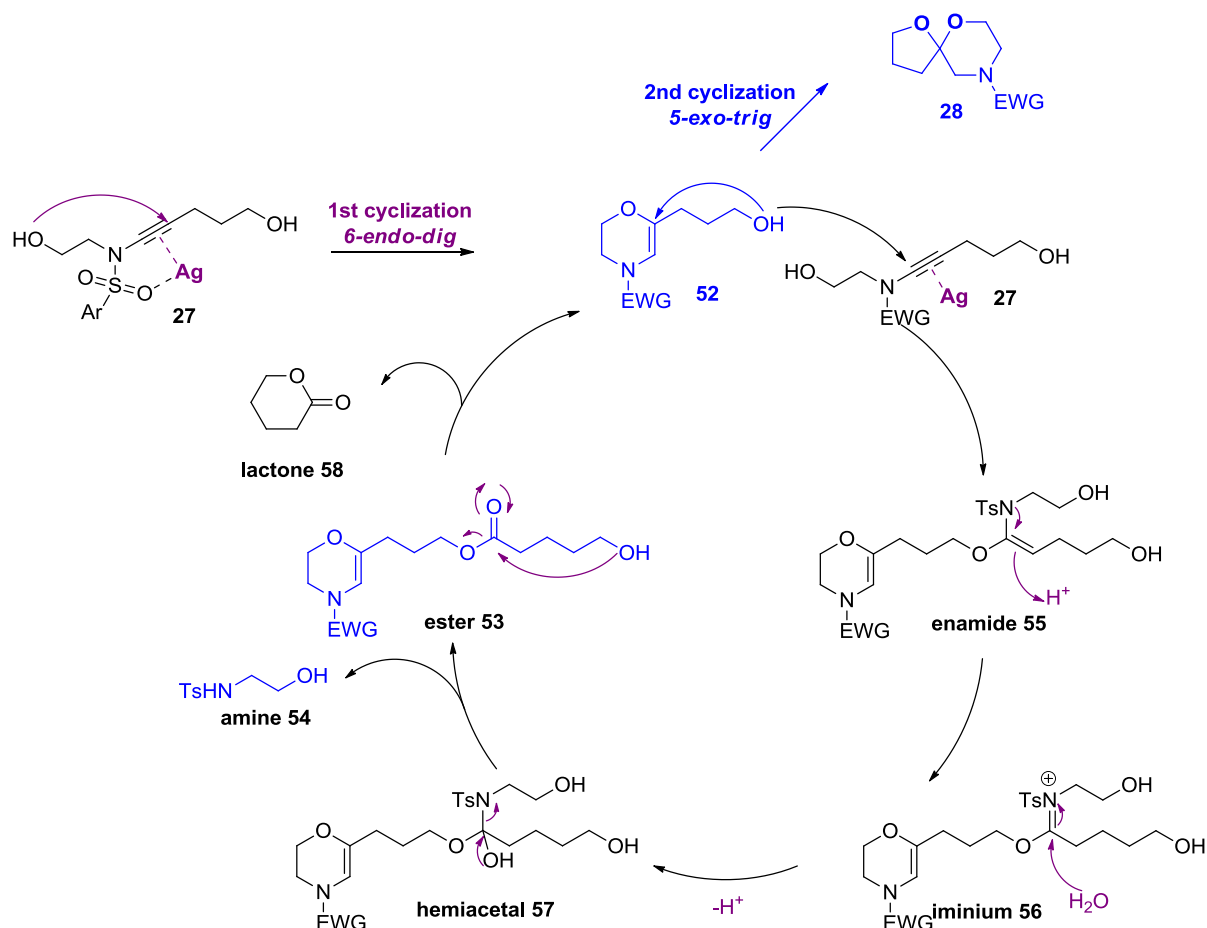


Scheme 138. Possible reaction path with pyrrole **21'** carrying a free hydroxyl group.

Concerning the global reaction mechanism, we assumed that the formation of unwanted side-products could be linked to the poor reactivity of the *endo*-methylene morpholine **52** (Scheme 139). Instead of performing the expected 5-*exo-trig* cyclization to spiroketal **28**, the latter intermediate might rather react in an intermolecular fashion with another ynamide diol molecule. This “self-condensation” process should be particularly favored in concentrated reaction medium or in the absence of any solvent. The attack of the hydroxyl end of **52** at the carbon α to the ynamide nitrogen would lead to enamide **55**, which might evolve to its iminium form **56** under Brønsted acid catalysis. The addition of water to the iminium would lead to hemiacetal **57**, which may cleave to release ester **53** and amine **54**. Finally, the attack of the hydroxyl end to the ester carbonyl of **53** may give back the morpholine intermediate **52**, along with a lactone **58**. It is noteworthy that such compound was never isolated during our experiments. The proposed mechanism enabled to account for the formation of aminoalcohol

54 and ester **53** from reaction intermediate **52**. It is also consistent with the fact that both alcohol **52** and ester **53** can afford spiroketal **28** in the end.

The low yields of spiroketal obtained using our Ag-USY catalyzed method might be explained by the poor reactivity of the 6-*endo* cyclization product which formed first. Consequently, degradation and side reactions partly occurred, especially favored by long reaction time and high temperature.



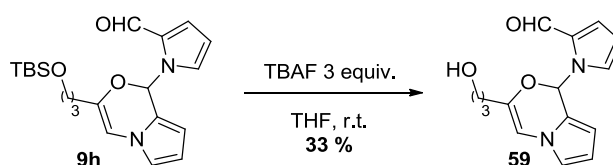
Scheme 139. Proposed reaction mechanism for the formation of products **28**, **52**, **53** and **54**.

5.2. Toward the tricyclic core of acortatarin A

Besides these attempts of Ag-USY catalyzed spiroketalization of ynamide diol substrates, we were attracted to the transformation of pyrrole morpholine bicycle **9h**, obtained from an unexpected copper-catalyzed amidative coupling/cyclization cascade (Scheme 140). This precursor might provide interesting alternatives toward a straightforward synthesis of acortatarin A.

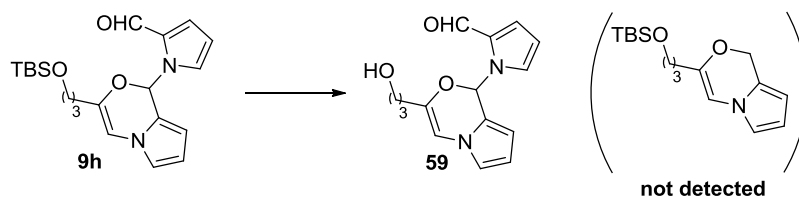
Scheme 140. Transformation of precursor **9h** into the tricyclic core of acortatarin A.

One of the main objectives was the deprotection of the silylated alcohol in view of performing the second cyclization. Usual conditions using fluoride ions turned out to be not suitable, the silyl group staying relatively inert in the presence of one equivalent TBAF. With 3 equivalents, conversion went to completion according to TLC monitoring. However, the resulting alcohol was recovered in a modest 33 % yield (Scheme 141).

Scheme 141. Deprotection of the silyl group of **9h** using fluoride ions

Interestingly, attempts to cleave the exceeding pyrrole moiety using various conditions suggested that organic acids seemed more suitable to remove the protecting silyl group. Indeed, the *N,O*-acetal remained untouched and the major product was most often the deprotected alcohol (Table 24).

Table 24. Attempts to cleave the exceeding pyrrole moiety.



Entry	Reagent	Solvent	T (°C), t (h)	Yield
1	Et ₃ SiH 2.5 equiv.	TFA	r.t., 30 min	- ^a
2	TFA 10 mol%	MeOH	r.t., 3 h	43 %
3	<i>p</i> TSA.H ₂ O 1 equiv.	THF:H ₂ O (9:1)	r.t., 16 h	70 %

^a Degradation occurred.

Triethylsilane in TFA as solvent were too harsh conditions, leading only to degradation of the starting material (entry 1). 10 mol% trifluoroacetic acid in methanol afforded a moderate 43

% yield, while milder *p*-toluenesulfonic acid monohydrate provided the best result with 70 % alcohol **59** after one night at room temperature (entries 2 - 3).

Our efforts to cleave the exceeding pyrrole-2-carboxaldehyde unit being unsuccessful, we even though decided to attempt the remaining 5-*exo-trig* cyclization under Ag-USY catalysis (Table 25).

Table 25. Ag-USY catalyzed transformation of alcohol **59**.

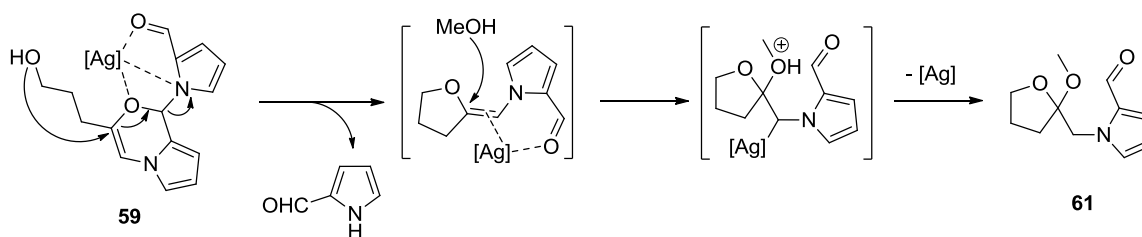
Entry	Solvent	T (°C), t (h)	Result
1	-	90 °C, 24 h	7e 16 %, conversion 77 % ^a
2	MeOH	90 °C, 48 h	7e 8 %, 61 43 % ^{a,b}

^a Presence of unidentified side products. ^b With 5 mol% Ag-USY.

When the reaction was performed neat at 90 °C in a sealed tube with 2 mol% Ag-USY, the formation of several compounds was detected by TLC. Unfortunately, only one could be isolated in sufficient amount (16 % yield) and was found to be pyrrole-2-carboxaldehyde **7e**. In addition, the conversion was not complete since 23 % of the starting alcohol **59** was also recovered. Nevertheless, this first result suggested that the reaction conditions promoted the desired pyrrole cleavage. When using methanol as solvent, a major product clearly appeared among others upon TLC monitoring. The latter was identified as the acetal **61** (entry 2), isolated in 43 % yield. This major product along with 8 % yield of **7e** confirmed that pyrrole cleavage actually took place in the presence of Ag-USY as catalyst.

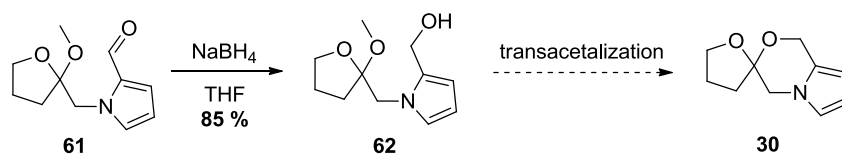
Acetal **61** originated from the opening of the morpholine ring previously formed under copper catalysis. Again, a cascade mechanism may be suspected, involving the expected 5-*exo-trig* cyclization, with simultaneous *N,O*-acetal cleavage, possibly favored by coordination of the silver catalyst to the aldehyde oxygen and pyrrole nitrogen (Scheme 142). This cascade would release the pyrrole-2-carboxaldehyde moiety. Upon silver activation, the remaining highly

reactive *exo*-methylene bond would be finally trapped by the addition of methanol, affording acetal **61** in the end.



Scheme 142. Proposed reaction mechanism for the synthesis of acetal **61**.

This unexpected result got us closer than ever to the tricyclic target **30** (Scheme 143). Reduction of the aldehyde to the alcohol in the presence of sodium borohydride afforded acetal **62** in 85 % yield. The last step we need to set up is a transacetalization reaction, eliminating methanol and building the desired spiro[4.5]ketal **30** at the same time.

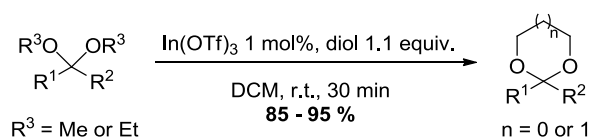


Scheme 143. Final steps toward the tricyclic core of acortatarin A.

Acetal exchange strategies are well-known in the literature, but most methods rely on complicated catalysts or harsh reaction conditions using stoichiometric Brønsted or Lewis acids, toxic solvent and high temperature for the azeotropic removal of water.³⁶³ Interestingly, Graham and co-workers recently found that indium(III) triflate catalyzed the transacetalization of diols and triols under solvent free conditions, at room temperature (Scheme 144).³⁶⁴

³⁶³ (a) Ortholand, J.-Y.; Vicart, N.; Greiner, A. *J. Org. Chem.* **1995**, *60*, 1880–1884. (b) Sülü, M.; Venanzi, L. M. *Helv. Chim. Acta* **2001**, *84*, 898–907. (c) Ranu, B. C.; Jana, R.; Samanta, S. *Adv. Synth. Catal.* **2004**, *346*, 446–450. (d) Čorić, I.; Vellalath, S.; List, B. *J. Am. Chem. Soc.* **2010**, *132*, 8536–8537.

³⁶⁴ Smith, B. M.; Kubczyk, T. M.; Graham, A. E. *Tetrahedron* **2012**, *68*, 7775–7781.

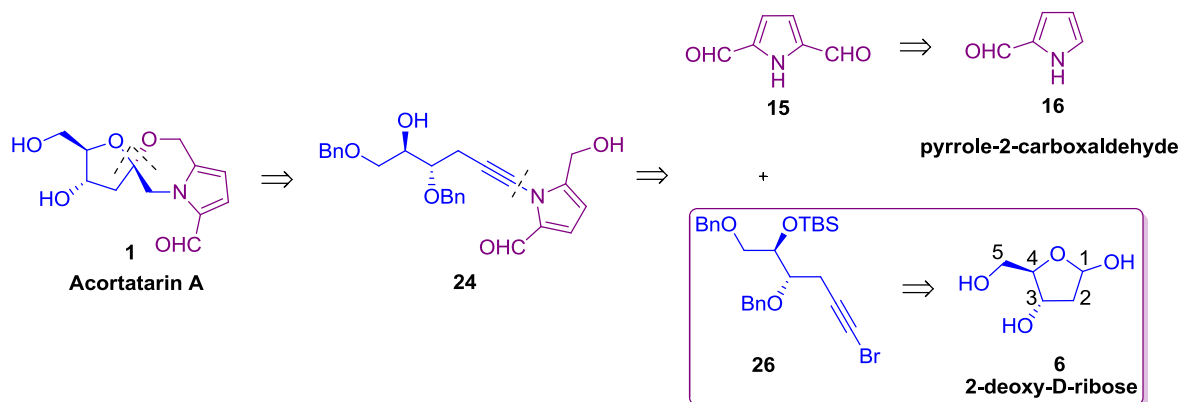


Scheme 144. Indium(III)-catalyzed transacetalization of diols by Graham et al.

As a perspective we aim to apply this mild methodology to the last step of our short synthesis of the tricyclic scaffold of acortatarin A. If successful, an indium-zeolite catalyzed variant may be considered, which would maximize the number of heterogeneously catalyzed steps in the total synthesis, and strengthen its environmental friendly nature.

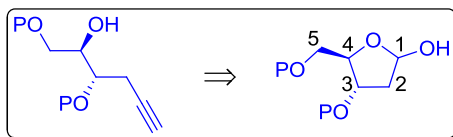
6. Synthesis of the sugar moiety of acortatarin A

When working on the development of a suitable methodology to access the core of acortatarin A, we embarked at the same time on the synthesis of the sugar moiety. Our strategy was based on the preparation of the alkynyl bromide derivative **26** from chiral pool available 2-deoxy-D-ribose **6** (Scheme 145).



Scheme 145. Retrosynthetic approach to acortatarin A.

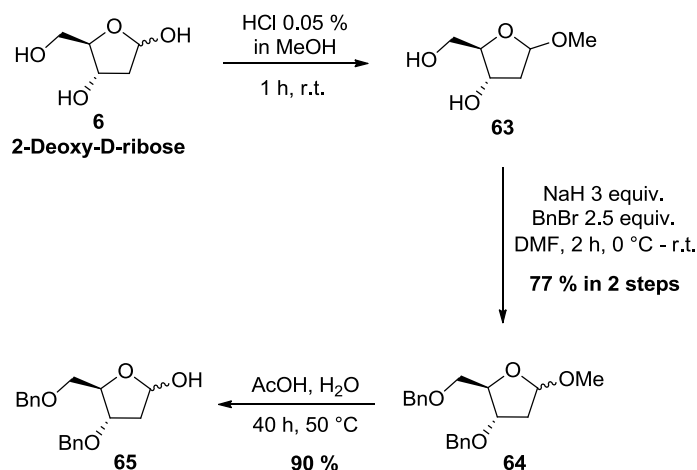
The key step in the synthesis of the bromo alkyne **26** was the formation of the triple bond. As the hemiacetal functionality already present in the ribose derivative could be seen as a masked aldehyde, we proposed that the triple bond was obtained by a one carbon homologation reaction (Scheme 146).



Scheme 146. Key step toward bromoalkyne **26** : a one carbon homologation reaction

The Seyfert-Gilbert homologation³⁶⁵ or the Corey-Fuchs methodology³⁶⁶ could thus be employed to synthesize the terminal alkyne. The former strategy is advantageous from a total synthesis point of view, in so far as it is a one-step procedure, contrary to the Corey-Fuchs alternative performed in two steps. In order to avoid any side-reaction, we decided to protect the two hydroxyl functional groups at position 3 and 5 before engaging in this key transformation. It will always be possible to skip such steps if they prove unnecessary.

The synthesis of 3,5-dibenzyl protected 2-deoxy-D-ribose was already reported in the literature, and used by Jagadeesh and co-workers in the first total synthesis of acortatarin A.³²³ We decided to employ the same methodology, carried out in 3 steps. 2-deoxy-D-ribose **6** was first converted to its acetal **63**, before benzylation of the remaining two alcohols using sodium hydride/benzyl bromide. These two steps gave the protected ribose derivative **64** in an overall 77 % yield (Scheme 147).³⁶⁷ Removal of methanol under acidic conditions at 50 °C for 40 h released the hemiacetal **65** in 90 % yield.³⁶⁸



Scheme 147. Synthesis of hemiacetal **65** from 2-deoxy-D-ribose **6**.

³⁶⁵ Gilbert, J. C.; Weerasooriya, U. *J. Org. Chem.* **1982**, *47*, 1837–1845.

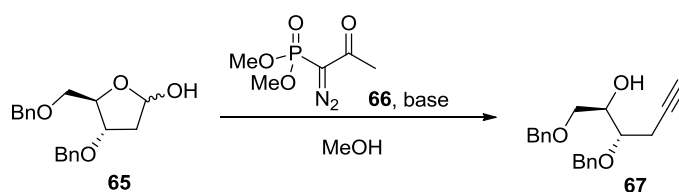
³⁶⁶ Corey, E. J.; Fuchs, P. L. *Tetrahedron Lett.* **1972**, *13*, 3769–3772.

³⁶⁷ Takahashi, T.; Hirose, Y.; Iwamoto, H.; Doi, T. *J. Org. Chem.* **1998**, *63*, 5742–5743.

³⁶⁸ Adamo, M. F. A.; Pergoli, R. *Org. Lett.* **2007**, *9*, 4443–4446.

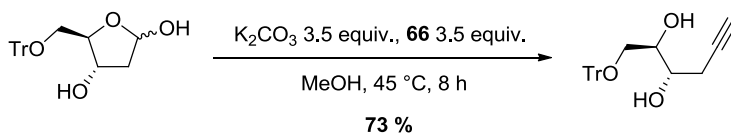
With this ribose derivative in hands, we were ready to engage in the synthesis of the terminal alkyne.

The Ohira-Bestmann modification of the Seyfert-Gilbert homologation is known to proceed under milder conditions, enabling the conversion of sensitive substrates such as enolizable aldehydes.³⁶⁹ It relies on the use of dimethyl 1-diazo-2-oxopropylphosphonate or Bestmann-Ohira reagent **66** (Scheme 148).



Scheme 148. Seyfert-Gilbert homologation of **65** using the Bestmann-Ohira reagent.

In the literature, such homologation using Bestmann-Ohira reagent **66** was already carried out on substrates quite similar to our hemiacetal sugar derivative **65**. In particular, Demailly and co-workers reported that glyco-1-ynitols could be synthesized *via* this method, which tolerated even free hydroxyl groups.³⁷⁰ They stated that higher temperature was necessary to counterbalance the lower reactivity of the hemiacetal substrates. To avoid decomposition of the phosphonate at this temperature, the authors mentioned that the latter was added slowly. With their procedure, 2-deoxy-D-ribose protected only in position 5 with a trityl group yielded 73 % of the corresponding glycol-1-ynitol, using 3.5 equivalent of the base and the phosphonate, at 45 °C (Scheme 149).



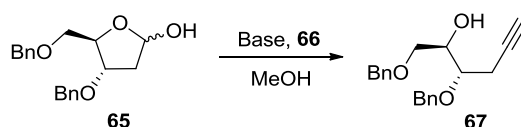
Scheme 149. Homologation of a mono-protected 2-deoxy-D-ribose by Demailly et al.

³⁶⁹ (a) Ohira, S. *Synth. Commun.* **1989**, *19*, 561–564. (b) Müller, S.; Liepold, B.; Roth, G. J.; Bestmann, H. J. *Synlett* **1996**, *1996*, 521–522.

³⁷⁰ Thierry, J. C.; Frechou, C.; Demailly, G. *Tetrahedron Lett.* **2000**, *41*, 6337–6339.

Due to the similarity of our substrate with these aldoses, we first attempted to prepare alkyne **67** by the procedure of Demailly and co-workers (Table 26, entry 1).³⁷⁰ However, the reaction mixture quickly turned brown upon heating of the hemiacetal solution in methanol. After the end of the phosphonate addition, TLC monitoring and ¹H NMR confirmed that mostly degradation occurred, 45 % benzyl alcohol being recovered as single product. Concluding that ribose derivative **65** was not stable at high temperature, we tested a milder procedure, adding this time the sugar on the Bestmann-Ohira reagent. After 3 h at room temperature, the conversion seemed complete and 35 % of desired alkyne **67** was isolated (entry 2).

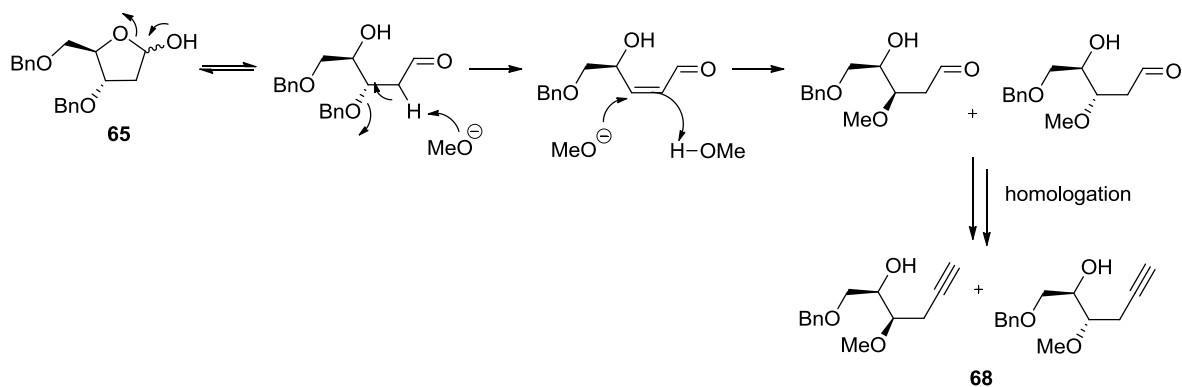
Table 26. Synthesis of alkyne **67** from hemiacetal **65** using Bestmann-Ohira reagent.



Entry	Base	66	Solvent	T (°C), t (h)	Yield
1	K ₂ CO ₃ 3 eq.	3 eq. ^a	MeOH	reflux, 3 h	- ^b
2	K ₂ CO ₃ 3 eq.	3 eq.	MeOH	0 °C - r.t., 3 h	35 %
3	K ₂ CO ₃ 2 eq.	1.5 eq.	MeOH	0 °C - r.t., 22 h	30 % ^c
4	K ₂ CO ₃ 3 eq.	3 eq.	THF/MeOH 8/2	0 °C - r.t., 23 h	24 % ^d
			THF/MeOH 1/1	r.t., 20 h	

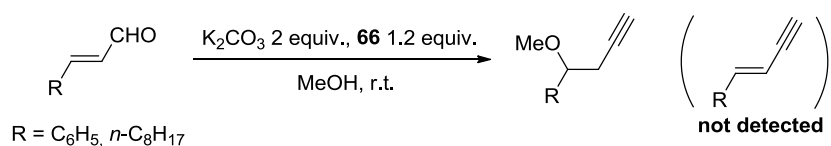
^a **66** was added slowly to the reaction mixture (0.29 mL/h). ^b Degradation occurred and 45 % benzyl alcohol was recovered. ^c 13 % benzyl alcohol and 3 % diastereomers **68** isolated. ^d 8 % benzyl alcohol and 7 % diastereomers **68** isolated.

Suspecting that this low yield may be due to degradation, we reasoned that 3 equivalents of base and phosphonate were not necessary, one or two equivalents being theoretically required. With 2 equivalents of K₂CO₃ and 1.5 equivalent of phosphonate, the reaction proceeded smoothly in 22 h. However, only 30 % of alkyne was still recovered (entry 3). In addition, 13 % benzyl alcohol was isolated and 3 % of a 1:1 mixture of diastereomers **68**, resulting from the elimination of a benzyl ether substituent and subsequent addition of methanol. We assumed that these two diastereomers may be formed by a E2 elimination reaction, in which the acidic proton α to the carbonyl would be trapped by the methanolate base, with concomitant elimination of the benzyl protecting group (Scheme 150). Subsequent addition of methanolate to the double bond would provide two intermediates, which could undergo the homologation and lead to diastereomers **68**.

Scheme 150. Proposed reaction mechanism for the formation of diastereomers **68**.

In order to avoid this side reaction, we tried to reduce the amount of methanol, by using a 8/2 mixture of THF/methanol as solvent (entry 4). Although the reaction proceeded under these conditions, conversion remained low after 23 h. Therefore, methanol was added until having a 1/1 ratio of the two solvents. After 20 h, reaction was complete but yielded only 24 % alkyne, along with 8 % benzyl alcohol and 7 % diastereomers **68**.

Our first attempts to increase the yield of alkyne being unsuccessful, we assumed that our benzyl substituted hemiacetal **65** was not a suitable candidate for this homologation reaction. Isolated examples reported by Bestmann and co-workers supported this hypothesis. In the first publication disclosing the Bestmann-Ohira conditions,^{369b} the authors indicated that α,β -unsaturated aldehydes could not be converted to the expected enynes. Instead, the main isolated products were the corresponding propargylic methyl ethers (Scheme 151).

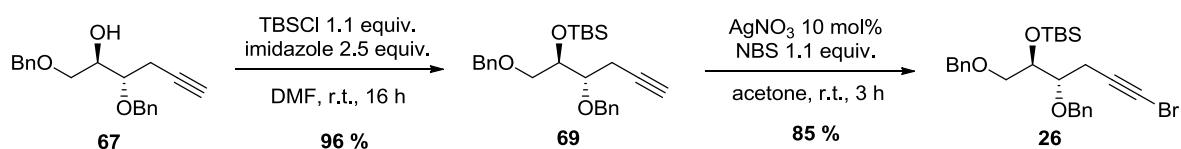


Scheme 151. Formation of propargylic methyl ethers under the Bestmann-Ohira conditions.

The authors assumed that initial conjugate addition of methanol and subsequent homology took place.

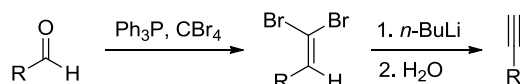
With sufficient amount of the alkyne **67**, we were able to finish the synthesis of the sugar moiety. The remaining two steps were the protection of the free alcohol and bromination of the terminal alkyne, in view of the amidative cross-coupling with the pyrrole derivative. Classical silylation conditions using TBSCl and imidazole in DMF afforded 96 % of the

protected alcohol **69** (Scheme 152). Bromination of the alkyne was mediated by *N*-bromosuccinimide and silver nitrate as catalyst, according to the method of Weichert et al.³⁷¹ After 3 h in acetone at room temperature, the expected alkynyl bromide **26** was isolated in 85 % yield (Scheme 152).



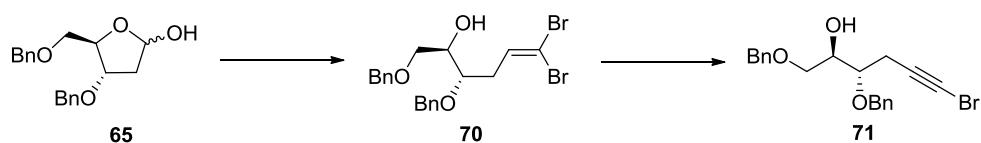
Scheme 152. Final steps toward the synthesis of bromoalkyne **26**.

Since the Bestmann-Ohira conditions were not perfectly suitable to the transformation of hemiacetal **65** to alkyne **67**, we started considering the Corey-Fuchs alternative, proceeding in two steps (Scheme 153).



Scheme 153. The Corey-Fuchs methodology to prepare alkynes from aldehydes.

In order to develop a straightforward synthesis of compound **26**, we reasoned that the alkynyl bromide could be directly accessed from the adjustment of the Corey-Fuchs methodology, providing the dibromoalkene **70**. The latter could, after dehydrohalogenation reaction, yield the desired bromoalkyne **71** (Scheme 154).

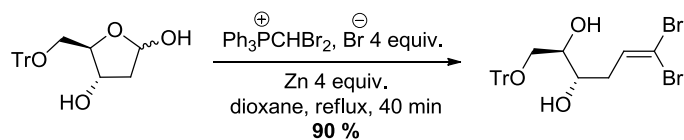


Scheme 154. Application of the Corey-Fuchs strategy to our substrate.

Protection of the alcohol could be performed afterwards if necessary. Using this strategy, the total number of steps would be identical to the synthesis based on the Bestmann-Ohira conditions.

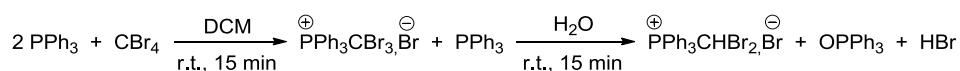
³⁷¹ Hofmeister, H.; Annen, K.; Laurent, H.; Wiechert, R. *Angew. Chem.* **1984**, *96*, 720–721.

Demilly and co-workers also investigated the synthesis of dibromoalkenes from aldoses carrying free hydroxyl groups.³⁷² They obtained good yields using a fourfold excess of dibromomethyltriphenylphosphonium bromide and a fourfold excess of zinc, in refluxing dioxane (Scheme 155).



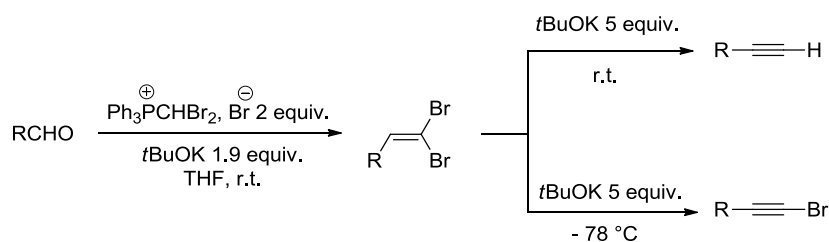
Scheme 155. Synthesis of dibromoalkenes from aldoses by Demilly et al.

Contrary to the Corey-Fuchs methodology in which the ylide is generated *in situ* from CBr_4 and PPh_3 , they prepared and isolated the phosphonium salt before the reaction, using the procedure of Ramirez et al. (Scheme 156).³⁷²⁻³⁷³



Scheme 156. Preparation of the phosphonium salt by Ramirez et al.

Demilly et al. indicated that the methodology of Rassat and co-workers, using the same phosphonium salt in combination with *t*BuOK in THF was efficient only for protected aldoses carrying no free hydroxyl groups.³⁷⁴ Initially, Rassat et al. developed these conditions in order to perform the one-pot synthesis of alkynes and bromoalkynes from aldehydes (Scheme 157).³⁷⁴



Scheme 157. One-pot synthesis of alkynes and bromoalkynes by Rassat et al.

³⁷² Dolhem, F.; Lièvre, C.; Demilly, G. *Tetrahedron Lett.* **2002**, *43*, 1847-1849.

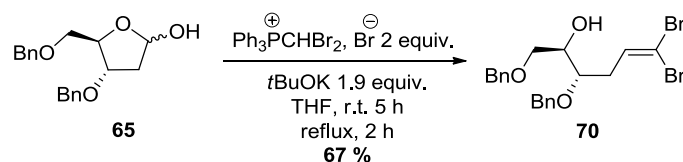
³⁷³ Desai, N. B.; McKelvie, N.; Ramirez, F. *J. Am. Chem. Soc.* **1962**, *84*, 1745-1747.

³⁷⁴ Michel, P.; Gennet, D.; Rassat, A. *Tetrahedron Lett.* **1999**, *40*, 8575-8578.

Depending on the temperature of the second addition of *t*BuOK, they managed to isolate either the aldehyde (room temperature) or bromoalkyne (-78 °C). However, the authors indicated that the result strongly depended on the nature of the aldehyde, some aromatic substrates being directly converted to the alkyne even at low temperature.

Based on these informations, we decided to test the conditions of Rassat et al., in order to check whether dibromoalkene **70** could actually be formed from hemiacetal **65**.

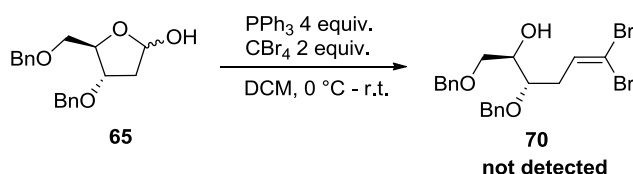
Dibromomethyltriphenylphosphonium bromide was prepared according to the adjusted method of Demailly et al. (Scheme 156).³⁷² Hemiacetal **65** was added to the mixture of the phosphonium salt and *t*BuOK in THF (Scheme 158).



Scheme 158. Synthesis of dibromoalkene **70** using the conditions of Rassat et al.

After 5 h at room temperature, the mixture was heated at reflux for 2 hours, in order to achieve complete conversion. We were pleased to isolate the desired dibromoalkene in 67 % yield. Although conversion was difficult to assess by TLC monitoring, only 4 % of starting material could be isolated, confirming that nearly all hemiacetal reacted.

Control experiment using the classical Corey-Fuchs conditions indicated that they were not suitable to our substrate (Scheme 159).



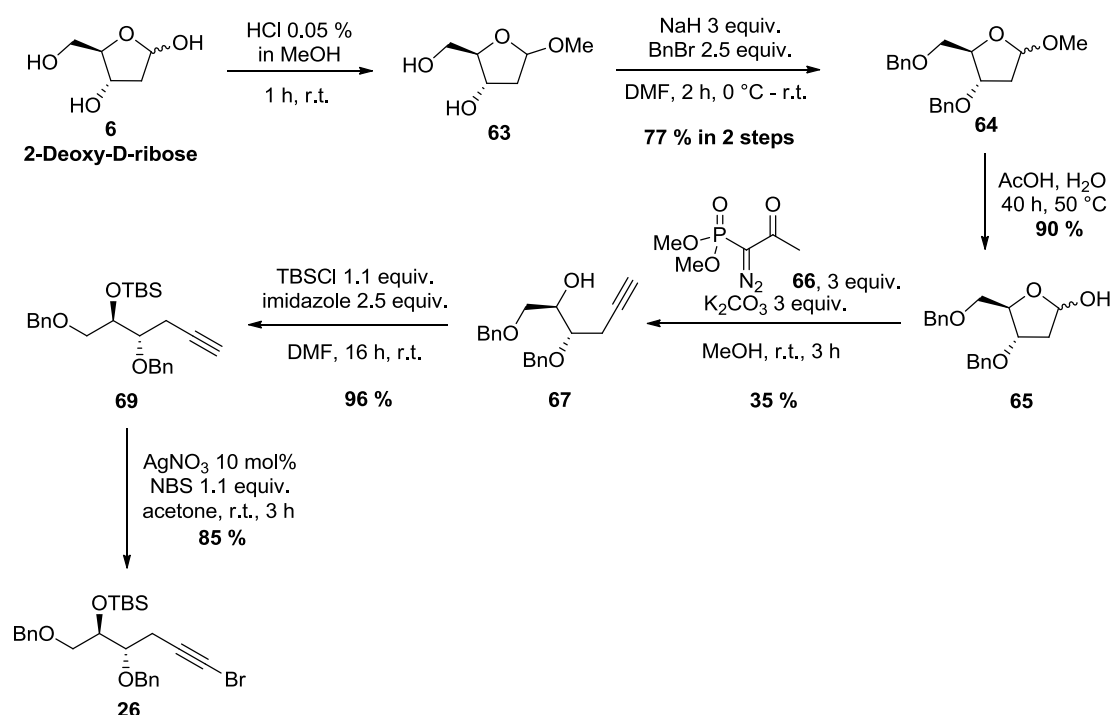
Scheme 159. Attempt to prepare **70** using the classical Corey-Fuchs conditions.

Indeed, no trace of alkene **70** could be detected, and only small amounts of unidentified products were recovered. It is likely that side reactions may have occurred in the presence of PPh_3Br_2 , generated during the reaction of PPh_3 and CBr_4 . The preparation of the phosphonium salt before the reaction may be an important factor of success, due to the sensitivity of our hemiacetal **65**.

As a perspective, we still have to find suitable conditions for the dehydrohalogenation of alkene **70** to bromoalkyne **71**. We could start with the conditions of Rassat, using a second addition of *t*BuOK at low temperature.³⁷⁴

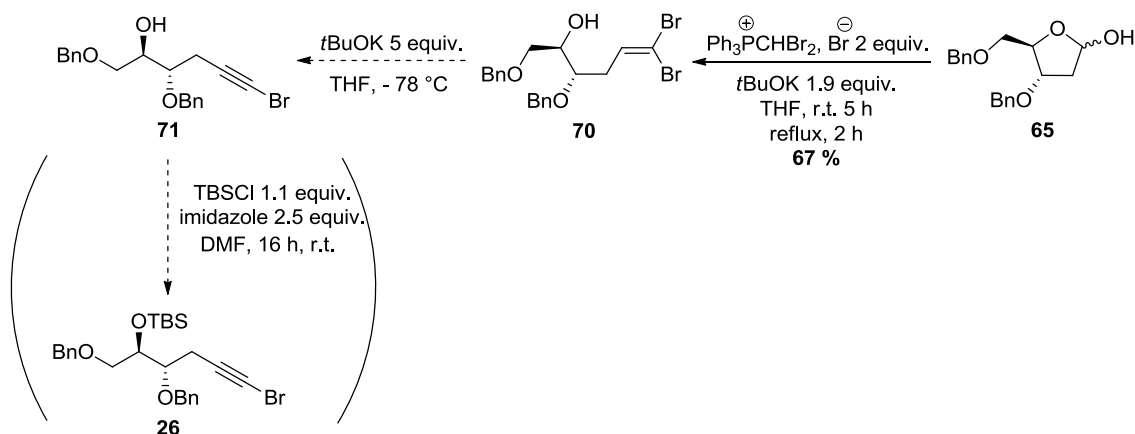
7. Perspectives concerning the total synthesis of acortatarin A

At the present stage, we have accomplished the synthesis of the sugar moiety of acortatarin A. The bromoalkyne **26** was obtained in 20 % over 6 steps from 2-deoxy-D-ribose (Scheme 160).



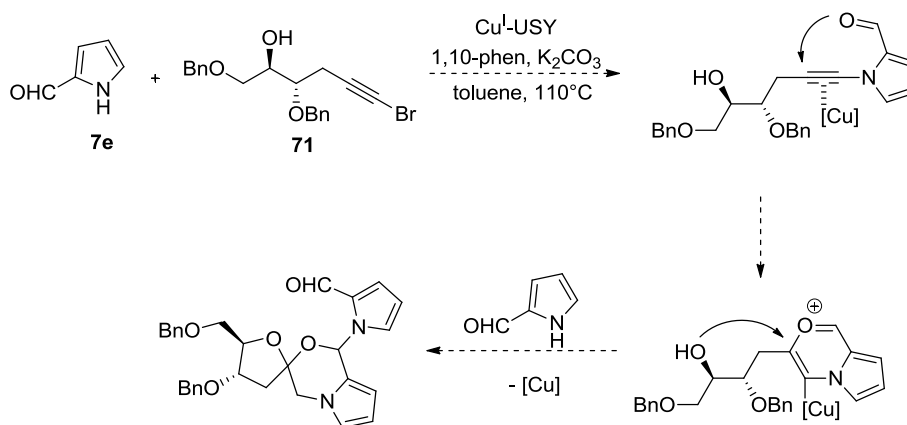
Scheme 160. Achieved synthesis of the sugar moiety of acortatarin A.

The key step of this synthesis is the transformation of hemiacetal **65** to alkyne **67**, which is currently unsatisfying using the Bestmann-Ohira conditions. In order to improve the overall yield of the synthesis, a Corey-Fuchs type strategy may be considered (Scheme 161). Based on this methodology, hemiacetal **65** would be converted to dibromoalkene **70**, and then to bromoalkyne **71** using a dehydrohalogenation reaction. We still must find suitable conditions for this transformation, but the first attempt to synthesize the dibromoalkene precursor was a success, affording the desired product in 67 % yield.



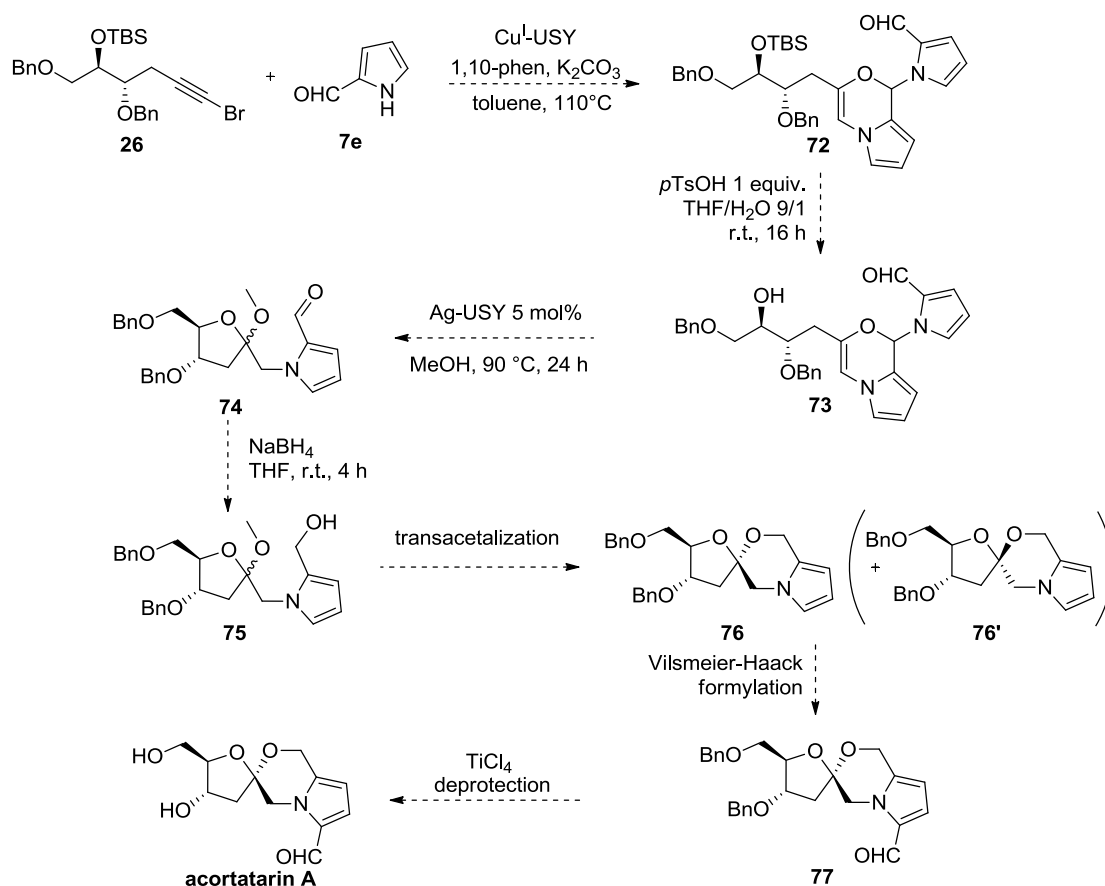
Scheme 161. Possible improvement of the homologation reaction.

In the current synthesis of bromoalkyne **26** (Scheme 160), the free hydroxyl group of alkyne **67** was protected by a silyl, before bromination of the alkyne. This step was necessary considering the bromination conditions, using silver nitrate. Without suitable protection, the alcohol may be prone to attack the triple bond under silver catalysis, and form undesired heterocyclic products. Considering that the alcohol protection is not absolutely necessary to perform the amidative cross-coupling, we could skip this step once we obtained bromoalkyne **71** (Scheme 161). Based on the tandem coupling/cyclization cascade observed in the *N*-alkynylation of pyrrole-2-carboxaldehyde, it would be also interesting to check whether the free alcohol would hopefully cyclize upon coupling with the pyrrole (Scheme 162).

Scheme 162. Possible coupling/cyclization cascade between pyrrole **7e** and bromoalkyne **71**.

If this reaction does not lead to interesting results, we can still explore the coupling of pyrrole-2-carboxaldehyde with fully protected bromoalkyne **26**.

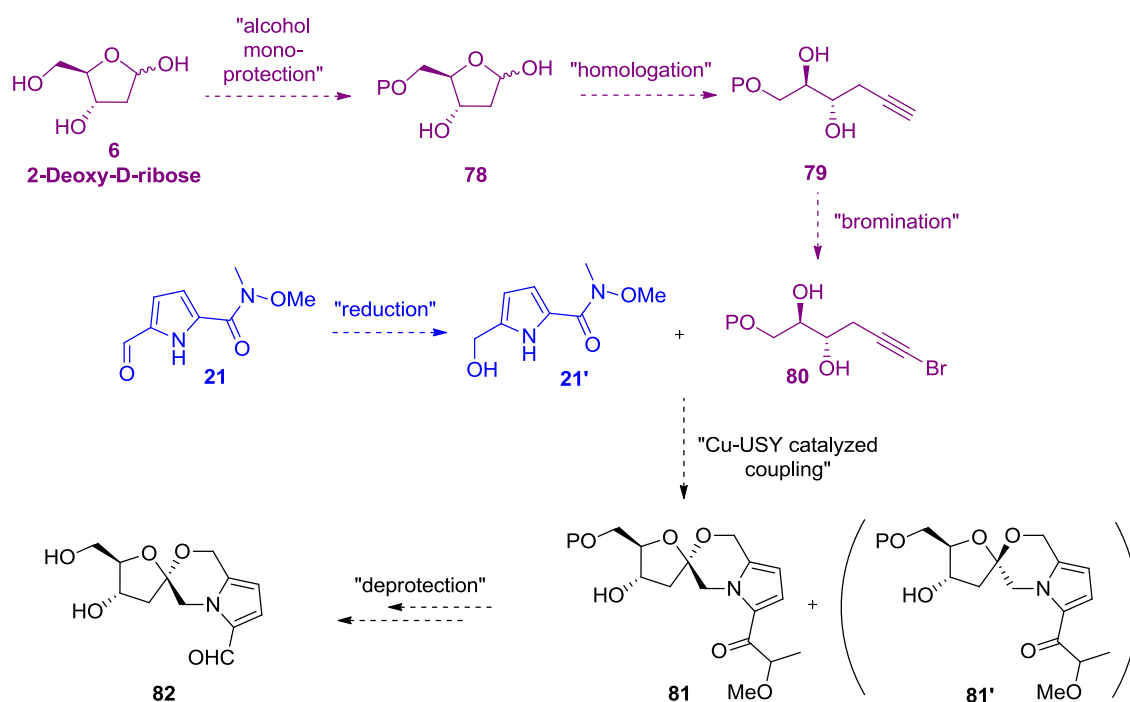
From the results obtained with the protected 5-bromopent-4-yn-1-ol model, we could propose the following reaction sequence (Scheme 163).



Scheme 163. Proposed total synthesis of acortatarin A based on current results.

N-alkynylation of pyrrole-2-carboxaldehyde with bromoalkyne **26** followed by 6-*endo* cyclization and oxonium trapping would lead to the *endo*-methylene morpholine derivative **72**, according to our preliminary experiments. After deprotection of the silylated alcohol, Ag-USY catalysis in methanol at 90 °C would promote the expected 5-*exo-trig* cyclization and subsequent cascade affording acetal **74**. Reduction of the aldehyde and transacetalization of compound **75** would yield a mixture of spiroketal isomers **76** and **76'**. To finish the sequence, the desired diastereoisomer would undergo Vilsmeier-Haack formylation of the pyrrole fragment, and final deprotection of the benzyl ethers, to give acortatarin A.

Since the protection of alcohol at position 3 in 2-deoxy-D-ribose is not absolutely necessary in the following steps, we could also envisage a more straightforward approach based on the initial mono-protection of alcohol at position 5, directly followed by the homologation reaction leading to alkyne **79** (Scheme 164). It is noteworthy that hemiacetals similar to **78**, bearing free hydroxyl groups, were effectively converted in such homologation reaction under the conditions of Demailly and co-workers.³⁷⁰



Scheme 164. Proposed shorter synthesis of acortatarin A.

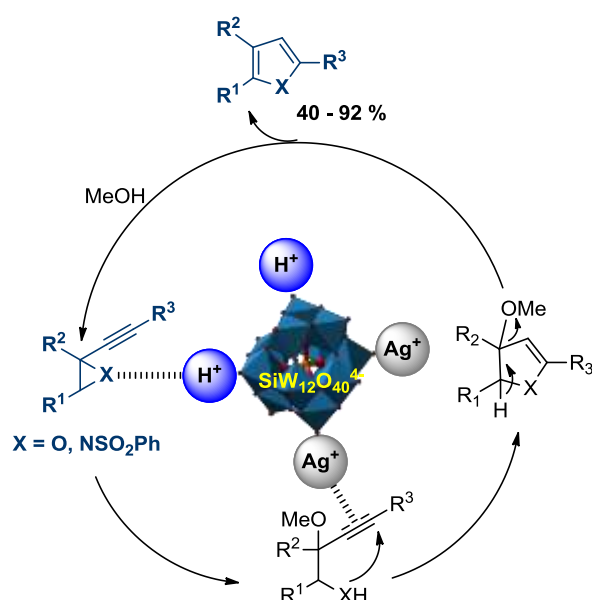
The alkynyl bromide coupling partner **80** would then be obtained after bromination of the terminal alkyne. Suitable reaction conditions should be found in order to avoid side reactions between the free hydroxyl groups and the alkyne. On the other hand, the pyrrole fragment **21'** could be accessed after reduction of the formyl substituted pyrrole **21** (obtained in 3 steps according to the procedure of Aponick and co-workers).³²¹ Copper-catalyzed coupling between pyrrole fragment **21'** and the bromo alkyne derivative **80**, possibly mediated by Cu-USY zeolite, could directly yield the tricyclic core of acortatarin A **81**, along with its stereoisomer **81'**. After deprotection of the Weinreb amide and the alcohol at position 5, acortatarin A could be finally obtained.

Conclusion

Conclusion

Based on all the results presented in this manuscript, we can conclude that the main objective of this Ph.D. thesis was reached. Indeed, we managed to develop greener pathways toward small attractive building blocks, using metal-doped solids as heterogeneous catalysts.

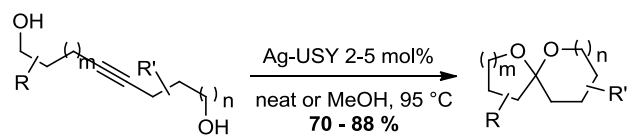
We demonstrated that polyoxometalates were suitable heterogeneous supports for the rearrangement of alkynyloxiranes to furans, able to provide in a single catalyst the bifunctional acid/silver properties, necessary for the rearrangement (Scheme 165). The screening of reaction conditions showed that $\text{Ag}_2\text{H}_2\text{SiW}_{12}\text{O}_{40}$ was the most suitable heteropolyacid candidate, as efficient in terms of yields and reaction rate as the combination of silver triflate and *p*-toluenesulfonic acid, employed in the usual homogeneous conditions.²⁶⁰ Silver-doped polyoxometalates are stable materials, easy to prepare, handle, and could be recycled up to four times without significant loss of yield in this reaction. These versatile supports, easily tunable, open the way for other applications in organic synthesis.



Scheme 165. Ag-POM catalyzed rearrangement of alkynyloxiranes to furans.

In another part of the thesis, we successfully developed a green synthesis of ketals and spiroketals, based on the silver-zeolite catalyzed dihydroalkoxylation of alkynediols. This atom-economic and straightforward method has never been reported under silver catalysis. In addition, most of the substrates could be efficiently converted in the presence of only 2 mol% Ag-USY, without solvent (Scheme 166).

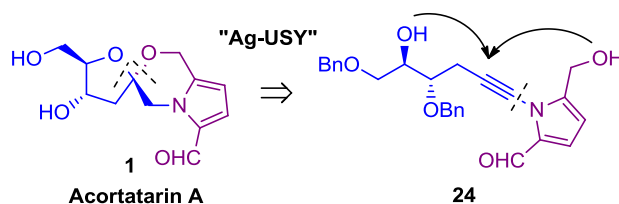
Conclusion



Scheme 166. Ag-USY catalyzed dihydroalkoxylation of alkyne diols.

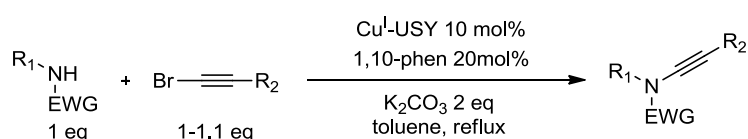
Moreover, the presence of methanol dramatically increased the reaction rate, without incorporation of the latter. Hydrogen-bonding catalysis could be at the origin of this acceleration.³¹⁴ The catalyst could be recycled at least 5 times, without loss of activity.

As a long term objective, we aimed to apply this environmental friendly spiroketalization strategy to the synthesis of acortatarin A, a potential inhibitor of Reactive Oxygen Species (ROS) (Scheme 167).



Scheme 167. Ag-USY catalyzed spiroketalization strategy for the synthesis of acortatarin A.

In the course of the work, we demonstrated the potential of a copper-zeolite catalyzed cross-coupling of alkynylbromides and *N*-nucleophiles, for the synthesis of ynamides (Scheme 168).

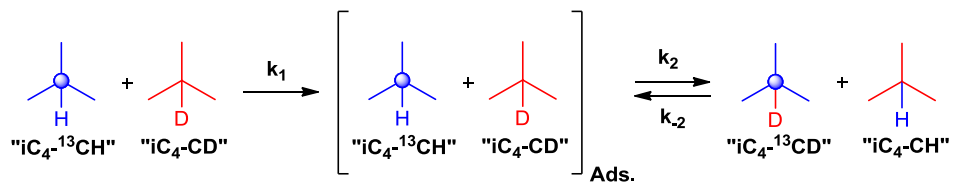


Scheme 168. Cu-USY catalyzed cross-coupling of alkynylbromides and *N*-nucleophiles.

For the moment, the total synthesis has not been completed but promising results supported the feasibility of our approach.

The second objective of the Ph.D. has also been reached. The synthesis of ²H and ¹³C labeled isobutanes could be carried out in sufficient yields and purities to perform the hydride transfer study. The kinetic of the H/D exchange between the two molecules could be directly monitored by *in situ* NMR at different temperatures, allowing the access to the energetic

parameters of the reaction: the rate constant and the activation energy. Experimental data suggested that the reaction proceeded *via* the formation of two intermediate adsorbed species (Scheme 169), and the calculated apparent activation energy was consistent with a carbenium-type mechanism, as supported by Sommer and co-workers.



Scheme 169. Two-step hydride transfer between ^2H and ^{13}C labeled isobutanes.

Conclusion

Experimental Data

Experimental Data

1. Activation of small alkanes on solid acids

1.1. General information

Proton (^1H NMR) and Carbon (^{13}C NMR) nuclear magnetic resonance spectra were recorded on Bruker Avance Spectrometers at 400 or 500 MHz. Chemical shifts are given in part per million (ppm) on the delta scale. The solvent peak was used as reference value. For ^1H NMR: $\text{C}_2\text{D}_2\text{Cl}_4 = 5.98$ ppm. For ^{13}C NMR: $\text{C}_2\text{D}_2\text{Cl}_4 = 73.81$ ppm. Data are presented as follows: chemical shift, multiplicity (s = singlet, d = doublet, t = triplet, q = quartet, qt = quintet, sext = sextuplet, m = multiplet), coupling constants (J/Hz) and integration. Reagents and solvents were purified using standard means. All other chemicals were used as received except where otherwise noted in the experimental text. All other extractive procedures were performed using non distilled solvents and all aqueous solutions used were saturated (satd).

1.2. Synthesis of ^2H and ^{13}C labeled isobutanes

Isobutane-2- d_1 ($i\text{C}_4\text{-CD}$) was synthesized according to a modified procedure reported by Sassi and co-workers.³⁷⁵



Isobutane-2- d_1 .

To a solution of *tert*-butyl-magnesium chloride (1.7 M in THF, 11.8 mL, 20 mmol) was added dropwise a solution of D_2O (0.48 g, 24 mmol, 1.2 equiv.) in dry THF (1 mL), and the produced gases were collected in a cold trap at -117 °C (ethanol and liquid nitrogen), connected on the top of the condenser by a polyethylene tube and a rubber cap. After addition of all the deuterium oxide, the reaction mixture was heated up to the boiling point, to release all dissolved gases. Then, 0.1 mL of Br_2 was added to the condensed gases in the cold trap, and the valves of the trap were closed. After 0.5 h, the crude isobutane-2- d_1 was progressively warmed up to room temperature and bubbled through two traps containing an aqueous solution of $\text{Na}_2\text{S}_2\text{O}_3$ (5.3 g $\text{Na}_2\text{S}_2\text{O}_3 \cdot 5\text{H}_2\text{O}$ in 13 mL of solution), and collected in a final ball-shape glassware containing brine. To finish, the gas was condensed a second time in a cold

³⁷⁵ Sassi, A.; Goepfert, A.; Sommer, J.; Esteves, P. M.; Mota, C. J. *J. Labelled Compd. Radiopharm.* **1999**, *42*, 1023–1030.

Experimental Data

trap at $-196\text{ }^{\circ}\text{C}$ (liquid nitrogen), pumped under vacuum in order to discard the presence of air, before being stored in the ball-shape glassware containing brine.

Yield: 27 % (121 mL, 5.4 mmol). ^1H NMR ($\text{C}_2\text{D}_2\text{Cl}_4$, 500 MHz): $\delta=0.87$ ppm (t, $J=1.0$, 9 H).

^{13}C NMR ($\text{C}_2\text{D}_2\text{Cl}_4$, 500 MHz): $\delta=24.6$, 22.7 ppm (t, $^1J_{\text{C-D}}=19.7$).



Isobutane-2- C^{13} .

To a solution of methyl magnesium bromide (3 M in diethyl ether, 22.4 mL, 67.3 mmol) under argon at $0\text{ }^{\circ}\text{C}$ was added dry diethyl ether (44 mL) and ethyl acetate-2- C^{13} (2.0 g, 22.4 mmol). After addition of all the ethyl acetate-2- C^{13} , the reaction mixture was allowed to warm to room temperature. After stirring overnight at room temperature, saturated NH_4Cl was added (120 mL) and the solution was extracted with diethyl ether (3x60 mL). Careful evaporation of the solvent under reduced pressure afforded the crude *tert*-butyl alcohol-2- C^{13} , which was directly used in the next step without further purification.

To a solution of *tert*-butyl alcohol-2- C^{13} (1.54 g, 20.5 mmol) in TFA (10 mL) at $0\text{ }^{\circ}\text{C}$ was added triethylsilane (7.15 g, 61.5 mmol, 3 equiv.). After addition of all the triethylsilane, the reaction mixture was heated up to $50\text{ }^{\circ}\text{C}$ for 2 h. The produced gases were directly bubbled at the outlet of the condenser in a ball-shape glassware containing brine. Then, the crude gaseous mixture was condensed in a cold trap at $-117\text{ }^{\circ}\text{C}$, 0.1 mL Br_2 was added and the valves of the trap were closed. After 0.5 h, the crude isobutane-2- C^{13} was progressively warmed up to room temperature and bubbled through two traps containing an aqueous solution of $\text{Na}_2\text{S}_2\text{O}_3$ (5.3 g $\text{Na}_2\text{S}_2\text{O}_3 \cdot 5\text{H}_2\text{O}$ in 13 mL of solution), and collected in a final ball-shape glassware containing brine. To finish, the gas was condensed a second time in a cold trap at $-196\text{ }^{\circ}\text{C}$ (liquid nitrogen), pumped under vacuum in order to discard the presence of air, before being stored in the ball-shape glassware containing brine.

Yield: 37 % in 2 steps (186 mL, 8.29 mmol). ^1H NMR ($\text{C}_2\text{D}_2\text{Cl}_4$, 400 MHz): $\delta=1.69$ (decoupled doublet, $^1J_{\text{C-D}}=126.0$, $^3J_{\text{H-H}}=7.0$, 1 H), 0.87 ppm (dd, $^2J_{\text{H-C}}=4.0$, $^3J_{\text{H-H}}=7.0$, 9 H).

^{13}C NMR ($\text{C}_2\text{D}_2\text{Cl}_4$, 500 MHz): $\delta=24.8$, 23.2 ppm.

1.3. *In situ* MAS NMR experiments

All NMR spectroscopic experiments were conducted under MAS by using a 500 MHz NMR spectrometer equipped with an Avance Bruker console. ^1H and ^{13}C NMR spectra were

recorded at a Larmor frequency of 500.1 and 125.8 MHz with a spinning rate of 5 kHz. For both nuclei, chemical shifts were referenced to tetramethylsilane (TMS) at $\delta = 0.0$ ppm. A Hahn echo sequence was used for ^1H NMR spectra with a delay between the 90° and 180° pulses of 200 μs , synchronized to one rotor period. Typically, a recycle delay of 2.1 s, acquisition time of 0.2 s, and radiofrequency field of 87 kHz were used. $^{13}\text{C}\{^1\text{H}\}$ MAS spectra were obtained with a high-power decoupling (hpdec) Bloch decay sequence using a pulse duration of 4.5 μs corresponding to a flip angle of 90° , a relaxation delay of 2.8 s, and a number of scan of 256. Under these experimental conditions all measurements were fully quantitative, as verified according to preliminary T_1 relaxation times saturation-recovery experiments.

A 50/50 mixture of the two gases was prepared for all *in situ* MAS NMR experiments. Specific homemade device was used to activate the catalyst, load the gas and seal the 4 mm NMR rotor without expose to the ambient atmosphere prior to each experiment. Around 50 mg of USY zeolite (Si/Al = 11; 4.33 mmol H acid/g) was first treated at 250 $^\circ\text{C}$ for 54 h and subsequently outgassed at room temperature for 3 h ($< 10^{-7}$ mbar). Then, 0.5 mL of the 50/50 gaseous mixture $i\text{C}_4\text{-}^{13}\text{CH}/i\text{C}_4\text{-CD}$ (0.4 mmol $i\text{C}_4/\text{g}$) was introduced. The H/D exchange kinetics experiments were recorded simultaneously in ^1H and ^{13}C detection within a temperature range of 297–327 K along a period ranging from ca. 25 to 90 h, depending on the temperature.

2. Ag-H-POMs catalyzed rearrangement of alkynyloxiranes to furans

2.1. General Information

Proton (^1H NMR) and Carbon (^{13}C NMR) nuclear magnetic resonance spectra were recorded on Bruker Avance Spectrometers at 300, 400 or 500 MHz. Chemical shifts are given in part per million (ppm) on the delta scale. The solvent peak was used as reference value. For ^1H NMR: $\text{CDCl}_3 = 7.26$ ppm or $\text{C}_6\text{D}_6 = 7.16$ ppm. For ^{13}C NMR: $\text{CDCl}_3 = 77.0$ ppm or $\text{C}_6\text{D}_6 = 128.0$ ppm. Data are presented as follows: chemical shift, multiplicity (s = singlet, d = doublet, t = triplet, q = quartet, qt = quintet, sext = sextuplet, m = multiplet), coupling constants (J/Hz) and integration. X-ray diffraction (XRD) patterns were acquired on a D8 Advance Bruker AXS powder diffractometer ($\theta/2\theta$) using monochromatized Cu-K α radiation in the range of 2θ from 5° to 60° . Infrared spectra were recorded neat on an ALPHA Bruker FT-IR apparatus. Wavelengths of maximum absorbance (ν_{max}) are quoted in wave numbers (cm^{-1}). Scanning Electron Microscopy (SEM) was operated on a JEOL FEG 6700F microscope working at 9 kV accelerating voltage. EDX spectra were acquired using 20 kV primary electron voltage to determine the composition of the material. Mass spectra were recorded by ElectroSpray Ionization (ESI) or Electronic Impact (EI). Analytical Thin Layer Chromatography (TLC) were carried out on silica gel 60 F₂₅₄ plates with visualization by ultra violet, KMnO_4 , *p*-anisaldehyde or molybdophosphoric acid/ $\text{Ce}(\text{SO}_4)_2 \cdot 4\text{H}_2\text{O}$. Flash column chromatographies were carried out using silica gel 60 (40-63 μm) and the procedure includes the subsequent evaporation of solvents *in vacuo*. Reagents and solvents were purified using standard means. All other chemicals were used as received except where otherwise noted in the experimental text. All other extractive procedures were performed using non distilled solvents and all aqueous solutions used were saturated (satd).

2.2. Preparation of silver-containing POMs

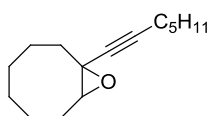
Silver substituted polyoxometalates were prepared by a controlled cationic exchange method³⁷⁶: 12-tungstosilicic acid hydrate ($\text{H}_4\text{SiW}_{12}\text{O}_{40} \cdot 25\text{H}_2\text{O}$; 5.33 g; 1.6 μmol) was dissolved in 20 mL of distilled water under vigorous stirring. The appropriate amount of an

³⁷⁶ (a) Okamoto, K.; Uchida, S.; Ito, T.; Mizuno, N. *J. Am. Chem. Soc.* **2007**, *129*, 7378–7384. (b) Tatematsu, S.; Hibi, T.; Okuhara, T.; Misono, M. *Chem. Lett.* **1984**, 865–868.

aqueous solution of AgNO_3 (0.1 mol.L^{-1}) was then added to the former solution at room temperature under vigorous stirring. The metal content, x in $\text{Ag}_x\text{H}_{4-x}\text{SiW}_{12}\text{O}_{40}$, can therefore be properly adjusted. The milky solution was then allowed to age overnight, before removing the water under vacuum. The remaining salt was dried in an oven at 393 K for 12 h.

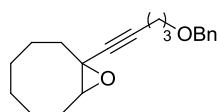
2.3. Characterization of the products

Alkynyloxiranes **1a-l** and alkynylaziridine **1m** were synthesized according to procedures reported elsewhere.³⁷⁷



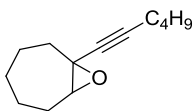
1-(hept-1-yn-1-yl)-9-oxabicyclo[6.1.0]nonane **1a**.^{377a}

Yield: 61% in 3 steps; $^1\text{H NMR}$ (CDCl_3 , 300 MHz): $\delta=3.02$ (dd, $J=10.4$, $J=4.2$, 1 H), 2.18 (t, $J=7.0$, 2 H), 2.20-2.10 (m, 2 H), 1.60-1.31 (m, 16 H), 0.89 ppm (t, $J=7.1$, 3 H).



1-(5-(benzyloxy)pent-1-yn-1-yl)-9-oxabicyclo[6.1.0]nonane **1b**.³⁷⁸

Yield: 24% in 3 steps; $^1\text{H NMR}$ (CDCl_3 , 300 MHz): $\delta=7.30$ -7.19 (m, 5 H), 4.44 (s, 2 H), 3.48 (t, $J=6.0$, 2 H), 2.94 (dd, $J=7.3$, $J=4.3$, 1 H), 2.27 (t, $J=7.0$, 2 H), 2.12-2.01 (m, 2 H), 1.74 (q, $J=6.7$, 2 H), 1.64-1.09 ppm (m, 10 H).



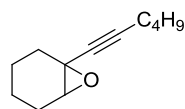
1-(hex-1-yn-1-yl)-8-oxabicyclo[5.1.0]octane **1c**.^{377a}

Yield: 27% in 3 steps; $^1\text{H NMR}$ (CDCl_3 , 300 MHz): $\delta=3.20$ (dd, $J=6.9$, $J=3.7$, 1 H), 2.17 (t, $J=6.9$, 2 H), 2.18-1.89 (m, 4 H), 1.76-1.38 (m, 10 H), 0.88 ppm (t, $J=7.2$, 3 H).

³⁷⁷ (a) Blanc, A.; Tenbrink, K.; Weibel, J.-M.; Pale, P. *J. Org. Chem.* **2009**, *74*, 4360–4363. (b) Blanc, A.; Tenbrink, K.; Weibel, J.-M.; Pale, P. *J. Org. Chem.* **2009**, *74*, 5342–5348. (c) Södergren, M. J.; Alonso, D. A.; Bedekar, A. V.; Andersson, P. G. *Tetrahedron Lett.* **1997**, *38*, 6897–6900.

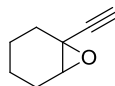
³⁷⁸ Borghèse, S.; Louis, B.; Blanc, A.; Pale, P. *Catal. Sci. Technol.* **2011**, *1*, 981–986.

Experimental Data



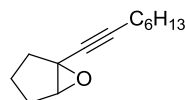
1-(hex-1-yn-1-yl)-7-oxabicyclo[4.1.0]heptane **1d**.^{377a}

Yield: 33% in 3 steps; ¹H NMR (CDCl₃, 300 MHz): δ =3.28 (t, J =2.6, 1 H), 2.19 (t, J =6.8, 2 H), 2.15-1.93 (m, 2 H), 1.89 (td, J =5.9, J =2.6, 2 H), 1.51-1.15 (m, 8 H), 0.9 ppm (t, J =7.1, 3 H).



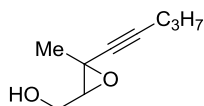
1-ethynyl-7-oxabicyclo[4.1.0]heptane **1e**.^{377a}

Yield: 60%; ¹H NMR (CDCl₃, 400 MHz): δ =3.33 (t, J =2.4, 1 H), 2.30 (s, 1 H), 2.18-2.08 (m, 1 H), 2.03-1.95 (m, 1 H), 1.92-1.85 (m, 2 H), 1.43-1.17 ppm (m, 4 H).



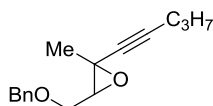
1-(oct-1-yn-1-yl)-6-oxabicyclo[3.1.0]hexane **1f**.^{377a}

Yield: 24% in 3 steps; ¹H NMR (CDCl₃, 300 MHz): δ =3.56 (m, 1 H), 2.19 (t, J =7.1, 2 H), 2.11 (dd, J =13.5, J =7.8, 1 H), 1.96 (dd, J =14.0, J =8.1, 1 H), 1.82-1.24 (m, 12 H), 0.87 ppm (t, J =6.8, 3 H).

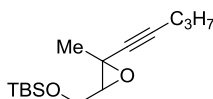


(3-methyl-3-(pent-1-yn-1-yl)oxiran-2-yl)methanol **1g**.

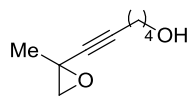
Prepared following the procedure reported by Blanc et al.^{377b} in 47% overall yield (371 mg, 2.41 mmol, 2 steps) as a colorless oil from 3-methylpent-2-en-4-yn-1-ol (981 mg, 10.2 mmol). R_f = 0.20 (cyclohexane/EtOAc 20%). IR (neat) ν_{\max} 3379, 2964, 2933, 2873, 2238, 1443, 1379, 1339, 1305, 1255, 1106, 1055, 1020, 933, 857, 735, 589, 545 cm⁻¹. ¹H NMR (300 MHz, CDCl₃): δ =3.87 (d_{ab}, J =12.4, J =4.9, 2 H), 3.07 (t, J =5.4, 1 H), 2.18 (t, J =7.1, 2 H), 1.66 (bs, 1 H), 1.53 (sext, J =7.1, 2 H), 1.55 (s, 3 H), 0.97 ppm (t, J =7.3, 3 H). ¹³C NMR (500 MHz, CDCl₃): δ =86.1, 64.1, 62.9, 52.4, 24.0, 22.2, 22.1, 20.9, 13.6 ppm. LRMS (ESI, positive mode): m/z : calcd for C₉H₁₄NaO₂ 177.09, found 177.09.


3-((benzyloxy)methyl)-2-methyl-2-(pent-1-yn-1-yl)oxirane 1h.^{377b}

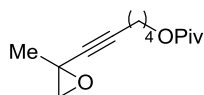
Yield: 40% in 3 steps; ¹H NMR (CDCl₃, 300 MHz): δ= 7.38-7.27 (m, 5 H), 4.60 (ab, *J*=11.8, 2 H), 3.75 (d_{ab}, *J*=11.2, *J*=4.8, 2 H), 3.09 (t, *J*=5.2, 1 H), 2.16 (t, *J*=7.0, 2 H), 1.53 (s, 3 H), 1.50 (sext, *J*=7.2, 2 H), 0.96 ppm (t, *J*=7.3, 3 H).


tert-butyldimethyl((3-methyl-3-(pent-1-yn-1-yl)oxiran-2-yl)methoxy)silane 1i.

Prepared following the procedure reported by Blanc et al.^{377b} in 35% overall yield (315 mg, 1.17 mmol, 3 steps) as a colorless oil from 3-methylpent-2-en-4-yn-1-ol (981 mg, 10.2 mmol). *R*_f = 0.74 (cyclohexane/EtOAc 20%). IR (neat) *v*_{max} 2958, 2930, 2857, 1463, 1253, 1134, 1084, 1006, 939, 835, 776, 735, 666 cm⁻¹. ¹H NMR (300 MHz, CDCl₃): δ=3.84 (d_{ab}, *J*=11.6, *J*=5.3, 2 H), 2.99 (t, *J*=5.1, 1 H), 2.18 (t, *J*=7.1, 2 H), 1.54 (s, 3 H), 1.53 (sext, *J*=7.1, 2 H), 0.98 (t, *J*=7.3, 3 H), 0.91 (s, 9 H), 0.10 ppm (s, 6 H). ¹³C NMR (500 MHz, CDCl₃): δ=85.7, 77.7, 64.7, 63.4, 52.5, 26.1 (3xCH₃), 23.9, 22.1, 20.9, 18.6, 13.6, -4.9, -5.0 ppm. LRMS (ESI, positive mode): *m/z*: calcd for C₁₅H₂₈NaO₂Si 291.18, found 291.17.

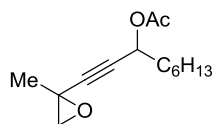

6-(2-methyloxiran-2-yl)hex-5-yn-1-ol 1j.^{377a}

Yield: 57% in 2 steps; ¹H NMR (CDCl₃, 300 MHz): δ=3.67 (t, *J*=6.0, 2 H), 2.96 (d, *J*=5.7, 1 H), 2.72 (d, *J*=5.7, 1 H), 2.24 (t, *J*=7.0, 2 H), 1.72-1.55 (m, 6 H), 1.53 ppm (s, 3 H).


6-(2-methyloxiran-2-yl)hex-5-yn-1-yl pivalate 1k.^{377a}

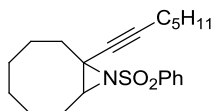
Yield: 50% in 2 steps; ¹H NMR (CDCl₃, 300 MHz): δ=4.07 (t, *J*=6.4, 2 H), 2.96 (d, *J*=5.5, 1 H), 2.72 (d, *J*=5.5, 1 H), 2.23 (t, *J*=7.0, 2 H), 1.77-1.68 (m, 2 H), 1.62-1.54 (m, 2 H), 1.53 (s, 3 H), 1.20 ppm (s, 9 H).

Experimental Data



1-(2-methyloxiran-2-yl)non-1-yn-3-yl acetate **11**.^{377a}

Yield: 57% in 2 steps; ¹H NMR (CDCl₃, 300 MHz): δ=5.36 (t, *J*=6.7, 1 H), 3.00 (d, *J*=5.5, 1 H), 2.74 (d, *J*=5.5, 1 H), 2.07 (s, 3 H), 1.77-1.70 (m, 2 H), 1.55 (s, 3 H), 1.45-1.28 (m, 8 H), 0.89 ppm (t, *J*=6.9, 3 H).

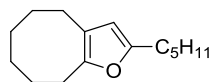


1-(hept-1-yn-1-yl)-9-(phenylsulfonyl)-9-azabicyclo[6.1.0]nonane **1m**.³⁷⁸

Yield: 24% in 3 steps; ¹H NMR (300 MHz, CDCl₃): δ=7.60-7.51 (m, 3 H), 7.45 (t, *J*=7.8, 2 H), 5.81 (s, 1 H), 2.90 (t, *J*=6.1, 2 H), 2.75 (t, *J*=7.6, 2 H), 2.40 (t, *J*=5.9, 2 H), 1.65-1.51 (m, 6 H), 1.44-1.22 (m, 8 H), 0.88 ppm (t, *J*=6.9, 3 H).

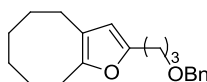
General procedure 1 for the synthesis of furans from alkynyloxiranes

A mixture of alkynyloxirane (0.45 mmol), naphthalene (0.05 mmol, internal standard) and Ag_xH_{4-x}SiW₁₂O₄₀ (*x* = 0, 1, 2, 3, 4; 5 mol%/Ag) in dichloromethane (4 mL) and methanol (0.45 mL) was stirred at room temperature for an appropriate time. Samples (0.2 mL) were taken to assess the amount of furan and the kinetic of the reaction. After completion of the reaction, the solvent was removed in vacuo. The resulting product was separated from the catalyst by washing with *n*-pentane. The product thus obtained was charged on a small silica gel column and eluted with *n*-pentane to afford pure furan. The recovered catalyst was finally dried in an oven for 10 min at 120 °C prior to reuse. The amount of catalyst was calculated to have 5 mol % of silver in each test. The kinetic of the reaction was followed by NMR and yields were assessed relative to the internal standard (naphthalene).



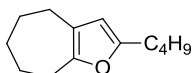
2-pentyl-4,5,6,7,8,9-hexahydrocycloocta[*b*]furan **2a**.^{377a}

¹H NMR (300 MHz, CDCl₃): δ=5.70 (s, 1 H), 2.71 (m, 2 H), 2.55-2.46 (m, 4 H), 1.71-1.45 (m, 10 H), 1.34-1.30 (m, 4 H), 0.90 ppm (t, *J*=6.2, 3 H).



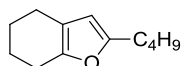
2-(3-(benzyloxy)propyl)-4,5,6,7,8,9-hexahydrocycloocta[*b*]furan 2b.³⁷⁸

¹H NMR (300 MHz, CDCl₃): δ=7.28-7.18 (m, 5 H), 5.63 (s, 1 H), 4.43 (s, 2 H), 3.43 (t, *J*=6.4, 2 H), 2.60 (m, 4 H), 2.40 (t, *J*=6.1, 2 H), 1.85 (q, *J*=6.4, 2 H), 1.67-1.35 ppm (m, 8 H).



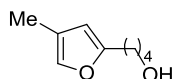
2-butyl-5,6,7,8-tetrahydro-4*H*-cyclohepta[*b*]furan 2c.^{377a}

¹H NMR (300 MHz, CDCl₃): δ=5.73 (s, 1 H), 2.71 (m, 2 H), 2.52 (t, *J*=7.6, 2 H), 2.42 (m, 2 H), 1.77-1.54 (m, 8 H), 1.40 (sext, *J*=7.4, 2 H), 0.93 ppm (t, *J*=7.3, 3 H).



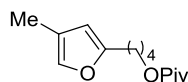
2-butyl-4,5,6,7-tetrahydrobenzofuran 2d.^{377a}

¹H NMR (300 MHz, CDCl₃): δ=5.79 (s, 1 H), 2.60-2.54 (m, 4 H), 2.40-2.37 (m, 2 H), 1.85-1.78 (m, 2 H), 1.75-1.66 (m, 2 H), 1.58 (qt, *J*=5.7, 2 H), 1.39 (sext, *J*=7.4, 2 H), 0.94 ppm (t, *J*=7.3, 3 H).



4-(4-methylfuran-2-yl)butan-1-ol 2j.³⁷⁹

¹H NMR (500 MHz, CDCl₃): δ=7.05 (s, 1 H), 5.86 (s, 1 H), 3.66 (t, *J*=6.4, 2 H), 2.60 (m, *J*=7.3, 2 H), 1.97 (s, 3 H), 1.69 (m, 2 H), 1.61 (m, 2 H), 1.36 ppm (br s, 1 H, OH).

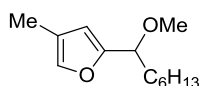


4-(4-methylfuran-2-yl)butyl pivalate 2k.^{377a}

¹H NMR (300 MHz, CDCl₃): δ=7.05 (s, 1 H), 5.85 (s, 1 H), 4.06 (t, *J*=6.1, 2 H), 2.60 (t, *J*=6.7, 2 H), 1.98 (s, 3 H), 1.70-1.66 (m, 4 H), 1.19 ppm (s, 9 H).

³⁷⁹ Hashmi, A. S. K.; Sinha, P. *Adv. Synth. Catal.* **2004**, *346*, 432-438.

Experimental Data

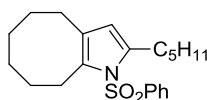


2-(1-methoxyheptyl)-4-methylfuran 2l.^{377a}

¹H NMR (300 MHz, C₆D₆): δ =6.96 (s, 1 H), 5.99 (s, 1 H), 4.07 (t, J =6.8, 2 H), 3.06 (s, 3 H), 2.06-1.82 (m, 2 H), 1.79 (s, 3 H), 1.50-1.20 (m, 8 H), 0.84 ppm (t, J =6.8, 3 H).

General procedure 2 for the synthesis of pyrrole from alkynylaziridine

A mixture of alkynylaziridine (0.45 mmol), naphthalene (0.05 mmol, internal standard) and Ag₂H₂SiW₁₂O₄₀ (10 mol%/Ag) in dichloromethane (4 mL) and methanol (0.45 mL) was stirred at room temperature for an appropriate time. Samples (0.2 mL) were taken to assess the amount of pyrrole. The kinetic of the reaction was followed by NMR and yield was assessed relative to the internal standard (naphthalene).



2-pentyl-1-(phenylsulfonyl)-4,5,6,7,8,9-hexahydro-1H-cycloocta[b]pyrrole 2m.³⁷⁸

¹H NMR (300 MHz, CDCl₃): δ =7.60-7.51 (m, 3 H), 7.45 (t, J =7.8, 2 H), 5.81 (s, 1 H), 2.90 (t, J =6.1, 2 H), 2.75 (t, J =7.6, 2 H), 2.40 (t, J =5.9, 2 H), 1.65-1.51 (m, 6 H), 1.44-1.22 (m, 8 H), 0.88 ppm (t, J =6.9, 3 H).

3. *Synthesis of ketals and spiroketals under Ag-zeolite catalysis*

3.1. General information

Proton (^1H NMR) and Carbon (^{13}C NMR) nuclear magnetic resonance spectra were recorded on Bruker Avance Spectrometers at 75, 300, 400 or 500 MHz. Chemical shifts are given in part per million (ppm) on the delta scale. The solvent peak was used as reference value. For ^1H NMR: $\text{CDCl}_3 = 7.26$ ppm or $\text{C}_6\text{D}_6 = 7.16$ ppm. For ^{13}C NMR: $\text{CDCl}_3 = 77.0$ ppm or $\text{C}_6\text{D}_6 = 128.0$ ppm. Data are presented as follows: chemical shift, multiplicity (s = singlet, d = doublet, t = triplet, q = quartet, qt = quintet, sext = sextuplet, m = multiplet), coupling constants (J/Hz) and integration. X-ray diffraction patterns (XRD) were recorded on a Bruker D8 Advance diffractometer, with a Ni detector side filtered Cu $K\alpha$ radiation (1.5406 \AA) over a 2θ range of $5\text{-}60^\circ$ and a position sensitive detector using a step size of 0.02° and a step time of 2 s. Infrared spectra were recorded neat on an ALPHA Bruker FT-IR apparatus. Wavelengths of maximum absorbance (ν_{max}) are quoted in wave numbers (cm^{-1}). SEM images were acquired with a Hitachi S4800 FEG microscope equipped with an EDS system (EDX) for elemental analysis. EDX spectra were acquired using 20 kV primary electron voltage to determine the composition of the material. XPS spectra were obtained using a Multilab 2000 XPS machine (Thermo). The pressure inside the chamber is 5.10^{-9} mbar during the analysis and the incident beam is Al $K\alpha$ radiation ($h\nu = 1486.6 \text{ eV}$). The spectra have been calibrated relative to the C $1s_{1/2}$ binding energy of contamination carbon, which was fixed at 285 eV. Mass spectra were recorded by ElectroSpray Ionization (ESI) or Electronic Impact (EI). Analytical Thin Layer Chromatography (TLC) were carried out on silica gel 60 F₂₅₄ plates with visualization by ultra violet, KMnO_4 , *p*-anisaldehyde or molybdophosphoric acid/ $\text{Ce}(\text{SO}_4)_2 \cdot 4\text{H}_2\text{O}$. Flash column chromatographies were carried out using silica gel 60 (40-63 μm) and the procedure includes the subsequent evaporation of solvents *in vacuo*. Reagents and solvents were purified using standard means. All other chemicals were used as received except where otherwise noted in the experimental text. All other extractive procedures were performed using non distilled solvents and all aqueous solutions used were saturated (satd).

3.2. Ag-zeolites preparation

Procedure by ionic exchange

Ag^I-USY was prepared using standard ion-exchange method.³⁸⁰ Commercial NH₄USY (CBV500 Zeolyst international, Si/Al=2.8, 2.0 g) was exchanged by contacting the material with a 0.1 M aqueous AgNO₃ solution (50 mL). The resulting white suspension was vigorously stirred overnight at 80 °C in the dark. After the first ion-exchange, the solution was cooled, filtered through nylon membrane (0.2 μm), washed with copious amounts of water and dried in an oven for 24 h at 110 °C. The resulting white solid was then submitted to a second ion-exchange by following the same procedure described above. After drying for 24 h at 110 °C, the resulting white powder was finally dehydrated at 550 °C overnight.

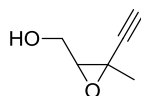
Procedure by solid exchange

HUSY zeolite (CBV500 Zeolyst international, Si/Al=2.8) was obtained after calcination of its NH₄-form during 15 h at 823 K. Ag⁺-exchanged USY zeolite was prepared by mixing 1g of dry HUSY with an appropriate mass of silver nitrate (Acros Organics, >99% purity, melting point 485 K) to obtain a physical mixture containing loadings of Ag at 20 mol%. The mixture was ground with a mortar and pestle rapidly in order to achieve an intimate mixture of the two solids. The ground HUSY/AgX mixture was then loaded into a tubular reactor. The reactor was sealed and connected to a flow manifold. The intimate mixture of the solids was heated to 723 K at 10 K.min⁻¹ under N₂ flow (40 mL/min). The exchange temperature was held isothermal and the duration was set to 72 h.

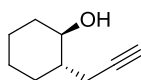
3.3. Characterization of the products

Alkynols **3c-d** and alkyne diols **5a-h** were synthesized according to procedures reported elsewhere.³⁸¹⁻³⁸⁴

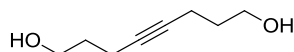
³⁸⁰ N. D. Hutson, B. A. Reisner, R. T. Yang, B. H. Toby, *Chem. Mater.* **2000**, *12*, 3020–3031.

**(3-ethynyl-3-methyloxiran-2-yl)methanol 3c.**³⁸¹

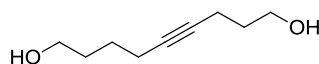
¹H NMR (300 MHz, CDCl₃): δ =3.92 (dd, J =12.2, 5.0, 1 H), 3.84 (dd, J =12.4, 5.9, 1 H), 3.09 (t, J =5.3, 1 H), 2.38 (s, 1 H), 1.63 (br s, 1 H, OH), 1.57 ppm (s, 3 H).

**(1R,2S)-2-(prop-2-yn-1-yl)cyclohexanol 3d.**³⁸¹

¹H NMR (300 MHz, CDCl₃): δ =3.36 (td, J =10.0, 4.6, 1 H), 2.43 (ddd, J =17.0, 4.4, 2.8, 1 H), 2.29 (ddd, J =17.0, 6.8, 2.8, 1 H), 1.97 (t, J =2.8, 1 H), 1.87-1.81 (m, 1 H), 1.77-1.69 (m, 1 H), 1.67-1.62 (m, 2 H), 1.48-1.36 (m, 1 H), 1.30-1.12 ppm (m, 4 H).

**Oct-4-yne-1,8-diol 5a.**³⁸²

Yield: 26% in 3 steps; ¹H NMR (CDCl₃, 300 MHz): δ =3.76-3.70 (m, 4 H), 2.26 (t, J =6.9, 4 H), 1.76-1.67 (m, 4 H), 1.57 ppm (br s, 2 H, 2 OH).

**Non-4-yne-1,9-diol 5b.**³⁸³

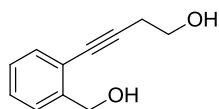
Yield: 32% in 4 steps; ¹H NMR (CDCl₃, 400 MHz): δ =3.77 (t, J =6.2, 2 H), 3.68 (t, J =6.2, 2 H), 2.33-2.25 (m, 2 H), 2.24-2.16 (m, 2 H), 2.06-1.96 (br s, 2 H, 2 OH), 1.80-1.63 (m, 4 H), 1.62-1.52 ppm (m, 2 H).

³⁸¹ Pale, P.; Chuche, J. *Eur. J. Org. Chem.* **2000**, 1019–1025.

³⁸² T. von Hirschheydt, V. Wolfart, R. Gleiter, H. Irgangtinger, T. Oeser, F. Rominger, F. Eisenträger, *J. Chem. Soc., Perkin Trans. 2* **2000**, 175–183.

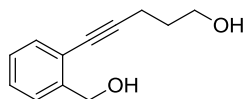
³⁸³ K. Ravindar, M. S. Reddy, P. Deslongchamps, *Org. Lett.* **2011**, 13, 3178–3181.

Experimental Data



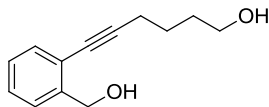
4-(2-(hydroxymethyl)phenyl)but-3-yn-1-ol **5c**.³⁸⁴

Yield: 73%; ¹H NMR (CDCl₃, 300 MHz): δ =7.42-7.25 (m, 4 H), 4.77 (s, 2 H), 3.83 (t, J =5.8, 2 H), 2.70 ppm (t, J =6.2, 2 H).



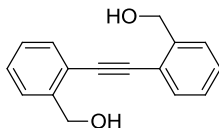
5-(2-(hydroxymethyl)phenyl)pent-4-yn-1-ol **5d**.³⁸⁴

Yield: 90%; ¹H NMR (CDCl₃, 300 MHz): δ =7.37-7.34 (m, 2 H), 7.24-7.17 (m, 2 H), 4.78 (s, 2 H), 3.73 (t, J =6.4, 2 H), 3.18 (br s, 2 H, 2 OH), 2.51 (t, J =6.8, 2 H), 1.79 ppm (m, 2 H).



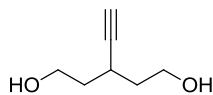
6-(2-(hydroxymethyl)phenyl)hex-5-yn-1-ol **5e**.³⁸³

Yield: 61%; ¹H NMR (CDCl₃, 300 MHz): δ =7.40-7.17 (m, 4 H), 4.76 (s, 2 H), 3.71-3.66 (m, 2 H), 2.48 (t, J =6.5, 2 H), 1.93 (br s, 2 H, 2 OH), 1.76-1.67 ppm (m, 4 H).



(Ethyne-1,2-diylbis(2,1-phenylene))dimethanol **5f**.³⁸⁴

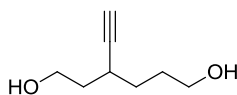
Yield: 32% in 3 steps; ¹H NMR (CDCl₃, 300 MHz): δ =7.59-7.27 (m, 8 H), 4.87 (s, 4 H), 1.28 ppm (br s, 2 H, 2 OH).



3-ethynylpentane-1,5-diol **5g**.³⁸⁴

Yield: 18% in 2 steps; ¹H NMR (CDCl₃, 300 MHz): δ =3.82 (t, J =6.4, 4 H), 2.74 (m, 1 H), 2.12 (d, J =2.6, 1 H), 1.83-1.64 ppm (m, 4 H).

³⁸⁴ Messerle, B. A.; Vuong, K. Q. *Organometallics* **2007**, *26*, 3031–3040.

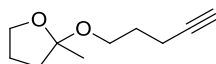


3-ethynylhexane-1,6-diol 5h.³⁸⁴

Yield: 13% in 2 steps; ¹H NMR (CDCl₃, 300 MHz): δ =3.83 (t, J =6.0, 2 H), 3.69 (t, J =6.2, 2 H), 2.59 (m, 1 H), 2.11 (d, J =2.4, 1 H), 1.89-1.50 ppm (m, 6 H).

General Procedure 3 for the Silver(I)-Zeolite Catalyzed Synthesis of Ketals

To an alkynol or alkyne diol (1 mmol) neat or in MeOH (2 mL) was added Ag-USY (0.02 mmol; 0.02 equiv.) at room temperature. The resulting suspension was stirred at room temperature or 95 °C in a sealed tube. After reaction completion (monitored by thin-layer chromatography), the reaction mixture was diluted with CH₂Cl₂ and filtered through a Nylon membrane (0.2 μ m). The solvent was removed in *vacuum*, and the crude residue was purified by flash chromatography (*n*-pentane/Et₂O: 8/2).



2-methyl-2-(pent-4-yn-1-yloxy)tetrahydrofuran 4a.

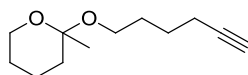
Prepared from the *general procedure 3* in 85% (170 mg, 1.01 mmol) as a colorless oil from pent-4-yn-1-ol (200 mg, 2.38 mmol). R_f = 0.81 (cyclohexane/EtOAc 40 %). IR (neat) ν_{\max} 3294, 2986, 2941, 2878, 1443, 1377, 1322, 1241, 1199, 1159, 1118, 1092, 1064, 1019, 904, 851, 628 cm⁻¹. ¹H NMR (300 MHz, C₆D₆): δ =3.73-3.68 (m, 2 H), 3.58-3.51 (m, 1 H), 3.40-3.33 (m, 1 H), 2.13 (td, J =7.0, 2.6, 2 H), 1.94-1.74 (m, 2 H), 1.81 (t, J =2.7, 1 H), 1.67-1.58 (m, 2 H), 1.55-1.41 (m, 2 H), 1.34 ppm (s, 3 H). ¹³C NMR (75 MHz, C₆D₆): δ =107.7, 84.5, 69.3, 67.8, 59.4, 38.9, 30.0, 25.2, 22.4, 16.0 ppm. LRMS (ESI, positive mode): m/z : calcd for C₁₀H₁₆NaO₂ 191.105, found 191.104.

Experimental Data



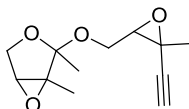
2-methoxy-2-methyltetrahydrofuran **4a'**.³⁸⁵

¹H NMR (300 MHz, CDCl₃): δ =3.77 (m, 2 H), 3.11 (s, 3 H), 1.99-1.58 (m, 4 H), 1.33 ppm (s, 3 H).



2-(hex-5-yn-1-yloxy)-2-methyltetrahydro-2H-pyran **4b**.

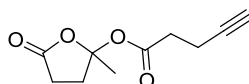
Prepared from the *general procedure 3* in 68% (136 mg, 0.69 mmol) as a colorless oil from hex-5-yn-1-ol (200 mg, 2.04 mmol). *R_f* = 0.67 (cyclohexane/EtOAc 20 %). IR (neat) ν_{\max} 3307, 2940, 2870, 1451, 1374, 1269, 1227, 1176, 1088, 1062, 1034, 967, 865, 810, 626 cm⁻¹. ¹H NMR (300 MHz, C₆D₆): δ =3.60-3.46 (m, 2 H), 3.42-3.35 (m, 1 H), 3.31-3.24 (m, 1 H), 2.01 (td, *J*=7.1, 2.8, 2 H), 1.94-1.76 (m, 1 H), 1.81 (t, *J*=2.7, 1 H), 1.72-1.67 (m, 1 H), 1.63-1.45 (m, 4 H), 1.44-1.17 (m, 4 H), 1.23 ppm (s, 3 H). ¹³C NMR (75 MHz, C₆D₆): δ =97.6, 84.7, 63.4, 61.6, 59.7, 36.7, 29.9, 26.4, 25.9, 25.3, 19.7, 19.0 ppm. LRMS (ESI, positive mode): *m/z*: calcd for C₁₂H₂₀NaO₂ 219.136, found 219.136.



2-((3-ethynyl-3-methyloxiran-2-yl)methoxy)-1,2-dimethyl-3,6-dioxabicyclo[3.1.0]hexane **4c**.³⁸¹

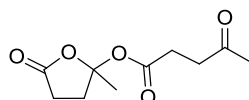
Prepared from the *general procedure 3* in 8% yield. ¹H NMR (300 MHz, C₆D₆): δ =3.90 (dd, *J*=11.2, 4.8, 0.5 H), 3.84 (dd, *J*=10.9, 6.1, 0.5 H), 3.78-3.71 (m, 1 H), 3.63 (t, *J*=10.3, 1 H), 3.42 (dd, *J*=10.1, 4.4, 1H), 2.94 (d, *J*=11.6, 1 H), 2.87-2.83 (m, 1 H), 1.83 (d, *J*=4.1, 1 H), 1.40-1.38 (m, 6 H), 1.27 ppm (s, 3 H).

³⁸⁵ Glatthar, R.; Spichty, M.; Gugger, A.; Batra, R.; Damm, W.; Mohr, M.; Zipse, H.; Giese, B. *Tetrahedron* **2000**, *56*, 4117–4128.



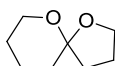
2-methyl-5-oxotetrahydrofuran-2-yl pent-4-ynoate 4e.

Prepared from the *general procedure 3* in 23% (69 mg, 0.35 mmol) as a colorless oil from pent-4-ynoic acid (300 mg, 3.06 mmol). $R_f = 0.76$ (EtOAc/cyclohexane 30 %). IR (neat) ν_{\max} 3286, 2922, 2850, 1787, 1739, 1416, 1385, 1266, 1161, 1117, 1078, 992, 936, 900, 797, 652, 522, 489, 402 cm^{-1} . ^1H NMR (300 MHz, C_6D_6): $\delta = 2.58\text{--}2.46$ (m, 1 H), 2.20–1.94 (m, 6 H), 1.75 (t, $J = 2.4$, 1 H), 1.56–1.48 (m, 1 H), 1.40 ppm (s, 3 H). ^{13}C NMR (75 MHz, C_6D_6): $\delta = 175.1$, 170.2, 109.0, 82.7, 70.0, 34.1, 33.0, 28.9, 26.2, 14.6 ppm. LRMS (ESI, positive mode): m/z : calcd for $\text{C}_{10}\text{H}_{12}\text{NaO}_4$ 219.061, found 219.063.



2-methyl-5-oxotetrahydrofuran-2-yl 4-oxopentanoate 4e'.

Prepared from the *general procedure 3* in 34% (112 mg, 0.52 mmol) as a colorless oil from pent-4-ynoic acid (300 mg, 3.06 mmol). $R_f = 0.48$ (EtOAc/cyclohexane 30 %). IR (neat) ν_{\max} 2933, 1788, 1741, 1714, 1413, 1362, 1267, 1155, 1117, 1078, 956, 928, 656, 524, 428 cm^{-1} . ^1H NMR (300 MHz, C_6D_6): $\delta = 2.64\text{--}2.52$ (m, 1 H), 2.32–1.99 (m, 6 H), 1.68 (s, 3 H), 1.67–1.56 (m, 1 H), 1.45 ppm (s, 3 H). ^{13}C NMR (75 MHz, C_6D_6): $\delta = 205.9$, 175.5, 171.6, 109.0, 37.7, 32.9, 29.5, 29.0, 29.0, 26.4 ppm. LRMS (ESI, positive mode): m/z : calcd for $\text{C}_{10}\text{H}_{14}\text{NaO}_5$ 237.074, found 237.073.

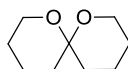


1,6-dioxaspiro[4.5]decane 6a.³⁸⁶

Prepared following the *general procedure 3* in 83% yield. ^1H NMR (C_6D_6 , 300 MHz): $\delta = 3.97\text{--}3.82$ (m, 2 H), 3.78–3.71 (m, 1 H), 3.61–3.54 (m, 1 H), 2.04–1.80 (m, 3 H), 1.66–1.61 (m, 2 H), 1.56–1.38 (m, 4 H), 1.28–1.20 ppm (m, 1 H).

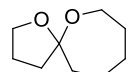
³⁸⁶ Ley, S. V.; Lygo, B.; Sternfeld, F.; Wonnacott, A. *Tetrahedron* **1986**, *42*, 4333–4342.

Experimental Data



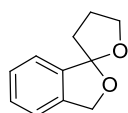
1,7-dioxaspiro[5.5]undecane 6b.³⁸³

Prepared following the *general procedure 3* in 36% yield. ¹H NMR (C₆D₆, 500 MHz): δ =3.69-3.64 (m, 2 H), 3.54 (ddt, J =10.9, 4.7, 1.6, 2 H), 1.49-1.42 (m, 2 H), 1.41-1.35 (m, 3 H), 1.33-1.16 ppm (m, 7 H).



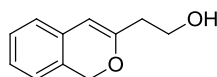
1,6-dioxaspiro[4.6]undecane 6b'.³⁸³

Prepared following the *general procedure 3* in 50% yield. ¹H NMR (C₆D₆, 500 MHz): δ =3.87-3.73 (m, 3 H), 3.57 (dtd, J =12.8, 3.5, 1.4, 1 H), 2.08-2.00 (m, 2 H), 1.91-1.81 (m, 2 H), 1.67-1.15 ppm (m, 8 H).



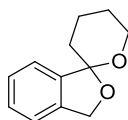
4,5-dihydro-3H,3'H-spiro[furan-2,1'-isobenzofuran] 6c.³⁸⁴

Prepared following the *general procedure 3* in 29% yield. ¹H NMR (CDCl₃, 300 MHz): δ =7.41-7.29 (m, 3 H), 7.23-7.20 (m, 1 H), 5.14 (d, J =12.6, 1 H), 4.93 (d, J =12.8, 1 H), 4.17-3.99 (m, 2 H), 2.35-2.03 ppm (m, 4 H).



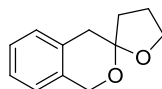
2-(1H-isochromen-3-yl)ethanol 6c'.³⁸⁴

Prepared following the *general procedure 3* in 41% yield. ¹H NMR (CDCl₃, 300 MHz): δ =7.19-6.91 (m, 4 H), 5.73 (s, 1 H), 5.07 (s, 2 H), 3.82 (t, J =6.1, 2 H), 2.47 ppm (t, J =6.1, 2 H).



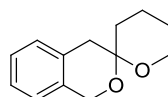
3',4',5',6'-tetrahydro-3H-spiro[isobenzofuran-1,2'-pyran] 6d.³⁸⁴

Prepared following the *general procedure 3* in 9% yield. ¹H NMR (CDCl₃, 300 MHz): δ =7.32-6.97 (m, 4 H), 5.15 (d, J =12.6, 1 H), 4.98 (d, J =12.8, 1 H), 4.10-4.04 (m, 1 H), 3.81-3.74 (m, 1 H), 2.22-1.78 ppm (m, 6 H).



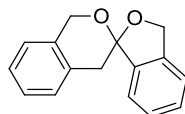
4,5-dihydro-3H-spiro[furan-2,3'-isochroman] 6d'.³⁸⁴

Prepared following the *general procedure 3* in 76% yield. ¹H NMR (CDCl₃, 300 MHz): δ =7.32-6.97 (m, 4 H), 4.90 (d, J =14.9, 1 H), 4.66 (d, J =14.9, 1 H), 3.98 (t, J =6.6, 2 H), 3.21 (d, J =16.3, 1 H), 2.80 (d, J =16.4, 1 H), 2.22-1.78 ppm (m, 4 H).



3',4',5',6'-tetrahydrospiro[isochroman-3,2'-pyran] 6e.³⁸⁷

Prepared following the *general procedure 3* in 88% yield. ¹H NMR (CDCl₃, 300 MHz): δ =7.16-7.10 (m, 2 H), 7.07-6.96 (m, 2 H), 4.79 (d, J =14.8, 1 H), 4.67 (d, J =14.8, 1 H), 3.76 (td, J =11.0, J =3.5, 1 H), 3.68-3.62 (m, 1 H), 2.87 (d, J =16.5, 1 H), 2.73 (d, J =16.5, 1 H), 2.01-1.56 ppm (m, 6 H).



3H-spiro[isobenzofuran-1,3'-isochroman] 6f.³⁸⁸

Prepared following the *general procedure 3* in 81% yield. ¹H NMR (C₆D₆, 300 MHz): δ =7.09-6.77 (m, 8 H), 5.19 (d, J =14.9, 1 H), 5.00 (d, J =12.6, 1 H), 4.77 (d, J =5.7, 1 H), 4.73 (d, J =3.6, 1 H), 3.42 (d, J =16.4, 1 H), 2.96 ppm (d, J =16.3, 1 H).

³⁸⁷ Ho, J. H. H.; Hodgson, R.; Wagler, J.; Messerle, B. A. *Dalton Trans.* **2010**, 39, 4062–4069.

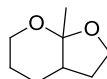
³⁸⁸ Padwa, A.; Krumpe, K. E.; Weingarten, M. D. *J. Org. Chem.* **1995**, 60, 5595–5603.

Experimental Data



6a-methylhexahydrofuro[2,3-*b*]furan 6g.³⁸⁴

Prepared following the *general procedure 3* in 81% yield. ¹H NMR (CDCl₃, 300 MHz): δ =3.92 (td, J =8.8, J =6.2, 2 H), 3.86 (td, J =8.8, J =3.8, 2 H), 2.49 (tt, J =8.8, J =3.4, 1 H), 2.21-2.11 (m, 2 H), 1.75-1.67 (m, 2 H), 1.48 ppm (s, 3 H).



7a-methylhexahydro-2H-furo[2,3-*b*]pyran 6h.³⁸⁴

Prepared following the *general procedure 3* in 65% yield. ¹H NMR (C₆D₆, 300 MHz): δ =4.04-3.96 (m, 1 H), 3.74-3.67 (m, 2 H), 3.37-3.30 (m, 1 H), 1.67-1.50 (m, 3 H), 1.43-1.29 (m, 4 H), 1.39 ppm (s, 3 H).

4. *Toward the total synthesis of Acortatarin A*

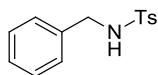
4.1. General Information

Proton (^1H NMR) and Carbon (^{13}C NMR) nuclear magnetic resonance spectra were recorded on Bruker Avance Spectrometers at 75, 300, 400 or 500 MHz. Chemical shifts are given in part per million (ppm) on the delta scale. The solvent peak was used as reference value. For ^1H NMR: $\text{CDCl}_3 = 7.26$ ppm or $\text{C}_6\text{D}_6 = 7.16$ ppm. For ^{13}C NMR: $\text{CDCl}_3 = 77.0$ ppm or $\text{C}_6\text{D}_6 = 128.0$ ppm. Data are presented as follows: chemical shift, multiplicity (s = singlet, d = doublet, t = triplet, q = quartet, qt = quintet, sext = sextuplet, m = multiplet), coupling constants (J/Hz) and integration. Infrared spectra were recorded neat on an ALPHA Bruker FT-IR apparatus. Wavelengths of maximum absorbance (ν_{max}) are quoted in wave numbers (cm^{-1}). Melting points were measured in open capillary tubes with a Stuart Scientific Melting Point Apparatus SMP3 and are uncorrected. Mass spectra were recorded by ElectroSpray Ionization (ESI) or Electronic Impact (EI). Analytical Thin Layer Chromatography (TLC) were carried out on silica gel 60 F₂₅₄ plates with visualization by ultra violet, KMnO_4 , *p*-anisaldehyde or molybdophosphoric acid/ $\text{Ce}(\text{SO}_4)_2 \cdot 4\text{H}_2\text{O}$. Flash column chromatographies were carried out using silica gel 60 (40-63 μm) and the procedure includes the subsequent evaporation of solvents *in vacuo*. Reagents and solvents were purified using standard means. All other chemicals were used as received except where otherwise noted in the experimental text. All other extractive procedures were performed using non distilled solvents and all aqueous solutions used were saturated (satd).

4.2. Cu-USY preparation

Commercial NH_4 -USY was placed in an oven and heated at 550 °C for 4 h to give H-USY. Subsequently, H-USY (1 g) and CuCl (475 mg, 1.1 equiv.) were mixed by using a mortar and charged in a closed reactor. The mixture of powders was heated at 350 °C for 3 days under a nitrogen flow, quantitatively yielding Cu^{I} -USY.

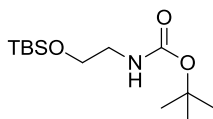
4.3. Characterization of the products



***N*-benzyl-4-methylbenzenesulfonamide 7a.**

To a mixture of benzylamine (2.6 mL, 23 mmol) and triethylamine (4.8 mL, 35 mmol) in CH₂Cl₂ (35 mL) was added *p*-toluenesulfonyl chloride (4.4 g, 23 mmol) in small portions at 0 °C. The reaction mixture was stirred for 1 h at room temperature. Distilled H₂O (50 mL) was added and the solution was extracted with CH₂Cl₂ (3 x 25 mL). The organic layers were combined, dried on Na₂SO₄ and evaporated under reduced pressure. The crude solid (6 g) was recrystallized from EtOH to give sulfonamide **1** (5.161 g, 19.75 mmol, 86% yield) as a colorless solid.

¹H-NMR (300 MHz, CDCl₃): δ=7.77 (d, *J*=8.1, 2 H), 7.33-7.25 (m, 5 H), 7.21-7.18 (m, 2 H), 4.60 (br s, 1 H, NH), 4.12 (d, *J*=6.2, 2 H), 2.44 ppm (s, 3 H). For complete characterization see the reference below.³⁸⁹



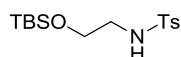
***tert*-butyl (2-((*tert*-butyldimethylsilyl)oxy)ethyl)carbamate 7b.**

To a solution of 2-aminoethanol (2.0 g, 33 mmol) in dry CH₂Cl₂ (73 mL) was added triethylamine (6.8 mL, 50 mmol) at room temperature. After 30 min the solution was cooled to 0 °C. Then a solution of di-*tert*-butyl dicarbonate (7.1 g, 33 mmol) in dry CH₂Cl₂ (19 mL) was added slowly. The mixture was stirred at room temperature overnight, quenched with NH₄Cl and extracted with CH₂Cl₂ (3 x 35 mL). The organic layers were combined, washed with brine, dried on Na₂SO₄ and evaporated under reduced pressure. The crude product was purified by flash chromatography on silica gel (EtOAc/cyclohexane: 6/4) to give *tert*-butyl (2-hydroxyethyl)carbamate (5.1 g, 32 mmol, 97% yield) as a colorless oil.

To a solution of *tert*-butyl (2-hydroxyethyl)carbamate (5.1 g, 32 mmol) in dry CH₂Cl₂ (72 mL) were added *tert*-butyldimethylsilyl chloride (5.2 g, 35 mmol), imidazole (3.2 g, 47 mmol) and 4-dimethylaminopyridine (0.58 g, 4.7 mmol). The mixture was stirred at room temperature overnight, quenched with distilled water and extracted with CH₂Cl₂. The organic layers were combined, washed with water, NH₄Cl, brine, dried on Na₂SO₄ and evaporated

under reduced pressure. The crude product was purified by flash chromatography on silica gel (EtOAc/cyclohexane: 1/9 - 2/8) to give *tert*-butyl (2-((*tert*-butyldimethylsilyl)oxy)ethyl)carbamate (8.0 g, 29 mmol, 92% yield) as a colorless oil.

¹H-NMR (300 MHz, CDCl₃): δ=4.83 (br s, 1 H, NH), 3.66 (t, *J*=5.2, 2 H), 3.22 (q, *J*=3.5, 2 H), 1.45 (s, 9 H), 0.90 (s, 9 H), 0.06 ppm (s, 6 H). For complete characterization see the reference below.³⁹⁰



***N*-(2-((*tert*-butyldimethylsilyl)oxy)ethyl)-4-methylbenzenesulfonamide 7c.**

To a solution of 2-aminoethanol (3.0 g, 49 mmol) and imidazole (6.7 g, 98 mmol) in CH₂Cl₂ (50 mL), under argon was added *tert*-butyldimethylsilyl chloride (7.8 g, 52 mmol). The reaction was stirred at room temperature for 2 hours, quenched with water and extracted with CH₂Cl₂. The combined organic phases were dried over MgSO₄, filtered and concentrated under reduced pressure to yield 2-((*tert*-butyldimethylsilyl)oxy)ethanamine (7.5 g, 43 mmol, 87% crude) as a transparent, yellow oil. Used without further purification.

To a solution of 2-((*tert*-butyldimethylsilyl)oxy)ethanamine (7.5 g, 43 mmol) in CH₂Cl₂ (21 mL) under argon, was added toluenesulfonyl chloride (9.0 g, 47 mmol). Once dissolved, the solution was cooled to 0 °C and triethylamine (6.4 mL, 47 mmol) was added. The reaction was stirred at room temperature for one hour, or until TLC indicated completion, and then quenched with water and extracted with CH₂Cl₂. The combined organic phases were washed with brine, dried over Na₂SO₄, filtered, and concentrated under reduced pressure. Purification by flash chromatography on silica gel (EtOAc/cyclohexane: 1/9) to afford *N*-(2-((*tert*-butyldimethylsilyl)oxy)ethyl)-4-methylbenzenesulfonamide (8.2 g, 25 mmol, 57% yield) as a colorless oil.

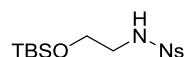
¹H-NMR (400 MHz, CDCl₃): δ=7.74 (d, *J*=8.3, 2 H), 7.31 (d, *J*=8.2, 2 H), 4.73 (t, *J*=5.6, 1 H, NH), 3.61 (t, *J*=5.0, 2 H), 3.04 (t, *J*=5.0, 2 H), 2.43 (s, 3 H), 0.84 (s, 9 H), 0.00 ppm (s, 6 H). For complete characterization see the reference below.³⁹¹

³⁸⁹ Shaabani, A.; Soleimani, E.; Hossein Rezayan, A. *Tetrahedron Lett.* **2007**, *48*, 2185–2188.

³⁹⁰ Molander, G. A.; Cormier, E. P. *J. Org. Chem.* **2005**, *70*, 2622–2626.

³⁹¹ Gandon, L. A.; Russell, A. G.; Güveli, T.; Brodewolf, A. E.; Kariuki, B. M.; Spencer, N.; Snaith, J. S. *J. Org. Chem.* **2006**, *71*, 5198–5207.

Experimental Data

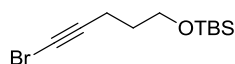


***N*-(2-((*tert*-butyldimethylsilyl)oxy)ethyl)-4-nitrobenzenesulfonamide 7d.**

To a solution of 2-aminoethan-1-ol (1.5 g, 25 mmol) in dry CH₂Cl₂ (60 mL) cooled at 0 °C were added triethylamine (5.0 mL, 37 mmol) and *para*-nosyl chloride (8.6 g, 26 mmol). The reaction mixture was stirred for 3 hours at room temperature and then was treated with sat. aq. NaHCO₃ (60 mL). The aqueous phase was extracted with CH₂Cl₂ (4 x 60 mL) and the combined organic layers were washed with brine (60 mL), dried over Na₂SO₄, concentrated under reduced pressure to give *N*-(2-hydroxyethyl)-4-nitrobenzenesulfonamide (5.7 g, 23 mmol, 92% crude) as a white solid. Used without further purification.

To a solution of *N*-(2-hydroxyethyl)-4-nitrobenzenesulfonamide (2.3 g, 9.3 mmol) in dry DMF (18 mL) at 0 °C were added imidazole (948 mg, 14 mmol) and *tert*-butyldimethylsilyl chloride (1.7 g, 11 mmol). The resulting solution was stirred at room temperature for 2 hours and then was treated with sat. aq. NaHCO₃ (30 mL). The aqueous phase was extracted with EtOAc (4 x 30 mL) and the combined organic layers were washed with brine (30 mL), dried over Na₂SO₄, concentrated under reduced pressure. The crude product was purified by chromatography over silica gel (cyclohexane/EtOAc, 9/1 – 8/2) to afford *N*-(2-((*tert*-butyldimethylsilyl)oxy)ethyl)-4-nitrobenzenesulfonamide (2.8 g, 7.8 mmol, 84% yield) as a colorless solid.

¹H-NMR (400 MHz, CDCl₃): δ=8.37 (d, *J*=8.8, 2 H), 8.06 (d, *J*=8.9, 2 H), 4.93 (t, *J*=5.8, 1 H, NH), 3.66 (t, *J*=5.0, 2 H), 3.12 (q, *J*=5.5, 2 H), 0.85 (s, 9 H), 0.01 ppm (s, 6 H). For complete characterization see the reference below.³⁹²



((5-bromopent-4-yn-1-yl)oxy)(*tert*-butyl)dimethylsilane 8a.

To a mixture of 4-pentyn-1-ol (3.0 g, 36 mmol) and DMF (11 mL) were added imidazole (6.1 g, 89 mmol) and *tert*-butyldimethylsilyl chloride (5.9 g, 39 mmol). The mixture was stirred at room temperature under argon overnight, then distilled water (75 mL) was added and the solution was extracted with petroleum ether (3 x 15 mL). The organic layers were combined, washed with distilled water (30 mL), brine (30 mL), dried on Na₂SO₄, filtered and evaporated under reduced pressure. The crude colorless liquid was purified by flash chromatography over

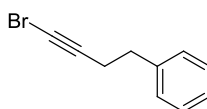
³⁹² Sabot, C.; Guerard, K. C.; Canesi, S. *Chem. Commun.* **2009**, 2941–2943.

silica gel using petroleum ether as eluent, to afford *tert*-butyldimethyl(pent-4-yn-1-yloxy)silane (4.2 g, 21 mmol, 59% yield) as a colorless liquid.

General procedure 4 for the bromination of terminal alkynes

A solution of the alkyne (5.0 mmol) in acetone (30 mL) is treated at room temperature with *N*-bromosuccinimide (6.0 mmol, 1.2 equiv.) and silver nitrate (0.50 mmol, 0.1 equiv.). The flask is protected from light with aluminum foil and stirred for one hour at room temperature. Then, the reaction mixture is poured with stirring into distilled water and the precipitate that is formed is filtered off over a pad of Celite and washed with ethyl acetate. The organic phase is washed with distilled water, dried on Na₂SO₄, and evaporated to dryness in *vacuo*. The crude product is purified by flash chromatography over silica gel.

((5-bromopent-4-yn-1-yl)oxy)(*tert*-butyl)dimethylsilane was prepared according to the *general procedure 4* in 74% yield (4.3 g, 15 mmol) as a colorless oil from *tert*-butyldimethyl(pent-4-yn-1-yloxy)silane (4.2 g, 21 mmol). *R_f* = 0.37 (cyclohexane 100 %). IR (neat) ν_{\max} 2953, 2928, 2857, 1471, 1253, 1103, 1005, 957, 833, 774, 662 cm⁻¹. ¹H-NMR (300 MHz, CDCl₃): δ =3.66 (t, *J*=6.0, 2 H), 2.28 (t, *J*=7.1, 2 H), 1.69 (qt, *J*=6.0, 2 H), 0.87 (s, 9 H), 0.03 ppm (s, 6 H). ¹³C NMR (500 MHz, CDCl₃): δ =80.2, 61.6, 37.9, 31.5, 26.1 (3xCH₃), 18.5, 16.4, -5.1 (2xCH₃) ppm. LRMS (ESI, positive mode): *m/z*: calcd for C₁₁H₂₁BrOSiH 277.06, found 277.07.



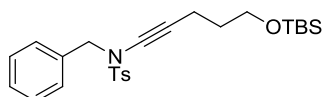
(4-bromobut-3-yn-1-yl)benzene 8b.

Prepared from the *general procedure 4* in 91% yield (1.5 g, 7.0 mmol) as a colorless liquid from 4-phenyl-1-butyne (1.0 g, 7.7 mmol). ¹H-NMR (300 MHz, CDCl₃): 7.38-7.22 (m, 5 H), 2.88 (t, *J*=7.5, 2 H), 2.54 ppm (t, *J*=7.9, 2 H). For complete characterization see the reference below.³⁹³

Experimental Data

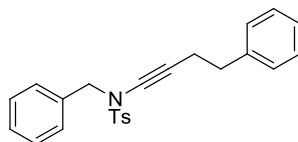
General Procedure 5 for the Cu-USY Catalyzed Synthesis of Ynamides

To a solution of alkynyl bromide (1.1 mmol, 1.1 equiv.) in 1 mL of freshly anhydrous toluene in a reaction vial were added the nitrogen nucleophile (1.0 mmol), K_2CO_3 (2.0 mmol, 2 equiv.), Cu-USY (0.10 mmol, 0.1 equiv.), and 1,10-phenanthroline (0.20 mmol, 0.2 equiv.). Argon was bubbled in the reaction mixture for 10 min before sealing the vial. The mixture was stirred at 65-110 °C until completion of the reaction, indicated by TLC monitoring. Upon completion, the reaction mixture was cooled to room temperature and diluted with 12 mL of dichloromethane. The resulting mixture was filtered through a pad of Celite, and the filtrate was concentrated in *vacuo*. The crude residue was purified using silica gel column flash chromatography (cyclohexane/ethyl acetate: 100 – 95 %) to give the expected ynamide.



***N*-benzyl-*N*-(5-((tert-butyldimethylsilyloxy)pent-1-yn-1-yl)-4-methylbenzenesulfonamide 9a.**

Prepared from the *general procedure 5* in 89 % (408 mg, 0.89 mmol) as a colorless oil from *N*-benzyl-4-methylbenzenesulfonamide (261 mg, 1.00 mmol). $R_f = 0.38$ (EtOAc/cyclohexane 2 %). IR (neat) ν_{max} 2952, 2928, 2856, 1685, 1597, 1496, 1456, 1360, 1252, 1167, 1090, 956, 834, 812, 775, 699, 666, 594, 545 cm^{-1} . 1H NMR (300 MHz, $CDCl_3$): $\delta = 7.72$ (d, $J = 8.4$, 2 H), 7.29-7.26 (m, 7 H), 7.07 (d, $J = 7.1$, 2 H), 4.42 (s, 2 H), 3.50 (t, $J = 6.0$, 2 H), 2.42 (s, 3 H), 2.23 (t, $J = 7.1$, 2 H), 1.55 (qt, $J = 6.6$, 2 H), 0.84 (s, 9 H), -0.02 ppm (s, 6 H). ^{13}C NMR (500 MHz, $CDCl_3$): $\delta = 144.4$, 137.0, 135.0, 129.7 (2xCH), 128.8 (2xCH), 128.6 (2xCH), 128.3, 127.9 (2xCH), 73.6, 70.6, 61.6, 55.7, 32.1, 26.1 (3xCH₃), 21.8, 18.5, 15.0, -5.2 (2xCH₃) ppm. LRMS (ESI, positive mode): m/z : calcd for $C_{25}H_{35}NO_3SSiNa$ 480.20, found 480.20.

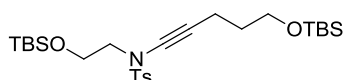


***N*-benzyl-4-methyl-*N*-(4-phenylbut-1-yn-1-yl)benzenesulfonamide 9b.**

Prepared from the *general procedure 5* in 92 % (205 mg, 0.53 mmol) as a colorless solid from *N*-benzyl-4-methylbenzenesulfonamide (150 mg, 0.57 mmol). $R_f = 0.40$ (EtOAc/cyclohexane

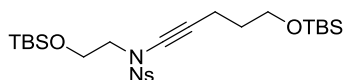
³⁹³ Okutani, M.; Mori, Y. *J. Org. Chem.* **2008**, *74*, 442–444.

10 %). IR (neat) ν_{\max} 3026, 2926, 2245, 1597, 1495, 1452, 1422, 1356, 1231, 1165, 1088, 1056 cm^{-1} . ^1H NMR (500 MHz, CDCl_3): δ =7.64 (d, J =8.3, 2 H), 7.27-7.15 (m, 10 H), 7.08 (dd, J =8.0, 1.7, 2 H), 4.39 (s, 2 H), 2.68 (t, J =7.3, 2 H), 2.47 (t, J =7.3, 2 H), 2.42 ppm (s, 3 H). ^{13}C NMR (500 MHz, CDCl_3): δ =144.2, 140.6, 134.8, 134.8, 129.6 (2xCH), 128.7 (2xCH), 128.5 (2xCH), 128.4 (2xCH), 128.3 (2xCH), 128.1, 127.7 (2xCH), 126.2, 74.2, 70.1, 55.6, 35.1, 21.6, 20.5 ppm. HRMS (ESI, positive mode): m/z : calcd for $\text{C}_{24}\text{H}_{23}\text{NSO}_2\text{Na}$ 412.131, found 412.134. Melting point: 66-67 °C.



***N*-(2-((tert-butyldimethylsilyl)oxy)ethyl)-*N*-(5-((tert-butyldimethylsilyl)oxy)pent-1-yn-1-yl)-4-methylbenzenesulfonamide 9f.**

Prepared from the *general procedure 5* in 74 % (1.56 g, 2.96 mmol) as a colorless oil from *N*-(2-((tert-butyldimethylsilyl)oxy)ethyl)-4-methylbenzenesulfonamide (1.32 g, 4.00 mmol). R_f = 0.43 (EtOAc/cyclohexane 10 %). IR (neat) ν_{\max} 2952, 2928, 2856, 2050, 1686, 1471, 1361, 1253, 1185, 1099, 1006, 938, 833, 775, 707, 582, 546 cm^{-1} . ^1H NMR (300 MHz, CDCl_3): δ =7.76 (d, J =8.4, 2 H), 7.30 (d, J =8.2, 2 H), 3.76 (t, J =6.4, 2 H), 3.61 (t, J =6.0, 2 H), 3.37 (t, J =6.2, 2 H), 2.42 (s, 3 H), 2.30 (t, J =7.1, 2 H), 1.65 (qt, J =6.6, 2 H), 0.86 (s, 9 H), 0.85 (s, 9 H), 0.02 (s, 6 H), 0.01 ppm (s, 6 H). ^{13}C NMR (500 MHz, CDCl_3): δ =144.4, 135.2, 129.8 (2xCH), 127.9 (2xCH), 73.6, 69.6, 61.8, 60.7, 53.6, 32.3, 26.2 (3xCH₃), 26.1 (3xCH₃), 21.8, 15.2, -5.1 (2xCH₃), -5.2 (2xCH₃) ppm. LRMS (ESI, positive mode): m/z : calcd for $\text{C}_{26}\text{H}_{47}\text{NO}_4\text{SSi}_2\text{Na}$ 548.27, found 548.27.

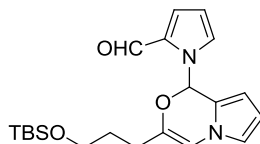


***N*-(2-((tert-butyldimethylsilyl)oxy)ethyl)-*N*-(5-((tert-butyldimethylsilyl)oxy)pent-1-yn-1-yl)-4-nitrobenzenesulfonamide 9g.**

Prepared from the *general procedure 5* in 91 % (2.11 g, 3.79 mmol) as a colorless oil from *N*-(2-((tert-butyldimethylsilyl)oxy)ethyl)-4-nitrobenzenesulfonamide (1.50 g, 4.16 mmol). R_f = 0.56 (EtOAc/cyclohexane 20 %). IR (neat) ν_{\max} 2952, 2929, 2856, 1607, 1532, 1472, 1374, 1348, 1311, 1253, 1175, 1103, 938, 832, 775, 738, 684, 659, 596, 576, 461 cm^{-1} . ^1H NMR (400 MHz, CDCl_3): δ =8.37 (d, J =8.8, 2 H), 8.10 (d, J =8.9, 2 H), 3.81 (t, J =5.9, 2 H), 3.64 (t, J =6.0, 2 H), 3.48 (t, J =5.8, 2 H), 2.34 (t, J =7.1, 2 H), 1.68 (qt, J =6.6, 2 H), 0.89 (s, 9 H), 0.86 (s, 9 H), 0.04 ppm (s, 12 H). ^{13}C NMR (500 MHz, CDCl_3): δ =150.7, 143.7, 129.1 (2xCH),

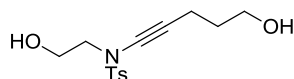
Experimental Data

124.4 (2xCH), 72.3, 70.9, 61.7, 60.4, 54.0, 32.2, 30.4, 27.1, 26.1 (3xCH₃), 26.0 (3xCH₃), 15.1, -5.1 (2xCH₃), -5.2 (2xCH₃) ppm. LRMS (ESI, positive mode): *m/z*: calcd for C₂₅H₄₄N₂O₆SSi₂Na 579.24, found 579.24.



1-(3-(3-((tert-butyldimethylsilyl)oxy)propyl)-1H-pyrrolo[2,1-c][1,4]oxazin-1-yl)-1H-pyrrole-2-carbaldehyde **9h**.

Prepared from the *general procedure 5* in 52 % (103 mg, 0.27 mmol) as a slightly orange oil from 1H-pyrrole-2-carbaldehyde (84 mg, 0.88 mmol). *R_f* = 0.40 (EtOAc/cyclohexane 10 %). IR (neat) ν_{\max} 2927, 2854, 1665, 1530, 1483, 1463, 1404, 1333, 1298, 1252, 1215, 1197, 1165, 1143, 1098, 1072, 1006, 962, 897, 833, 773, 740, 710, 605 cm⁻¹. ¹H NMR (400 MHz, CDCl₃): δ =9.63 (s, 1 H), 8.01 (s, 1 H), 6.97 (d, *J*=3.5, 1 H), 6.73 (s, 1 H), 6.39 (s, 1 H), 6.38 (s, 1 H), 6.24 (t, *J*=3.2, 1 H), 6.14 (d, *J*=3.5, 1 H), 7.00 (t, *J*=3.4, 1 H), 3.40-3.34 (m, 1 H), 3.29-3.23 (m, 1 H), 2.18-2.05 (m, 2 H), 1.49-1.39 (m, 1 H), 1.32-1.22 (m, 1 H), 0.84 (s, 9 H), -0.03 ppm (s, 6 H). ¹³C NMR (500 MHz, CDCl₃): δ =179.6, 141.2, 131.1, 129.4, 126.3, 118.9, 117.1, 110.2, 109.6, 106.5, 104.2, 77.7, 61.5, 29.7, 27.5, 26.1 (3xCH₃), 18.4, -5.2 (2xCH₃) ppm. LRMS (ESI, positive mode): *m/z*: calcd for C₂₁H₃₀N₂O₃SiNa 409.19, found 409.19.

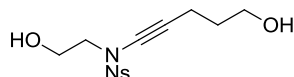


N-(2-hydroxyethyl)-*N*-(5-hydroxypent-1-yn-1-yl)-4-methylbenzenesulfonamide **27f**.

To a solution of *N*-(2-((tert-butyldimethylsilyl)oxy)ethyl)-*N*-(5-((tert-butyldimethylsilyl)oxy)pent-1-yn-1-yl)-4-methylbenzenesulfonamide **9f** (1.1 g, 2.0 mmol) in freshly anhydrous THF (23 mL) under argon was added TBAF (4.1 mL, 4.1 mmol, 2 equiv., 1 M in THF) at room temperature. The reaction mixture was stirred at room temperature for one hour. Then, saturated NH₄Cl was added and the solution was extracted with diethyl ether. Organic layers were combined, dried on MgSO₄, and concentrated in *vacuo*. The crude residue was purified using silica gel column flash chromatography (cyclohexane/ethyl acetate: 50 – 30 %) to give *N*-(2-hydroxyethyl)-*N*-(5-hydroxypent-1-yn-1-yl)-4-methylbenzenesulfonamide (0.49 g, 1.6 mmol, 81% yield) as a colorless solid.

R_f = 0.06 (EtOAc/cyclohexane 50 %). IR (neat) ν_{\max} 3227, 2958, 2938, 2913, 2892, 2864, 1594, 1478, 1444, 1349, 1280, 1218, 1163, 1109, 1074, 1047, 1029, 972, 931, 875, 858, 815,

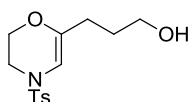
771, 703, 672, 583, 541, 494, 452 cm^{-1} . ^1H NMR (300 MHz, CDCl_3): δ =7.78 (d, J =8.4, 2 H), 7.33 (d, J =8.1, 2 H), 3.81 (q, J =5.7, 2 H), 3.71 (q, J =5.9, 2 H), 3.43 (t, J =5.3, 2 H), 2.44 (s, 3 H), 2.38 (t, J =6.8, 2 H), 1.86 (t, J =6.4, 1 H, OH), 1.73 (qt, J =6.4, 2 H), 1.44 ppm (t, J =5.5, 1 H, OH). ^{13}C NMR (300 MHz, CDCl_3): δ =144.9, 134.5, 130.0 (2xCH), 127.9 (2xCH), 73.6, 69.9, 61.7, 60.2, 53.9, 31.5, 21.9, 15.3 ppm. LRMS (ESI, positive mode): m/z : calcd for $\text{C}_{14}\text{H}_{19}\text{NO}_4\text{SNa}$ 320.09, found 320.09. Melting point: 93.8 – 94.0 $^\circ\text{C}$.



***N*-(2-hydroxyethyl)-*N*-(5-hydroxypent-1-yn-1-yl)-4-nitrobenzenesulfonamide 27g.**

To a solution of *N*-(2-((tert-butyldimethylsilyl)oxy)ethyl)-*N*-(5-((tert-butyldimethylsilyl)oxy)pent-1-yn-1-yl)-4-nitrobenzenesulfonamide **9g** (2.1 g, 3.8 mmol) in freshly anhydrous THF (43 mL) under argon was added TBAF (7.5 mL, 7.5 mmol, 2 equiv., 1 M in THF) at room temperature. The reaction mixture was stirred at room temperature for one hour. Then, saturated NH_4Cl was added and the solution was extracted with diethyl ether. Organic layers were combined, dried on MgSO_4 , and concentrated in *vacuo*. The crude residue was purified using silica gel column flash chromatography (cyclohexane/ethyl acetate: 80 – 30 %) to give *N*-(2-hydroxyethyl)-*N*-(5-hydroxypent-1-yn-1-yl)-4-nitrobenzenesulfonamide (0.33 g, 1.0 mmol, 27% yield) as a yellow solid.

R_f = 0.14 (EtOAc/cyclohexane 70 %). IR (neat) ν_{max} 3222, 3105, 2936, 2882, 1605, 1529, 1476, 1450, 1401, 1345, 1305, 1278, 1217, 1166, 1110, 1077, 1033, 976, 937, 878, 854, 831, 770, 738, 680, 646, 580, 490, 462 cm^{-1} . ^1H NMR (400 MHz, CDCl_3): δ =8.40 (d, J =8.8, 2 H), 8.12 (d, J =8.9, 2 H), 3.84 (t, J =4.9, 2 H), 3.73 (t, J =6.0, 2 H), 3.54 (t, J =5.3, 2 H), 2.42 (t, J =6.9, 2 H), 1.87 (br s, 1 H, OH), 1.76 (qt, J =6.4, 2 H), 1.58 ppm (br s, 1 H, OH). ^{13}C NMR (300 MHz, CDCl_3): δ =150.8, 143.0, 129.2 (2xCH), 124.5 (2xCH), 72.4, 71.0, 61.7, 59.8, 54.0, 31.4, 15.3 ppm. LRMS (ESI, positive mode): m/z : calcd for $\text{C}_{13}\text{H}_{16}\text{N}_2\text{O}_6\text{SNa}$ 351.06, found 351.06. Melting point: 80.8 – 81.0 $^\circ\text{C}$.

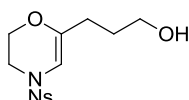


3-(4-tosyl-3,4-dihydro-2*H*-1,4-oxazin-6-yl)propan-1-ol 52f.

Prepared according to the *general procedure 3* in 36% (53 mg, 0.18 mmol) as a colorless oil from *N*-(2-hydroxyethyl)-*N*-(5-hydroxypent-1-yn-1-yl)-4-methylbenzenesulfonamide **27f** (0.30 g, 1.0 mmol).

Experimental Data

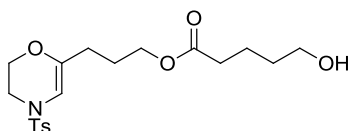
$R_f = 0.31$ (EtOAc/cyclohexane 50 %). IR (neat) ν_{\max} 3388, 2931, 2880, 1727, 1670, 1597, 1448, 1389, 1347, 1307, 1284, 1187, 1161, 1105, 1086, 1055, 981, 907, 815, 774, 736, 706, 668, 596, 547 cm^{-1} . ^1H NMR (400 MHz, CDCl_3): $\delta=7.61$ (d, $J=7.7$, 2 H), 7.29 (d, $J=8.0$, 2 H), 5.85 (s, 1 H), 3.57-3.52 (m, 4 H), 3.40 (t, $J=4.3$, 2 H), 2.39 (s, 3 H), 2.08 (t, $J=7.2$, 2 H), 1.74 (br s, 1 H, OH), 1.64 ppm (qt, $J=6.4$, 2 H). ^{13}C NMR (500 MHz, CDCl_3): $\delta=144.1$, 143.3, 133.9, 129.9 (2xCH), 127.6 (2xCH), 100.6, 63.2, 62.0, 43.2, 30.1, 28.6, 21.7 ppm. LRMS (ESI, positive mode): m/z : calcd for $\text{C}_{14}\text{H}_{19}\text{NO}_4\text{SNa}$ 320.09, found 320.09.



3-(4-((4-nitrophenyl)sulfonyl)-3,4-dihydro-2H-1,4-oxazin-6-yl)propan-1-ol 52g.

Prepared according to the *general procedure 3* in 8% (11 mg, 0.034 mmol) as a colorless oil from *N*-(2-hydroxyethyl)-*N*-(5-hydroxypent-1-yn-1-yl)-4-nitrobenzenesulfonamide **27g** (0.15 g, 0.46 mmol).

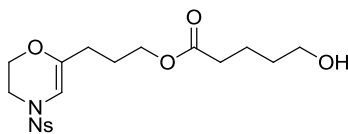
$R_f = 0.31$ (EtOAc/cyclohexane 50 %). ^1H NMR (400 MHz, CDCl_3): $\delta=8.38$ (d, $J=8.8$, 2 H), 7.96 (d, $J=8.8$, 2 H), 5.91 (s, 1 H), 3.67 (t, $J=4.2$, 2 H), 3.60 (t, $J=6.2$, 2 H), 3.50 (t, $J=4.1$, 2 H), 2.13 (t, $J=7.2$, 2 H), 1.68 (qt, $J=6.6$, 2 H), 1.51 ppm (br s, 1 H, OH).



3-(4-tosyl-3,4-dihydro-2H-1,4-oxazin-6-yl)propyl 5-hydroxypentanoate 53f.

Prepared according to the *general procedure 3* in 10% (20 mg, 0.050 mmol) as a colorless oil from *N*-(2-hydroxyethyl)-*N*-(5-hydroxypent-1-yn-1-yl)-4-methylbenzenesulfonamide **27f** (0.30 g, 1.0 mmol).

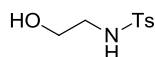
$R_f = 0.25$ (EtOAc/cyclohexane 50 %). IR (neat) ν_{\max} 3510, 2932, 2879, 1728, 1597, 1451, 1394, 1349, 1307, 1285, 1160, 1088, 1019, 975, 758, 706, 667, 581, 548 cm^{-1} . ^1H NMR (400 MHz, CDCl_3): $\delta=7.61$ (d, $J=8.3$, 2 H), 7.30 (d, $J=8.4$, 2 H), 5.85 (s, 1 H), 3.98 (t, $J=6.4$, 2 H), 3.63 (t, $J=6.4$, 2 H), 3.52 (t, $J=4.0$, 2 H), 3.41 (t, $J=4.0$, 2 H), 2.40 (s, 3 H), 2.34 (t, $J=7.2$, 2 H), 2.08 (t, $J=7.2$, 2 H), 1.75-1.67 (m, 4 H), 1.72 (br s, 1 H, OH), 1.59 ppm (qt, $J=6.0$, 2 H). ^{13}C NMR (300 MHz, CDCl_3): $\delta=173.9$, 144.2, 142.5, 133.9, 130.0 (2xCH), 127.6 (2xCH), 101.0, 63.4, 63.2, 62.5, 43.2, 34.1, 32.3, 28.7, 26.0, 21.8, 21.4 ppm. LRMS (ESI, positive mode): m/z : calcd for $\text{C}_{19}\text{H}_{27}\text{NO}_6\text{SNa}$ 420.15, found 420.14.



3-(4-((4-nitrophenyl)sulfonyl)-3,4-dihydro-2H-1,4-oxazin-6-yl)propyl 5-hydroxypentanoate 53g.

Prepared according to the *general procedure 3* in 10% (53 mg, 0.044 mmol) as a colorless oil from *N*-(2-hydroxyethyl)-*N*-(5-hydroxypent-1-yn-1-yl)-4-nitrobenzenesulfonamide **27g** (0.15 g, 0.46 mmol).

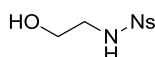
$R_f = 0.63$ (EtOAc/cyclohexane 70 %). $^1\text{H NMR}$ (400 MHz, CDCl_3): $\delta = 8.38$ (d, $J = 8.8$, 2 H), 7.94 (d, $J = 8.8$, 2 H), 5.87 (s, 1 H), 3.98 (t, $J = 6.5$, 2 H), 3.64 (t, $J = 6.3$, 2 H), 3.62 (t, $J = 4.6$, 2 H), 3.48 (t, $J = 4.7$, 2 H), 2.34 (t, $J = 7.1$, 2 H), 2.09 (t, $J = 7.2$, 2 H), 1.72 (sext, $J = 7.0$, 4 H), 1.62–1.56 ppm (m, 3 H).



***N*-(2-hydroxyethyl)-4-methylbenzenesulfonamide 54f.**

Prepared according to the *general procedure 3* in 55% (20 mg, 0.093 mmol) as a colorless oil from *N*-(2-hydroxyethyl)-*N*-(5-hydroxypent-1-yn-1-yl)-4-methylbenzenesulfonamide **27f** (0.1 g, 0.34 mmol).

$^1\text{H NMR}$ (300 MHz, CDCl_3): $\delta = 7.74$ (d, $J = 8.4$, 2 H), 7.29 (d, $J = 8.1$, 2 H), 5.15 (br s, 1 H, NH), 3.67 (t, $J = 4.9$, 2 H), 3.06 ppm (t, $J = 5.1$, 2 H). For complete characterization see the references below.³⁹¹



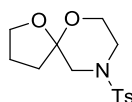
***N*-(2-hydroxyethyl)-4-nitrobenzenesulfonamide 54g.**

Prepared according to the *general procedure 3* in 39% (21 mg, 0.085 mmol) as a colorless oil from *N*-(2-hydroxyethyl)-*N*-(5-hydroxypent-1-yn-1-yl)-4-nitrobenzenesulfonamide **27g** (70 mg, 0.21 mmol).

$^1\text{H NMR}$ (400 MHz, CDCl_3): $\delta = 8.38$ (d, $J = 8.8$, 2 H), 8.07 (d, $J = 8.8$, 2 H), 5.09 (t, $J = 5.1$, 1 H, NH), 3.74 (t, $J = 5.0$, 2 H), 3.19 ppm (q, $J = 5.6$, 2 H). For complete characterization see the references below.³⁹⁴

³⁹⁴ (a) Iwaki, S.; Hanaoka, K.; Piao, W.; Komatsu, T.; Ueno, T.; Terai, T.; Nagano, T. *Bioorg. Med. Chem. Lett.* **2012**, 22, 2798–2802. (b) Knipe, A. C.; Lound-Keast, J. *J. Chem. Soc., Perkin Trans. 2* **1976**, 1741–1748.

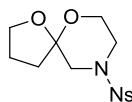
Experimental Data



9-tosyl-1,6-dioxa-9-azaspiro[4.5]decane **28f**.

Prepared according to the *general procedure 3* in 27% (39 mg, 0.13 mmol) as a colorless solid from *N*-(2-hydroxyethyl)-*N*-(5-hydroxypent-1-yn-1-yl)-4-methylbenzenesulfonamide **27f** (0.15 g, 0.50 mmol).

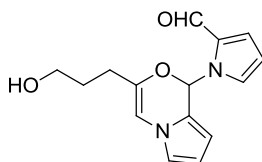
$R_f = 0.57$ (EtOAc/cyclohexane 50 %). IR (neat) ν_{\max} 2994, 2931, 2848, 1596, 1495, 1455, 1341, 1312, 1277, 1242, 1160, 1124, 1092, 1065, 1016, 974, 956, 898, 853, 830, 803, 758, 715, 655, 582, 548, 534, 487 cm^{-1} . ^1H NMR (400 MHz, CDCl_3): $\delta=7.64$ (d, $J=8.2$, 2 H), 7.33 (d, $J=8.2$, 2 H), 4.06 (td, $J=10.9$, 2.9, 1 H), 4.02-3.92 (m, 2 H), 3.61 (dt, $J=11.6$, 3.2, 1 H), 3.38-3.33 (m, 2 H), 2.67 (d, $J=11.4$, 1 H), 2.61 (dd, $J=10.6$, 3.1, 1 H), 2.44 (s, 3 H), 2.09-1.98 (m, 1 H), 1.97-1.86 (m, 2 H), 1.79-1.70 (m, 1 H). ^{13}C NMR (400 MHz, CDCl_3): $\delta=150.8$, 144.0, 129.9 (2xCH), 128.1 (2xCH), 103.8, 68.4, 60.4, 51.7, 45.1, 35.6, 23.9, 21.8 ppm. LRMS (ESI, positive mode): m/z : calcd for $\text{C}_{14}\text{H}_{19}\text{NO}_4\text{SNa}$ 320.09, found 320.09. Melting point: 158.8 – 160.0 $^\circ\text{C}$.



9-((4-nitrophenyl)sulfonyl)-1,6-dioxa-9-azaspiro[4.5]decane **28g**.

Prepared according to the *general procedure 3* in 14% (10 mg, 0.030 mmol) as a light yellow solid from *N*-(2-hydroxyethyl)-*N*-(5-hydroxypent-1-yn-1-yl)-4-nitrobenzenesulfonamide **27g** (70 mg, 0.21 mmol).

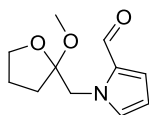
$R_f = 0.56$ (EtOAc/cyclohexane 50 %). IR (neat) ν_{\max} 3112, 2985, 2904, 2882, 2852, 1609, 1543, 1451, 1402, 1341, 1313, 1273, 1250, 1226, 1160, 1125, 1107, 1072, 1045, 1020, 993, 925, 904, 857, 842, 765, 743, 731, 708, 684, 607, 572, 553, 525, 486, 463 cm^{-1} . ^1H NMR (400 MHz, CDCl_3): $\delta=8.36$ (d, $J=8.8$, 2 H), 7.96 (d, $J=8.8$, 2 H), 4.00-3.85 (m, 3 H), 3.58 (dt, $J=11.7$, 2.5, 1 H), 3.49 (t, $J=11.3$, 2 H), 2.80 (d, $J=11.7$, 1 H), 2.74 (dd, $J=11.3$, 3.2, 1 H), 2.07-1.97 (m, 1 H), 1.95-1.85 (m, 2 H), 1.74-1.69 ppm (m, 1 H). ^{13}C NMR (400 MHz, CDCl_3): $\delta=150.4$, 142.8, 129.1 (2xCH), 124.5 (2xCH), 103.5, 68.4, 59.9, 51.4, 44.9, 35.7, 23.8 ppm. LRMS (ESI, positive mode): m/z : calcd for $\text{C}_{13}\text{H}_{16}\text{N}_2\text{O}_6\text{SNa}$ 351.06, found 351.06. Melting point: 136.0 $^\circ\text{C}$.



1-(3-(3-hydroxypropyl)-1H-pyrrolo[2,1-c][1,4]oxazin-1-yl)-1H-pyrrole-2-carbaldehyde 59.

To a solution of 1-(3-(3-((tert-butyldimethylsilyl)oxy)propyl)-1H-pyrrolo[2,1-c][1,4]oxazin-1-yl)-1H-pyrrole-2-carbaldehyde **9h** (0.18 g, 0.47 mmol) in THF/H₂O (3.6 mL, 9/1) was added *p*-toluenesulfonic acid monohydrate (89 mg, 0.47 mmol, 1 equiv.) at room temperature. The solution was stirred overnight at room temperature, and diethyl ether (9 mL) was added. The solution was washed with NaHCO₃ 5% (3x7 mL), brine (7 mL), dried on MgSO₄ and evaporated in *vacuo*. The crude product was purified by flash chromatography on silica gel (cyclohexane/EtOAc 90 – 20 %) to afford 1-(3-(3-hydroxypropyl)-1H-pyrrolo[2,1-c][1,4]oxazin-1-yl)-1H-pyrrole-2-carbaldehyde (90 mg, 0.33 mmol, 70%) as a slightly orange oil.

R_f = 0.22 (EtOAc/cyclohexane 40 %). IR (neat) ν_{\max} 3381, 3113, 2926, 2873, 2807, 2722, 1732, 1654, 1528, 1482, 1463, 1403, 1333, 1252, 1215, 1197, 1141, 1071, 1025, 1003, 896, 836, 739, 605 cm⁻¹. ¹H NMR (300 MHz, CDCl₃): δ =9.60 (d, *J*=0.9, 1 H), 7.98 (s, 1 H), 6.98 (dd, *J*=3.8, 1.6, 1 H), 6.72 (dd, *J*=2.7, 1.5, 1 H), 6.42 (s, 1 H), 6.38 (qt, *J*=1.5, 1 H), 6.24 (t, *J*=3.3, 1 H), 6.13 (dt, *J*=3.5, 0.5, 1 H), 7.00 (t, *J*=3.3, 1 H), 3.38-3.26 (m, 2 H), 2.22-2.02 (m, 2 H), 1.94 (s, 1 H, OH), 1.55-1.41 (m, 1 H), 1.39-1.27 ppm (m, 1 H). ¹³C NMR (500 MHz, CDCl₃): δ =179.7, 140.8, 131.1, 129.5, 126.5, 118.7, 117.2, 110.2, 109.6, 106.6, 104.4, 77.7, 61.3, 29.6, 27.4 ppm. LRMS (ESI, positive mode): *m/z*: calcd for C₁₅H₁₆N₂O₃Na 295.11, found 295.11.



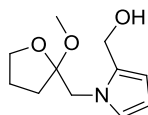
1-((2-methoxytetrahydrofuran-2-yl)methyl)-1H-pyrrole-2-carbaldehyde 61.

Prepared according to the *general procedure 3* in 42% (23 mg, 0.11 mmol) as a colorless oil from 1-(3-(3-hydroxypropyl)-1H-pyrrolo[2,1-c][1,4]oxazin-1-yl)-1H-pyrrole-2-carbaldehyde **59** (71 mg, 0.26 mmol).

R_f = 0.77 (EtOAc/cyclohexane 50 %). IR (neat) ν_{\max} 3116, 2953, 2883, 2830, 2721, 1655, 1528, 1477, 1403, 1370, 1315, 1265, 1220, 1189, 1152, 1125, 1074, 1044, 995, 963, 924, 894, 852, 852, 747 cm⁻¹. ¹H NMR (300 MHz, CDCl₃): δ =9.51 (d, *J*=0.9, 1 H), 7.08 (qt, *J*=1.3, 1

Experimental Data

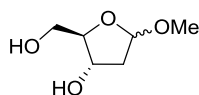
H), 6.89 (dd, $J=3.8, 1.8, 1$ H), 6.21 (dd, $J=4.0, 2.6, 1$ H), 4.81 (d, $J=13.9, 1$ H), 4.48 (d, $J=14.1, 1$ H), 3.95-3.89 (m, 1 H), 3.79-3.71 (m, 1 H), 3.27 (s, 3 H), 2.00-1.78 (m, 2 H), 1.72-1.60 ppm (m, 2 H). ^{13}C NMR (400 MHz, CDCl_3): $\delta=179.8, 133.3, 132.0, 125.2, 110.1, 108.4, 69.1, 50.5, 49.2, 32.1, 24.8$ ppm. LRMS (ESI, positive mode): m/z : calcd for $\text{C}_{11}\text{H}_{15}\text{NO}_3\text{Na}$ 232.09, found 232.10.



(1-((2-methoxytetrahydrofuran-2-yl)methyl)-1H-pyrrol-2-yl)methanol 62.

To a mixture of NaBH_4 (15 mg, 0.40 mmol, 4 equiv.) in THF (0.70 mL) under argon was added a solution of 1-((2-methoxytetrahydrofuran-2-yl)methyl)-1H-pyrrole-2-carbaldehyde **61** (21 mg, 0.10 mmol) in THF (0.50 mL). The resulting mixture was stirred at room temperature for 4 h. Then, saturated NH_4Cl and ethyl acetate were added at 0 °C. The organic phase was separated, washed with a pH 7 phosphate buffer ($\text{KH}_2\text{PO}_4/\text{NaOH}$), brine, dried on MgSO_4 , filtered and concentrated in *vacuo*. The crude product was purified by flash chromatography on silica gel (cyclohexane/EtOAc 90 – 20 %) to afford (1-((2-methoxytetrahydrofuran-2-yl)methyl)-1H-pyrrol-2-yl)methanol (18 mg, 0.085 mmol, 85%) as a colorless oil.

$R_f = 0.38$ (EtOAc/cyclohexane 50 %). IR (neat) ν_{max} 3396, 2949, 2882, 2832, 1486, 1463, 1428, 1298, 1192, 1123, 1071, 1043, 1020, 991, 924, 894, 848, 794, 771, 718 cm^{-1} . ^1H NMR (300 MHz, CDCl_3): $\delta=6.70$ (dd, $J=2.7, 1.8, 1$ H), 6.12 (dd, $J=3.7, 1.8, 1$ H), 6.06 (t, $J=3.1, 1$ H), 4.54 (s, 2 H), 4.26 (d, $J=14.6, 1$ H), 4.04 (d, $J=14.6, 1$ H), 3.98-3.91 (m, 1 H), 3.84-3.77 (m, 1 H), 3.24 (s, 3 H), 2.06-1.59 ppm (m, 5 H). ^{13}C NMR (400 MHz, CDCl_3): $\delta=133.0, 123.9, 109.5, 108.3, 107.6, 69.3, 56.2, 50.5, 49.4, 33.0, 24.6$ ppm. LRMS (ESI, positive mode): m/z : calcd for $\text{C}_{11}\text{H}_{17}\text{NO}_3\text{Na}$ 234.11, found 234.11.



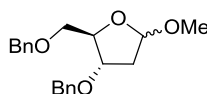
(2R,3S)-2-(hydroxymethyl)-5-methoxytetrahydrofuran-3-ol 63.

To 2.0 g (15 mmol) of 2-Deoxy-D-ribose **6** was added 30 mL of 0.05% HCl in methanol at room temperature. The mixture was stirred for one hour at the same temperature, and then the reaction was quenched by an addition of NaHCO_3 . The suspension was vigorously stirred for 20 min, filtered through Celite, and the filtrate was concentrated in *vacuo* to provide crude

(2*R*,3*S*)-2-(hydroxymethyl)-5-methoxytetrahydrofuran-3-ol (2.2 g, 15 mmol 100% crude) as a yellow oil, which was used for the next reaction without further purification.

¹H NMR of α and β -isomer of **63** (400 MHz, MeOD): δ =5.07 (dd, J =5.3, 2.2, 1 H), 5.02 (dd, J =5.5, 1.5, 1 H), 4.26 (td, J =6.2, 4.3, 1 H), 4.11 (qt, J =3.8, 1 H), 3.90 (qt, J =4.3, 1 H), 3.86 (t, J =4.7, 1 H), 3.66 (dd, J =11.8, 3.7, 1 H), 3.59 (td, J =12.0, 5.0, 2 H), 3.52 (dd, J =11.5, 6.5, 1 H), 3.35 (s, 3 H), 3.33 (s, 3 H), 2.34-2.27 (m, 1 H), 2.15 (ddd, J =13.4, 6.8, 2.3, 1 H), 2.02 (dt, J =13.4, 5.6, 1 H), 1.83 ppm (dq, J =13.8, 1.7, 1 H).

For complete characterization see the references below.³⁹⁵



(2*R*,3*S*)-3-(benzyloxy)-2-((benzyloxy)methyl)-5-methoxytetrahydrofuran **64.**

To a cooled (0 °C) suspension of 1.8 g (44 mmol, 3 equiv., 60% suspension in oil and washed with hexane) of NaH in 20 mL of DMF was added a solution of crude (2*R*,3*S*)-2-(hydroxymethyl)-5-methoxytetrahydrofuran-3-ol **63** in 10 mL of DMF and the slurry was stirred for one hour at room temperature. After the mixture was cooled to 0 °C, benzyl bromide (4.4 mL, 37 mmol, 2.5 equiv.) was added and the mixture was stirred for one hour at room temperature. The reaction was cooled to 0 °C, quenched by addition of dry methanol, poured into saturated NH₄Cl solution. The mixture was extracted with ethyl acetate. The organic layer was washed with brine, dried over Na₂SO₄, filtered and concentrated in *vacuo*. The crude product was purified by flash chromatography over silica gel (EtOAc/cyclohexane 0 – 20 %) to give (2*R*,3*S*)-3-(benzyloxy)-2-((benzyloxy)methyl)-5-methoxytetrahydrofuran (3.7 g, 11 mmol, 77% in 2 steps) as a yellow oil.

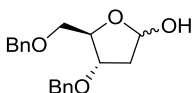
¹H NMR of α and β -isomer of **64** (400 MHz, CDCl₃): δ =7.33-7.26 (m, 20 H), 5.08 (dd, J =5.2, 2.1, 1 H), 5.05 (d, J =5.7, 1 H), 4.56-4.45 (m, 8 H), 4.27-4.21 (m, 2 H), 4.12 (td, J =6.2, 3.8, 1 H), 3.98-3.94 (m, 1 H), 3.56-3.46 (m, 4 H), 3.39 (s, 3 H), 3.29 (s, 3 H), 2.24-2.17 (m, 2 H), 2.11 (dt, J =13.3, 5.5, 1 H), 2.00 ppm (d, J =14.0, 1 H).

For complete characterization see the references below.^{395a-396}

³⁹⁵ (a) Adamo, M. F. A.; Pergoli, R. *Org. Lett.* **2007**, *9*, 4443–4446. (b) Chenault, H. K.; Mandes, R. F. *Tetrahedron* **1997**, *53*, 11033–11038.

³⁹⁶ Paul, G. J. C.; Théberge, R.; Bertrand, M. J.; Feng, R.; Bailey, M. D. *Org. Mass Spectrom.* **1993**, *28*, 1329–1339.

Experimental Data

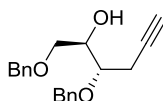


(4*S*,5*R*)-4-(benzyloxy)-5-((benzyloxy)methyl)tetrahydrofuran-2-ol **65.**

A stirred solution of (2*R*,3*S*)-3-(benzyloxy)-2-((benzyloxy)methyl)-5-methoxytetrahydrofuran **64** (5.3 g, 16 mmol) in AcOH/H₂O (162 mL, 80/20) was heated at 49 °C for 24 h. At this point an additional 54 mL of AcOH/H₂O (80/20) was added and the reaction mixture was allowed to stir at the same temperature for other 16 h. The solvent was then removed in *vacuo*, the resulting crude mixture treated with toluene to eliminate the residual acetic acid and the residue purified by flash chromatography over silica gel (EtOAc/cyclohexane 10 – 30 %) to give (4*S*,5*R*)-4-(benzyloxy)-5-((benzyloxy)methyl)tetrahydrofuran-2-ol (4.6 g, 15 mmol, 90 %) as a yellow oil.

¹H NMR of α and β -isomer of **65** (400 MHz, CDCl₃): δ =7.36-7.25 (m, 20 H), 5.54-5.50 (m, 1 H), 5.45 (dd, J =10.5, 3.4, 1 H), 4.60-4.41 (m, 8 H), 4.28-4.24 (m, 2 H), 4.10-4.09 (m, 1 H), 3.65-3.47 (m, 4 H), 3.34 (dd, J =10.1, 6.0, 1 H), 2.21-2.18 (m, 2 H), 2.11-2.09 ppm (m, 2 H).

For complete characterization see the references below.^{395a}

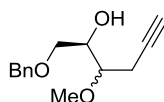


(2*R*,3*S*)-1,3-bis(benzyloxy)hex-5-yn-2-ol **67.**

To a mixture of K₂CO₃ (0.66 g, 4.8 mmol, 3 equiv.) in dry methanol (8 mL) under argon at 0 °C were added dimethyl (1-diazo-2-oxopropyl)phosphonate **66** dropwise (0.72 mL, 4.8 mmol, 3 equiv.) and a solution of (4*S*,5*R*)-4-(benzyloxy)-5-((benzyloxy)methyl)tetrahydrofuran-2-ol **65** (0.50 g, 1.6 mmol, 1 equiv.) in methanol (1 mL) dropwise. The mixture was stirred for 30 min at 0 °C and allowed to warm to room temperature. After 3 h, complete conversion was indicated by TLC monitoring. Saturated NH₄Cl was added (30 mL) and the solution was extracted by ethyl acetate (4x30 mL). Organic layers were combined, washed with brine (30 mL), dried over Na₂SO₄, filtered and concentrated under reduced pressure. The crude product was purified by flash chromatography over silica gel (EtOAc/cyclohexane 0 – 30 %) to give (2*R*,3*S*)-1,3-bis(benzyloxy)hex-5-yn-2-ol (0.17 g, 0.56 mmol, 35%) as a colorless oil.

R_f = 0.64 (EtOAc/cyclohexane 40 %). IR (neat) ν_{\max} 3433, 3290, 3030, 2919, 2866, 1721, 1496, 1454, 1363, 1260, 1206, 1073, 1027, 909, 818, 736, 697, 638, 467 cm⁻¹. ¹H NMR (300 MHz, CDCl₃): δ =7.36-7.24 (m, 10 H), 4.73 (d, J =11.3, 1 H), 4.51 (s, 2 H), 4.49 (d, J =8.6, 1 H), 3.93-3.88 (m, 1 H), 3.68-3.56 (m, 3 H), 2.64 (ddd, J =17.2, 4.8, 2.7, 1 H), 2.55 (ddd,

$J=17.0$, 5.5, 2.6, 1 H), 2.39 (br s, 1 H, OH), 2.00 ppm (t, $J=2.6$, 1 H). ^{13}C NMR (500 MHz, CDCl_3): $\delta=138.2$, 138.1, 128.7 (2xCH), 128.6 (2xCH), 128.2 (2xC_{quat}), 128.0 (4xCH), 81.2, 77.5, 77.4, 73.7, 72.6, 71.5, 70.9, 70.3, 20.7 ppm. LRMS (ESI, positive mode): m/z : calcd for $\text{C}_{20}\text{H}_{22}\text{O}_3\text{Na}$ 333.15, found 333.15.

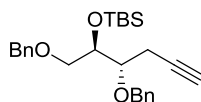


(2R)-1-(benzyloxy)-3-methoxyhex-5-yn-2-ol 68.

Prepared according to the synthetic procedure of **67**, with 2 equivalents K_2CO_3 and 1.5 equivalent dimethyl (1-diazo-2-oxopropyl)phosphonate **66**. The two diastereoisomers were isolated after 22 h, (11 mg, 0.047 mmol, 3%).

First isomer: $R_f = 0.54$ (EtOAc/cyclohexane 40 %). ^1H NMR (400 MHz, CDCl_3): $\delta=7.36$ -7.24 (m, 5 H), 4.55 (s, 2 H), 3.92-3.87 (m, 1 H), 3.66 (dd, $J=9.6$, 3.4, 1 H), 3.58 (dd, $J=9.6$, 6.1, 1 H), 3.41 (s, 3 H), 3.38-3.35 (m, 1 H), 2.60 (ddd, $J=17.1$, 4.8, 2.7, 1 H), 2.51 (ddd, $J=17.2$, 5.3, 2.7, 1 H), 2.42 (br s, 1 H, OH), 1.98 ppm (t, $J=2.6$, 1 H). ^{13}C NMR (300 MHz, CDCl_3): $\delta=138.1$, 128.7 (2xCH), 128.0, 128.0 (2xCH), 81.0, 79.6, 73.7, 71.1, 71.0, 70.2, 58.3, 20.0 ppm.

Second isomer: $R_f = 0.49$ (EtOAc/cyclohexane 40 %). ^1H NMR (400 MHz, CDCl_3): $\delta=7.36$ -7.24 (m, 5 H), 4.73 (d, $J=11.3$, 1 H), 4.55 (s, 2 H), 3.94 (qt, $J=5.0$, 1 H), 3.56 (d, $J=5.4$, 1 H), 3.46-3.42 (m, 1 H), 3.43 (s, 3 H), 2.56 (ddd, $J=17.0$, 6.5, 2.7, 1 H), 2.44 (ddd, $J=17.3$, 5.1, 2.6, 1 H), 1.98 (t, $J=2.7$, 1 H), (br s, 1 H, OH), 2.00 ppm (t, $J=2.6$, 1 H). ^{13}C NMR (300 MHz, CDCl_3): $\delta=138.2$, 128.6 (2xCH), 128.0, 128.0 (2xCH), 80.8, 79.3, 73.7, 71.4, 71.1, 70.4, 58.6, 19.9 ppm.



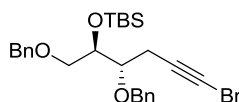
(((2R,3S)-1,3-bis(benzyloxy)hex-5-yn-2-yl)oxy)(tert-butyl)dimethylsilane 69.

To a mixture of (2R,3S)-1,3-bis(benzyloxy)hex-5-yn-2-ol **67** (0.50 g, 1.6 mmol, 1 equiv.) and DMF (1.0 mL) were added imidazole (0.33 g, 4.8 mmol, 3 equiv.) and *tert*-butyldimethylsilyl chloride (0.27 g, 1.8 mmol, 1.1 equiv.). The mixture was stirred at room temperature under argon overnight, then distilled water (25 mL) was added and the solution was extracted with petroleum ether (3 x 5 mL). The organic layers were combined, washed with distilled water (10 mL), brine (10 mL), dried on Na_2SO_4 , filtered and evaporated under reduced pressure.

Experimental Data

The crude colorless liquid was purified by flash chromatography over silica gel (EtOAc/cyclohexane 0 – 3 %), to afford (((2*R*,3*S*)-1,3-bis(benzyloxy)hex-5-yn-2-yl)oxy)(tert-butyl)dimethylsilane (0.66 g, 1.5 mmol, 96% yield) as a colorless liquid.

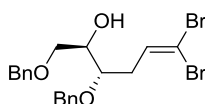
$R_f = 0.63$ (EtOAc/cyclohexane 10 %). IR (neat) ν_{\max} 2927, 2885, 2855, 1496, 1471, 1388, 1252, 1207, 1094, 1027, 833, 777, 734, 696, 633, 463 cm^{-1} . ^1H NMR (300 MHz, CDCl_3): $\delta=7.34\text{--}7.24$ (m, 10 H), 4.68 (d, $J=11.5$, 1 H), 4.57 (d, $J=11.5$, 1 H), 4.49 (s, 2 H), 3.97 (q, $J=4.8$, 1 H), 3.69 (q, $J=5.4$, 1 H), 3.58 (dd, $J=9.9$, 4.0, 1 H), 3.53 (dd, $J=10.0$, 4.8, 1 H), 2.56 (ddd, $J=17.1$, 4.9, 2.7, 1 H), 2.48 (ddd, $J=17.1$, 5.8, 2.7, 1 H), 1.97 (t, $J=2.6$, 1 H), 0.87 (s, 9 H), 0.05 ppm (d, $J=10.2$, 6 H). ^{13}C NMR (400 MHz, CDCl_3): $\delta=138.6$, 138.5, 128.5 (4xCH), 128.1 (2xCH), 127.9 (2xCH), 127.8, 127.7, 81.9, 78.4, 73.6, 73.0, 72.8, 71.9, 70.1, 27.1, 26.1 (3x CH_3), 20.7, -4.2, -4.6 ppm. LRMS (ESI, positive mode): m/z : calcd for $\text{C}_{26}\text{H}_{36}\text{O}_3\text{SiNa}$ 447.23, found 447.23.



(((2*R*,3*S*)-1,3-bis(benzyloxy)-6-bromohex-5-yn-2-yl)oxy)(tert-butyl)dimethylsilane **26**.

Prepared according to the *general procedure 4* as a colorless oil (0.66 g, 1.3 mmol, 85%) from (((2*R*,3*S*)-1,3-bis(benzyloxy)hex-5-yn-2-yl)oxy)(tert-butyl)dimethylsilane **69** (0.65 g, 1.5 mmol).

$R_f = 0.16$ (cyclohexane 100 %). IR (neat) ν_{\max} 2952, 2884, 1496, 1361, 1251, 1207, 1094, 1027, 833, 777, 734, 696, 606, 466 cm^{-1} . ^1H NMR (400 MHz, CDCl_3): $\delta=7.36\text{--}7.27$ (m, 10 H), 4.66 (d, $J=11.5$, 1 H), 4.57 (d, $J=11.6$, 1 H), 4.50 (s, 2 H), 3.96 (q, $J=4.6$, 1 H), 3.69 (q, $J=5.4$, 1 H), 3.59–3.52 (m, 2 H), 2.58 (dd, $J=10.0$, 4.8, 1 H), 2.51 (dd, $J=17.1$, 4.8, 1 H), 2.51 (dd, $J=17.1$, 5.9, 1 H), 0.88 (s, 9 H), 0.07 ppm (d, $J=8.8$, 6 H). ^{13}C NMR (500 MHz, CDCl_3): $\delta=138.5$ (2x C_{quat}), 128.5 (4xCH), 128.2 (2xCH), 127.9 (2xCH), 127.8, 127.8, 78.4, 77.9, 73.6, 73.0, 72.8, 71.9, 39.4, 26.1 (3x CH_3), 22.0, 18.4, -4.2, -4.7 ppm. LRMS (ESI, positive mode): m/z : calcd for $\text{C}_{26}\text{H}_{35}\text{BrO}_3\text{SiNa}$ 525.14, found 525.14.



(2*R*,3*S*)-1,3-bis(benzyloxy)-6,6-dibromohex-5-en-2-ol **70**.

Under an argon atmosphere, dibromomethyltriphenylphosphonium bromide (1.0 g, 2.0 mmol, 2 equiv.) and *t*-BuOK (0.21 g, 1.9 mmol, 1.9 equiv.) were dissolved in THF (10 mL). The

solution was stirred for a few minutes, and (4*S*,5*R*)-4-(benzyloxy)-5-((benzyloxy)methyl)tetrahydrofuran-2-ol **65** (0.31 g, 1.0 mmol, 1 equiv.) was then added. The mixture was stirred for 5 h at room temperature, and for 2 h at reflux in order to achieve complete conversion. The reaction was quenched at -78 °C by addition of brine (15 mL). The mixture was extracted twice with 10 mL of diethyl ether. Organic layers were combined, dried over Na₂SO₄ and concentrated. Chromatography on silica gel afforded (2*R*,3*S*)-1,3-bis(benzyloxy)-6,6-dibromohex-5-en-2-ol (0.31 g, 0.67 mmol, 67%) as a colorless oil.

*R*_f = 0.61 (EtOAc/cyclohexane 30 %). IR (neat) ν_{max} 3435, 3029, 2865, 1701, 1603, 1496, 1453, 1205, 1070, 1027, 910, 808, 778, 735, 696, 607, 467 cm⁻¹. ¹H NMR (400 MHz, CDCl₃): δ =7.36-7.25 (m, 10 H), 6.50 (t, *J*=7.2, 1 H), 4.58-4.56 (m, 4 H), 3.83-3.77 (m, 1 H), 3.64-3.54 (m, 3 H), 2.46 (t, *J*=6.3, 2 H), 2.37 ppm (d, *J*=4.9, 1 H). ¹³C NMR (500 MHz, CDCl₃): δ =138.0, 135.2 (2x C_{quat}), 128.7 (4xCH), 128.2 (2x C_{quat}), 128.1 (4xCH), 90.3, 77.7, 73.7, 72.5, 71.6, 71.0, 34.2 ppm. LRMS (ESI, positive mode): *m/z*: calcd for C₂₀H₂₂Br₂O₃Na 490.98, found 490.98.

Résumé

De nos jours, l'industrie chimique est de plus en plus confrontée à la question de son impact environnemental, et doit dans le même temps faire face à la diminution des ressources de matières premières importantes tels que les métaux de transition, tout en respectant des contraintes économiques. Ces travaux de thèse avaient pour but de tenter de répondre à ces exigences, par le développement de méthodologies de synthèse basées sur l'utilisation de catalyseurs hétérogènes recyclables. En combinant les propriétés catalytiques de certains ions métalliques avec les propriétés de catalyseurs solides tels que les polyoxométallates ou les zéolithes, nous avons pu mettre au point de nouveaux outils pour la synthèse organique. Les polyoxométallates dopés à l'argent ont démontré leur efficacité dans le réarrangement d'alcynyloxiranes en furanes. La synthèse de spiroacétals et d'acétals par dihydroalkoxylation d'alcyne diols a été effectuée pour la première fois en catalyse à l'argent, *via* l'utilisation de zéolithes. En perspective, nous avons mis en évidence les applications potentielles de ces procédés verts dans la synthèse totale de molécules plus complexes. Les premiers résultats suggèrent que de telles synthèses plus respectueuses de l'environnement ont tout intérêt à être davantage utilisées à l'avenir.

Mots-clés: chimie verte, catalyse hétérogène, polyoxométallates, furanes, zéolithes, spiroacétals, alcanes.

Abstract

Nowadays, the modern chemical industry has to deal with increasing environmental concerns, including the disposal of waste and its economic impact, or the diminution of important worldwide resources such as transition metals. In this Ph.D. thesis, we aimed to bring improvement in this area by the development of green processes, based on the use of recyclable heterogeneous catalysts. By combining the catalytic properties of several metal cations with the properties of solid catalysts such as polyoxometalates or zeolites, we were able to set up new tools for organic synthesis. Silver-doped polyoxometalates proved to be very efficient catalysts in the rearrangement of alkynyloxiranes to furans. Acetals and spiroketals were synthesized by dihydroalkoxylation of alkynediols under catalysis with silver-zeolites. As a perspective, we highlighted the potential applications of such green procedures in the total synthesis of more complex molecules. The first results suggested that these environmental friendly processes should gain increasing interest in the future.

Key-words: Green Chemistry, heterogeneous catalysis, polyoxometalates, furans, zeolites, spiroketals, alkanes.